Anne-Katrin Marten

Operation of meshed high voltage direct current (HVDC) overlay grids - From operational planning to real time operation

Ilmenauer Beiträge zur elektrischen Energiesystem-, Geräte- und Anlagentechnik (IBEGA)

Herausgegeben von
Univ.-Prof. Dr.-Ing. Dirk Westermann
(Fachgebiet Elektrische Energieversorgung) und
Univ.-Prof. Dr.-Ing. Frank Berger
(Fachgebiet Elektrische Geräte und Anlagen)
an der Technischen Universität Ilmenau.

Band 12

Anne-Katrin Marten

Operation of meshed high voltage direct current (HVDC) overlay grids

From operational planning to real time operation

Universitätsverlag Ilmenau
2015

Impressum

Bibliografische Information der Deutschen Nationalbibliothek
Die Deutsche Nationalbibliothek verzeichnet diese Publikation in der Deutschen Nationalbibliografie; detaillierte bibliografische Angaben sind im Internet über http://dnb.d-nb.de abrufbar.

Diese Arbeit hat der Fakultät für Elektrotechnik und Informationstechnik der Technischen Universität Ilmenau als Dissertation vorgelegen.

Tag der Einreichung:	6. Januar 2015
1. Gutachter:	Univ.-Prof. Dr.-Ing. Dirk Westermann (Technische Universität Ilmenau, Deutschland)
2. Gutachter:	Prof. Dr. Dirk van Hertem (Katholieke Universiteit Leuven, Belgien)
3. Gutachter:	Prof. Dr.-Ing. Jutta Hanson (Technische Universität Darmstadt, Deutschland)
Tag der Verteidigung:	30. April 2015

Technische Universität Ilmenau/Universitätsbibliothek
Universitätsverlag Ilmenau
Postfach 10 05 65
98684 Ilmenau
www.tu-ilmenau.de/universitaetsverlag

Herstellung und Auslieferung
Verlagshaus Monsenstein und Vannerdat OHG
Am Hawerkamp 31
48155 Münster
www.mv-verlag.de

ISSN 2194-2838 (Druckausgabe)
ISBN 978-3-86360-112-6 (Druckausgabe)
URN urn:nbn:de:gbv:ilm1-2015000216

Acknowledgement

This work has been done during my time as a research fellow at the Power Sytems Group at Technische Universität Ilmenau, Germany. To all people that I have been in regular contact with, whether it be colleagues at Technische Unversität Ilmenau, from other international universities or industrial partners, I would like to express my sincere thanks and apprechiation. My special thanks go to the following important personalities:

Prof. Dirk Westermann gave me the opportunity to start my master degree studies in a scientific oriented study program at the Technische Universität Ilmenau. During that time he encouraged and challenged me in the field of HVDC and operation of power systems which defined my way down to this thesis. The best master thesis award 2012 didn`t only awarded me but also his commitment as well as quality of teaching and supervision. When I started as a research fellow in his group he was continuously supporting me with fruitful discussions, challenging projects, teaching duties, the possibility to take part in several international and national conferences as well as working groups. For that and his excellent supervision I would like to express my special thanks.

Prof. Dirk van Hertem from KU Leuven, Belgium, inspired me during several conferences by his presentations and critical discussions we had about operation of HVDC systems and related political and standardization issues. So I was very happy to have him as one of my reviewers for this thesis and would like to thank him for this work and being a part of the promotion committee.

Prof. Jutta Hanson from Technische Universität Darmstadt, Germany, is well known for her compence in the field of HVDC and power systems in general from a scientific as well as from an industrial point of view. I got to know her during research projects and our working group activities which underlined my impression of her. I would like to thank her for being a reviewer for this thesis and her work within the promotion committee.

Also Prof. Frank Berger, Prof. Jürgen Petzoldt and Dr. Uwe Rädel all from Technische Universität Ilmenau took an active part in the promotion committee as proven experts in their individual fields of interests. For that I would like to express my thanks to.

For the exceptional working environment and our special co-worker relationship as well as for a number of refreshing free time activities, several HVDC and off-topic related discussions I would like to thank my colleagues (and friends!) M.Sc. Robert Schwerdfeger, M.Sc. Florian Sass, Dipl.-Ing. Steffen Schlegel, M.Sc. Teng Jiang and M.Sc. Martin Wolfram.

Besides many other colleagues from the industry I would like to express my special thanks to Dipl.-Ing. Wilfried Fischer for inspiring me with his unique character, his special effort for supporting young engineers and wide spread knowledge in HVDC and AC power system equipment.

For their support I would also like to thank my friends, parents and especially my husband for his continuous patience and encouragement.

Abstract

There is an increasing demand for long distance bulk power transmission worldwide and particularly in Europe. Energy turnaround from conventional to renewable energy generation is one of the main drivers. This implies that a significant percentage of electricity production is generated remotely from load centers, by huge wind farms, for example. This new transmission objective can be met with high voltage direct current (HVDC) transmission. An HVDC grid is favored for redundancy as well as economic reasons. As this HVDC grid will be a new network layer above the existing AC transmission layer, it is referred to as an "overlay" HVDC grid.

This thesis proposes a three stage operation management strategy for future HVDC overlay grids. The architecture is comprised of tertiary, secondary and primary control instances which reflect the hierarchy of AC system operation. All control methods have been validated by numerical case studies on a reference grid which is a representative of a typical interconnected network situation in central Europe.

The proposed **tertiary control** ensures coordination among all HVDC converters and with the underlaying AC system. It serves as an example of converter reference value determination in a 15 minutes time interval. Therefore a mixed AC/DC optimal power flow method is proposed which is capable of solving this nonlinear optimization problem based on a complete set of topological and other state information of the entire grid.

In the event of having different transmission system operators (TSO) operating only a subset of converters of the HVDC overlay grid, the optimization problem becomes increasingly complex since each TSO might have its own optimization objectives. This problem is addressed by another multiple objective function approach. The proposed method superimposes particular cost functions of related TSO which yields system-wide cost functions as a basis for AC/DC power flow optimization.

The s**econdary control** instance adapts the tertiary control's converter reference values within the 15 minute interval to the actual grid requirements, particularly in the event of grid disturbances. An algorithm is proposed that identifies significant deviations from the actual power flow schedule by a wide are monitoring system. Converter power references are adapted in order to optimally share the deviations between the AC system and the HVDC overlay grid. Since data availability is key for the robust operation of this method, backup mechanisms for data acquisition is also proposed.

The **primary control** ensures DC energy balance, which is referred to as the energy stability of HVDC grids. Converter reference values for active power need to be adjusted in the event of a mismatch between active power fed to and drawn from the HVDC grid. As the time constants within a DC grid are very small, this is a fast, local control based on p-v-characteristics; the converter's power reference is adjusted in accordance with deviation of the

DC node voltage from its reference. Furthermore, a continuous *p*-*v*-characteristic is proposed as well as two appropriate parameterization methods. One emulates already existing piecewise linear *p*-*v*-characteristics for DC node voltage control and the other performs an automatic parameterization according to available balancing power provision capabilities on related AC point of common couplings. The latter significantly reduces the additional loading of the AC transmission grid with DC balancing power flows as the AC nodes, which are the most technically feasible, are utilized to provide the most DC balancing power.

Kurzfassung

Weltweit, aber besonders in Europa, steigt der Bedarf große Leistungen über weite Strecken zu transportieren. Dies ist hauptsächlich in der Energiewende und dem damit zusammenhängenden stark ansteigenden Anteil Erneuerbarer Energien und deren Erzeugungszentren begründet. Ein bedeutender Teil der Erneuerbaren Energien wird zukünftig weitab der Lastzentren produziert. Zur Lösung dieser daraus resultierenden neuen Transportaufgabe ist die Hochspannungsgleichstromübertragung (HGÜ) besonders geeignet. Eine redundante und damit auch wirtschaftliche Ausführung stellt das vermaschte HGÜ-Netz dar, das in der Energieversorgungsnetzhierarchie eine neue Netzebene dargestellt und somit als Overlay-HGÜ-Netz bezeichnet wird.

Diese Arbeit widmet sich der Fragestellung der Betriebsführung eines Overlaynetzes. Dazu wird eine dreistufige Betriebsführung vorgeschlagen. In Anlehnung an die im europäischen AC-Verbundnetz bestehende Dreiteiligkeit wird eine Untergliederung in folgende Regelungsinstanzen vorgenommen: Tertiär-, Sekundär und Primärregelung.

Die **Tertiärregelung** übernimmt die Koordinierungsaufgabe der Umrichter untereinander und mit dem unterlagerten AC-Netz im Rahmen einer Betriebsplanung. Es ist ein betriebstypisches Aktualisierungsintervall von 15 Minuten vorgesehen, indem die Umrichtersollwerte vorgegeben werden. Deren Bestimmung erfolgt durch ein auf dieses nichtlineare Problem zugeschnittenen AC/DC Optimal Power Flow. Dieses Verfahren fußt auf der Verfügbarkeit aller AC- und DC-Netzinformationen im Gebiet des Overlaynetzes. Im Falle einer föderalen Organisation eines HGÜ-Overlaynetzes in Europa müssen die Zielsetzungen mehrere Übertragungsnetzbetreiber (ÜNB) bei der Bestimmung eines Umrichtersollwertfahrplans berücksichtig werden. Für diesen Fall wird hier eine Methode vorgeschlagen, die mittels eines Aushandlungsprozesses die ÜNB spezifischen Kostenfunktionen für den Einsatz von HGÜ-Umrichtern in der entsprechenden Regelzone zu einer für das gesamte Overlaynetz gültigen Zielfunktion konsolidiert. Dabei werden Grenzwerte der einzelnen beteiligten ÜNB ebenso berücksichtigt wie lokale Zielfunktionen.

Die **Sekundärregelung** passt die von der Tertiärregelung vorgegebenen Umrichtersollwerte innerhalb des 15-min-Betriebsintervalls vor allem im Fall von Störungen an. Dafür

wird ein Verfahren vorgeschlagen, das sich der Informationen eines Weitbereichsüberwachungssystems bedient, um signifikante Abweichung der geplanten Leistungsflüsse zu erfassen. Die Umrichterwirkleistungssollwerte werden entsprechend angepasst. Eine Aufteilung von unplanmäßigen Leistungsflüssen zwischen AC und DC-Netz sorgt für eine Entlastung des AC-Netzes und beugt Betriebsmittelüberlastungen und dadurch verursachten Instabilitätsphänomenen vor.

Die **Primärregelung** gewährleistet das Gleichgewicht zwischen ein- und ausgespeister Wirkleistung in das / aus dem HGÜ-Overlaynetz. Ist die diesbezügliche Leistungsbilanz ausgewogen, ist das Energiegleichgewicht, die sogenannte Energiestabilität, gewahrt. Die DC-Zeitkonstanten sind klein. Nur eine dezentral (am Umrichterstandort) angeordnete Regelung kann zeitlich angemessen reagieren. Diese nutzt eine *p*-*u*-Regelcharakteristik, die die Umrichtersollleistung entsprechend der Abweichung von der DC-Sollspannung anpasst. Dafür werden eine kontinuierliche *p*-*u*-Charakteristik sowie Verfahren zu deren Parametrierung vorgeschlagen. Für die Bereitstellung von DC-Regelleistung besonders geeignete AC-Knoten können so angemessen für das HGÜ-Overlaynetz genutzt werden. Die Funktionalität des hier vorgeschlagenen dreiteiligen Betriebsführungsverfahrens für vermaschte HGÜ-Netze wird anhand von numerischen Fallstudien auf Basis einer typischen Netztsituation in Zentraleuropa validiert.

Table of contents

1 Introduction and Motivation

1.1 Historical power system development in Europe and ambitious visions

High demand for electrical power has emerged in heavily industrialized nations such as in Western Europe during the last hundred years. With these increased power demands, energy generation and transmission has also developed. Today's power system is based on power plants generating electrical power from coal, oil, gas or nuclear power close to centers of consumption interconnected with an AC transmission system to balance small fluctuations in available electrical energy in some regions.

In the beginning of Europe`s electrification, single generating units supplied a very small surrounding area with power, at this time primarily for lightning. An increasing demand which was also driven by the industrial sector, forced a connection of several nearby generating units to smaller grids, still with a limited expansion. In the beginning of 20th Century there has been a number of coexisting small AC systems. The ever increasing demand for electrical energy in Germany in the 1920's and the shortage of coal (main primary energy source at this time apart from water which is not available in the main load centers) pushed a development towards interconnection of these asynchronous zones in order to share generation potentials. There was also a similar need in other European countries. For instance in France a powerful interconnection was needed in order to balance seasonally fluctuating energy generation (depending on water supply) in the south. The interconnection of regional energy suppliers over short distance using 110 kV lines no longer met the demand. In April 1930, an 800 km long 220 kV overhead line achieved an interconnection between hydro power plants in the German Alps and coal power plants in the west of Germany at main industrial centers. [1] This has been the beginning of Europe's interconnected AC power system which today, still maintains a highly reliable energy supply.

At this time even longer interconnections have also been discussed in order to make use of larger hydro energy resources, such as in Norway, for sustainable and sufficient provision of energy supply. But it was also apparent that AC is not the appropriate technology to overcome challenges associated with such long distance transmissions. However, high voltage direct current (HVDC) was favored by some instead. At this time it was not only unclear how to operate such HVDC systems and how to extinguish DC faults but also how to generate high DC voltages, as a transformation, such as in AC, is not possible. Hence, this technology had to withstand much criticism and challenging technical problems. [1] This is still the case today. Some of these challenges, such as high voltage DC/DC transformation, have been resolved, nowadays a number of new challenges beside technical issues moved to the foreground such as various resistance from the populace or long approval procedures.

During world war two HVDC developments were pushed politically and several ideas of interconnecting Europe's energy resources emerged (as in Fig. 1.1) with typical intensions

of this time as HVDC provides the possibility to create a wide spread cable system for bulk energy transmission protected from airstrikes. [1] However, the basic technical idea of interconnecting all available energy recourses among Europe to supply load centers is still the same. This is an option for a future-proof and sustainable energy supply which is currently even more up-to-date in Europe even if there is no natural but a more idealistically driven shortage of existing energy sources today than in the first half of the 19th century. Nowadays this early idea of a meshed European HVDC system is rediscovered for long distance bulk power transmission with a major difference that some key challenges of former times are solved today, and this makes realization more likely. However, there are still challenging aspects to be solved on the way towards a meshed HVDC topology in Europe as is later explained in subchapter 1.3

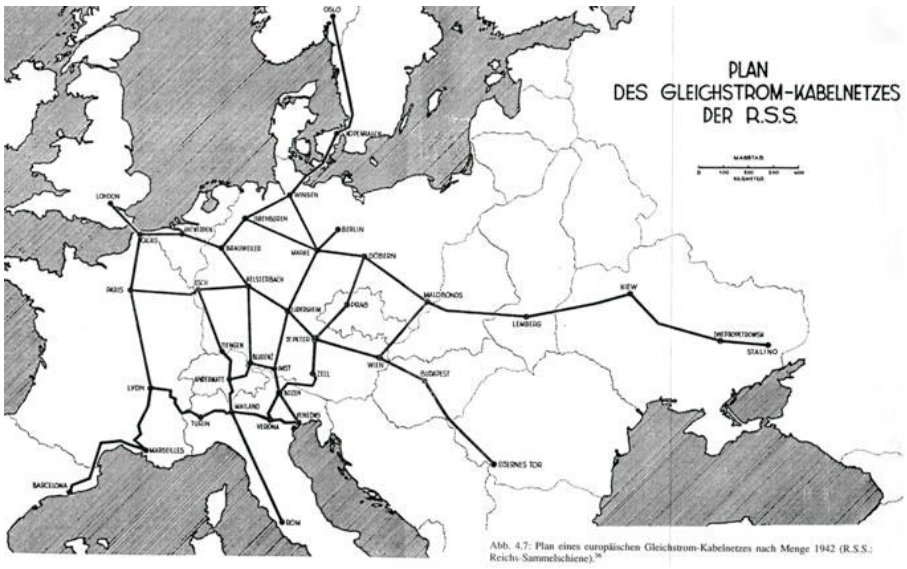

Abb. 4.7: Plan eines europäischen Gleichstrom-Kabelnetzes nach Menge 1942 (R.S.S.: Reichs-Sammelschiene).[36]

Fig. 1.1: Early idea of a European HVDC grid in cable technology. [1]

1.2 Challenges for Europe's power system today

1.2.1 Renewable Energies

The energy turnaround in Europe which is also known as *Energiewende* is a main target of the European Commission mainly driven by de-carbonization issues. Therefore, the Energy Roadmap 2050 defines ten structural changes for the transformation of Europe's energy system. It includes a share of renewable energies of at least 55% in overall energy consumption by 2050 [2]. Other scenarios within the Energy Roadmap 2050 assume an even higher share of renewable energy of up to 97% (high renewable scenario) while assuming the availability of significant electricity storages [2].This tremendous change in energy generation patterns is accompanied by high investments in the transmission system infrastructure. This is a transition from a system with high fuel costs towards a system with high capital expenditure. The Energy Roadmap 2050 estimates investment costs to be in the

range of 1.5 to 2.2 trillion Euro[1] between 2011 and 2050 for the future-ready European transmission system, whereby more renewable energies induce more investments in the transmission system [2].

As these are quite general and long-term targets, more short term targets are defined by the European commission in order to make sure that long term targets can be reached in time. The decisive 20-20-20 energy targets define EU wide key objectives for the year 2020 in order to reduce the greenhouse gas emissions by 20% (based on figures in 1990), to increase the share of overall energy consumption produced by renewable recourses by 20% and to improve overall energy efficiency by 20% [3], [4]. Assuming these targets will be met in 2020, the European Council has agreed to the 2030 framework which is going even further. This framework aims to reduce greenhouse gases by at least 40%, a share of overall energy consumption provided by renewable energy resources to at least 27% as well as an increase in energy efficiency by at least 27% [5].

Driven by these ambitioned European and national targets the amount of renewables used for electricity generation is continuously increasing. In 2013, 35 GW of new electricity generation capacity was installed. 73% of this (25 GW) is accounted for new renewable energy generation facilities. Approximately 11.2 GW of the renewable generation capacity are wind power units which is a slight decrease of 8% compared to figures in 2012. In total the installed wind power generation capacity was at 117.3 GW by the end of 2013. [6] Given that the installation costs are much smaller, most generating units of wind power are onshore. Only 5.6% is installed offshore [6]. As such, 1.6 GW have been installed in 2013. This is an increase of 34% compared to figures in 2012 [7]. However, as there is a high population density in Europe there is much more potential for offshore wind power plants to be installed in the years to come and this is also indicated by the tendency of offshore and onshore wind power plant installations. Fig. 1.2 shows the share of installed wind generation capacity in the European seas in 2013.

As the amount of installed offshore wind installation capacity is increasing every year, new installations of photovoltaics has been decreasing in Europe since 2012, due to political decisions. Almost 11 GW photovoltaic capacity was connected to the European grid in 2013 [8]. Of which, 3.3 GW have been installed in Germany although it is not one of the sunniest countries in Europe. However, this is still a 50% reduction compared to figure in 2011. The overall installed photovoltaic capacity by the end of 2013 was 81.5 GW although this will increase only slightly in the years to come. [8]

In 2012, the overall energy generation from volatile renewable energies (wind and photovoltaic) was approximately 280 TWh and the overall share of renewables of gross electricity consumption in Europe was 680 TWh (23.5%) [9]. The distribution among the European countries differs greatly, as can be seen in Fig. 1.3 a). This is due to different capacities of renewable energy use and various political influences. Other than conventional generation,

[1] $1.5 – 2.2\ 10^{12}$ €

renewables cause significant cross border load flows and energy trading. The energy exchange of each European country in 2012 is indicated in Fig. 1.3 b). With a further increase in the use of renewable energy in the form of wind and photovoltaics for Europe's electricity demand, a significant increase in power transmission capacity is necessary due to the volatile character of these energy resources and their geographical dependency.

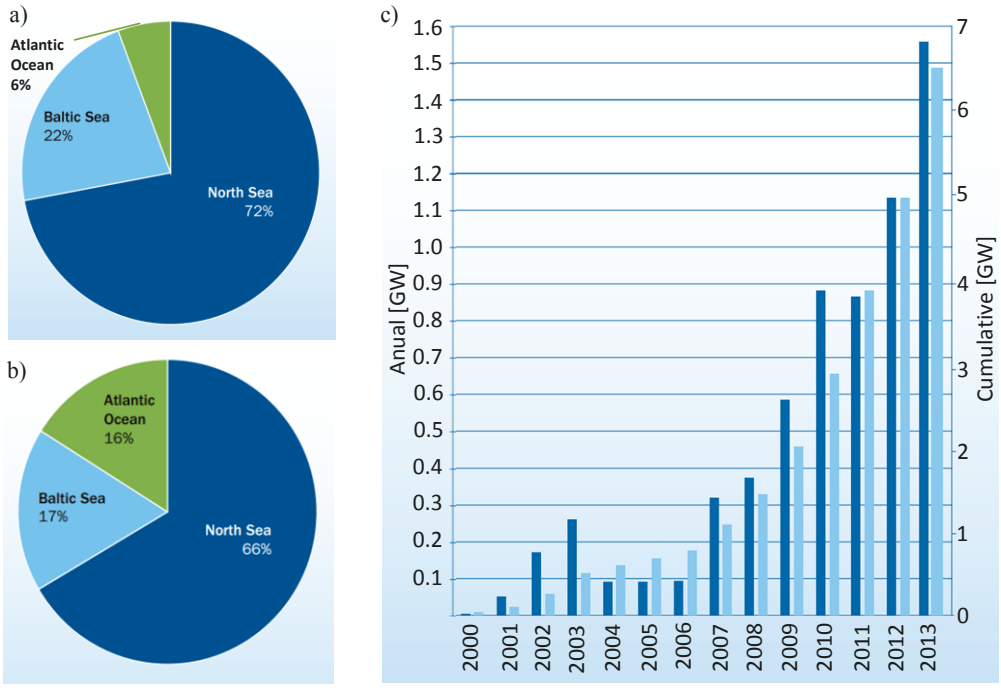

Fig. 1.2: Installed offshore wind power generating capacity by sea in the end of 2013 - a) installed in 2013, b) cumulative and c) cumulative annual offshore wind installations. [7]

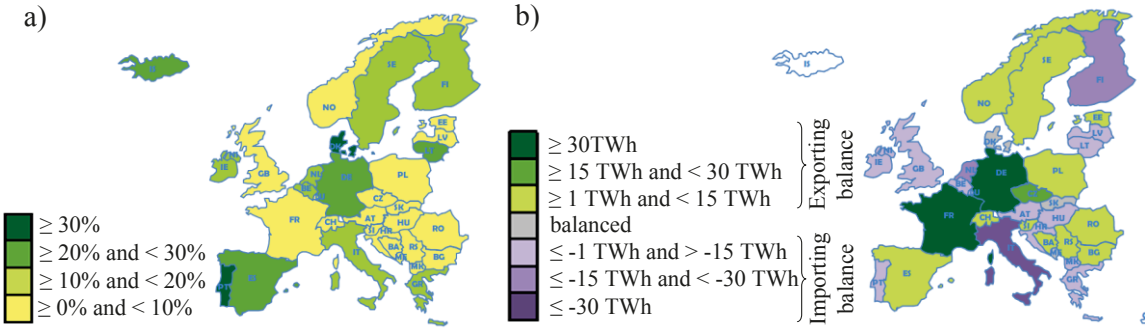

Fig. 1.3: Share of renewable energy generation excluding hydro power in 2013 (a) and exchanged energy in 2013 (b) per country. [10]

Storage capacities are an important issue in order to compensate renewables' volatile character. However, there is a lack of storage technologies feasible for bulk energy. An exception to this, however, is pumped hydro storage. This technology is also highly dependent on geographical conditions which are only available in selected European countries. The European Commission has published a study which identifies the potential for pumped hydro storages per country. Norway and Spain have the highest available capacities [11],

which can be used for certain locally generated overcapacity from renewables. Even more potential is available in Turkey which could become Europe's electricity storage as is shown in Fig. 1.4. A potential of 123 TWh has been identified which is approximately 10 times higher than the already used storage capacity [11]. However, there is a need to overcome long distances in order to connect these storages with Europe's load centers.

Hydro power has been used since the beginning of electrification in Europe and is already a key component in today's energy mix. However, there is still a European-wide potential of another 600 TWh to be generated per year (status as of 2010), which would mean a doubling of the potential used today [12]. In Turkey, Norway, Sweden, Iceland, Spain and France alone there is a capacity for another 180 TWh, 82 TWh, 65 TWh, 52 TWh, 38 TWh and 35 TWh respectively [12]. Again, these main capacities are only available in a few countries and the majority of these have a significant distance to load centers. This highlights the need for long distance bulk power transmission in order to utilize this seasonal dependent base load potentials.

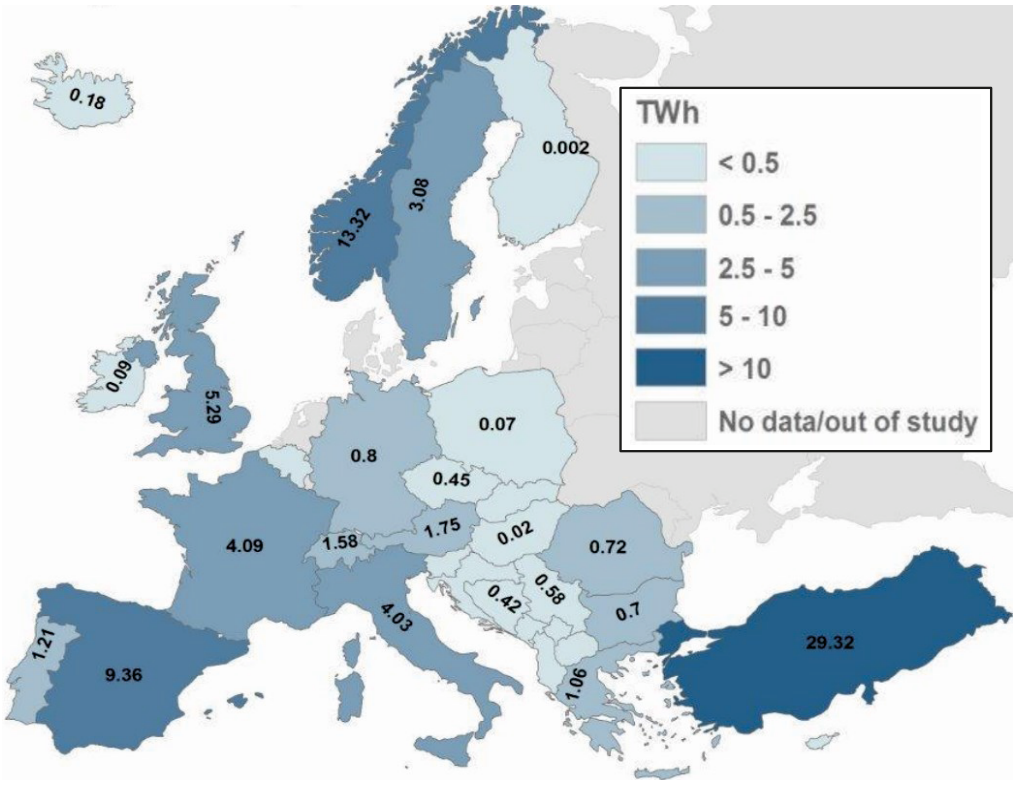

Fig. 1.4: Realizable potential for pumped hydro storage assuming that one reservoir out of two already exists, a second one can be built, maximum distance to an existing transmission grid is 20 km and taking into account environmental, social and infrastructural restrictions. [11]

1.2.2 Definition of the new transmission task and first steps towards a solution

In the previous subchapter, renewable energies as the reason for future transmission grid challenges have been examined in terms of its present situation and its potential to be used

in order to reach Europe's energy goals by 2050. Significant potential for further renewable energy generation as well as the linked storage potential for volatility compensation are located far from load centers as is summarized in Fig. 1.5. This is not only a challenge for the existing AC grid but a redefinition is also required to identify its primary tasks in the future. The existing AC grid is therefore not designed to overcome this new transmission challenge, and DC technology is the most suitable solution that is known today:

Long distance bulk power transmission in varying directions.

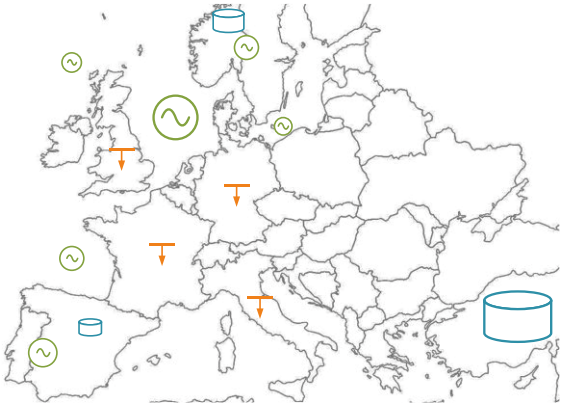

Fig. 1.5: Areas for high renewable energy generation and storage potential as well as main load centers in Europe.

For this special transmission task, the advantages of HVDC transmission with respect to AC transmission are:

- Direct integration of offshore wind power
- Integration of asynchronous areas for market coupling issues
- Absence of reactive power demand even for very long distances and cables. This also enables theoretically unlimited transmission distances.
- More economic, also due to the absence of reactive power (no compensation)
- AC/DC converter stations have to be actively controlled. This prevents unintended power flow paths and power oscillations can be inherently damped.

The identified demand for long distance bulk power transmission and the feasibility of DC to overcome this challenge is also reflected in the current version (2014) of Europe's Ten Year Network Development Plan (TYNDP). Although the TYNDP includes market integration as a driver for grid extension, transmission of renewable energy is another consideration. Before 2030 interconnection capacities will double and therefore a need for additional or upgraded transmission infrastructure of approximately 48,000 km will be necessary. Of this, 17,300 km will be DC subsea cables used to connect offshore wind farms to onshore systems as well as improving the interconnection of the UK, for example. Additionally, approximately 6,000 km of DC transmission infrastructure is requires onshore. Thus, more than 40% of total additional transmission infrastructure is DC. [13] Fig. 1.6 a) shows the projects identified within the TYNDP.

Four of these projects particularly stand out and can be seen as lighthouse projects in Europe. These are the four HVDC point-to-point (P2P) interconnections planned in Germany until 2034 [14]. These are also shown in Fig. 1.6 b). Renewable energies accounted for 25.4% of Germany's electricity consumption [15]. Due to geographical and meteorological conditions renewable energy generation from wind in Germany is primarily located in the north as well as in the east. Increasingly, wind is also being utilized in the North and Baltic Sea. More than 36,500 GWh wind power was generated in Germany's northern region[2] in 2012 [16]. These extensive geographical distances must therefore be bridged in order to supply load must be transmitted via Germany's planned HVDC corridors.

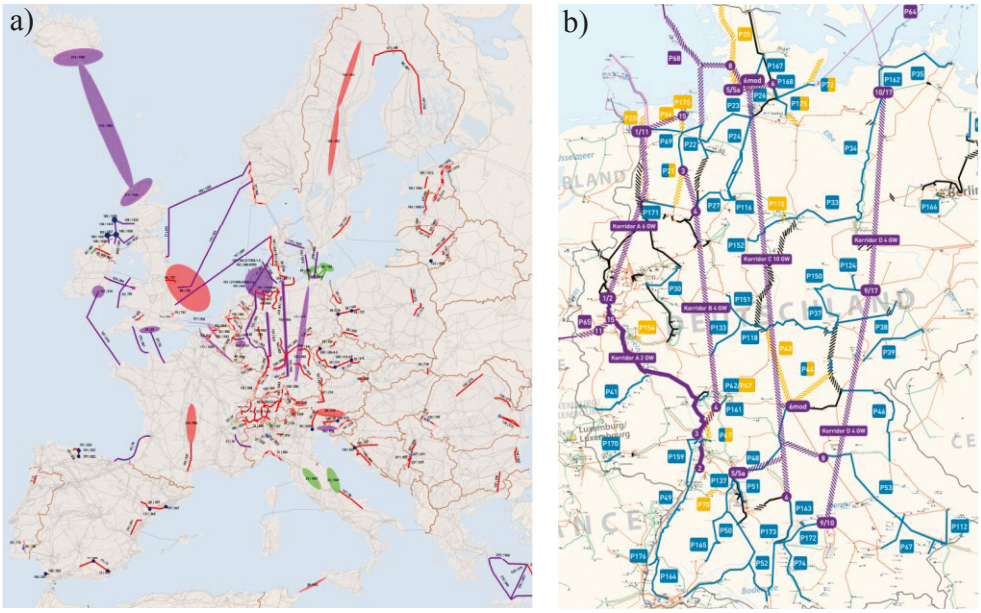

Fig. 1.6: a) Ten Year Network Development plan until 2030 [13] and b) Netzentwicklungsplan of the German TSOs for 2034 [14].

HVDC in general is a suitable solution for onshore bulk power transmission over longer distances. As overhead lines increasingly face public resistance, more and more areas are favoring underground alternatives. However, underground solutions are confined to very short distances using AC technology or require exponential high reactive power compensation efforts. This is not required using HVDC technology and HVDC underground lines are not physically limited in length. Recent developments in HVDC cables (525 kV and up to 2.6 GW) [17] as well as progress in the field of gas insulated transmission lines (GIS) [18] makes these solutions become more realistic.

In general HVDC technology has made considerable progress in regards to power and voltage ratings as well as converter technology. With the commercial introduction of voltage source converters (VSC) in the 1990's, the demand on reactive power and connection to weak AC systems is no longer problematic. Furthermore, with the invention of multi-level converter (MMC) technology (also VSC) in 2001, the high loss of VSC compared to line

[2] Mecklenburg Vorpommern, Brandenburg, Saxony-Anhalt, Schleswig-Holstein and Lower Saxony

commutated converter (LCC) technology was reduced significantly. As VSC technology is also capable of building meshed HVDC grids the realization of the early vision from the beginning of last century (see Fig. 1.1) is closer than ever before. There are, however, still many technical challenges regarding HVDC grids, and this is a major focus in current research. Besides political challenges these issues are mainly related to various technological components and system operation. This issue will be discussed in more detail in chapter 2.

The general concept of interconnecting all regions with their specific energy generation specialties (as is indicated in Fig. 1.7) has not been altered since the beginning of last century. Other than hydro power this will mainly be other renewable such as wind, solar and also significant storage capacities. There are already projects in planning and under construction, which could serve as a nucleus for a future meshed European HVDC grid as: INELFE [19], Europagrid Adriatic [20], Western HVDC Link [21] and the planned four HVDC corridors in Germany [14].

Fig. 1.7: A possible option for a pan-European HVDC grid. [22]

If the transmission task itself is considered, it could be solved using state of the art P2P. The more HVDC interconnections are set into operation in a transmission system the more important this new transmission layer becomes and the more additional requirements step into the foreground. The most essential requirement is reliability. The same degree of reliability with P2P interconnections, requires much higher monetary effort as each P2P line needs two converter stations.

Taking into account a meshing option, reliability is provided to the very most extend by the meshes itself. In this case, the most expensive equipment (converters) is used in a much more efficient way. Additionally, when considering fluctuating main transmission directions and paths, the intensity of exploration of converter capacities is much higher using a grid than a P2P connection. It is inherent in P2P connections that only one transmission path is able to be served. This information is summarized in Tab. 1-1. From a technological, as well as economical point of view, a meshed HVDC topology is therefore the most efficient solution for expected challenges of the European transmission grid.

Tab. 1-1: Requirements related to Europe's additional future transmission tasks.

	P2P connection	HVDC overlay grid	Meshed HVAC overlay grid
Bulk power long distance transmission	✓	✓	× Reactive power demand increases with transmission distance; compensations costs affect its economic efficiency
Inherent redudancy	(×) A redundancy can be provided with P2P connections with another parallel P2P system is installed and both are operated accordingly	✓	✓
Controllability of power flows dedicated for long distance transmission	✓	✓	(×) Additional equipment would be necessary
Fluctuating transmission directions	(✓) If the line (or a part of it) is in mass impregnated cable technology, immediate power flow reversal is impossible	✓	✓
Fluctuating transmission paths	×	✓	✓

1.3 Current research activities and initiatives related to HVDC in Europe

Today's network planning for the interconnected onshore grid focuses on projects which strengthen existing transmission lines or corridors. Building new lines or corridors is for the most part limited by length and based on conventional AC technology, preferably in overhead line design. ENTSO-E criticizes this forthcoming approach as such marginal improvements will not be enough to reach the ambitious renewable energy targets of 2050 [25]. New approaches are needed which significantly strengthen the European transmission capacity. Therefore the use of new technologies and new operation methodologies is inevitable to continue a stable and sustainable energy supply.

Major projects and initiatives in Europe such as Twenties, BestPath, Friends of the Supergrid and North Seas Countries' Offshore Grid Initiatives are focusing on new technologies such as HVDC, and even an HVDC network code has been drafted and is about to become into European law. However, the main focus is on technology, economical and regulatory aspects, HVDC grid topology and, in Twenties, also on operation of offshore HVDC grids [26]-[29].

Addressing these issues is essential to prepare the transmission grid for future challenges; however, as grid requirements differ with regards to offshore HVDC grids (interconnecting asynchronous areas) the operation of an HVDC grid itself and in parallel to a synchronous AC grid is vital as well.

1.4 Scope of this work and main contributions of the thesis

This work addresses the following research question: *How is it possible to operate a meshed HVDC grid overlaying an interconnected AC grid in order to maintain its own stability and interact with the AC system to ensure secure operation of both AC and DC in such a way that an optimal operation point of the overall system can be reached?*

Short term events as faults in the AC transmission grid as well as in the HVDC grid are assumed to be cleared. Possible contributions of the HVDC converters that are not related to HVDC grid's transmission tasks as AC voltage control or a contribution for AC grid damping will not be considered here.

Increasing the share of renewable energies by up to almost 100% requires a tremendous change to the energy supply system. A particular role corresponds to the transmission system which was built to transmit small amounts of power between neighboring areas. Bulk potential for renewable is mostly removed from load centers, thus bulk power has to be transmitted over long distances. This is a challenge for the transmission system which can be overcome by introducing a new transmission layer based on HVDC.

For redundancy reasons and for scenarios with fluctuating transmission directions (maybe varying with season or daytime) meshed structures are reasonable. If the same level of redundancy should be provided with P2P topologies, much more financial and space effort are necessary than for a meshed HVDC grid.

Most existing HVDC projects are in P2P topology and the first multi-terminal using MMC technology was established in 2014, connecting Nan'ao Island's wind power with the mainland in Guangdong area in China [46]. However, a meshed HVDC topology does not exist and operation methods are required beforehand. This work deals with the operation of meshed HVDC grids for public electricity supply systems. Presented methods are also applicable for P2P and multi-terminal topologies in an early stage of an HVDC grid, for example. As such, it focuses on general operation methods in real time operation, up to day ahead operational planning.

In subchapter 2.3 system operation hierarchy is presented and includes primary (local), secondary (semi-local) and tertiary (central) control instances following the structure in AC systems. Functionalities for each control instance are addressed here as can also be seen in Fig. 1.8. A European HVDC grid will be a new grid layer above the existing AC transmission grid. A definition of concrete data to be provided is proposed by the operational planning instance. This includes information on converter power, AC and DC voltage reference values, parameter of local DC node voltage control characteristics, individual DC node voltage limits and emergency schedules in case of a disturbance. In subchapter 2.3.3 it is explained that it is not reasonable to split responsibilities within the HVDC grid and give it to every involved TSO. It is much more beneficial to define a new responsibility instance with a global view on the HVDC and AC transmission system adequately controlling their HVDC system. As TSC and CORESO are in charge of larger AC transmission areas, either of these institutions could incorporate the responsibility of the new HVDC grid.

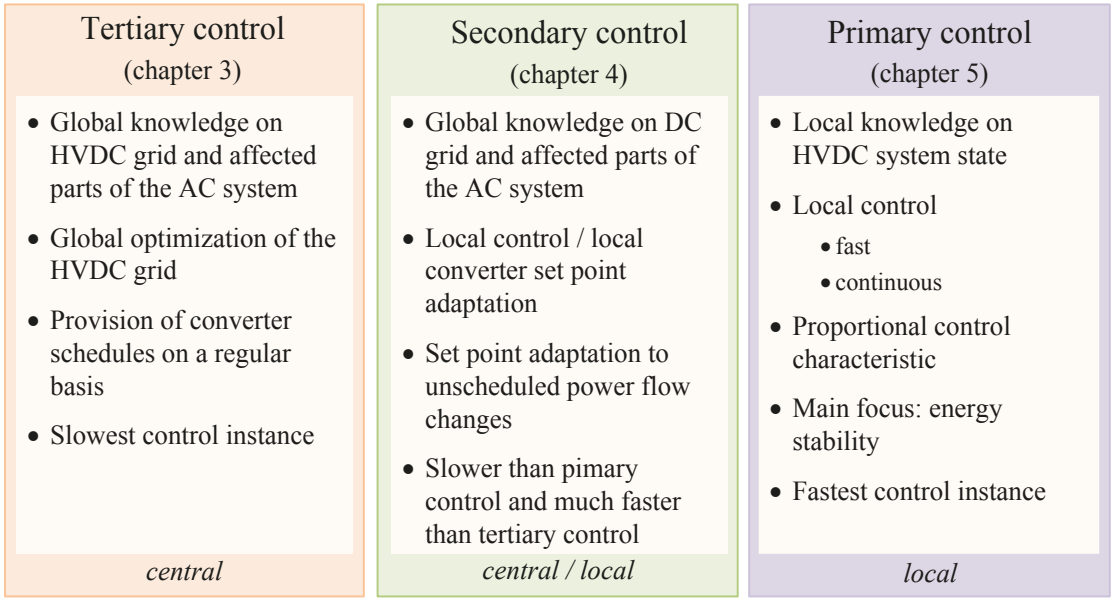

Fig. 1.8: General HVDC control hierarchy concept this work is focusing on including primary, secondary and tertiary control instances.

One of its tasks is operational planning for the entire HVDC grid in order to meet market requirements and to ensure a safe operation of the overall transmission grid. Thus, chapter 3 proposes a centralized coordination using a mixed AC/DC OPF solved with an artificial intelligence optimization method (also see Fig. 1.8). Conventional optimization methods are not suitable as they promote non-convergence or convergence in local minima particularly when having highly non-linear equipment such as HVDC converters. Operational planning is dedicated to tertiary control as indicated in Fig. 1.8. Additionally a coordination method without having a centralized control instance is presented in subchapter 3.3. This can be used in an early stage of a meshed HVDC grid when only a limited number of converters and TSOs are involved.

Operational planning is based on forecasts and market results, which define the generation patterns. If the grid's topology, generation or load pattern change in real operation, converter schedules given by operational planning are subject to adaptation as they do not automatically change. Within the AC or DC system a change of topology and / or load and generation pattern causes an automatic adaptation of power flows according to the grid impedances. However, converters as coupling equipment between both systems need an active change in reference values in order to take part in significantly changed load flow patterns and thus give maximum contribution to keep the entire system stable. A method to overcome this challenge is proposed in chapter 4. It is based on phasor measurement unit (PMU) / wide area monitoring system (WAMS), which provides voltage angle information to identify significant global power changes. PMU based technology has been commercially available for a number of years and is adopted for the realization of control functions. Here, local converter reference values are adapted without global optimization process, which is time consuming. A global re-coordination of all converters after a disturbance could therefore take place afterwards. Additionally back-up procedures are proposed for the rare event of PMU or WAMS tripping. Adaptation of converter reference values to the actual system state are dedicated to secondary control (see Fig. 1.8).

Finally, the smallest time horizon is considered maintaining DC energy balance. Time constants in DC systems are much smaller than in AC systems. Consequently, it is reasonable to have local control mechanisms in order to maintain DC energy balance. Some state of the art piecewise linear local control characteristics can lead to DC oscillations. Influencing factors are analyzed in subchapter 5.2. It is found that continuous local control characteristics can significantly decrease the sensitivity of the DC system against DC oscillations. As such, subchapter 5.3 proposes a continuous control characteristic that can emulate the basic idea behind state of the art local control characteristics (subchapter 5.4) but which can also be used to dynamically vary the control characteristic based on local AC grid characteristics (subchapter 5.5). According parameterization is also presented. As local DC node voltage control is the fastest control instance and modifies converter power references with a proportional control in order to maintain the DC energy equilibrium, it is dedicated to be the primary control instance (see Fig. 1.8). A conclusion and an outlook of this work are given in chapter 6.

1.5 General Definitions

When introducing new technologies always goes along with using different vocabulary having the same aspects, topologies or methods in mind. However, until there is consensus on the vocabulary used, this will lead to confusion. The subject of meshed HVDC grids is at an early stage. Thus, some general definitions are given in this subchapter in order to define its meanings in relation to this document.

HVDC: At the time of writing (end of 2014) there has been no standardised definition for HVDC. Even if it is clear that direct current is addressed, the minimum voltage level for HVDC is unclear. For the onshore HVDC grids which are in the focus of this work, a minimum voltage level of 200 kV is assumed. A future HVDC grid as it is favored in this work is intended for voltage levels of 500 kV or 800kV, ideally as bipolar technology (±500 kV or ±800 kV) for reasons of redundancy and power capacity. Bipolar HVDC systems are assumed in this work. It is assumed that technological gaps between these assumptions and the available technology today will soon be resolved. This is also a subject in subchapter 2.1. HVDC considered in this manner is mostly used for bulk power (1 GW and above [43]) long distance transmission.

AC system and AC grid: In general an AC system includes the AC grid and all connected equipment, loads and generating units. If the AC grid is considered loads and generating units are out of scope.

HVDC system and HVDC grid: An HVDC grid as it is used here refers to the network, including busbars, lines and other equipment as DC breakers and DC/DC converters (if applicable and necessary), as well as its topology. Here an HVDC grid is defined as a meshed HVDC topology including at least one mesh. Radial sections can also be a part of the HVDC grid if at least one mesh is existent. In this work it is assumed that no loads or generating units are directly connected to the HVDC system but only via a converter. Hence, HVDC grid and HVDC system are used synonymously in this work with the exception that an HVDC system can also imply a P2P or radial multi-terminal topology without meshes.

Overlay HVDC grid / system: An overlay HVDC grid or system is a special kind of an HVDC grid / system that is overlaying a synchronous AC grid. It does not exclude the HVDC interconnection of asynchronous zones if at least two converters of the HVDC system are within a synchronous zone.

Multiterminal HVDC: An HVDC grid is also a multi-terminal topology known as multi-terminal direct current (MTDC). In contrast to an HVDC grid, a MTDC does not necessarily include meshes but can also have solely radial topology.

Operation of HVDC grids as it is used in this work addresses larger time scales such as operational planning up to two days ahead, day ahead and intraday time frames, as well as real time operation. This focuses on normal operation and operation in disturbed conditions by means of adapting converters reference values. It does not include fault handling, inner converter control and consideration of transient phenomena. This is also addressed and illustrated in subchapter 2.3.1.

2 Challenges corresponding to meshed HVDC grids

To date, there is not yet been an HVDC grid built worldwide. There are therefore many challenges which current and future research and engineering need to address. These challenges can be categorized as either asset or operation related issues.

2.1 Components

DC/DC converters: When considering HVDC grids, there are additional challenges which must be considered than for P2P or small radial multi-terminal systems. Without the use of additional equipment in meshes such as DC/DC converters, DC power flows cannot be actively controlled on a specified line [O-17], [48]. Given that these devices are not typically needed in today's HVDC P2P schemes, they are not commercially available and there lacks a common strategy to operate them in a meshed HVDC topology.

Fault clearing equipment: There is a major problem related to DC faults in meshed HVDC schemes. Multiple lines and converters can feed the fault and single line currents cannot be limited without having capable line current controlling devices. Depending on the converter technology used, the DC fault can also be fed by the AC system and both systems are affected. By using full bridge VSC converters, this problem can be avoided, however during converter operation there is a significant increases in investment costs and losses. Given that a full bridge converter is capable of controlling DC fault currents, it is therefore also possible they are utilized for DC fault clearing. Problems may occur when considering very large HVDC grids when the whole system needs to be shut down using full bridge converters. In this case, DC circuit breakers may become necessary.

Regarding the requirements for AC circuit breakers, the DC equivalent has to cope with much steeper fault current gradients, the absence of current zero crossings, fast decreasing DC voltages which may cause problems for some converter topologies, and no overcurrent capability of power electronic equipment as converters resulting in the requirement for very fast DC fault current interruption. First approaches for DC circuit breaker exist [23], [24]. Questions are still posed as to whether or not these solutions, among others, will be ultimately carried out due to monetary effort it takes (two breakers are needed for each line). It is also unclear whether the DC breakers are able to be up scaled to ultra-high DC voltages with bulk power ratings.

Multi-Vendor grids: Most P2P HVDC connections are from a single manufacturer. This will change for an HVDC grid as there are a number of converters required. However, it lacks of standardization for HVDC equipment applied to so-called multi-vendor grids. It is therefore unclear if different converter topologies and particularly converter control methods will negatively interact with each other. As topology and control differs from manufacturer to manufacturer, there also lacks simple yet not oversimplified models to represent all relevant converter characteristics. On this basis it is also difficult to define standards or

standardized behavior of converters without putting one or more manufacturers at a disadvantage. It is very unlikely that an HVDC grid spanning Europe with a number of converters is able to be successfully delivered by a single manufacturer due to multiple reasons:

- Limited production and installation capacities of single manufacturers
- Contracting of single projects (parts of the future meshed HVDC overlay grid) is based on a free market related to:
  - Economic considerations
  - Technical considerations, such as HVDC technology, is under rapid development (therefore, useful technical advances will be a competitive advantage)

Public resistance is a very important issue that is related to the (visible) HVDC components and thus is mentioned here. The public resistance against overhead transmission lines in densely populated areas such as Western Europe is very high. Thus, long distance underground transmission will be necessary for some areas. On the other hand, this grid extension still lags behind the increasing share of renewable so it would therefore be necessary to make up for lost time. Furthermore, building underground transmission lines is usually much more time consuming than building overhead lines. Additionally, there is a lack of procedure and standardization for manufacturing and laying extended cables. Possible solutions are an onsite production of endless cables, a pre-manufacturing of cable sleeves in the factory or using gas insulated lines (GIL). However, none of these solutions are close to becoming commercially available.

Converters voltage and power rating: Converter technology suited for HVDC grids (VSC technology) have been commercially available since the late 1990's. Bulk power and low loss converters have been available since market introduction of VSC development in MMC technology in 2007 [30], [31]. With the advent of VSC meshed HVDC grids became feasible and in particular, MMC decreased losses, which is particularly important with regards to bulk power transmission. But MMC and also VSC technologies in general are relatively new. Thus, classical LCC technology's biggest advantage is the availability for ultra high voltages and power ratings. This must be catched up by VSC technologies in order to economically meet bulk power transmission demands in Europe.

Former challenges regarding the "transformation" of DC voltages to ultra high voltage levels are accomplished for some decades with the development of LCC. Since the late 1990's self-commutated converters have become available and converters with very low reactive power demand have been available since 2001 [32]. Newer converter topologies are also available with DC fault current blocking capabilities (full bridge converter topology). But as previously described, there still remain some challenges regarding HVDC overlay grid components.

2.2 Operation

However, operation methodologies are equally important to the utilization of appropriate equipment in meshed HVDC grids. To make use of assets it is essential to have adequate HVDC overlay grid operation and sufficient technological capabilities. In general the implementation of a grid offers basic advantages over P2P connections, such as:

- Increased system stability
- Redundancy
- Flexibility for changing transmission paths during certain periods

Additional advantages result from an HVDC overlay grid:

- Lower transmission losses
- Inherent controllability of coupling equipment (converters)
- Relief of the underlaying AC transmission layer by an adjustable amount in means of:
  - Transmission of scheduled power flows (operational planning)
  - Transmission of unscheduled power flows (real time operation):
    - balancing power flows
    - power flows after parallel transmission equipment trip
    - supply of islanded areas

As converters between the AC transmission and the HVDC overlay grid must be actively controlled, algorithms must be developed and implemented in order to make use of those advantages.

DC energy balance: In order to ensure stable DC grid operation the DC energy balance has to be maintained at any point in time as a vital control requirement. The input has to meet the output power of the HVDC grid, otherwise an energy surplus or energy deficiency results in an immediate and significant change of DC voltage. This is described in more detail in chapter 5. Many local control characteristics have therefore been proposed and tested on a numerical basis. However, most of these characteristics require improvement according to the overall dynamic system behavior when applied to multiple converters within a single HVDC grid.

Guaranteeing the energy balance is vital for any HVDC system, but operational methodologies are necessary not only for operating an isolated HVDC grid but also for an integrated operation within an interconnected parallel AC system. Extensive research has been conducted on controlling an HVDC system interconnecting AC offshore networks with AC onshore networks as this would be the first possible application in Europe. Essentially, controlling HVDC systems interconnecting asynchronous AC system is very important. Directly after the implementation of such an HVDC system, possibly as a meshed topology, there is the challenge of distributing the offshore wind energy among the continental load centers over a great distance to the shorelines. A meshed HVDC onshore grid is a feasible

solution. For the operation of both types of HVDC systems or meshed grids an understanding of the overall system including the DC and AC part(s), is necessary.

Automatic participation in unscheduled power flow changes: Considering an onshore HVDC grid is accompanied with the idea of creating a backbone for the entire electricity grid. As coupling devices between the AC and the DC grid, the converters do not automatically take part in the power flow pattern. This is different when considering a single AC or DC grid where power flows are distributed along the grid according to its impedances in normal and disturbed operation. The automatic behavior of a converter must be actively controlled for operational planning issues as well as for fast adaptation of converter references after disturbances.

Maintaining N-1 security: The general motivation for an HVDC system is the transmission of bulk power (besides coupling of asynchronous AC networks). However, disturbances can also affect parts of the DC system. This must be taken into consideration during the HVDC grid planning process as well as for operational issues. The possibility of faults must be considered in operational planning in terms of maintaining N-1 criteria or available margins for emergency situations, for example. Additionally, the creation of emergency schedules can be taken into account. During the operational planning stage, emergency schedules are used to calculate for various possible disturbances as well as to communicate to the converters. If any of these disturbances take place an autonomous switch to the relevant emergency schedule maintains stable operation at any time without the time consuming central recalculation of schedules after the disturbance. This requires a local and explicit identification of the disturbances which may not be possible in any case. Each converter should therefore be equipped with autonomous mechanisms to take part in significant changes of the power flow pattern in order to avoid overloading any equipment. It is also possible to use such mechanisms to bridge the time in case of central identification of the explicit disturbance.

DC fault identification: The absence of natural zero crossings and consequently lower damping effect of the system's inductances with respect to the fault current rise, not only cause challenges for fault extinguishing equipment but also for fault identification. Due to the high fault current rise in DC systems and the absence of overcurrent capability of semiconductors (e.g. in converters) fault identification must be very fast depending on line length and technology (due to traveling wave characteristics) between 1 ms and 4 ms [33]. The overall fault detection and clearing process must be significantly faster than 10 ms at least if only DC circuit breakers are used for DC fault clearing. Therefore, for fault clearing a time of about 5 ms remains. Several methods for DC fault identification in meshed HVDC grids are proposed in the literature. Concepts that are based on differential current such as in [34], [35] are unacceptable for extended HVDC grids due to communication delay [36], [37]. Another solution is proposed in [38] introduced as the Handshaking Method. Each node identifies a potentially faulted connected line, before the entire HVDC system shuts down and opens fast disconnectors of identified potentially faulted lines. When the HVDC

system is energized again a decision on a faulted line is made by comparing the voltage on both side of each open disconnector. This approach can generate a conflict with two general fault clearing requirements; namely: selectivity and speed. Other approaches are based on wavelet analyses [39]-[42] or identification of current and voltage gradients [44], [45]. However, a final decision on a specific solution is still pending.

HVDC grid responsibility: As a meshed onshore HVDC grid will span a wide area of the existing AC grid, it is likely that also multiple TSOs are involved. It is likely that each TSO will only have a limited number of converters within its responsibility area with regards to the overall number of converters within the HVDC grid. This raises the question of responsibility for the entire HVDC grid. A more detailed discussion on this topic is made in subchapter 2.3.3.

Standardization of operation: As with the technological issues, there is also a lack of standardization with regards to operation. A standardization of HVDC grid operation is of particular interest if the HVDC grid responsibility and operation is shared among several instances and for coordination between the HVDC grid and AC grid operation. So far there are no requirements to be met for different operation and control instances within the HVDC grid. ENTSO-E created the first HVDC grid code which is in the current version and focuses on the effect of the HVDC converters on the AC grid rather than on the operation of the HVDC system [26]. Consequently, a CENELEC working group was created which focuses on all topics related to operation of meshed HVDC grids [O-28].

2.3 System operation hierarchy and responsibility

Once the most important technological and political challenges regarding the setup of a meshed onshore HVDC grid are solved, it comes to operational requisition. As a new transmission layer with different characteristics, transmission tasks and geographical expansion, there are basically two questions:

- How to operate a meshed HVDC system that spans an existing, in operation AC system in order to maintain a stable operation of the DC system, relieving the AC by the DC grid to keep AC system stability, to guaranty an overall economic operation that also includes market aspects?
- Who will be responsible for this new grid layer? This issue can go through a dynamic process with changing topology and covered area of the HVDC grid during its development phase.

The first question is generally described in subchapter 2.3.1 and special categories are subject for more detailed analyses in chapters 3 (HVDC overlay grid operational planning), 4 (Autonomous local reference value adaptation) and 5 (DC energy balance). Possible responsibility is discussed in subchapter 2.3.3.

2.3.1 Structure of system operation hierarchy – state of the art

System operation of the European AC system is subdivided in three control levels primary, secondary and tertiary. Using load frequency control as an essential part of AC system operation, the primary control is a frequency containment process with a proportional control characteristic. As a steady state frequency error occurs, secondary control, which is slower activated than primary control, is a frequency restoration process with an integral control character that also restores pre-disturbance power exchange among control areas. The tertiary control gives new schedule afterwards in order to relieve control reserves. [47]

This concept was transferred to an HVDC grid operation hierarchy by [O-17], [48]-[53], [129]. Tertiary control layer is intended to determine converter power schedules based on global information and using an optimal power flow calculation (OPF). This OPF is only able to consider the DC system or in addition also the AC system in order to find an optimal operating point for the overall system.

As optimal power flow may do not or do not exactly take all converter and DC transmission losses into account, there is a DC energy imbalance without any disturbances and therefore an adaptation of converter power reference values is necessary. This is one of the issues for secondary control [51]. Secondary control is also needed when primary control was active due to any disturbance within the DC grid to reset converter's set point in order to reestablish pre-disturbance conditions, regarding power exchange between system areas or on specific tie lines for example [49], [50], [52], [53]. Additionally secondary control can specify primary control parameters for set point achievement [49].

Primary control of HVDC grids according to [49]-[53] is represented by DC node voltage control limiting the deviation of DC voltage if any disturbance within the DC system takes place or energy balance is not met due to other reasons. This is achieved by adapting converter's power using voltage droop control characteristic, for example, as it is described in subchapter 5.1. A concept for HVDC grid operation hierarchy according to [49]-[53] and [129] is shown in Fig. 2.1.

2.3.2 Structure of system operation hierarchy - extension of state of the art HVDC control hierarchy definitions

The existing definitions, particularly for secondary control instances, do not take into account parallel operation of an AC and DC grid. Only a stable operation of each single grid (AC and DC) is considered. Assuming one major task of the HVDC grid to relieve the AC grid, also unscheduled and significant AC power flow changes affecting AC transmission corridors parallel to DC lines should be a subject of immediate adaptation of converter power reference values. This maintains AC system stability even in case of large disturbances (for more details see subchapter 4.3). This control function has characteristics of secondary but also primary control to a certain extent. It will have a higher hierarchy level than

DC node voltage control while it is determining new converter power set points and is a part of *autonomous adaptation control* in Fig. 2.2.

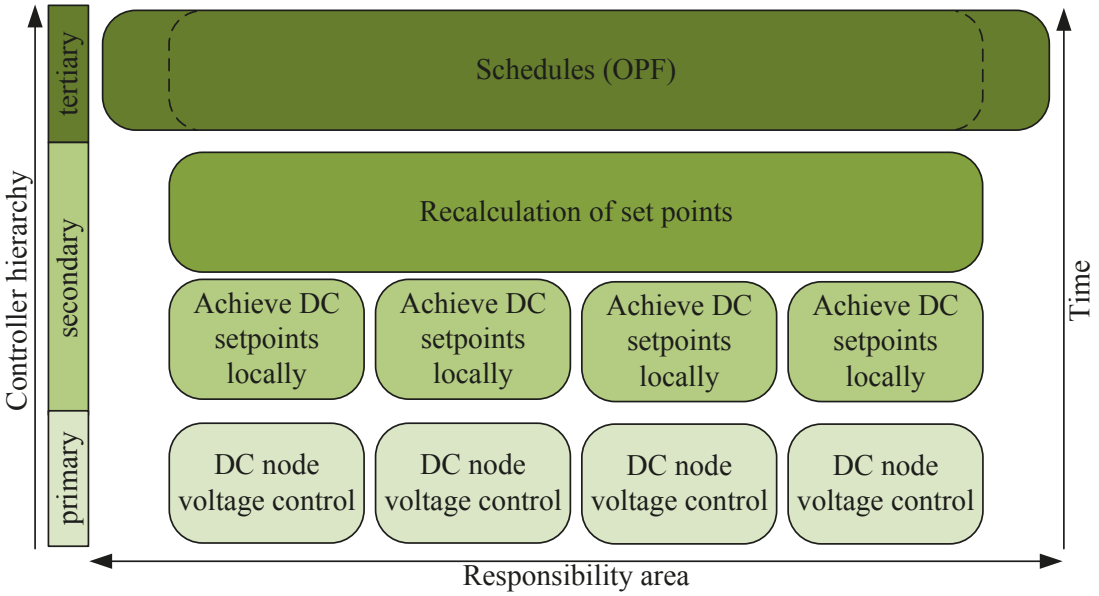

Fig. 2.1: Sate of the art - HVDC grid control hierarchy and instances.

Converters can have different kind of DC control modes, which is not limited to DC node voltage control. Converters' control mode can also be defined to constant power control, for example. Thus, the lowest level of control instances is redefined to *local converter DC control mode* as shown in Fig. 2.2.

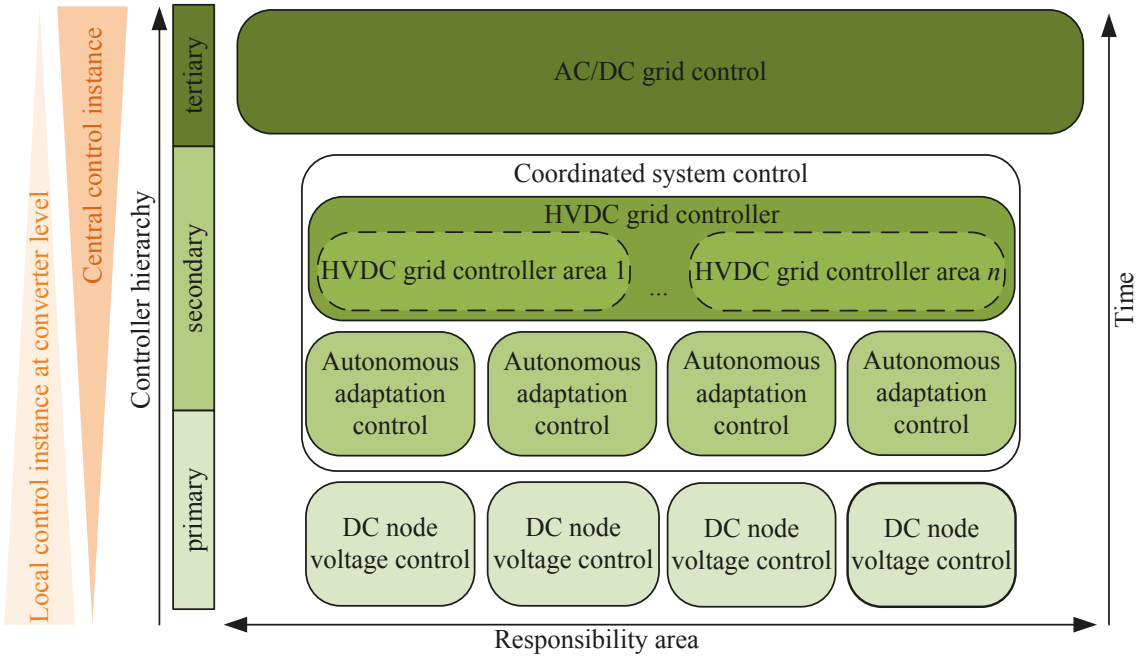

Fig. 2.2: HVDC grid control hierarchy and instances.

Secondary control is not limited to reestablish pre-disturbance conditions / power exchanges or determining primary control parameters. For overall system security reasons even a fundamental redefinition of reference values is possible after a major disturbance.

Therefore, an optimization can be made in advance for a number of possible disturbances calculating the optimal converter set points. Those will be stored locally at each converter. When any of these considered disturbances takes place in reality, converter set points are already given and need only to be activated locally. This is the secondary control instance of *autonomous adaptation control* in Fig. 2.2.

This control instance can only be effective for those scenarios that have been considered previously. Any other disturbances or set of disturbances will be covered by redefining a set point by the *HVDC grid controller*. Depending on the size of the HVDC system there will be a single, or for larger HVDC grid, a few of HVDC grid controllers responsible for a defined area of the HVDC grid as indicated in Fig. 2.2. An HVDC grid controller has a global view on its responsibility area and can perform optimization processes if major disturbances took place. In order to realize short computation times, a division of large HVDC grids in several responsibility areas is necessary. The global view of an HVDC grid controller is given by the corresponding part of the DC grid and major information from directly connected AC parts. HVDC grid controller and autonomous adaptation control are *coordinated system control* instances as it is also defined by CENELEC [O-17] and Cigré WG B4.58 [O-17], [48].

As the HVDC grid controller provides set point adaptations on a short term (in-between schedules) and, depending on the size of the HVDC grid, only optimized for a limited area, the overall AC/DC optimization will be performed by the *AC/DC grid controller* [O-17], [48]. This tertiary control instance ideally performs a mixed AC/DC OPF with a global view. As such, it is possible that the central control instance is not in place and probably even not necessary from the beginning building an extended meshed HVDC grid. Chapter 3 addressesalso a dispersed coordination case in subchapter 3.3.

2.3.3 HVDC grid system responsibility and integration into AC system operation

With regards to a meshed onshore HVDC system overlaying the existing AC system there will be a much smaller number of nodes (or converters) than the AC transmission system. Thus, it is realistic to assume that each European TSO will have one to ten converters within its responsibility area. This leads to a total number of approximately fifty to 200 converters distributed throughout Europe. This is also in line with the current structure of today's AC grid. The lower the grid layer voltage level, the more nodes per unit area the system will have (see Fig. 2.3). As the HVDC overlay grid would represent the highest voltage level in the grid it will have the lowest number of converters per unit area.

When a future European HVDC overlay grid spans a number of TSO responsibility areas it is no longer reasonable to leave responsibility for converters to the AC TSOs. The possible influence of having only one converter owned by a single TSO, for example, is too small. It is far more reasonable to define a new grid responsibility layer for the HVDC overlay grid namely the HVDC TSO. An HVDC TSO can make use of the full power of

the HVDC grid due to its wider system view while also monitoring the AC transmission layer for HVDC operation purposes.

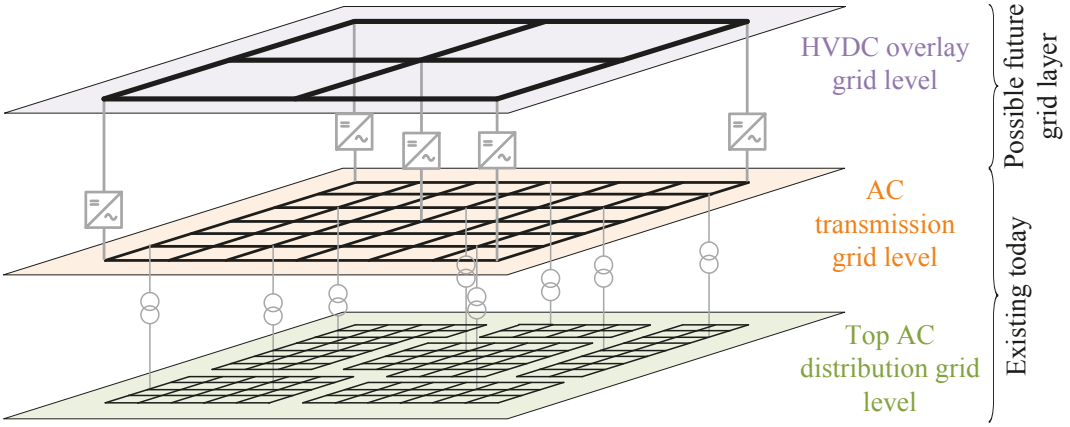

Fig. 2.3: Abstract representation of different voltage level grid layers.

The need for more global system monitoring capabilities has already been identified by some European TSO's for the AC transmission layer. Consequently, they joined together in global monitoring initiatives / organizations. The most important of these are the Transmission System Operator Security Cooperation (TSC) currently located in Munich (Germany) and the **CO**o**R**dination of **E**lectricity **S**ystem **O**perators (CORESO) currently located in Brussels (Belgium). Taking the covered area into account, the Electricity Coordinating Center (EKC) located in Belgrade (Serbia) is also an important organization; however, EKC was quite inactive during the last years regarding official coordination actions. All are monitoring a wide area of the AC transmission system across the borders of a single TSO. Hence, they can detect system security endangering system states caused by events or forecasts in responsibility areas of other TSOs. Today this is even more important than in the past since cross border trading, wind generation and general electricity transmission are significantly and continuously increasing which necessitates a more global system view. As these organizations are already dealing with a wide system view they are predestinated to provide development towards an HVDC TSO.

As the need for coordination among TSO is increasing among others due to increasing cross-border energy trade, significantly increased renewable energy infeed, installation of power flow controlling devices and transit power flows (in neighboring TSO areas) also caused by increasing transmission distances ENTSO-E identified the increased level of interdependency among TSOs leading to a fundamental need for coordination among TSOs. Thus ENTSO-E mentions Regional Security Cooperation Initiatives (RSCI) in its actual network code on operational security as an exemplary manner for exchanging experiences and information, using a common grid model and alarming system among TSOs [54], [55].

TSO Security Cooperation (TSC)

TSC has been monitoring the AC transmission systems of member TSO as well as some of their neighboring TSOs since July 2009. Up until 2014, TSC has been joining forces of 12

TSOs namely: APG (Australia), HOPS (Croatia), CEPS (Czech Republic), Energinet.dk (Denmark), 50 Hertz Transmission (Germany), Amprion (Germany), Tennet TSO (Germany), Transnet BW (Germany), MAVIR (Hungary), PSE (Poland), ELES (Slovenia), Swissgrid (Switzerland) and Tennet TSO (the Netherlands) [56]. Thus TSC can cover a wide continuous area of the synchronous continental European AC transmission grid as it is shown in Fig. 2.4 a).

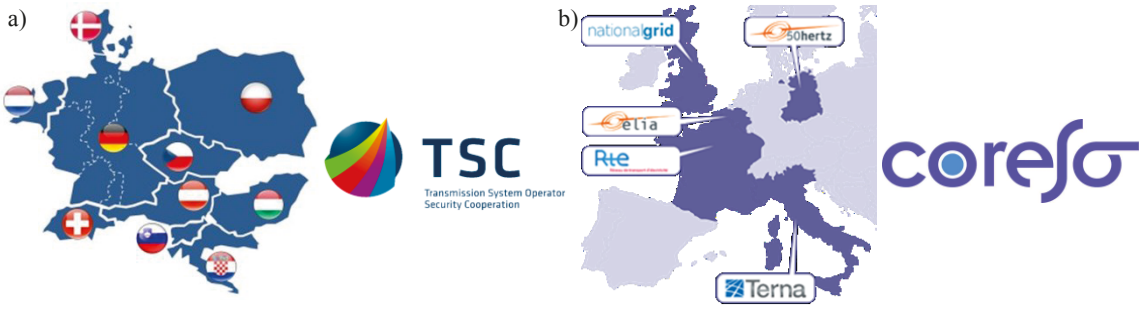

Fig. 2.4: a) Countries of TSC's member TSOs [56] and b) Countries of CORESO's Shareholder TSOs [57].

TSC intends to maintain and improve security of European electricity supply through intensive collaborations among European TSOs. Therefore TSC continuously develops coordinated procedures as well as remedial actions. For this purpose TSC collects operational forecast data of all members and some neighbouring TSOs and merges all of them in a data base. This enables TSC to make N-1 calculations to identify system security status. Those results are accessible by all of TSC's members. TSO experts analyze these results, decide on counter measures and implement them in their control centers. TSC is still undergoing further developments which are among other categorized in three phases: 1st phase – day ahead planning, 2nd – Intraday planning and 3rd – near to real time monitoring. [56]

In order to pool expertise of members, share information and expertise and fulfil its goals TSC founded its jointed office in Munich in October 2013 where TSC's permanent TSO security panel as a group of experts from its members is located, as well as the shared IT platform for data exchange and N-1 security assessment, including advanced methods for choosing appropriate remedial actions. [56]

Coordination of Electricity System Operators (CORESO)

CORESO has been providing its service for its shareholder TSOs, which are shown in Fig. 2.4 b), since February 2009. CORESO's portfolio includes two day ahead, day ahead, intraday and close to real time services. For its two day ahead service CORESO merges the best two-day ahead congestion forecast (D2CF) files from Elia, RTE, TenneT (Netherlands), Amprion and Transnet BW and day ahead congestion forecast (DACF) files of other TSO. Results are provided to member TSOs which is used to identify cross border capacities. This information is also used for the market coupling process. Since 2012 CORESO also operates a flow based prototype. Hence, CORESO enables TSO in the central west

Europe (CWE) area coordinating remedial actions e.g. by means of phase shifting transformers. In the future this will also include other remedial actions. The same procedure for cross border capacities is proceeded for the central south European (CSE) area while the two best D2CF of RTE, Terna, Swissgrid, Eles and APG are merged by CORESO. Additionally, the import capacity for Italy's northern border is optimized by CORESO. Prospectively, CORESO will provide security analyses, including an automatic tool for calculating the best set of remedial actions, among others which including phase shifting transformers and redispatch. [57]

For its day ahead services, CORESO merges day ahead congestion forecasts (DACF) from all continental European TSOs and computes N-1 calculations, including line and generator trips, for 24 time steps a day for the CWE and central east European (CEE) area as well as two time steps (peak and off-peak load) for the CSE area. Therefore, security risks in continental Europe can be identified one day ahead. Finally, identified congestions are analyzed and remedial actions are specified by CORESO. Afterwards they are discussed, agreed and tracked with affected TSO while TSO have the final responsibility. [57]

Within CORESO's intraday and close to real time business, measured system data is gathered, analyzed and compared to CORESO's forecasts before it is shared with participating TSOs. If necessary, day ahead forecasts are updated according to this new information and post fault analyses are carried out. [57]

Thus, CORESO's main business also focuses on day ahead and intraday security analyses including grid monitoring and coordination management of remedial actions as is also performed by TSC for its TSOs. [57]

Electricity Coordinating Center (EKC)

Since 2007 EKC coordinated the south east European (SEE) area. At the same time EKC also provides consulting and research services. Its special initiative for coordination within SEE is named Southeast European Cooperative Initiative Transmission System Planning Project (SECI TSP). Within this project, EKC collects input data from Romania, Hungary, Slovenia, Croatia, Bosnia and Herzegovina, Serbia, Montenegro, Albania, Greece, Bulgaria and Turkey for continuously updating the regional transmission system model. This model is used to perform power system analyses and coordination among TSO of SEE while experts from participating TSO are also involved. [58]

As previously shown, TSC and CORESO in particular, already have basic observation methods for coordinating several TSOs and equipment with wide area impact. As such they are predestinated to become a European ISO.

2.4 Reference Grid

It is suggested in subchapter 1.2.2 that there is a planning process ongoing in Germany to built four P2P HVDC transmission lines in order to transmit bulk power from offshore wind

to the load centers in the south and in the West of Germany. As those four P2P connections will be the first long distance onshore transmission lines in Europe and as they are comparably close together, they could be a nucleus for a European overlay HVDC transmission grid. Hence, Germany is exemplarily taken to set up the reference grid used for numerical case studies of this work.

Thus, the DC reference grid is inspired by the local conditions in Germany regarding load centers, expected areas with lack as well as with surplus of generation due to renewable energy infeed and it covers the connection to neighboring AC transmission grid s (see Fig. 2.5). In total the DC grid consists of 10 converters and is interconnected with 15 DC lines.

An AC system is underlayed with a higher degree of meshing. The AC part includes 6 AC nodes in Germany and another 7 to represent the first mesh of some neighboring states. It is not the intention to copy the existing ENTSO-E AC transmission grid for the considered area but to create a simplified topology that can be used to emulate Germany's typical power flows from North / North-East to Sooth/West. All AC nodes are connected to a power plant in order to be as flexible as possible regarding the creation of different power flows. Challenges related to reactive power are not considered in this work. Thus, it is permissible to connect a power plant to all AC nodes. All 6 AC nodes representing Germany and 4 nodes representing adjacent parts of the AC transmission grid are connected to the overlayed HVDC grid (see Fig. 2.5). All 13 AC nodes are interconnected with 26 AC lines.

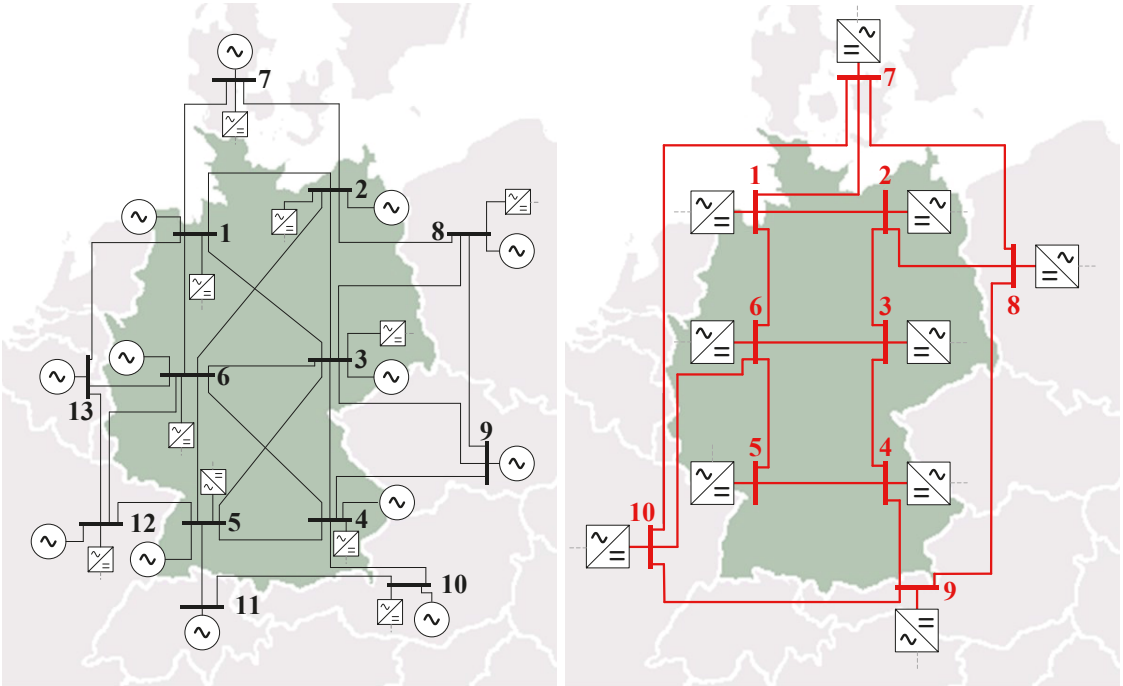

Fig. 2.5: Reference grid including the AC (left) and DC part (right) – basis for numerical case studies in this work.

For numerical case studies in chapter 3 and 5 the described reference grid is modified in accordance with related requirements for the reference grid. The reference grid remains unchanged in chapter 4 as it already meets the requirements there.

3 HVDC overlay grid operational planning – Tertiary control

Operational planning is the widest time horizon covered in this work which is a part of AC/DC grid control as explained in subchapter 2.3.2 and illustrated in Fig. 3.1. It represents the determination and definition of converter reference operating points in terms of days or hours ahead operational planning. An optimal operating point is focused based on the intended AC and DC grid topology at the considered point in time as well as results from electricity market and load forecasts. Both are considered as given inputs.

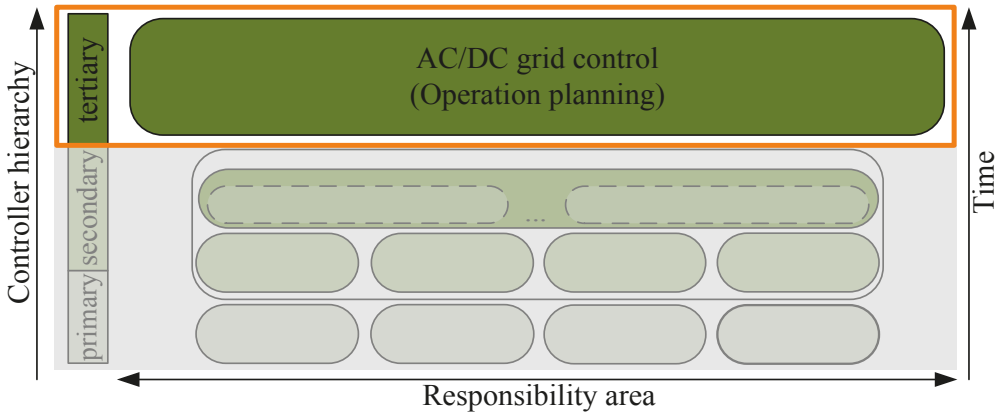

Fig. 3.1: Operation instance focussed in chapter 3.

Thus, main results from HVDC grid operational planning are converter schedules for defined time intervals of 15 minutes, for example, as it is shown in Fig. 3.2. These schedules include converter power and its DC node voltage reference value. Depending on DC node voltage control strategy (see chapter 5) a control characteristic can also be provided with each schedule. This can be defined in two different ways: First, by providing a certain control mode as is described for state of the art DC node voltage control strategies (as in Fig. 5.5) with related parameters whereas the second way is only based on provision of control parameters for a flexible control characteristic while its shape and inherent control mode representation is solely dependent on its parameterization (as proposed in subchapters 5.4 and 5.5). However, an operational planning control layer will provide each converter with:

- Active power reference
- DC node voltage reference
- DC node voltage control characteristic (see chapter 5)
- AC node voltage reference or reactive power reference

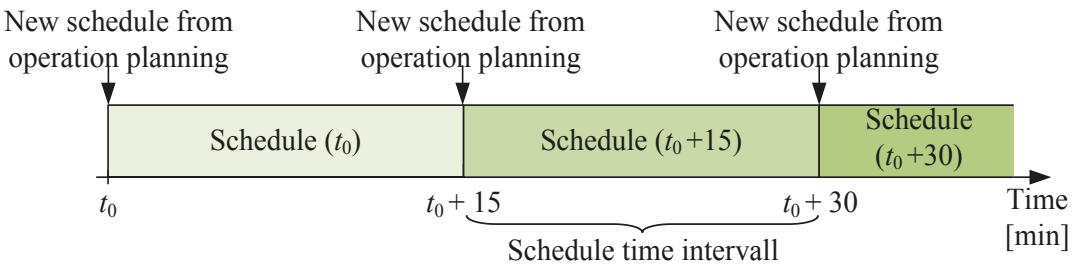

Fig. 3.2: Scheduling of converter reference values.

A global requirement for an entire HVDC grid must be met which is the equilibrium between infeed into the HVDC grid and output into the AC system, that is, the HVDC system itself has almost no storage capability. As is described in chapter 5 an energy balance must be maintained. As this chapter is concerned with operational planning, there are no energy reference values provided for each converter although there are power reference values which are provided for a schedule period. Therefore, hereinafter in this chapter power balance requirements will be used. According to (3.1) converter $p_{\text{loss\_conv}}$ and DC line losses $p_{\text{loss\_DC\_line}}$ off all i converters and all m lines of a DC system must also be taken into account. Although small deviations from this balance or DC equipment trips are covered by additional control units, as described in chapter 5, significant deviations that are also found during normal operation will have a negative effect on AC system operation. Converter power reference values can deviate significantly from physical ones if a balance is not ensured during operational planning. It may result in equipment overloading and AC as well as DC system instabilities. The necessity for the described balance had previously been identified when multiterminal or meshed HVDC grids were technologically not able to become realized and even not necessary [59]. Even if (3.1) is merely a constraint, it is the most important consideration during HVDC grid operational planning.

$$\frac{de_{\text{DC}}}{dt} = \sum_{i=1}^{n_{Conv}} p_{\text{conv},i} + \sum_{i=1}^{n_{Conv}} p_{\text{loss\_conv},i} + \sum_{m=1}^{n_{DC\_line}} p_{\text{loss\_DC\_line},m} = 0 \tag{3.1}$$

While only considering an HVDC converter as a local controllable generating or load unit and neglecting (3.1) during operational planning, DC balancing control (known as DC node voltage control) will balance the system during operation and converter power may differ a lot from its schedule. Consequently AC system states may also differ significantly. As described scheduled reference values can differ from physical ones due to DC balancing control (DC node voltage control in chapter 5) but can also be adapted to changed AC power flow patterns (significantly deviating from schedule) as described in chapter 4.

Operational planning should cover a global DC energy balance when providing converter reference values as far as possible[3]. This fact is endorsed in subchapter 5.2.5. If the overall AC/DC grid would remain undisturbed provided reference values will also be physical, even if this is a more idealistic than realistic scenario. Besides DC energy balance as a constraint for reference value determination active power, DC node voltage and AC node voltage (or reactive power) reference values can be subject to an optimization process in order to fulfill certain objective functions. Determination of these values regarding an optimization is a subject of this chapter.

This optimization is the main focus of this chapter. Thus subject of subchapter 3.1 is OPF as a method for calculating an optimal system state according to an objective function. In

[3] Losses can vary according to climatic conditions, equipment aging and related parameter variations. Normally that influences energy balance only marginally compared to uncoordinated converter reference values.

subchapter 3.1.1 a state of the art review is made according to optimization methods in general and their application for power system OPF. For the most common optimization algorithms for optimal power flow problems, significant disadvantages are identified that are even more important when it comes to application of FACTS and HVDC equipment. These are a high risk for non-convergence or convergence in local minima and their vulnerability to initial condition definition. Thus subchapter 3.1.4 identifies an artificial intelligence optimization method namely differential evolution (DE) to be the most suitable method for mixed AC/DC OPF problems. Furthermore, there are three different methods of HVDC converter coordination as mentioned in subchapters 3.2, 3.3 and 3.4. These are a centralized coordination and optimization carried out by an independent system operator as a future vision, a decentralized coordination that is only applicable for small grids. For example, when a meshed HVDC grid is in an early stage and inherent coordination of HVDC transmission capacities are an issue for the future energy market, this is also addressed shortly as a non technical option. For a centralized optimization a numerical case study is carried out that identifies significant improvement potential for that method.

3.1 Optimal Power Flow

Today a technically optimal operation of power systems is determined using an OPF. This was first proposed for an overall power system in 1949 [60]. At this time it was intended to combine mathematical descriptions for transmission losses and incremental fuel losses for power plants in such a way that minimal operation losses / costs occur. Algorithms and problem formulation have been quite basic since computer engineering was in its infancy while certain publications of this time argued that cost savings justify the use of a computer. The first OPF solution as it is known today was proposed in 1968 [61]. Today's OPF challenges are not related to computer engineering or related costs but to integration of new power electronic equipment as HVDC converter or FACTS as power flow controlling or impacting devices. Especially in Europe another limiting constraint is given by unbundling of generation and transmission of electric energy [62]. This prohibits the original idea of OPF of adjusting the generation pattern in order to achieve overall minimal generation costs. Operation of power systems in general became more difficult than in the past due to by higher transmission capacity utilization, longer transmission distances and almost non-deterministic volatile energy generation by renewable energies among other things. Consequently, today`s primary concern when using an OPF is to find a stable operating point for the system, fulfilling some constraints and minimizing one or more objective functions (OFs). While OFs changed from optimal power plant active power schedules towards multiple options or combinations of them such as:

- Minimal transmission losses
- Maximum stability margins concerning different stability indices
- Maintaining N-1 or N-x criterion

The last two points are referred to as security constrained OPF that are not addressed here. Since adjustment of active power generation should be avoided (if possible) due to unbundling, possible adjustments are: change of system topology (switching measures), change of reactive power schedules (power plants as well as FACTS and other compensating devices), influencing power flow controlling devices as phase shifting transformers, unified power flow controllers or other equipment and determining reference operation points for HVDC converters. The influence of storage schedules is not possible in all countries today since they are covered by the unbundling due to their definition as power plants or loads respectively.

An optimization problem is mostly defined to be a minimization problem as maximization problems can be formulated as minimization problems. Thus, the general optimization problem formulation is made according to (3.2) while F is the OF that may be a set of several OFs, u are input and x state variables of the system. Optimization problems using multiple OFs are known as multi objective optimization problems. The OF for such problems can be handled using a weighted sum method, as defined in (3.3), while each single OF $F_j(u,x)$ is weighted with a weighting factor a_i [63]. Therefore, an overall optimum is found instead of a single solution for each single OF $F_j(u,x)$ and a tradeoff between all OFs is made according to their weightings.

$$\min\left(F(u,x)\right) \tag{3.2}$$

$$F(u,x)=\sum_{j=1}^{n_{\mathrm{OF}}} a_j F_j(u,x) \tag{3.3}$$

Since there are more possible mathematical solutions than realistic ones (fulfilling system limits), constraints must be fulfilled simultaneously. Consequently, constraints are used to separate admissible from inadmissible state space areas. Constraints can be subdivided into k equality $h_k(u,x)$ and l inequality constraints $g_l(u,x)$ according to (3.4) and (3.5).

$$h_i(u,x)=0 \qquad \forall\ i=1...k \tag{3.4}$$

$$g_i(u,x)<0 \qquad \forall\ i=1...l \tag{3.5}$$

3.1.1 Requirements for an AC/DC optimal power flow optimization algorithm

An optimization method for mixed AC/DC systems should be capable of an extended permitted state space. In addition to an AC grid OPF or DC grid OPF, the total active power operation band $p_{\mathrm{VSC,AC,min}}$ to $p_{\mathrm{VSC,AC,max}}$ of all converters must be considered for a mixed AC/DC OPF. The more converters are included in the considered AC/DC grid, the more complex and multi dimensional the permitted state space will be. The state space for the AC as well as for the isolated DC grid can be limited quite successfully by the elaborative

selection of voltage amplitudes and voltage angles (for AC nodes). However, converters introduce many nonlinear relations and significantly increase system complexity.

Consequently, an optimization method for mixed AC/DC systems should be capable of extended permitted state spaces and a nonlinear optimization problem. Additionally the optimization result should not depend on initial conditions and a stable convergence should be ensured within an acceptable time range. OPF's objective target in this regard is to determine converter set points at least once within each schedule cycle (e.g. every 15 minutes). Thus, the computation effort of a suitable optimization method should enable periodical online calculations for large AC/DC systems. For this purpose, methods that meet this requirement can also be taken into account if they are using parallelization options that makes the computation time short enough. Additionally non-linear constraints, as well as a number of objective functions (multi objective functions), must be includable. Multi objective functionality is necessary in order to include different objectives such as loss minimization, system security issues, stability indices or stability margins. In summary, mixed AC/DC OPF optimization method requirements are:

- Active and reactive power consideration
- Stable convergence in global optimum
- Multi objective functions implementable
- No initial value problem
- Nonlinear constraints implementable
- Extended permissible state space
- Short computation time e.g. by parallelization of computation sequences

3.1.2 State of the art – optimization algorithms

This subchapter describes different strategies for solving optimization problems as described above. This includes the following according to [64]-[66]:

- Conventional methods
  - Linear programming method
  - Non-linear programming method
  - Interior point method
- Artificial Intelligence methods
  - Generic algorithm method
  - Differential Evolution
  - Particle Swarm Optimization

Linear programming method

One of the oldest optimization methods is linear programming (LP), originally proposed in 1968 [67]. This method linearizes the problem including its constraints and its OF around an operating point. Thus, all power flow calculations within an OPF are DC power flow calculations with the same disadvantages, for example, when there are no reactive and consequently no voltage and loss considerations. But this method can also be used for a first approach towards an economic dispatch when concerning security aspects, for example, line loading when no reactive power is considered. In [68] this method is also used for an

AC system with an integrated HVDC system without any considerations of reactive power and AC voltage control.

Non-linear programming method

LPs disadvantage in terms of reactive power consideration is overcome by a non-linear programming (NLP) method according to [61]. This method does not linearize the OF and constraints and solutions are calculated using algebraic methods such as the Newton and Lagrange multiplier method. Lagrange multiplier method is primarily based on penalty functions for violation of constraints' limits. The quadratic programming (QP) method is a special NLP method [69]. This method is only applicable for quadratic OF as in (3.6). Such formulation can be used for simple representations of generation costs and thus for energy generation dispatch problems for unbundled energy markets. QP uses linear or linearized constraints in the same way LP does.

$$F(u,x) = b + c \cdot u + d \cdot u^2 \tag{3.6}$$

A problem of linear and non-linear optimization methods is their convergence behavior. Only a single solution is calculated within each step of iteration, and this results in a slow convergence. Thus, they are not applicable for large systems. Additionally, they carry a high risk of finding local rather than global optima. This is further discussed in subchapter 3.1.3. Their major advantage is that they are suitable for describing complex economic energy problems. Thus, depending on the application a joint combination of these methods is possible. [64]

Interior point method

The next level of improvement was reached with interior point (IP) method which was theoretically invented in 1954 [70] and firstly applied to extended power systems in 1986 [71]. The search space for finding an optimal system state is limited to the non-linear permitted state space which is defined by its constraints. Consequently, its computation time is much smaller than that compared to the other conventional methods. Thus, IP is widely used and can be seen as a standard for OPF solutions with special focus on energy generation dispatch and market simulations. But the disadvantages of conventional methods mentioned above are still present using IP as dynamic aspects cannot be addressed and there still remains a risk of convergence in a local optimum (depending on the defined initial condition) and even a risk of non-convergence. [66]

Artificial intelligence methods

The generic term artificial intelligence (AI) method refers to a number of optimization algorithms. Three categories are: generic algorithm (GA) method, differential evolution (DE) and particle swarm optimization (PSO). Each method is based on heuristic optimization. Thus, the risk for a convergence in a local rather than global optimum as well as the risk

for non-convergence, are minimized. Additionally, formulation of transient stability aspects is possible using AF methods. [64] All three mentioned AI methods are capable of different kinds and numbers of OF‘s and constraints. Among others, this makes it possible to take power electronic based equipment, such as FACTS and HVDC devices into account. Additionally, there is theoretically no limitation in terms of network dimensions. [65]

Generic algorithm method

The first steps towards generic algorithm were made in 1970. As the name suggests this method is based on the evolution maxim “survival of the fittest” which implies that different solutions are generated within the permitted state space defined by constraints. Each different solution is compared and further developed or rejected. Today, GA is primarily used for design, allocation and operational planning for FACTS devices [72]. This is so since continuous as well as discrete parameters, such as tap changes, can be addressed. [73]

Differential Evolution

Invented in 1995 by [74], DE is a further development of GA and also based on evolutionary behavior. The main advantage of this algorithm is the high probability of finding the global optimum even when this concerns complex nonlinear problems. Additionally, DE is capable of representing non linear and differential equation based problems, which enables the algorithm to consider stability and security aspects in power systems such as FACTS devices. DE is mainly utilized for cost optimization problems within the energy market sector and day-ahead planning issues [75]. [76], [77]

Particle swarm optimization

As the name suggests this method imitates swarm behavior, a characteristic of bees or other animals flying or swimming in large numbers. This method was also invented in 1995 as an alternative to DE. It was first described in [78]. Parameterization is described as user-friendly. Today’s application is mainly focused on OF regarding security aspects, but it is also applicable for economic optimization problems. [79]

3.1.3 Convergence in local minima using conventional optimization methods

For conventional optimization methods, the problem of non-convergence or convergence in local minima is already mentioned above. Both problems can be caused by very extended state spaces as well as initial suboptimal conditions.

According to [80] the conventional formulation of Kirchhoff’s voltage law in polar coordinates for power flow description includes AC node voltages as well as voltage angle. This causes non-convex characteristics of the problem formulation. A non-convex system description bears the risk of more than one minimum within the permitted state space, namely one global and several local minima [81]. One physical description for the occurrence of local minima, this means more than one solution within the permitted state space is made in [81]. There a simple example is made with a two node test system (see Fig. 3.3 a). It is

well understood that this problem has two feasible power flow solutions if the line is not fully loaded (here at a load of p = 1.004 p.u.) one with a higher voltage at the PQ node and one with a lower voltage. Normally the latter case is avoided using appropriate constraints, but in certain scenarios there are instances, as shown in Fig. 3.3 b), where a low voltage solution also meets the voltage constraints given by the green horizontal lines. [81] identified the occurrence of local minima if loop flows, high voltage angle differences or an excess of reactive power occurred. It was also found, that a flat start deceases the risk of a convergence in a local minimum.

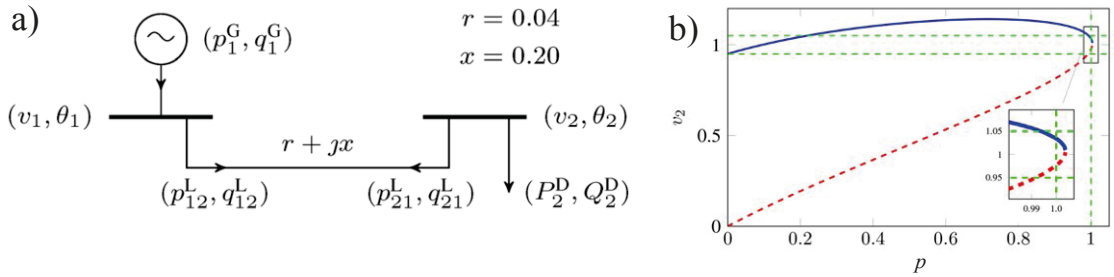

Fig. 3.3: Example for physical explanation of multi solutions within permitted state space a) test system, b) different load flow solution depending on variation of demand parameter p. [81]

The convergence into one of the local minima is higher when conventional methods are used [64], [65]. Additionally conventional methods bear a higher risk for non-convergence. Both are strongly influenced by the definition of initial values within a large state space. AI methods are much less susceptible to convergence in local minima, guarantee convergence and problems due to initial values are avoided.

3.1.4 Selection of the most suitable method for mixed AC/DC OPF problems

As mentioned in the previous subchapter, problems regarding convergence in local minima or even non-convergence are major. This is mostly caused by inappropriate initial values within a larger permissible state space. This primarily occurs when conventional optimization methods are used, as is summarized in Tab. 3-1.

However, this can be handled considering only an AC system. The permissible state space can be limited quite well by an elaborative selection of voltage amplitudes and voltage angles. Nevertheless, power generation and load patterns are given when considering an unbundled energy market. The situation differs significantly considering the additional DC grid which overlays the AC grid as is seen in this work. For the additional DC grid layer, DC node voltages and converter active power values are new variables to be considered during the optimization process. Thereby many of additional nonlinear correlations increase problem complexity. In particular the complete permissible operating range of converters' active power $p_{conv,AC}$, i.e. $p_{conv,AC,min}$ to $p_{conv,AC,max}$, must be considered for each

converter. The more converters are included in considerations the more complex and multi dimensional the permissible state space will be.

In accordance with requirements for a mixed AC/DC OPF only AI methods come into question. Particularly their stable convergence behavior and immunity to any initial values make those methods stand out. HVDC and FACTS have similar requirements when they are integrated in an OPF algorithm. AI methods have already been proven to be of value for OPF applications including FACTS, such as in [72] and [77]. Additionally evolutionary methods offer parallelization opportunities for fast computation times and a weighting of OFs is possible for such optimization methods in order to include more than one.

Tab. 3-1: Fulfilment of general requirements for an optimization method for OPF problems considering several optimization methods.

	LP	**NLP**	**IP**	**GA**	**DE**	**PSO**
Active and reactive power consideration	×	✓	✓	✓	✓	✓
Stable convergence in global optimum	×	×	×	(✓)	(✓)	(✓)
No initial value problem	×	×	×	✓✓	✓✓	✓✓
Short computation time e.g. by parallelization of computation sequences	✓✓✓	✓✓	✓	✓✓	✓✓	✓✓
Multi objective functions implementable	(✓)	✓	✓	✓	✓	✓
Nonlinear constraints implementable	×	×	✓	(✓)	(✓)	(✓)
Extended permissible state space	×	×	×	✓	✓	✓

Constraint handling is a more disadvantageous property of AI methods with regard to linear programming. AI methods were originally invented for unbounded optimization problems. Thus, for constraint problems such as OPFs, special constraint handling methods must be applied. A weighting integration into OF is also possible as a redefinition of variables if its limits are violated. This is also summarized in Appendix B. However, the advantages of AI methods with regard to linear programming methods outweigh this disadvantage which can be overcome with further research.

In subchapter 3.1.1 three AI methods are presented: GA, DE and PSO. [82] makes a comparison using 23 different OFs. DE was found to be the best performing algorithm in this study due to its robustness, fast convergence, converging in the global optimum in almost

every run and its simplicity since the algorithm is based only on a few parameters which are not as problem specific as the other methods. Additionally DE outperforms the other two methods with its immunity to any initial values [82]. Even if PSO is for the most part, the fastest method, it lacks in highly problem specific parameterization and some simulation runs are necessary for satisfactory results. There are also publications which apply GA, DE and PSO to OPF problems which confirm those results for the special power system OPF problems [63], [90], [91].

All AI methods must be parameterized. The number of essential parameters differs for each AI method. DE requires three, PSO five and GA six parameters for definition, while parameterization is problem specific. Thus, DE has a further advantage with regard to the other AI methods, with the lowest number of parameters to be defined for the mixed AC/DC OPF.

The advantages and disadvantages of GA, DE and PSO are summarized in Tab. 3-2. DE is found to be the most appropriate optimization method for converter reference value determination concerning mixed AC/DC system.

Tab. 3-2: Comparison of AI methods – GA, DE and PSO.

	GA	**DE**	**PSO**
Time until convergence	-	-	✓
Robustness	✓	✓✓	✓
Convergence in global optimum	✓	✓✓	✓
Parameterization effort	×	✓	-
Number of simulation runs for satisfying results	✓	✓	×

When computing an OPF a clear definition of system limits must be made. For a transmission system OPF distribution systems are mostly out of scope or only the highest distribution system layer is modeled. There are a number of TSOs in Europe with their own responsibility area. All of which make analysis for their responsibility area mostly including a wider observability area. However, so far there is no independent system operator (ISO) covering the whole European power system although organizations are in place with potential to take this role in the future (CORESO and TSO security cooperation - TSC) as discussed in subchapter 2.3.3.

Thus, subchapter 3.2 deals with a central optimization as a future initiative of a European ISO. This covers the preliminary intension for a mixed AC/DC OPF. Thus according subchapters 3.2.1 and 3.2.2 describe the objective function and the DE algorithm respectively. Subchapter 3.3 focuses on a decentralized coordination among TSOs having part in a common HVDC grid respectively. For remaining degrees of freedom DE can also be used for

optimization for the case described in subchapter 3.3 but with a much higher effort regarding coordination among TSOs.

3.2 Coordination with centralized master controller

Assuming the existence of a control instance monitoring a whole HVDC grid as well as the underlayed AC transmission level, by using a mixed AC/DC OPF a holistic consideration and therefore an optimization of the overall system is possible [O-11]. This is exemplarily shown in this subchapter for minimization of overall system losses from the perspective of an ISO.

3.2.1 Objective function and constraint definition

As it is necessary when considering an unbundled energy sector active power generation p_{gen} provided by conventional power plants as well as renewable energy and vertical system loads characterized by p_{load} and q_{load} are unchangeable input parameters. Degrees of freedom are:

- AC node voltages v_{AC}
- DC node voltages v_{DC}
- reactive power generation q_{gen} for the AC grid (by converters and power plants)
- active power schedules for converter stations seen from the AC side $p_{\mathrm{conv,AC}}$

Consequently, the optimization vector u' results to (3.7) [86] - [89].

$$u' = \begin{bmatrix} |v_{\mathrm{AC}}| & \delta_{v_{\mathrm{AC}}} & p_{\mathrm{conv,AC}} & q_{\mathrm{gen}} & v_{\mathrm{DC}} \end{bmatrix} \tag{3.7}$$

This optimization vector contains redundant information, since $p_{\mathrm{conv,AC}}$ and q_{gen} can be calculated using the reduced optimization vector u according to (3.8). Within each iteration step, attention must be made to ensure power limits of power plants and converters are respected.

$$u = \begin{bmatrix} |v_{\mathrm{AC}}| & \delta_{v_{\mathrm{AC}}} & v_{\mathrm{DC}} \end{bmatrix} \tag{3.8}$$

Here a simplified converter model is used which represents its losses $p_{\mathrm{conv,loss}}$ and the power balance between the AC $p_{\mathrm{conv,AC}}$ and DC side $p_{\mathrm{conv,DC}}$ as in (3.9). VSC in MMC technology have significant advantages with regard to pulse with modulation (PWM) based technology. The most important are smoother DC current as well as lower losses, first and formost, of approximately 1% which is almost comparable to LLC losses of approximately 0.75% [93]. A simplified loss definition is assumed in (3.10). It includes a voltage dependent part while voltage is assumed to be constant, thus, this part α is constant, a converter current i_{conv} dependent part β and part γ depending quadratically on the converter current i_{conv}. The constant voltage dependent losses become active as soon as the converter starts operating.

The coefficients are estimated according to Appendix A to $\alpha = 0.5234\%$, $\beta = 0.2097\%$ and $\gamma = 0.3146\%$.

$$0 = p_{\text{conv,AC}} + p_{\text{conv,DC}} + p_{\text{conv,loss}} \tag{3.9}$$

$$p_{\text{conv,loss}} = \left[\alpha + \beta \cdot \frac{i_{\text{conv}}}{i_{\text{conv,nominal}}} + \gamma \cdot \left(\frac{i_{\text{conv}}}{i_{\text{conv,nominal}}} \right)^2 \right] \cdot p_{\text{conv,nominal}} \tag{3.10}$$

$$i_{\text{conv}} = \frac{\sqrt{p_{\text{conv,AC}}^2 + q_{\text{conv,AC}}^2}}{\sqrt{3} v_{\text{conv,AC}}} \tag{3.11}$$

Since the minimization of overall system losses is intended, the objective function is defined accordingly in (3.12) including AC transmission losses $p_{\text{AC,loss}}$, DC transmission losses $p_{\text{DC,loss}}$ and converter losses $p_{\text{conv,loss}}$ which include all losses related to the converter and its AC and DC switch yard. Equation constraints g are listed in (3.13) - (3.17). An OPF considers a steady state, thus active and reactive power balances are given at AC nodes and active power balance at DC nodes respectively. Formulation (3.15) implies that no DC generation or load is directly connected to the DC grid except via a converter. However, implementation is still possible. (3.16) and (3.17) define the slack node.

$$F = \sum p_{\text{AC,loss}} + \sum p_{\text{DC,loss}} + \sum p_{\text{conv,loss}} \tag{3.12}$$

$$g_{1,p} = 0 = p_{\text{gen},p} + p_{\text{conv,AC},p} - p_{\text{load},p} - \sum_i p_{\text{lines},pi} \tag{3.13}$$

$$g_{2p} = 0 = q_{\text{gen},p} - q_{\text{load},p} - \sum_i q_{\text{lines},pi} \tag{3.14}$$

$$g_{3q} = 0 = p_{\text{conv,DC},q} - \sum_n p_{\text{lines},qn} \tag{3.15}$$

$$\left| v_{\text{Slack,AC}} \right| = 1 \tag{3.16}$$

$$\delta_{v_{\text{Slack,AC}}} = 0 \tag{3.17}$$

Inequality constraints define operational limits as permitted AC and DC voltage bands (see (3.18), (3.19)), converter and power plant limits (see (3.20), (3.21)) as well as maximum permitted AC and DC line loadings (see (3.22) and (3.23)). It is worth noting that $q_{\text{gen},p}$ includes reactive power provided by power plants and compensation units at AC node p while reactive power of converters is covered by converters' apparent power limits.

$$\left| v_{\text{AC,min},p} \right| \le \left| v_{\text{AC},p} \right| \le \left| v_{\text{AC,max},p} \right| \tag{3.18}$$

$$\left| v_{\text{DC,min},q} \right| \le \left| v_{\text{DC},q} \right| \le \left| v_{\text{DC,max},q} \right| \tag{3.19}$$

$$s_{\text{conv,min},p} \le s_{\text{conv},p} \le s_{\text{conv,max},p} \tag{3.20}$$

$$q_{\text{gen,min},p} \le q_{\text{gen},p} \le q_{\text{gen,max},p} \tag{3.21}$$

$$\left|s_{ij}\right| \leq s_{ij,\max} \tag{3.22}$$

$$\left|p_{km}\right| \leq p_{km,\max} \tag{3.23}$$

3.2.2 Differential evolution algorithm

As OF, equality and inequality constraints of the given problem are already defined in the previous subchapter, the used DE optimization algorithm is described in more detail hereinafter. The DE method is one of the evolutionary programming methods and was originally invented by [74]. Like all evolutionary programming methods, the DE optimization process is based on crossover, mutation and selection. The general algorithm approach is shown in Fig. 3.4.

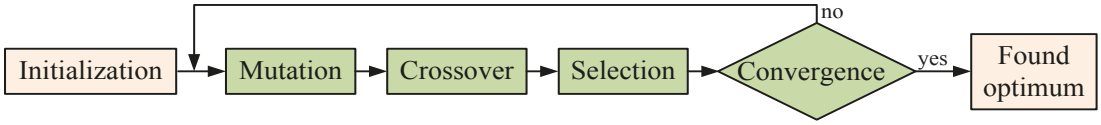

Fig. 3.4: General flow chart of differential evolution optimization algorithm.

For initialization issues the first population vector $P^{(G)}$ with a number of NP populations is created according to (3.24) [83] which represents the first generation G. The more populations are initially created, the more the state space can be covered while searching the global optimum, however, the higher the computation time will be. Each population $x_s^{(G)}$ consists of a d-dimensional vector itself while d represents the number of variables according to (3.8). Vector elements $x_{rs}^{(G)}$ change during the evolutionary process and thus with each generation G as described in following sections. During initialization values of each vector element $x_{rs}^{(G)}$ of $x_s^{(G)}$ are selected within their limits (e.g. voltage limits) according to (3.26) [83]. As shown in Fig. 3.4 the initial and all following generations G are modified by mutation using a mutation constant f_M and crossover of populations using a crossover constant CR. After modification the new populations are selected using OF and initially defined constraints, in that some are maintained and others will be rejected while the total number of populations NP remains unchanged. The populations undergo this evolutionary process until the algorithm converges which is the case when all populations have an equal or almost equal vector $x_s^{(G)}$.

$$P^{(G)} = \left[x_1^{(G)} \quad x_2^{(G)} \quad \ldots \quad x_s^{(G)} \quad \ldots \quad x_{NP}^{(G)} \right] \tag{3.24}$$

$$x_s^{(G)} = \left[x_{|v_{AC,1}|s}^{(G)} \quad x_{|v_{AC,2}|s}^{(G)} \quad \ldots \quad x_{rs}^{(G)} \quad \ldots \quad x_{|v_{DC,1}|s}^{(G)} \quad \ldots \quad x_{|v_{DC,k}|s}^{(G)} \right] = u \tag{3.25}$$

$$x_{rs,\min} \leq x_{rs}^{(0)} \leq x_{rs,\max} \tag{3.26}$$

As indicated in subchapter 3.1.4 the number of populations NP, mutation constant f_M and crossover constant CR significantly determine the optimization process and represent DE's three control parameters. Hereinafter the stages of DE's algorithm are further explained.

Initialization

As mentioned above, populations are created to resolve intitialization issues while each population is a vector x_s containing all system variables x_{rs}. The system variables are determined by a random number while this first population includes only system values from the permitted state space according to (3.27) [83].

$$x_{rs}^{(0)} = x_{rs,\min} + \text{rand}(0,1) \cdot (x_{rs,\max} - x_{rs,\min}) \tag{3.27}$$

Mutation

The first as well as additional populations will run through a mutation process until there is convergence. For that purpose, for each population $x_s^{(G)}$ of a generation G, mutation vectors $v_s^{(G)}$ are created containing of elements $v_{rs}^{(G)}$. Ten different strategies [4] are therefore proposed in [84]. One of them selects the vector $x_{r\text{best}}^{(G)}$ which is the best known at that point and is modified by summation of 4 randomly selected parameter values $x_{rs1}^{(G)}$, $x_{rs2}^{(G)}$, $x_{rs3}^{(G)}$ and $x_{rs4}^{(G)}$ from actual populations of generation G. Summation of four randomly selected values is weighted with the mutation parameter f_M according to (3.28). Normally, the mutation parameter f_M is between 0.4 and 1 [77]. Meanwhile, a larger value f_M increases level of mutation. This will usually cause a lower risk of converging in a local minimum [92].

$$v_{rs}^{(G)} = x_{r\text{best}}^{(G)} + f_M \cdot \left(x_{rs1}^{(G)} + x_{rs2}^{(G)} - x_{rs3}^{(G)} - x_{rs4}^{(G)} \right) \quad \text{with } s1, s2, s3, s4 \in [1...NP] \tag{3.28}$$

Crossover

In order to further increase diversity of new vectors and in order to avoid convergence in a local minimum, an additional crossover is performed after mutation. For that purpose mutation vectors $v_s^{(G)}$ and original vectors $x_s^{(G)}$ (parent vector) are crossed (see Fig. 3.5) using crossover constant CR according to (3.29) [83]. This crossover method is named binominal crossover was found to outperform other methods in its application [83].

$$u_{rs}^{(G)} = \begin{cases} v_{rs}^{(G)} & \text{if } (\text{rand}[0,1] \le CR) \\ x_{rs}^{(G)} & \text{otherwise} \end{cases} \tag{3.29}$$

Crossover constant CR directly determines the resulting trial vector $u_s^{(G)}$ while CR's value is between 0 and 1. Thus, a crossover constant of $CR = 1$ indicates that the trial vector $u_s^{(G)}$

[4] Other strategies according to [84] are:

$v_{rs}^{(G)} = x_{rs1}^{(G)} + f_\text{M} \cdot (x_{rs2}^{(G)} - x_{rs3}^{(G)})$

$v_{rs}^{(G)} = x_{r\text{best}}^{(G)} + f_\text{M} \cdot (x_{rs2}^{(G)} - x_{rs3}^{(G)})$

$v_{rs}^{(G)} = x_{rs}^{(G)} + f_{\text{M1}} \cdot (x_{r\text{best}}^{(G)} - x_{rs}^{(G)}) + f_{\text{M2}} \cdot (x_{rs1}^{(G)} - x_{rs2}^{(G)})$

$v_{rs}^{(G)} = x_{rs5}^{(G)} + f_\text{M} \cdot (x_{rs1}^{(G)} + x_{rs2}^{(G)} - x_{rs3}^{(G)} - x_{rs4}^{(G)})$

$v_{rs}^{(G)} = x_{r\text{best}}^{(G)} + f_{\text{M1}} \cdot (x_{rs1}^{(G)} - x_{rs2}^{(G)}) + f_{\text{M2}} \cdot (x_{rs3}^{(G)} - x_{rs4}^{(G)})$

will be equal to the mutation vector $v_s^{(G)}$. The smaller the CR is chosen, the more elements of the trial vector $u_s^{(G)}$ will come from the parent vector $x_s^{(G)}$.

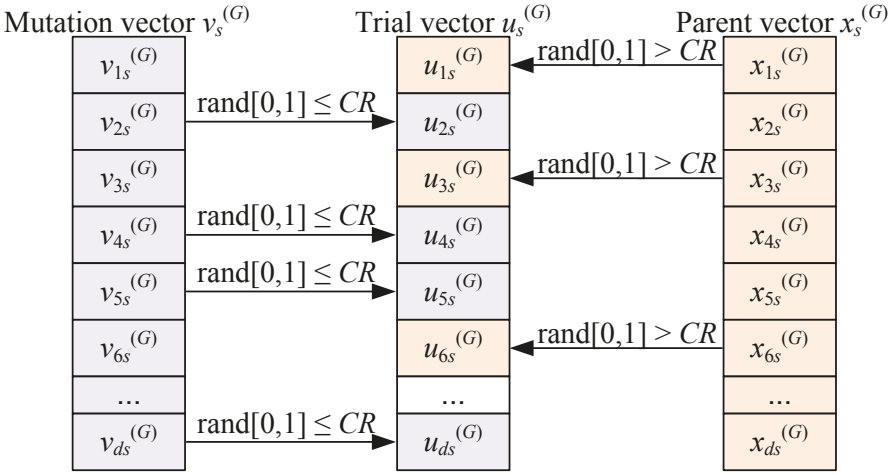

Fig. 3.5: Crossover principle.

Selection

The last part of each iteration compares trial vectors $u_s^{(G)}$ with their parent vectors $x_s^{(G)}$ using OF's value $F_{\text{fitness}}(x,u)$ (see appendix (A.5)). That of both vectors is maintained for the next generation (G+1), that has the smaller / better OF value $F_{\text{fitness}}(x,u)$ according to (3.30) [83]. This process is passed by each vector couple $u_s^{(G)}$ and $x_s^{(G)}$ of each population. Violation of constraints must also be considered during selection. Although the scope of this work does not allow for a more in depth explanation, some basics are given in Appendix B.

$$x_s^{(G+1)} = \begin{cases} u_s^{(G)} & \text{if } (F_{\text{fitness}}(u_s^{(G)},x) < (F_{\text{fitness}}(x_s^{(G)},x)) \\ x_s^{(G)} & \text{otherwise} \end{cases} \tag{3.30}$$

3.2.3 OPF numerical case study

The numerical case study in this subchapter intends to provide an impression on the convergence behavior using DE for a mixed AC/DC OPF problem. On the other hand, further potential is identified to improve problem formulation in order to achive satisfying results as an outlook for further work. For that purpose the used grid model, which is a modification of the previously described reference grid (see subchapter 2.4), and DE parameterization are described at first before simulation results are presented.

Grid model

The requirements for the grid model used in this work for OPF numerical case study are:

- *Simplified grid structure* as DE's convergence is complex and different from that of conventionally used methods. For a better understanding a limited number of grid nodes is therefore advantageous and allows for a better understanding of the convergence process and problem handling.

- *Sufficient number of AC and DC nodes* so that an OPF is still reasonable to be performed.
- *Meshed AC and DC grid structure:* The OPF described in this work, should be used for a meshed overlay HVDC grid. Thus, the AC as well as the DC grid should have a meshed topology.

Fig. 3.6 presents the grid model including a meshed AC as well as a meshed DC part. This is used for a numerical OPF case study and shows the reduction of the reference grid model described in subchapter 2.4. It still has generators for all AC nodes and most but not all AC nodes are connected to the DC grid. The number of AC as well as of DC nodes is significantly reduced with regard to the reference grid.

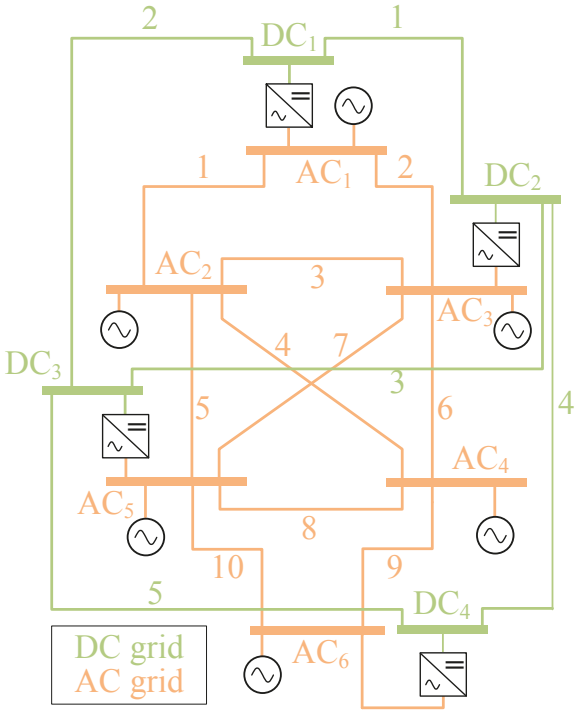

Fig. 3.6: AC and DC part of the grid model for OPF numerical case studies.

Due to its meshed structure on both the DC north-south as well as east-west side, main transmission paths are possible as could be the case for a future German or European overlay grid. The grid model contains six AC (AC_1 – AC_6) and four DC nodes (DC_1 – DC_4) while the degree of meshing within the AC grid is significantly higher using ten lines with regard to the DC part meshing using five lines. Grid topology, line parameters, converter power limits, generation and load at AC nodes as well as reactive power limits are described in Appendix C.

Parameterization of differential evolution for mixed AC/DC OPF

In subchapter 3.1.4 DE algorithm is described as using three user defined parameters for its evolutionary optimization: number of populations *NP*, mutation parameter f_M and crossover constant *CR*. In [63], [77], [83] and [91] application of DE is used for OPF and in [77] it

also includes FACTS. Based on their parameter selection a decision is made for mixed AC/DC OPF as shown in Tab. 3-3. In order to cover a wide area of the state space a number of populations $NP = 100$ is selected for the mixed AC/DC OPF. The mutation parameter f_M is defined to be 0.9 which is a mean value of the proposed range in [77] where FACTS are included in the OPF. The crossover constant CR is proposed to be approximately the same value as in [63], [77], [83] and [91] of 0.8. This value is therefore set for the mixed AC/DC OPF. For mutation, a strategy, such as in (3.28), is implemented.

Tab. 3-3: Parameter selection for DE mixed AC/DC OPF.

	NP	f_M	***CR***
[63]	60	0.8	0.8
[77]	10-30	0.8 - 0.95	0.5 - 0.8
[91]	20	0.8	0.8
[83]	50	0.7	0.8
Selected for mixed AC/DC OPF	100	0.9	0.8

As defined in subchapter 3.2.1, constraints are included in the optimization by two different strategies. AC and DC voltage constraints are handled using feasibility preserving (see Appendix B) while for all other penalty factors of the constraints are used in order to directly include them into the OF such as in (3.31) and (3.32) (see Appendix B). Static penalty factors $penalty_p$ are used while their values for different constraints are given in Tab. 3-4. Original OF $F(x,u)$ for reducing overall losses is weighted with $k_{\text{fitness}} = 100$.

$$F_{\text{fitness}}(x,u) = k_{\text{fitness}} \cdot F(x,u) + F_{\text{penalty}}(x,u) \tag{3.31}$$

$$F_{\text{penalty}}(x,u) = \sum_{u} k_{\text{penalty},u} \cdot penalty_u(u,x) \tag{3.32}$$

Tab. 3-4: Penalty factors for different constraints as implemented.

Penalty index *p*	**Constraint**	k_{penalty}
1	AC active power balance (see (3.13))	300
2	DC power balance (see (3.15))	300
3	Converter capacity (see (3.20))	50
4	Reactive power limits (see (3.21))	50
5	AC transmission capacity (see (3.22))	1,000
6	DC transmission capacity (see (3.23))	1,000

The optimization process terminates when between 3,000 and 8,000 iterations are passed, when all constraints are fulfilled and the convergence criterion according to (3.33) is met. I.e. when the objective function result of the best population $x_{\text{best}}^{(G)}$ changd by a maximum of 0.01% during the past 300 iterations respectively generations G.

$$\varepsilon \leq 0.01\% \tag{3.33}$$

$$\varepsilon = \frac{x_{\text{best}}^{(G-300)} - x_{\text{best}}^{(G)}}{x_{\text{best}}^{(G)}} \tag{3.34}$$

Numerical case study – results

The convergence of DE is different to conventional optimization algorithms used for OPF problems. Due to the integration of constraints in the OF using penalty factors, not only the original OF is minimized but in the beginning of the optimization process constraints are fulfilled first. This is described in the beginning. Following on from this the optimization results are presented and discussed. Thereby, potential for further improvement of the algorithm is identified.

Convergence of DE

DE is based on a stochastic evolution of its populations. Thus, each optimization will have another trajectory. Even if operating points differ slightly from simulation to simulation a tendency towards a single operating point can be seen in Tab. 3-5. For the given generation and load pattern in Appendix C 40 simulations are carried out. As defined for convergence criteria, results of all 40 simulations fulfill the given constraints. Please refer to Appendix D for corresponding simulation result details.

Convergence patterns of DE algorithms in general can be derived in two sections. In the first section, the constraint violations decease rapidly while OF is subject to significant fluctuations due to randomly selected populations and higher ratings of constraint violations (see Fig. 3.7). However, the overall value of $F_{\text{fitness}}(x,u)$ continuously decreases. Within the second section constraints are not violated or are only marginally violated and the progress of $F_{\text{fitness}}(x,u)$ is mainly determined by the optimization of the original OF $F(x,u)$ which represents minimization of total losses. The transition from one section to the other differs from simulation to simulation. Hence, a wide span of iterations is set for convergence criteria.

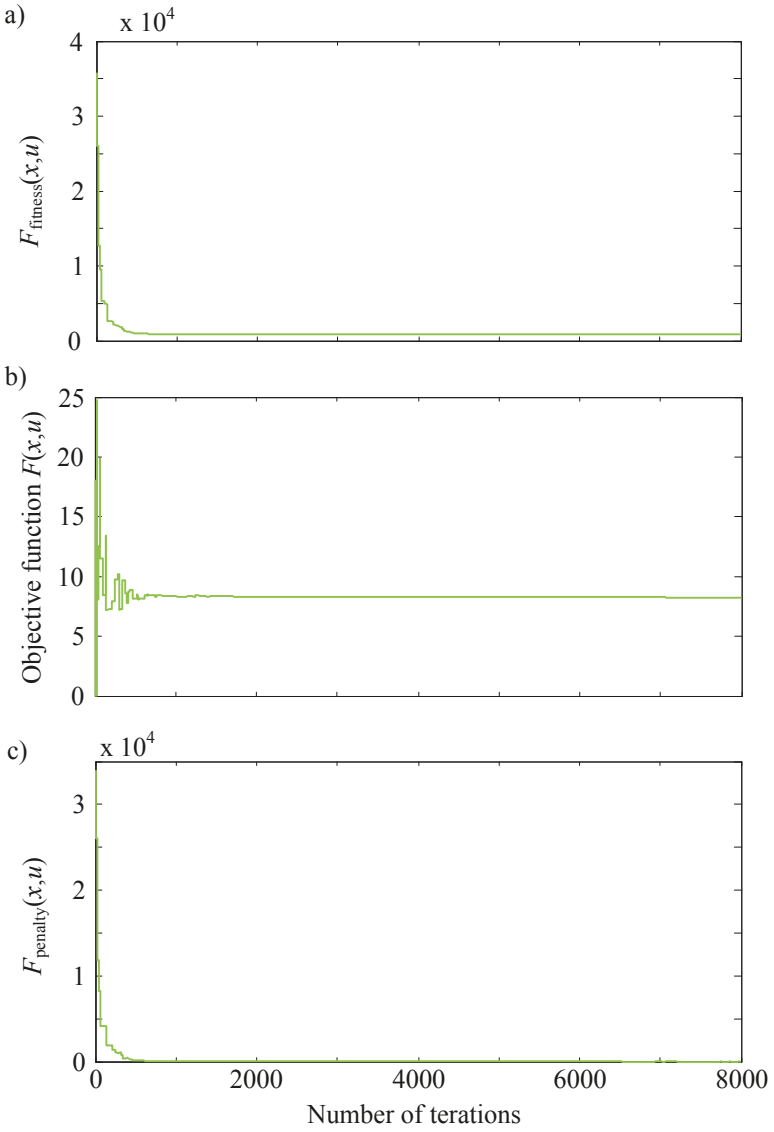

Fig. 3.7: Convergence pattern of DE algorithm for mixed AC/DC OPF a) $F_{\text{fitness}}(x,u)$ including OF $F(x,u)$ and summation of penalty functions $F_{\text{penalty}}(x,u)$, b) objective function $F(x,u) = P_{\text{loss}}$ and c) summation of penalty functions $F_{\text{penalty}}(x,u)$.

Discussion of results

Taking all 40 simulation runs into account the algorithm takes 5362 iterations on average until convergence. The average overall system losses are 847.8 MW (4.3 % of the overall generated power) while the maximum and minimum values are 897.5 MW and 822.4 MW respectively. The variation of results is shown in Fig. 3.9. Among 40 optimization results, 13 match the best found solution (global optimum) with an accuracy of 1%. In Tab. 3-5 an analysis is made for all results that correspond to the global optimum with an accuracy of 1% or 5% while the positive and negative variability and the mean value (absolute and in percentage) are considered.

With such results which deviate up to 5% from the optimum, the results that deviate the most from the global optimum have some AC and / or all DC voltages at or nearby their lower bound. The results which deviate from the global optimum by a maximum of 1%, meet global optimums voltage values quite well. An exception for this is AC voltage angle δ_{vAC6} which varies a lot for all simultations. Its effect on the optimization result is low since it is a low load and low generation node.

Tab. 3-5: Voltage information for global optimum found and the variability and mean values for other local optima found with OF results maximum 105% or 101% of the global optimum.

		OF results maximum 105% of the global optimum result			OF results maximum 101% of the global optimum result		
	Opt.	**Variability**		**Mean value**	**Variability**		**Mean value**
$\lvert v_{AC1}\rvert$	1.017	1.024	0.950	1.005 *(98.8%)*	1.021	1.009	1.017 *(100%)*
$\lvert v_{AC2}\rvert$ (Slack)	1.00	1.000	1.000	1.000 *(100%)*	1.000	1.000	1.000 *(100%)*
$\lvert v_{AC3}\rvert$	1.050	1.050	1.049	1.050 *(100%)*	1.050	1.049	1.050 *(100%)*
$\lvert v_{AC4}\rvert$	1.050	1.050	0.950	1.024 *(97.5%)*	1.050	1.025	1.045 *(99.5%)*
$\lvert v_{AC5}\rvert$	1.050	1.050	0.950	1.026 *(97.7%)*	1.050	1.024	1.044 *(99.4%)*
$\lvert v_{AC6}\rvert$	1.050	1.050	0.950	1.028 *(97.9%)*	1.050	0.958	1.037 *(98.7%)*
δ_{vAC1}	40.32	44.16	39.93	41.00 *(101.7%)*	40.82	40.08	40.34 *(100%)*
δ_{vAC2} (Slack)	0.00	0.00	0.00	0.00 *(100%)*	0.00	0.00	0.00 *(100%)*
δ_{vAC3}	9.43	10.56	7.90	9.20 *(97.6%)*	9.75	7.92	9.13 *(96.8%)*
δ_{vAC4}	-7.90	-7.71	-9.23	-8.31 *(105.2%)*	-7.71	-8.50	-7.99 *(101.1%)*
δ_{vAC5}	-9.94	-9.30	-10.32	-9.97 *(100.3%)*	-9.30	-10.10	-9.85 *(99.1%)*
δ_{vAC6}	4.00	6.69	-3.73	3.61 *(90.2%)*	6.30	3.78	4.63 *(115.9%)*
v_{DC1}	1.050	1.050	0.986	1.042 *(99.2%)*	1.050	1.050	1.050 *(100%)*
v_{DC2}	1.027	1.028	0.962	1.019 *(99.2%)*	1.028	1.027	1.027 *(100%)*
v_{DC3}	1.020	1.020	0.954	1.011 *(99.1%)*	1.020	1.019	1.019 *(100%)*
v_{DC4}	1.016	1.018	0.950	1.008 *(99.2%)*	1.017	1.016	1.016 *(100%)*

In general, results that deviate significantly from the best found optimum (assumed as global optimum) have either DC voltages and / or AC voltages on the lower voltage band, as can be seen in Appendix D.

There are several results that did not find the global optimum. This is mainly caused by the heuristic characteristic of differential evolution and the chosen mutation strategy using the best known vector so far x_{best}, in (3.28) for example, but also by the defined number of populations. A further increase in the number of populations together with increased num-

ber of minimum and maximum iteration steps per optimization will lead to a more satisfactory variation of results. As this also implies a significant increase in computation time the effect of further limiting the state space is analyzed below.

Due to its heuristic character there is always the possibility that a vector at or nearby the global optimum is not selected by randomly defining vectors within the permitted area. As mentioned, the chosen mutation strategy and number of populations favors this additionally. When the randomly chosen vectors in the beginning of the mutation process do not include any vector nearby the global optimum, it is possible that the area around it will not be covered during optimization. New created vectors within the optimization process will, to a certain extent, be based on x_{best} and on other randomly chosen vector elements of the current population. Thus, the optimization will focus on the area around the best chosen vector so far. This is exemplarily shown for the DC node voltage v_{DC1} and v_{DC4} in Fig. 3.8. The longer the optimization process lasts, the more a certain area is focused. If the heuristic process did not generate an initial vector close to the global optimum, this will fail.

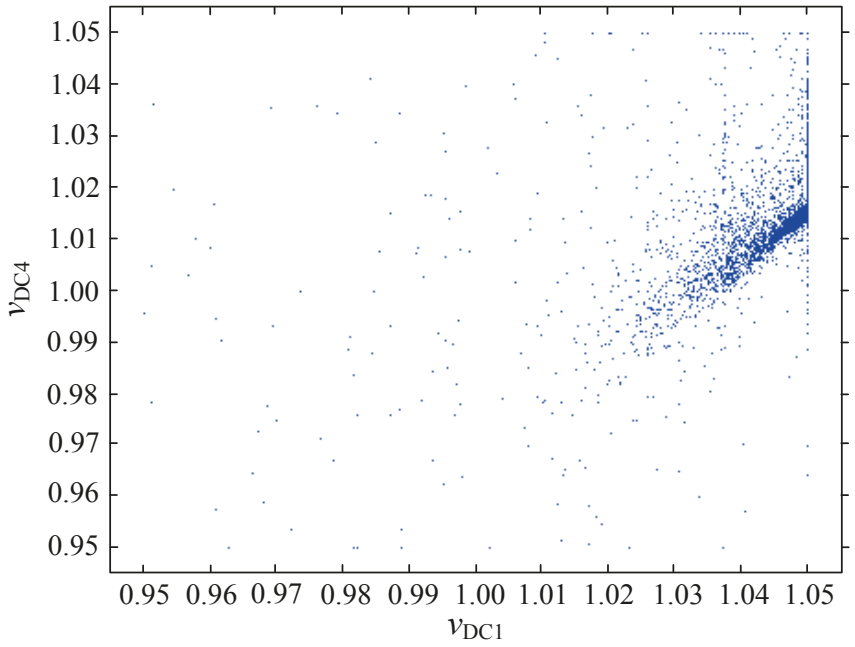

Fig. 3.8: Convergence of differential evolution algorithm exemplarily shown for the DC voltages at DC node DC1 with the highest infeed and DC voltage and DC4 with the lowest DC voltage.

If x_{best} is not used, the number of necessary iterations and iteration time will increase drastically. However, the complete permitted area will be covered equally during optimization. But this leads to another option changes mutation strategy during optimization starting with no consideration of x_{best} and then switching over to considering x_{best}. [85] proposes such a strategy for DE programming in general. As this is not made for OPF or mixed AC/DC OPF problems a deeper analysis in future work is necessary.

The permitted state space is quite large, thus a high number of possible state vectors can be generated. Limiting the permitted state space to the most feasible region also increases the probability for finding the global optimum. This is exemplarily made for a further limitation of AC voltage magnitudes ($v_{AC,min}$ = 1.00, $v_{AC,max}$ = 1.05) and for both a limitation of AC and DC magnitudes ($v_{AC,min}$ = 1.00, $v_{AC,max}$ = 1.05, $v_{DC,min}$ = 1.00, $v_{DC,max}$ = 1.05). A further 20 simulations are carried out for each, and the found optima are shown in Fig. 3.10 and Fig. 3.11 respectively (detailed simulation results are provided in Appendix D). Nevertheless, occurrence of local minima cannot be avoided, even if the number of solution close to the global optimum increases with a smaller permitted state space. Additionally the difference between local and global optima is more significant. Local minima can still be identified by DC voltages at the lower voltage band.

An identification of local minima solutions can be made afterwards if the maximum DC voltage is not near to the maximum permitted DC voltage.

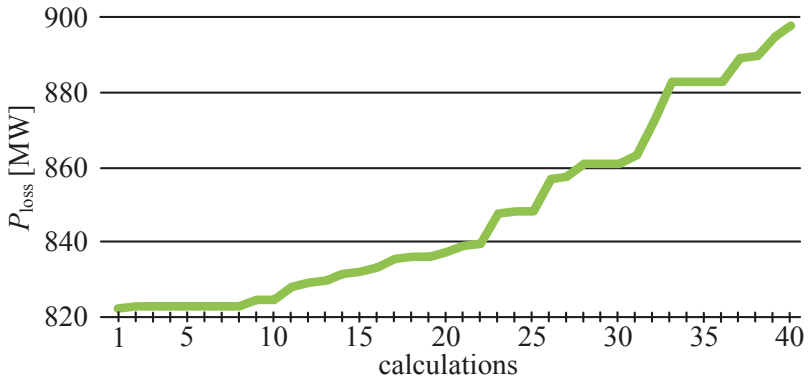

Fig. 3.9: Merit order of optimization results for 40 simulations with AC voltages between 0.95 p.u. and 1.05 p.u. and DC voltages between 0.95 p.u. and 1.05 p.u.

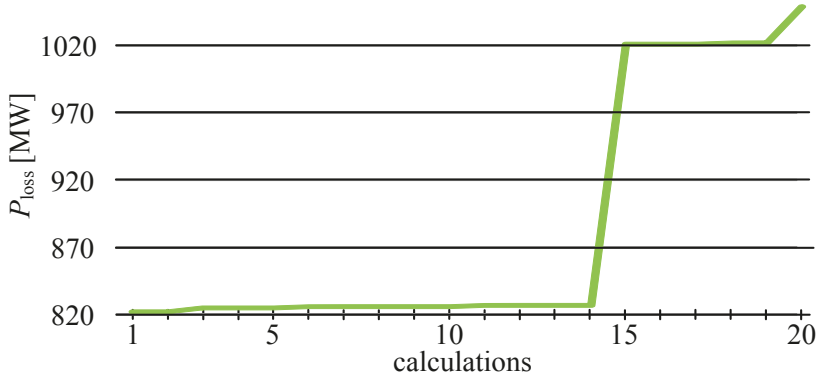

Fig. 3.10: Merit order of optimization results for 20 simulations with AC voltages between 1.00 p.u. and 1.05 p.u. and DC voltages between 0.95 p.u. and 1.05 p.u.

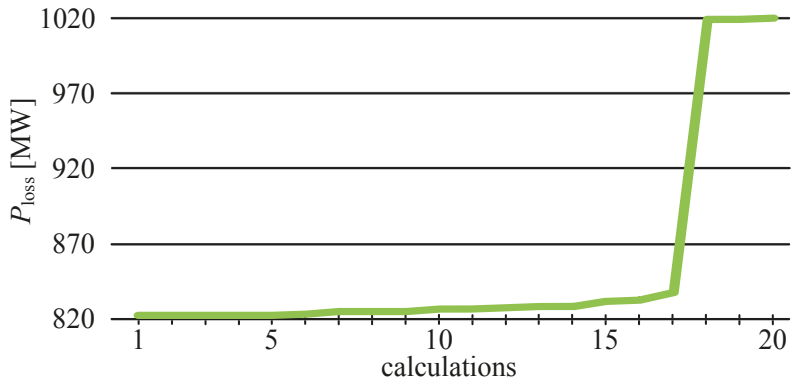

Fig. 3.11: Merit order of optimization results for 20 simulations with AC voltages between 1.00 p.u. and 1.05 p.u. and DC voltages between 1.00 p.u. and 1.05 p.u.

Validation of maximum number of iterations and acceleration of computation

In order to validate the maximum number of iterations a further simulation is carried out for 20,000 iterations. The total losses in this case decreased to p_{loss} = 822MW which is the same optimum found when a maximum of 8,000 iterations is defined. This is also true for values of corresponding state space variables (v_{AC} and v_{DC}). Thus, a maximum number of 8,000 iterations is sufficient.

As optimization results are not always but mostly close to the global optimum, this could also be realistically implemented in a future European ISO (as suggested in subchapter 2.3.3) by running multiple simulations in parallel for the same load and generation pattern and end by filtering the most optimal of these, as was done here. This can be a tradeoff between number of iterations and accuracy of final results.

A further acceleration of the overall optimization process could be reached by further limiting the constraints, particularly in AC voltage magnitudes. Limiting the permitted state space also limits search area to more realistic or likely values. AC voltage magnitudes at the transmission level particularly, will be normally in a much smaller range assuming enough reactive power capacity. However, a dynamic extension of permitted AC node voltage magnitudes is possible with respect to reactive power limits during the optimization process.

3.2.4 Conclusion

In this subchapter it is assumed that an ISO exists with a global view on the HVDC overlay grid and all relevant parts of the underlaying AC transmission system. This enables an system operator to run a global optimization with inherent coordination between AC and HVDC grid as well as between the converters. An alternative perspective is discussed in subchapter 3.3 assuming the absence of an ISO with a distributed responsibility for the HVDC grid and its converters among several TSOs.

In subchapter 3.1 DE was identified to be the most appropriate method for mixed AC/DC OPF problems. A more detailed explanation of DE algorithm is given in this subchapter. Further DE is applied to an AC/DC test grid. A typical convergence pattern is presented as well as a number of simulations for the same test grid and load or generation patterns. Unlike conventional optimization methods DE's convergence is not dependent on initial conditions but differs from simulation to simulation. It is shown that DE does not always find the global optimum in each simulation but the effect of slightly limiting the permitted state space was shown. This leads to a much higher probability in finding the global optimum and a significantly clearer distinction between global and local optima. The possibility of several parallel optimizations makes the identification of a global optimum much more likely than with conventional optimization methods.

3.3 Coordination without centralized master controller

As previously mentioned and as discussed in greater detail in subchapter 5.2, coordination of converter power reference values is not only essential for the DC grid but also for the AC grid. An imbalance in the DC grid will directly affect the AC grid since DC balancing power is sourced from the AC system via converters. Thus, input and output of the HVDC system and its losses must be balanced.

The optimization of converter reference values (schedules) as described in subchapter 3.2 assumes a global knowledge about the HVDC grid and AC transmission system as found in an ISO. Today's responsibility for the European transmission system is devided by a number of TSOs and no coordinating ISO is in place. Taking this into consideration a global optimization (as described in subchapter 3.2) would be impossible with the current organizational structure found today. This subchapter therefore proposes a methodology that allows an overall optimization and coordination of converter reference values which also maintains current distributed transmission grid responsibility. This means that responsibility for the AC transmission system remains the same and responsibility for converters is distributed among all TSOs according to converters AC PCC in the TSOs responsibility area.

3.3.1 Basic concept

As described in subchapter 3.2 for converter scheduling, schedules are calculated for a defined pre-conceived time frame which is characterized by a certain grid topology, load and generation pattern. As one of the primary tasks of the HVDC grid is to relieve the AC grid of bulk power long distance power flows, avoiding equipment overload and ensuring system instability in general converter reference values are subject to upper and lower limits. As long as these limits are within the converter power limits they define a limited permissible operation range, otherwise the whole operating range is allowed. Fig. 3.12. illustrates some limit introducing factors. Some of these limits can cause both an upper and a lower limit and restrict the permissible operation range. HVDC converters are designed for their

AC PCC, which means that their nominal power can be transmitted by the surrounding AC transmission grid. In case of a changed transmission grid topology, due to maintenance for example, a converter's permissible operation range is restricted by thermal line limits for example. This must be taken into account for converter scheduling.

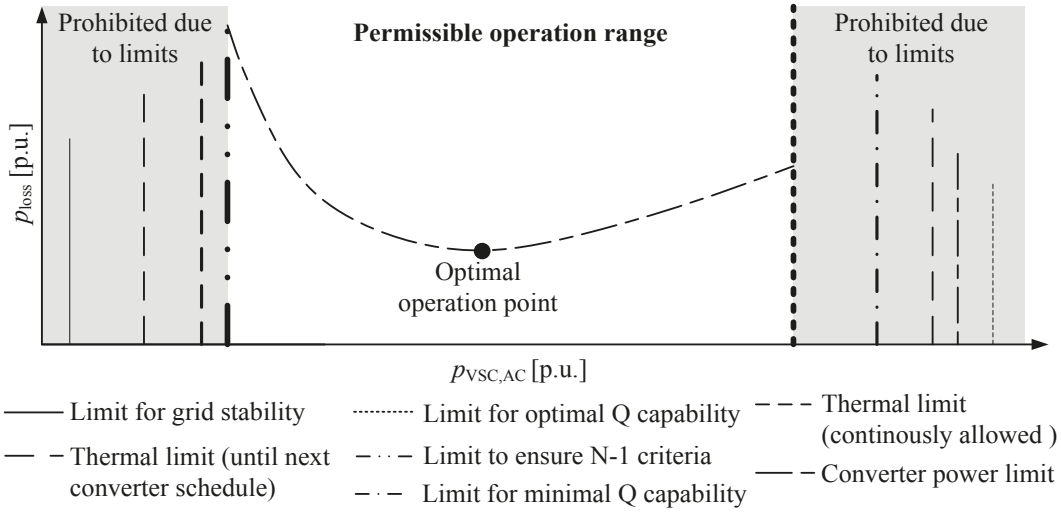

Fig. 3.12: Converter reference value limitation and permissible operation range which can be a subject for further optimization.

The most restrictive lower and upper limits define a permissible operation range from which any operation point can be chosen. Thus, this permissible operation range can be used for any kind of operating point optimization (e.g. with the objective of minimal losses or maximization of stability margins). This is illustrated in Fig. 3.12.

In the unlikely event that limits for one converter are very restrictive and there is no permissible operation range, certain restrictions can be reduced (as N-1 criterion) or completely neglected (as a continuously permissible thermal limit) as long as system security is maintained until the next schedule update.

If an HVDC system only interconnects points within the area of one single TSO, the optimization of converter power reference values will automatically result in global optimum since the HVDC system and mainly influenced parts of the AC system are included in a single optimization. This is not the case if areas of different TSOs are connected via the HVDC system given that each TSO will calculate the point of optimal operation for its own part of the system but not for the overall system. It is possible that the responsibility for the entire HVDC system will not be given only one of both involved TSOs as detailed grid information will mostly be not provided to the other TSO making a global optimization difficult.

The proposed coordination process of two or more TSOs is based on the aforementioned definition of permissible operation range using upper and lower limits and an OF for the remaining permissible operation range. This OF is solely dependent on the converter reference power and allows an optimization of converter power reference. Here it is assumed

that all TSO agreed on overall losses as a common optimization target. Any other target or set of targets is also possible even if they difer from TSO to TSO just a common normalization is necessary. For further considerations in this subchapter it is assumed that AC transmission losses are covered by the TSO that incur losses and that DC transmission losses (including converter and substation losses) are shared between exchanging TSOs. It is worth mentioning that power independent losses of the converter occur as soon as the HVDC system is energized.

It is also possible to modify the loss dependent optimization into a cost of loss dependent optimization. If both TSOs have significantly different energy procurement costs, optimization results may differ from loss dependent optimization. This would mean a higher weighting of optimization trajectories of converters in high energy procurement cost areas. Consequently, this implies that the cost of losses will partially be transferred to the area with lower energy procurement costs.

In subchapter 3.3.2 and 3.3.3 a coordination of an HVDC P2P interconnection between two adjacent and two remote TSOs are considered as basic examples. The general approach which is also applicable for converter coordination of unmeshed and meshed multi-terminal HVDC schemes is described in subchapter 3.3.4.

3.3.2 HVDC converter coordination of two adjacent areas

This subchapter considers an HVDC P2P connection between two adjacent TSOs as illustrated in Fig. 3.13 a). The aforementioned limits for converter power and OF for further optimization are handed between each TSO. If the permissible operation range of both converters do not have a common permissible operation band, some limits can be reduced (e.g. N-1 criterion) or removed (e.g. continuously permitted thermal limit) as long as a secure operation is ensured until next schedule. Critical limits, such as the limit for grid stability or the thermal limit (permitted until next converter schedule), must not be removed or reduced. If no common permissible operation band can be found the HVDC system is out of operation until a permissible operation band is found, for example when tripped lines under maintenance are back in operation. Thus, a scheduled power exchange between both considered TSOs $p_{\text{exchange21}}$ or $p_{\text{exchange12}}$, permissible operation ranges and optimization trajectories (OF) of both converters are known by both TSOs.

Depending on the AC transmission system topology and the location of the converters, optimal operation points of both converters may be different for perspectives of both considered TSOs. If the converter of TSO 1 is located electrically close to the borders of TSO 2 and that of TSO 2 is located electrically far from the border (see Fig. 3.13 a) it is likely to be more reasonable for TSO 2 to activate the HVDC system for a low value of transmission power than for TSO 1. This can even be the case if an activation of the HVDC system is reasonable from a global point of view (see Fig. 3.13 b).

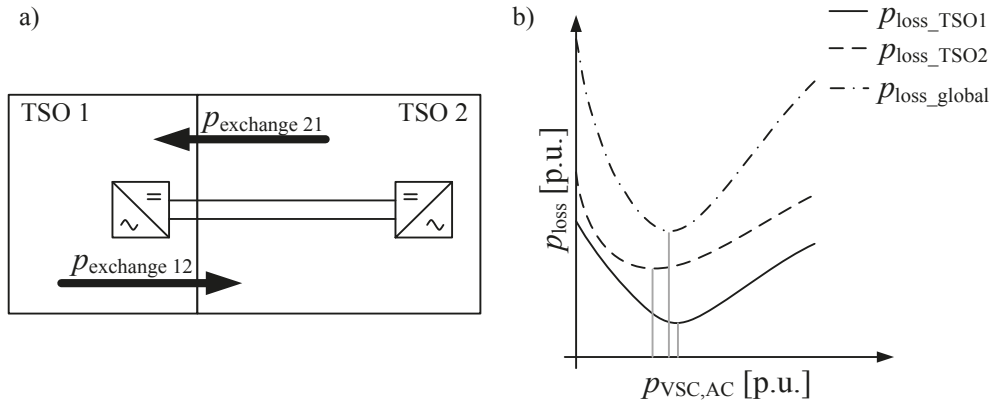

Fig. 3.13: HVDC connection between two adjacent TSOs (a) and composition of global losses (b)

With the OFs of both converters p_{loss_TSO1} and p_{loss_TSO2} a global optimization can be emulated adding both trajectories in order to generate a global one p_{loss_global}, such as in (3.39). The minimum of that emulated global OF p_{loss_global} according to (3.40) can be seen as an approximated global optimal operation point and would mostly be between both local minima of each converter (see Fig. 3.13 b). p_{VSC_AC} addresses the transmitted power through the HVDC P2P scheme and represents the physical converter power of the receiving converter on the AC side. Losses are only respected in the OF. Transit AC power flows through areas of other adjacent TSOs are neglected using this decentralized approach.

$$p_{loss\_global}(p_{VSC\_AC}) = p_{loss\_TSO1}(p_{VSC\_AC}) + p_{loss\_TSO2}(p_{VSC\_AC}) \tag{3.35}$$

$$\min_{P_{VSC\_AC}} \left(p_{loss\_global}(p_{VSC\_AC}) \right) \tag{3.36}$$

3.3.3 HVDC converter coordination of two remote areas

In addition to the described situation of having two directly adjacent TSOs, this subchapter considers an HVDC P2P interconnection between remote TSO areas with one or more TSO(s) in between. In this case the permissible operation range can also be further affected by limits of the transit TSO(s). As a minimum requirement the grid stability limit and the minimum thermal limit (permitted until next converter schedule) should be maintained for the transiting TSO(s).

Unlike in the previous subchapter 3.3.2 TSO(s) which do not have a direct part in the HVDC P2P interconnection are considered as well. They are affected by transit AC power flows dependent on the converter reference values. The more transit TSOs are considered within the interconnected AC system the more the decentralized optimization result will fit the global optimum.

Thus, any further restricting limits introduced by the responsibility area of not directly HVDC scheme involved TSO(s) (transit TSO(s)) and OF of those additionally considered

TSO area(s) are included in the consideration, as described in subchapter 3.3.2. The final OF for this extended optimization problem results is shown in Fig. 3.14 and (3.37).

$$p_{\text{loss\_global}}(p_{\text{VSC\_AC}}) = p_{\text{loss\_TSO1}}(p_{\text{VSC\_AC}}) + p_{\text{loss\_TSO2}}(p_{\text{VSC\_AC}}) + \sum_{i=1}^{n_{\text{transit\_TSO}}} p_{\text{loss\_transit\_TSO,i}}(p_{\text{VSC\_AC}}) \tag{3.37}$$

$$\min_{p_{\text{VSC\_AC}}} \left(p_{\text{loss\_global}}(p_{\text{VSC\_AC}}) \right) \tag{3.38}$$

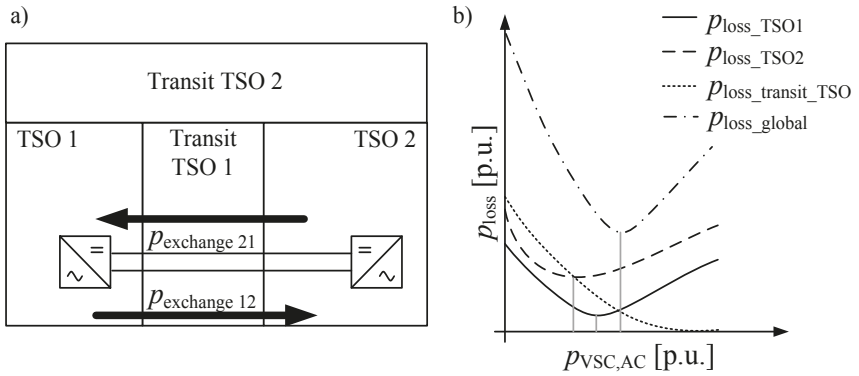

Fig. 3.14: HVDC connection between two not directly adjacent TSOs (a) and composition of global losses (b).

3.3.4 HVDC converter coordination of a multi-terminal HVDC scheme

A decentralized coordination of converter reference values becomes more complex the more TSOs and converters are involved. In a multi-terminal HVDC system (meshed or unmeshed) limits for P2P exchanges between two particular converters / TSOs cannot be defined in advance if there are multiple exchanges between converters. Furthermore, voltage dependent losses (power independent losses α in (3.10)) should be neglected in the initial step. They are in place as soon as the HVDC converter is in operation. When finalizing the optimization (after definition of all preliminary exchanges via the HVDC system) it is examined whether or not the determined HVDC transmission is still the best global solution additionally considering voltage dependent losses. Once the converter serves for more than one power exchange such constant losses are divided to all exchanges pro rata and are not fully applied for each single exchange.

For local optimization each TSO provides an OF for each planned exchange $p_{\text{exchange},i}$ with another TSO having an HVDC converter within the same HVDC scheme (see Fig. 3.15). These OF only consider current / power dependent DC losses and all affected AC losses. All possible converter power reference values are respected for each power exchange optimization process, that is starting from 0% up to 100% utilization of the HVDC converter for each power exchange $p_{\text{exchange},I}$ at first without considering the limitations.

Using all provided OFs including those of transit TSO(s), each converter owning TSO starts an optimization process for each of its planned exchanges separately first. As each involved TSO makes the calculations a redundant optimization is always running. This can be used for schedule verification. The result $p_{\text{conv;AC,exchange},x}$ is a part of the final converter power

reference value for each planned exchange. So far the process is comparable to the previously described processes of P2P connections but without previous limit consideration.

The sum of all optimization results $p_{conv;AC,exchange,x}$ for all power exchanges $p_{exchange,i}$ of one particular converter is its (temporary) total power reference value p_i (see Fig. 3.15). This value is temporary since limit violations are investigated in the next step.

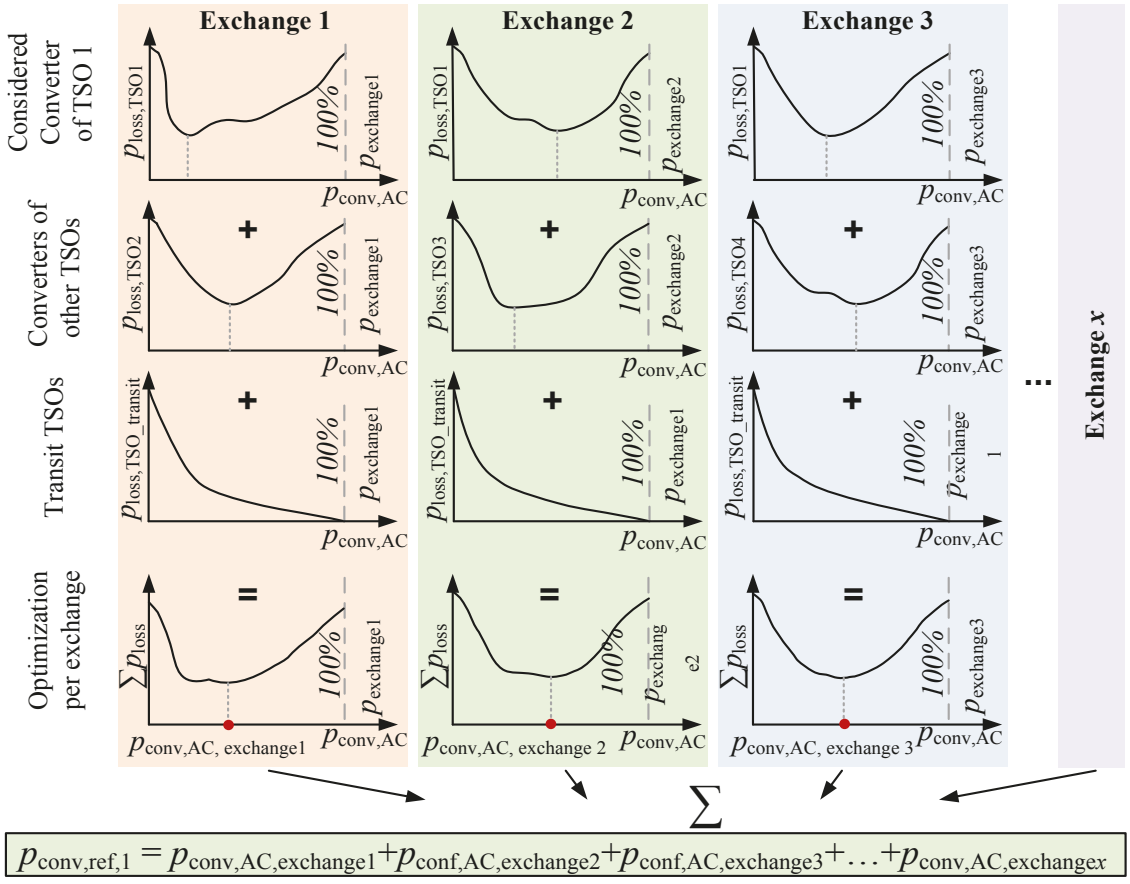

Fig. 3.15: Optimal operation point calculation with multiple TSOs in a multi-terminal or meshed HVDC grid – part I: temporarily total power reference value $p_{conv,ref,i}$.

Each temporary converter power reference value $p_{conv,ref,i}$ is examined according to limit violations. As a result, each TSO provides a positive $\Delta p_{pos,margin,i}$ and negative margin value $\Delta p_{neg,margin,i}$ for each of its converters. This is illustrated in Fig. 3.16 a).

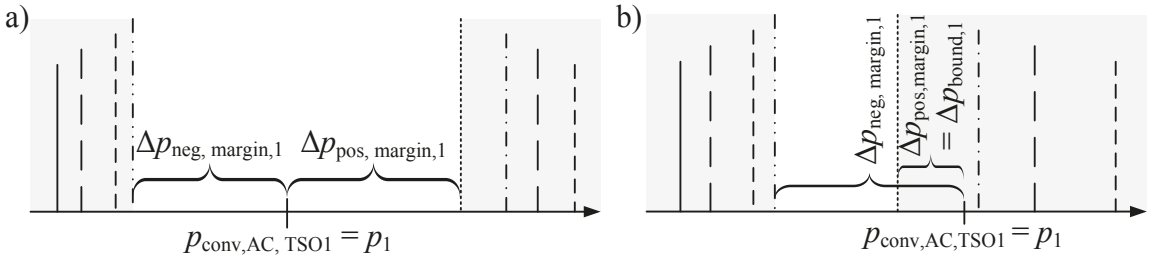

Fig. 3.16: Limit violation examination for temporarily converter power reference values– a) without limit violation, b) with limit violation ($\Delta p_{pos,\ margin,i}$ with negative sign).

Both values $\Delta p_{\text{pos,margin},i}$ and $\Delta p_{\text{neg,margin},i}$ define how much the temporary converter power reference value could change in both positive and negative direction until one of its defined limits is violated. These two values also inherently give information on whether or not a limit has already been violated. In such cases the corresponding margin value $\Delta p_{\text{pos,margin},i}$ or $\Delta p_{\text{neg,margin},i}$ has a negative sign as is illustrated in Fig. 3.16 b). If both $\Delta p_{\text{pos,margin},i}$ and $\Delta p_{\text{neg,margin},i}$ have a negative sign the converter is deactivated for the scheduled period as no permissible operation range exists. In the event that only one of both values has a negative sign it provides inherent information about how much its converter reference value must change until converter power complies with all limits. Thus, boundary violation $\Delta p_{\text{bound},i}$ of converter i is defined according to (3.39).

$$\Delta p_{\text{bound},i} = \begin{cases} \Delta p_{\text{pos,margin},i} & \text{if } \Delta p_{\text{pos,margin},i} < 0 \\ \Delta p_{\text{neg,margin},i} & \text{if } \Delta p_{\text{neg,margin},i} < 0 \\ 0 & \text{if } \Delta p_{\text{pos,margin},i} \geq 0 \text{ and } \Delta p_{\text{neg,margin},i} \geq 0 \end{cases} \tag{3.39}$$

If $\Delta p_{\text{bound},i}$ of any converter is not equal to zero a further corrective intervention is necessary. In order to comply with all limits of that converter with $\Delta p_{\text{bound},I} < 0$ its power reference p_i must be modified by $\Delta p_{\text{bound},i}$. For DC energy balance reasons this amount of power must be provided by the converters which are supposed to exchange power with the considered converter i. In order to distribute $\Delta p_{\text{bound},i}$ as low-loss as possible, another optimization is used. Here the optimization trajectories (see Fig. 3.15) are utilized again for OF in (3.40) which minimizes the loss for corrective adaptation Δp_j of other converter reference values in order to meet the constraint given in (3.41). That constraint ensures that the exact needed power difference $\Delta p_{\text{bound},i}$ is provided by other converters. This is exemplarily illustrated in Fig. 3.17. The second constraint (3.42) ensures that adaptation of one temporarily converter power reference value p_i does not cause limit violation for any other converter.

$$\min\left(\sum_j \Delta p_{\text{loss},j}(\Delta p_j) \right) \tag{3.40}$$

$$-\Delta p_{\text{bound},i} = \sum_j \Delta p_{\text{conf,ref},j} \tag{3.41}$$

$$\Delta p_{\text{pos,margin},j} \geq \Delta p_{\text{conv,ref},j} \geq -\Delta p_{\text{neg,margin},j} \tag{3.42}$$

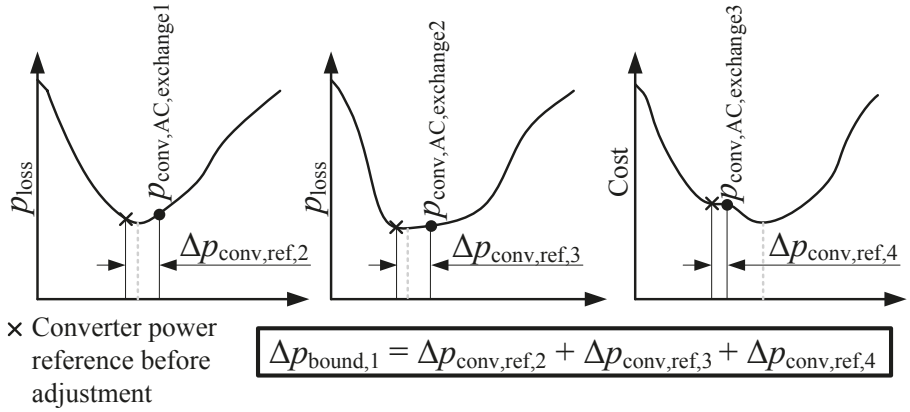

Fig. 3.17: Provision of $\Delta p_{\text{bound,1}}$ by other converters exchanging power with TSO 1 by adapting the power reference value calculated during first optimization process.

If $\Delta p_{\mathrm{bound},i}$ is non zero for more than one converter the adaptation process as described above will be applied at the converter, beginning with the largest $\Delta p_{\mathrm{bound},i}$. After each adaptation all converters provide adjusted positive and negative margin values and power references for potential subsequent adaptations.

3.3.5 Conclusion

The proposed method for global converter coordination on a local basis maintains full responsibility and a subjective controllability of each single TSO including converters within its area, however, certain difficulties arise. First a neutral third party must maintain a correct process by verifying reports of TSOs for plausibility, for example, and properness of their procedure during optimization and coordination with other TSOs. Second, the procedure of global coordination on a local basis becomes more complex the more TSOs are involved. Consequently, when a certain number of involved TSOs exceeds, coordination efforts are no longer justifiable and may take too long. This can therefore be a coordination method in very early stages of a European HVDC overlay grid, but it is necessary that this is eventually replaced by a method as explained in subchapter 3.2, for example, if a certain number of involved TSO and converters is exceeded.

3.4 Inherent coordination by energy transmission market

Besides the two described technical coordination concepts in subchapter 3.2 with a master controller instance (HVDC grid controller; see subchapter 2.3.2) and in subchapter 3.3 without having a centralized master controller, there is another market based option. This includes an inherent coordination of converter power reference values.

There will still in the future be cross border energy trading and possibly much more than is seen today. This is also one major driving force towards the implementation of an onshore HVDC grid. It is also possible that there are two different energy markets to trade. One is the conventional market that we have today which uses the AC transmission system for cross border trading and the other market could use the HVDC system for cross border trading. If all converter reference values are scheduled by this market based option there is an inherent coordination of converter reference values while DC transmission losses must be covered by adjusting converter power.

The most important disadvantage of this solution is the absence of any technical optimization either in overall AC and DC transmission losses, or in security or stability issues of the overall system. Maybe, this disadvantage could be overcome by integrating security and stability issues into the market as it is made in other areas e.g. the United States.

3.5 Conclusion

The most important issue in the operation of an HVDC overlay grid is the reasonable integration into AC transmission system operation and the coordination of all converters in order to prevent significant DC balancing control activation. This issue is discussed for the operational planning instance in this chapter.

On the one hand it is discussed from a centralized perspective assuming an instance that has an overview over and control of the HVDC grid and the affected parts of the AC transmission grid as well. This can also be assumed as the best solution from a technical optimum perspective given that all affected parts of the entire system are considered for optimization issues. Here an artificial intelligence optimization method (differential evolution) is used for mixed AC/DC OPF problems and the general convergence behavior, optimization results and further potential for improvement are identified.

On the other hand such an instance is so far not in place in Europe and it is a likely scenario that in early stages of a European overlay grid the responsibility for converters and the HVDC grid in general will be distributed among several TSOs. In such a case a global optimization is difficult and a distributed optimization and coordination is proposed in this chapter as well.

Another scenario is that reference values for converters are not provided according to technical objectives but only according to realized energy trades. In such a case HVDC transmission capacities are subject to commercial exploration. As this work focuses on technical options this is only mentioned as a possible scenario but not further discussed or analyzed.

4 Autonomous local reference value adaptation – Secondary control

In subchapter 2.3.2 the different control instances, primary, secondary and tertiary control, are introduced for HVDC grid operation. The previous chapter 3 describes operational planning thereby determining converter reference values in terms of their schedules as a part of tertiary control. Unscheduled changes of AC system's topology and/or generation/load pattern can significantly influence AC power flows and affect system stability. Thus, an adaptation of converter's reference values is necessary in order to perform HVDC overlay grid's preliminary task of relieving and supporting the AC grid. This control task can be subdivided in two sequences. One is adapting the converter reference values locally and therefore very quickly, whereas the other optimizes the adaptation of reference values later on. The local converter reference value adaptation which is based on global measurements (as indicted in Fig. 4.1) is in the focus of this chapter.

The optimization of converter reference value adaptation is not addressed in this work but is comparable to the optimization described for operational planning in chapter 3. This optimization will be performed possibly focusing on a smaller part of the grid as the computation time response and the computation speed requirements are more restrictive compared to tertiary control as it is described in subchapter 2.3.2.

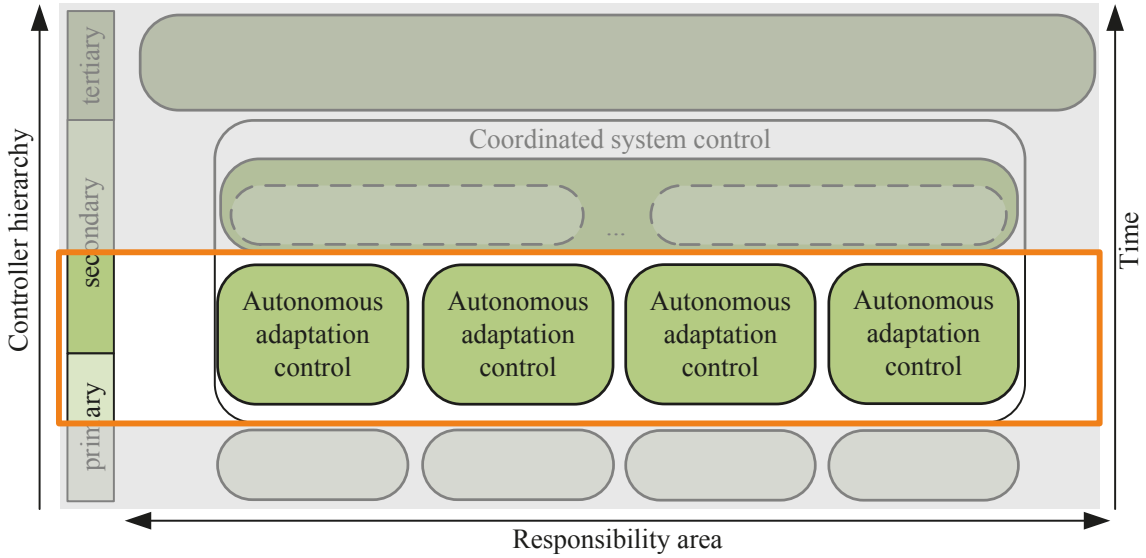

Fig. 4.1: Operation instance focused in chapter 4.

4.1 Requirements

The operational planning instance (tertiary control) assumes a certain generation and load pattern as well as a defined grid topology. Based on this information (possibly taking into account any uncertainty) optimal converter reference values are defined in order to meet an OF or set of OFs as described in chapter 3.

During operation significant deviations from the previously assumed grid state can occur. This may be caused by one of the following scenarios:

- Scenario 1: Significant deviation from renewable energy generation forecast
- Scenario 2: Power plant trip
- Scenario 3: Converter trip
- Scenario 4: AC line trip
- Scenario 5: Islanding of a part of the grid

In AC/DC converters it is inherent that they do not automatically take part in power distribution between the AC and DC grid, if the system state changes. Rather, converters control their reference values as much as possible and if the reference value is not adapted to the actual system state, its behavior will be equal to the pre-disturbance situation. Assuming that the current trend holds, more and more conventional power plants will be decommissioned and only a few within Europe will remain. Targets of this manner of different European countries can even lead to a situation that any remaining conventional power plants will concentrate in some countries, while other countries have no or almost no remaining conventional power plants.

As conventional power plants are the preferred source for balancing power provision in order to make the most of renewable energy sources, there may be balancing power hot spots in Europe. This would mean that balancing power flows have to be transmitted over long distances. In case of scenario 1 or 2 it is therefore reasonable to share the balancing power flows between the AC and DC grid. This share of power flows also limits the amount of transmission reserves to be maintained for such disturbed situations.

This is also true for other disturbances that significantly change AC power flows, such as in scenario 3 and 4 (converter or AC line trip). Power can be provided even to an islanded area power from the rest of the AC grid, via the HVDC overlay grid if an adaptation of reference values is implemented accordingly.

The requirements for an appropriate algorithm to adapt converter reference values in case of disturbances within the AC grid are:

- Detection of significant changed AC power flows (power flow direction and amount) from a global perspective
- Fast adaptation of converter reference values in the range of some hundred milliseconds
- Converter reference values as given by a tertiary control instance (chapter 3) should be respected as unaffected in undisturbed operation
- Share between AC and DC grid definable

4.2 State of the Art

4.2.1 Adaptation of converter reference values after a disturbance

A key motivation for the establishment of meshed HVDC grids are large offshore wind power plants as has been intended several years ago for the north sea in Europe [94] (see Fig. 4.2). Another example is that on the east coast of the United States of America (Atlantic Wind Connection) or other remote renewable energy production locations as is proposed for an Asian Supergrid using wind and solar power from the Gobi desert to provide load centers in the east Asian region [95]. Thus, all state of the art methods for automatic converter reference value adaptation after a disturbance, deal with phenomena that arise with regards to asynchronous AC grids interconnected with an HVDC system.

Fig. 4.2: Vision of the European Offshore Supergrid. [94]

Since there are no AC lines interconnecting these HVDC linked areas only loss of generation or load is considered which affects load frequency control of the disturbed area. Thus, only those converters of the disturbed areas are affected firstly and the methods presented hereinafter include the other AC areas in the balancing power provision process by modifying converters' power reference values accordingly. In consequence the balancing power is distributed across several AC areas.

Existing methods for participation of an HVDC system in load frequency control are therefore based on frequency deviation at the AC point of common coupling as it is for power plants within the AC grid. HVDC converters realizing a connection to another asynchronous AC area can be seen as a generating unit for a single AC grid, which justifies the analogy that balancing power must be provided by another AC grid.

[96] and [97] are methods that connect offshore wind power generation with the onshore AC grid by using P2P and a multiterminal HVDC system respectively. The onshore AC converter(s) adapt their active power reference value according to the onshore system frequency. As a result the power output of the windmills is regulated using pitch angle control.

A similar concept is proposed by [100]. The motivation for this approach is that a VSC converter can provide balancing power to an AC grid much faster than a conventional power plant. For that approach it is assumed that an HVDC system interconnects two asynchronous areas. When the frequency drops below 49.5Hz the necessary amount of balancing power is determined and the converters power reference value is adapted accordingly. When frequency reaches a value above 49.95 Hz the converters decrease the amount of transmitted balancing power while the conventional generating units in the disturbed area increase balancing power output by the same amount until the active power reference value of the converter reaches its initial value. With this method the frequency dip is much smaller than it would be if only a conventional balancing power provision were used, since more power plants provide balancing power (power plants of the disturbed and the undisturbed HVDC connected AC system).

[101] and [102] also use the frequency deviation as a control variable for load frequency control support by a multi terminal HVDC system and this does not require communication within the HVDC system since a voltage droop control is used for DC energy equilibrium.

The necessity for participation of an HVDC scheme in load frequency control has already been identified. All approaches, as previously described, are based on frequency deviation at the converter's AC point of common coupling used as controlled variable [96]-[106]. If such an algorithm is applied to an overlay HVDC grid, it would mean that in case of a frequency deviation at the AC side of one converter n its reference power p_n would change, according to (4.1). While Δf_n is the frequency deviation at the corresponding AC PCC and $k_{\Delta f,n}$ the frequency control droop of converter n. Assuming an ideal frequency step, a change in power reference would result as it is shown in Fig. 4.3 from point 1 to 2.

$$\Delta p_{\mathrm{conv,ref},n,f} = \Delta f_n \cdot k_{\Delta f,n} \tag{4.1}$$

A frequency deviation would cause a converter power reference change. While the continuous process would include a simultaneous change in DC voltage due to DC energy imbalance, the power reference would also be affected by voltage control. Assuming a straightforward voltage droop characteristic as most of the aforementioned references use, the change in reference power due to the voltage control can be described according to (4.2). The total change in reference value (frequency droop and DC voltage droop) results from (4.3). This is illustrated in Fig. 4.3 by a change from point 1 to 3.

$$\Delta p_{\mathrm{conv,ref},n,v} = \Delta v_{DC,n} \cdot k_{\Delta v_{DC},n} \tag{4.2}$$

$$\Delta p_{\mathrm{conv,ref},n} = \Delta v_{DC,n} \cdot k_{\Delta v_{DC},n} + \Delta f_n \cdot k_{\Delta f,n} \tag{4.3}$$

Numerous converters are involved when considering an entire HVDC grid. The total power of the n converters within the HVDC system in (4.4) are derived from (4.3) and include the pre-disturbance converter reference values $p_{\mathrm{conv,ref},n}$.

$$p_{\mathrm{DC}} = \sum_{i=1}^{n} p_{\mathrm{conv,ref},n} + \Delta v_{\mathrm{DC},n} \cdot k_{\Delta v_{\mathrm{DC}},n} + \Delta f_n \cdot k_{\Delta f,n} \tag{4.4}$$

When modifying (4.4) in such a way that losses are excluded, the converter references sum up to zero and voltage would be the same at all DC nodes. Furthermore, the total DC system power p_{DC} should be equal to zero for $t \to \infty$ in order to maintain the energy equilibrium (see chapter 5) and frequency deviation between node of the interconnected AC system will become equal to zero for $t \to \infty$ as well. Those assumptions lead to (4.5) if charging / discharging of DC system capacitances is neglegted.

$$p_{\mathrm{DC}} = \Delta v_{\mathrm{DC}} \sum_{i=1}^{n} \cdot k_{\Delta v_{\mathrm{DC}},n} + \Delta f \sum_{i=1}^{n} \cdot k_{\Delta f,n} \overset{!}{=} 0 \tag{4.5}$$

Thus DC voltage deviation further increases from point 3 in Fig. 4.3 until $\Delta p_{\mathrm{conv,ref},n,v} = -\Delta p_{\mathrm{conv,ref},n,f}$. That is the change in power reference value due to frequency droop is equal to the negative change in power reference value as a result of DC node voltage droop control (see Fig. 4.3 transition from point 3 to 4). Thus, the effect of frequency control of the HVDC system disappears after a short time due to reasons of DC energy equilibrium.

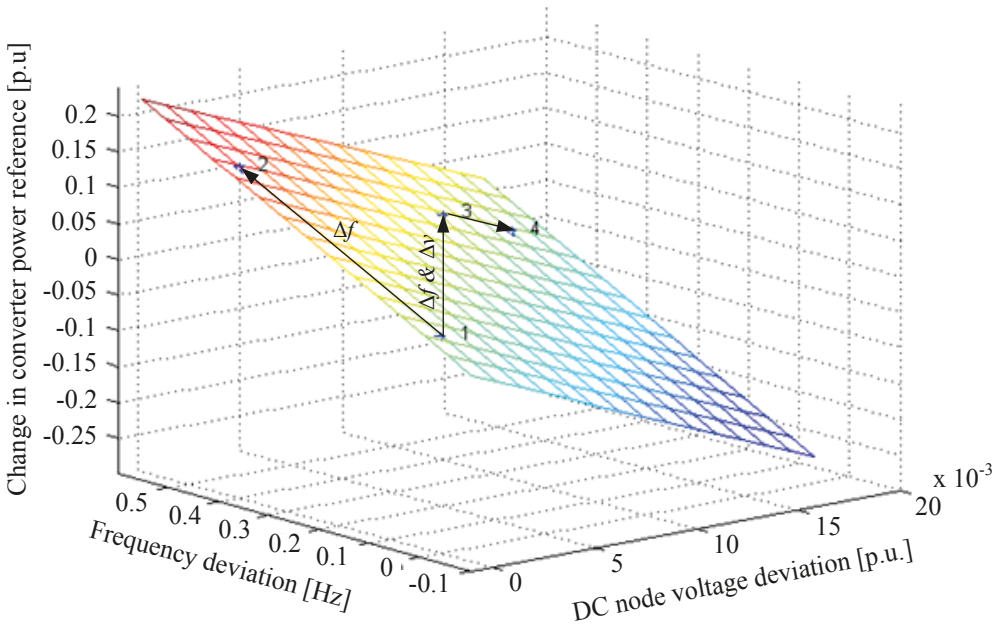

Fig. 4.3: Change in converter's power reference according to DC voltage and AC frequency deviation using frequency droop control (1→2) or frequency and DC node voltage droop control (1→3→4) according to (4.1) and (4.4)/(4.5) respectively.

Tab. 4-1 summarizes which functionalities are already covered by state of the art or state of research algorithms and which functionalities, particularly for overlay HVDC grids, remain unsolved. Necessary converter reference value adaptations for HVDC grids interconnecting asynchronous AC system, as it is the case for offshore HVDC grids, already exist. Algorithms for an autonomous adaptation of converter reference values for overlay HVDC

grids (e.g. for balancing power tranmission) are not within the state of research or even state of the art.

Using state of the art or research methods, the overlay HVDC grid spanning a single synchronous zone is only taking part in primary load frequency control in the case of an AC power imbalance (scenario 1 or 2). That is at least for some seconds before frequency deviation is the same at all AC nodes within the synchronous AC system. The amount of balancing power transmitted through the HVDC grid is less, the smaller the frequency differences between the converter AC PCCs becomes. From this moment balancing power is no longer transmitted via the HVDC grid as the DC energy equilibrium must also be met (see (4.5)).

Tab. 4-1: Already existing algorithms (✓) regarding HVDC converter reference value adaptation and further need for research (✗).

Functionality provided / delivered by HVDC grid	HVDC grid interconnecting asynchronous AC systems	Overlay HVDC grid without interconnections between asynchronous AC systems	Overlay HVDC P2P connection
Support of load frequency control (additional balancing power)	✓	- (not possible as no power generation or storage capacity within the HVDC grid)	- (not possible as no power generation or storage capacity within the HVDC grid)
Support of the AC transmission system in case of unscheduled power flow changes	- (not possible as no parallel AC grid exists)	✗ (required according to subchapter 4.3)	✓ (inherently given by emulation of an AC line)
Support of the AC transmission system in case of unscheduled power flow changes respecting converter schedules	- (not possible as no parallel AC grid exists)	✗ (required according to subchapter 4.3)	✗ (AC line is emulated in normal and disturbed operation)

Secondary and tertiary load frequency control caused power flow deviations, as well as other unscheduled power flow changes, will not be transmitted through HVDC grid. An abrupt and unscheduled load flow change can cause an equipment overload or instability if there is not a fast algorithm to make use of the HVDC transmission capacity.

For the first European onshore HVDC project in MMC technology (INELFE, P2P) several control functions are proposed. There are two realization options for determination of converter's reference power [108]:

- In proportion to parallel transmitted AC power
- As a function of the voltage angle differences on both AC sides of the P2P connection (emulation of an AC line)

Both approaches overcome the natural blocking behavior of an HVDC system by emulating an AC link but do apply for just a P2P connection.

The requirements as given in subchapter 4.1 are not fulfilled by any of the already existing algorithms. Thus, subchapter 4.3 introduces an algorithm for the mentioned purpose applicable for overlay HVDC grids as defined by the requirements according to subchapter 4.1. Therefore, it is reasonable to detect global AC power flow changes between converter AC PCCs as the overlay HVDC grid can take part in those power flow changes. Unscheduled power flow changes affecting shorter distances must only be covered by the AC transmission system.

Thus, it is necessary to use wide area information to have a global overview on power flow changes. As information provided by a SCADA will take much longer than the required some hundred milliseconds (after a disturbance took place) wide area measurement data provided by PMUs and a WAMS is the most reasonable solution to derive information about unscheduled global power flow changes. Appendix F therefore gives an overview on how a PMU and WAMS function and which delays are included.

4.3 Angle Gradient Method

Active power flows between node *i* and *j* can be described according to (4.6) and Fig. 4.4.

$$p_{ij} = \frac{r_{ij} \cdot v_i^2 - v_i \cdot v_j \cdot r_{ij} \cdot \cos(\Delta\delta) + v_i \cdot v_j \cdot x_{ij} \cdot \sin(\Delta\delta)}{r_{ij}^2 + x_{ij}^2} \tag{4.6}$$

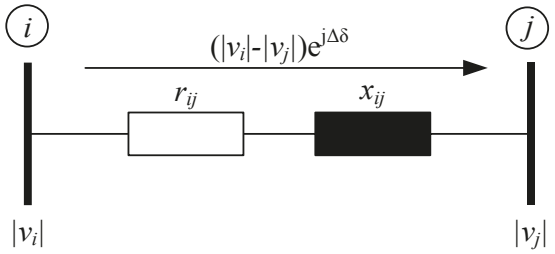

Fig. 4.4. Model for power flows on AC transmission lines according to (4.6)**.**

Using permissible simplifications for the transmission grid layer (see Appendix E) (4.6) becomes (4.7). This formula gives a simplified description for power flows within grids with an *r*/*x* ratio much smaller than 1. This is true for the transmission and the upper level

of the distribution level in Europe. These are the grid levels affected / relieved by the HVDC system.

$$p_{ij} = \frac{v_i v_j}{x_{ij}} \sin(\Delta\delta) \tag{4.7}$$

According to this, the main influencing factor for power flows between two nodes in the considered AC grid level is the angle difference between both Δδ.

Voltage magnitudes at the transmission grid level can be assumed to be constantly close to 1 p.u.. Thus voltage magnitudes do not significantly affect AC power flows according to (4.7).

Contrary to power flow controlling devices affecting a specific line impedance and thus mainly the power flow on a specific line, the HVDC system relieves a whole AC sector between two converter connected AC nodes. The AC grid impedance between those is constant if no significant topology change takes place within the considered sector to be relieved. Thus, it is feasible to use angle differences in order to detect power flow changes while voltage angle differences can be measured using a WAMS as described in Appendix F.

The voltage angle difference between HVDC converter's AC PCCs or nearby nodes therefore give information about global power flow gradients that can be affected by the HVDC system. As described in chapter 3 the tertiary control (operational planning) defines power reference values according to, for example, a forecasted electrical energy generation and system load pattern to meet an optimum. A power flow pattern then results. Power flows can deviate from this pattern as a consequence of:

- Unscheduled significant change of load
- Unscheduled significant change of electrical energy generation
    - Trip of conventional power plant
    - Connection trip of a renewable energy infeed
    - Significant deviation from renewable energy infeed forecast
- Trip of transmission equipment
- AC/HVDC converter trip

In order to avoid such abrupt unscheduled power flow changes to negatively influence system stability or overload transmission equipment, an adaptation of the scheduled converter active power reference values is necessary.

A change in power flow patterns can be detected using PMUs and a WAMS. It can be assumed that PMUs are available within each new protection device [116] and therefore at or even nearby each new HVDC converter station. Given that the proposed method is founded on measuring changes in voltage angle differences in the grid to allocate power flow changes, it has been named angle gradient method (AGM) and was first published in

[O-1], [O-8]. The basic concept of the AGM and of deriving global power flow information from WAMS data is shown in Fig. 4.5.

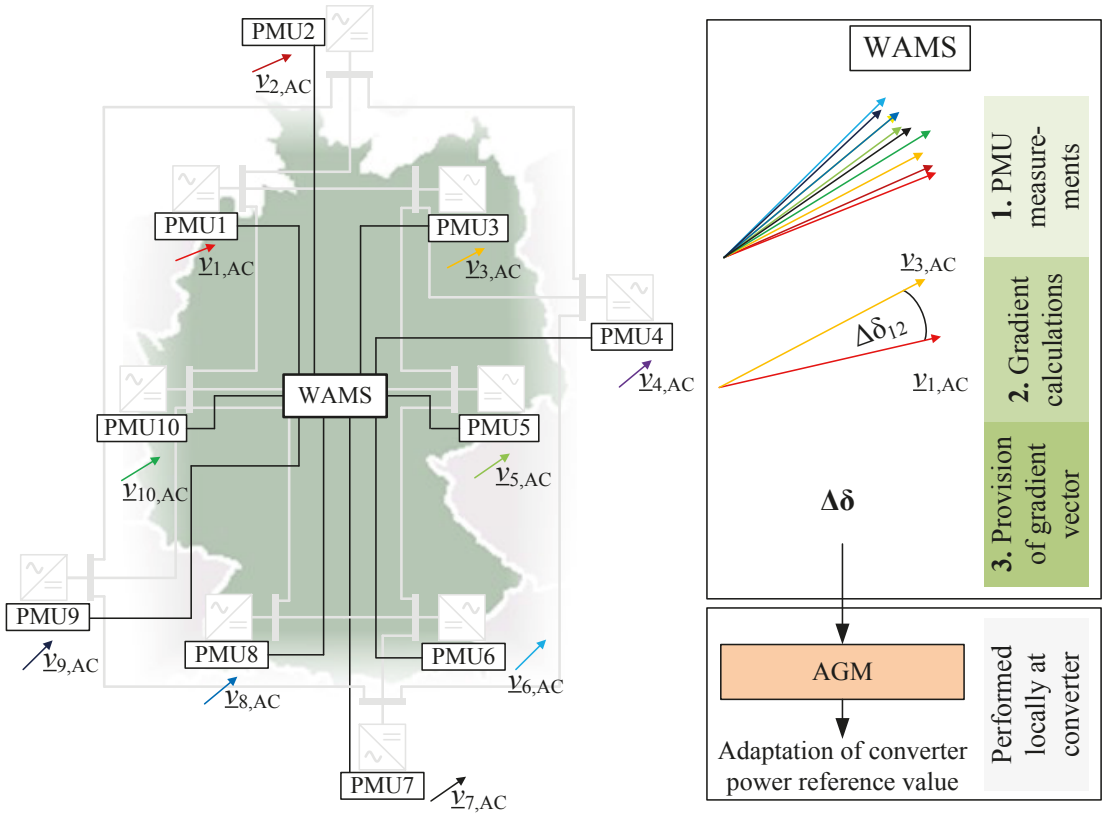

Fig. 4.5: Functionality of WAMS exemplary for an HVDC grid with 10 converters.

For further considerations regarding the AGM, each converter is assigned to a particular HVDC converter observability area. This area consists of one or more AC nodes around the converter's AC PCC. This approach is illustrated in Fig. 4.6. Furthermore, converter's AC PCC is defined as HVDC converter observability area center node within each HVDC converter observability area.

Using the angle gradient information provided by WAMS, power flows between HVDC converter observability area center nodes of directly adjacent responsibility areas are calculated using (4.7). A continuous comparison of this value with power flows resulting from the latest schedule and forecast information identifies significant power flow changes in its direction and magnitude.

$$\Delta p_{\text{schedule},ij} = p_{\text{WAMS},ij} - p_{\text{schedule},ij} \tag{4.8}$$

Since a HVDC converter observability area can be directly connected to several others, power flows on one connection can be transit power flows. Considering, for example, an unscheduled power flow from node 6 to node 2 in Fig. 4.6, the HVDC converter observability area of node 3 will be a transit area. Unscheduled power flows are intended to be commutated into the HVDC grid at their origin and should not be considered for intermediate / transit HVDC converter observability areas. Thus, power flow exchanges of an

HVDC converter observability area center node adds up with other HVDC converter observability area center nodes, and transit power flows are eliminated. The change in power flows with regard to the latest schedule can be determined by (4.9) where C is the set of HVDC converter observability area center nodes of directly adjacent HVDC converter observability areas to the considered HVDC converter observability area.

$$\Delta p_{\text{schedule},i} = \sum_{j \in C} \left(p_{\text{WAMS},ij} - p_{\text{schedule},ij} \right) \tag{4.9}$$

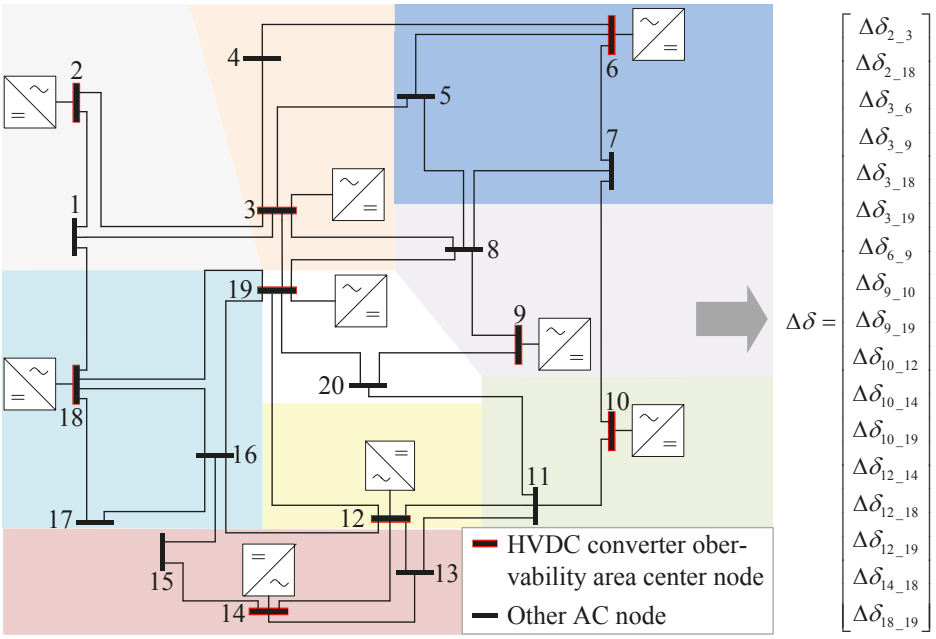

Fig. 4.6: Approach of HVDC converter observability area (marked with different colours) and HVDC converter observability area center node assignment.

$\Delta p_{\text{schedule},i}$ is the deviation between the scheduled and the actual power flow and is subject to be shared between the AC and HVDC grid.

In order to get as close as possible to a potential optimum, for example, regarding system losses as well as stability and maximum load margins, the AGM makes use of the latest schedule. As described in chapter 3 the schedule is a result of an optimization process ideally of the overall AC/DC system. Thus the optimization output includes information about the AC/DC power flow division at each HVDC converter observability area center node i and a power flow sharing factor $k_{\text{AC\_DC},i}$ will be defined according to (4.10) considering converters' reference value $p_{\text{ref,schedule}}$ and all scheduled AC power flows parallel to the DC lines. $k_{\text{AC\_DC},i}$ will vary depending on both systems (AC and DC) loading and switching state, for example.

$$k_{\text{AC\_DC},i} = \frac{\sum_{j \in C} p_{\text{schedule},ij}}{p_{\text{ref,schedule},i}} \tag{4.10}$$

According to the power flow sharing factor $k_{\text{AC\_DC},i}$, $\Delta p_{\text{schedule},i}$ is shared between the AC and DC grid respectively. The amount of unscheduled power flow that is supposed to be

commutated to the HVDC grid is added to the latest converter schedule value. Consequently, the adjusted converter reference values can be determined according to (4.11).The entire process is sketched in Fig. 4.7.

$$p_{\mathrm{conv,ref},i} = p_{\mathrm{ref,schedule},i} + k_{\mathrm{AC\_DC},i} \cdot \Delta p_{\mathrm{schedule},i} \tag{4.11}$$

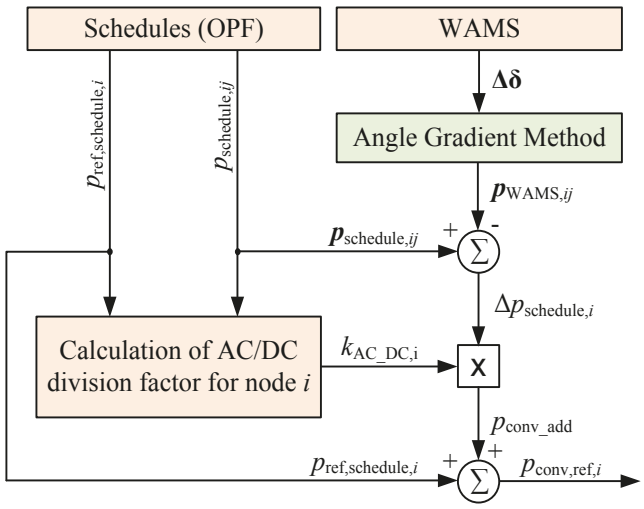

Fig. 4.7: Calculation of converter`s adapted reference value combining schedules and results of AGM in consequence of a disturbance.

Fast reaction as a result of a disturbance (as mentioned on page 65 in the context of AGM) means a required reaction within 1-3 seconds. WAMS' time delay of 50-200 ms (see Appendix F) can be considered to be noncritical, that is it will not negatively affect AGM's performance.

In addition to the fast local adaptation of converter reference values after a disturbance, a centralized optimization of converter power reference adaptation is another option. This centralized calculation of optimal adaptations will take much longer than the AGM, primarily due to a much higher calculation effort but must be significantly faster than tertiary control (see chapter 3). However, the calculation algorithm used for tertiary control and its coordinated adaptation of converter reference values (as slower part of secondary control) can be the same.

In this case, AGM will serve as a fast converter reference value adaptation avoiding equipment overloading immediately after the disturbance. Later on an optimized re-definition of converter power reference values will be provided by the slower part of the secondary control, which is not part of this thesis.

4.4 Numerical case studies

In order to verify the proposed AGM, some test scenarios are defined in order to show its effect if unscheduled power flows in the AC grid occur. As mentioned on page 65 those unscheduled power flows can be caused by:

- Unscheduled significant change of load
- Unscheduled significant change of electrical energy generation
    - Trip of conventional power plant
    - Connection trip of a renewable energy infeed
    - Significant deviation from renewable energy infeed forecast
- Trip of transmission equipment
- AC/HVDC converter trip

The first two imply a mismatch in the AC power balance. As an AC power imbalance affects the AC system's frequency this will imply the activation of load frequency control. Thus, balancing power flows propagate through the AC grid. Scenario 1 represents a corresponding numerical case study (power plant trip).

The trip of AC transmission equipment represented by an AC line trip is demonstrated in scenario 2. A multiple AC line trip can result in the electrical islanding of an AC area. With an existing overlay HVDC grid this can be the only remaining interconnection between the synchronous AC grid and the electrical island. Scenario 3 shows the effect of the AGM if an islanding within the AC grid occurs simultaneously with a converter trip within the electrically islanded area.

Summarizing, the following three scenarios show the positive impact of AGM's converter reference value adaptation in case of disturbances within the AC grid:

- Scenario 1: Power plant trip
- Scenario 2 : AC line trip
- Scenario 3: HVDC grid as single remaining interconnection with an electrically islanded AC area

Scenario1 implies the activation of load frequency control. For AGM two levels of this control are of interest. These are primary and secondary load frequency control. Primary control is a joint action of all TSOs within the European synchronous AC system while secondary control is supposed to be activated only in the disturbed control area / block [122]. In order to reproduce both control levels of load frequency control for scenario 1, the reference grid as introduced in subchapter 2.4 (see Fig. 2.5) is split in several control areas CAs (see Fig. 4.8):

- CA West
- CA North
- CA Germany
- CA East
- CA South

Primary and secondary load frequency control levels are of interest when considering the impact of AGM as both are active for a maximum of 15 minutes. This is equal to the update interval of tertiary control as proposed in chapter 3. Tertiary control level of load frequency control becomes active after a longer time horizon after the disturbance took place (15 minutes) and thus, it is a subject for consideration within operational planning and not for AGM considerations.

Synchronous machines are modelled with equation of motion and a time constant $T_a = 10$ s and a damping constant of $D = 2$. In order to avaoid effects related to reactive power phenomena and reaching of power plant power limits nominal power of power plants is defined to be 6 GW for each power plant in CA Germany and CA North, 13 GW for CA East, 8GW for CA South and 44 GW for CA West.

DC energy balance within the reference grid is continuously ensured by an implementation of a *p-v*-characteristic for DC node voltage control as described in chapter 5.

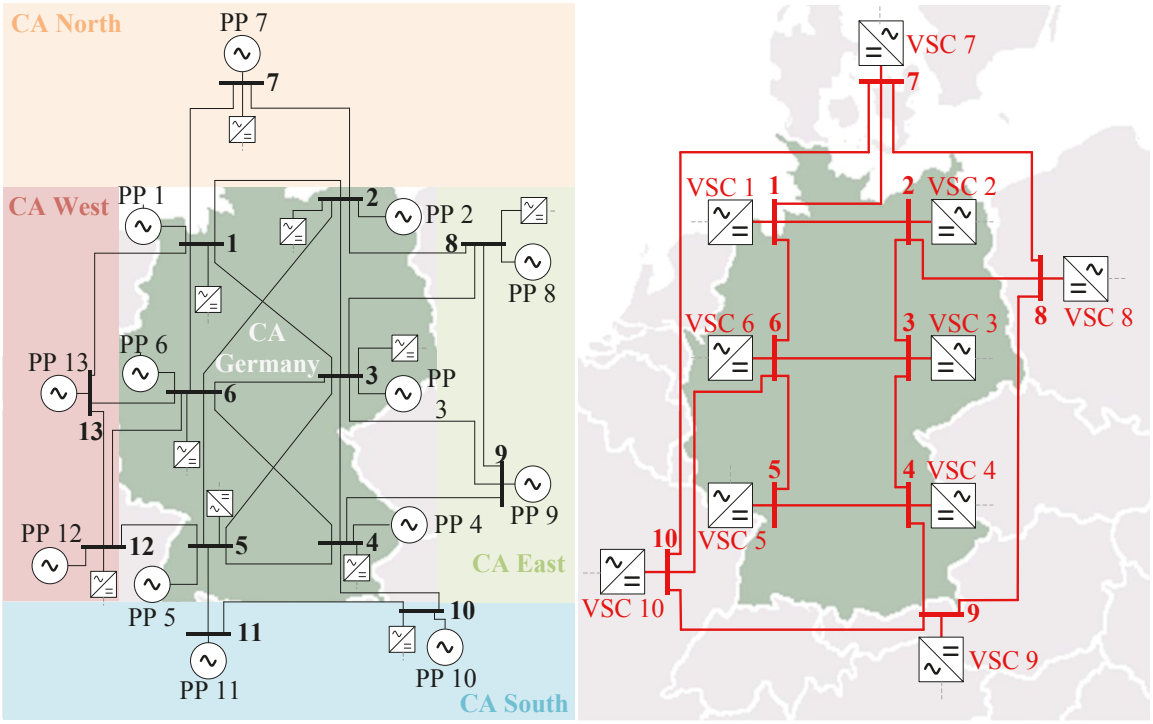

Fig. 4.8: Left: AC part of the reference grid and fictive control areas (CAs), Right: DC part of the reference grid.

4.4.1 Scenario 1 - Power Plant trip

For scenario 1 a power plant trip at AC node 6 (power plant (pp) 6 in Fig. 4.8) is assumed. Due to the power plant trip all power plants of the reference grid start their balancing power generation as part of the European primary load frequency control according to [122] (energy market aspects are neglected here). It is replaced by secondary control a short time after. Thus, only power plants of the disturbed CA Germany generate balancing power on a term longer than a few seconds.

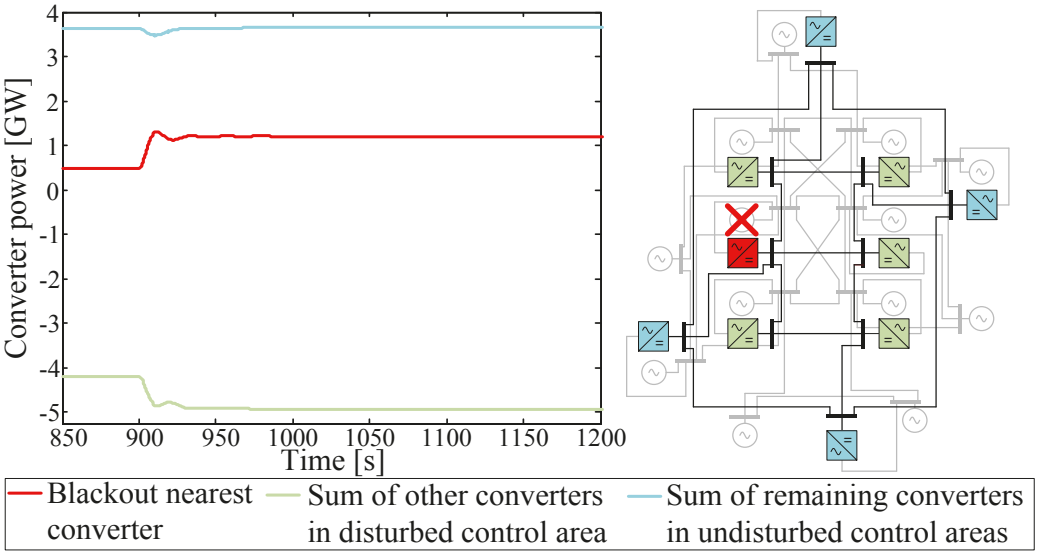

Fig. 4.9: HVDC converter power after trip of power plant 6.

Using WAMS data, AGM at VSC 6 (see Fig. 4.8) identifies the lack of power and at the other converters in CA Germany nearby power plants increase power generation. Thus, converter power reference values are adapted accordingly to take part in transmismitting balancing power. Fig. 4.9 shows that VSC 6 (close to tripped power plant) feeds more power from the DC to the AC grid and all other converters of the disturbed CA Germany (VSC 1 – VSC 5) feed more power from the AC to the DC grid.

Power plants of undisturbed control areas (CA, West, North, East and South) only take part in primary load frequency control for a short period of time immediately after disturbance takes place. Due to AGM, this is also reflected by converters' power (see Fig. 4.9)

It is also an indicator of improvement that power plants of undisturbed CAs are relieved by balancing power actions earlier than without AGM. This is exemplarily demonstrated by power plant 12 (see Fig. 4.10), which delivers slightly more peak power during primary load frequency control. Additionally this power plant generates balancing power for approximately 100 s. In the event that AGM is not used, it takes approximately 400 s. Further simulation results are shown in Appendix F.

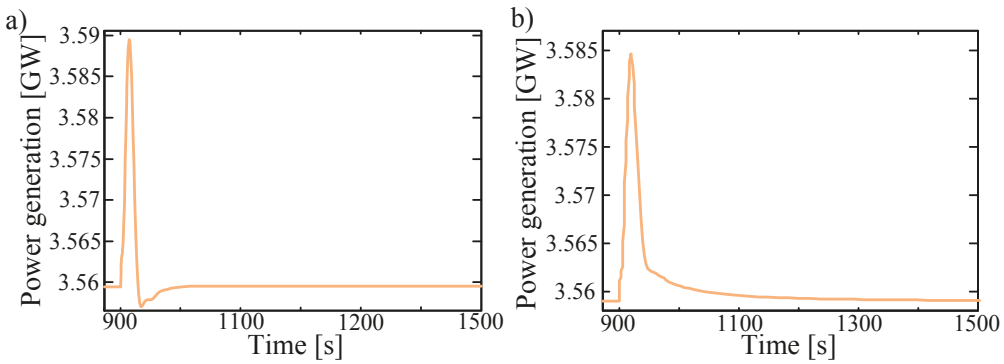

Fig. 4.10: Power generation of power plant 12 outside disturbed control area during load frequency control with (a) and without (b) AGM after trip of power plant 6.

4.4.2 Scenario 2 - AC line trip

As shown in the previous subchapter 5.4.1, AGM performs an automatic relief of the AC grid if its power flows deviate significantly from the schedule. The best results can be achieved by considering AC corridors that are directly in parallel to the overlay HVDC grid. In order to show AGM's effect on a line trip if its corridor is not in parallel to the overlay grid, AC line between node 13 and 1 is tripped.

Remaining interconnections of AC node 13, which is not directly connected to the overlay HVDC grid, are to AC node 6 and AC node 12. As well as AC node 1, both are directly connected to the overlay HVDC grid. Pre-disturbance AC power flows from AC node 1 to AC node 12 are redirected according to AC grid impedances. Thus, AC power flow increases between:

- AC node 1 and 6,
- AC node 6 and 12,
- AC node 6 and 13,
- AC node 5 and 12 and
- AC node 12 and 13.

This is also indicated by arrows in Fig. 4.11. AC-power flows parallel to DC corridors significantly change between:

- DC node 1 and 6 and
- DC node 1 and 12.

This is detected by the AGM and converter reference values are adapted accordingly on a local basis. Thus, a part of the pre-disturbance AC power flow between AC node 1 and 12 is redirected to the DC grid via converter VSC 1 and is fed back to the AC grid nodes 6 and 12 via converters VSC 5 and VSC 10 (see Fig. 4.11).

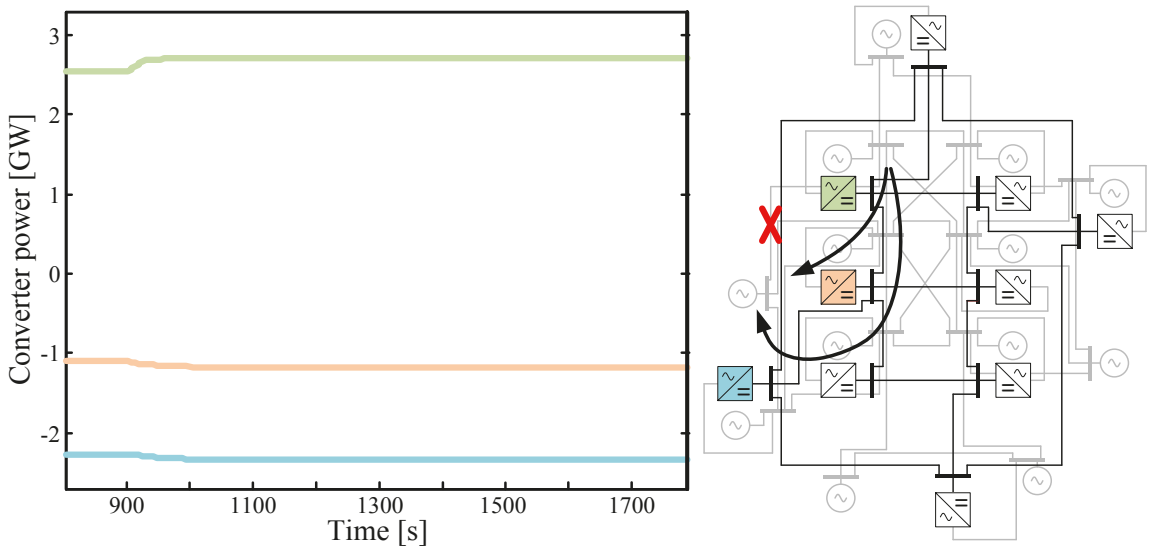

Fig. 4.11: HVDC converter power during and after an AC line 26 trip.

4.4.3 Scenario 3 - HVDC grid as single remaining interconnection with an electrically islanded AC area

Without an HVDC overlay grid an islanding process on the AC side can lead to significant power imbalances in both AC grids if there was a power exchange between both before the disturbance took place. Although the ad hoc group "Geographical distribution of reserves" [123] defines how much balancing power can be obtained from other CAs, an islanding can occur in the middle of a control area. Due to the full controllability of an HVDC system, this connection between the isolated AC area and the rest of the AC grid would remain and can transmit balancing power as well as the previous AC power flows between both areas.

In order to show the usefulness as well as functionally of AGM in that particular case a scenario is defined for the given reference grid, according to Fig. 4.12. Node 8 and 9 of CA East are isolated from the interconnected AC system. Simultaneously power plant 8 partially trips within the isolated area.

Due to the lack of power in CA East the voltage angle in this CA decreases and due to small pre-disturbance power flows from CA Germany to CA East there is a surplus of power in CA Germany which increases the voltage angle in that CA and decreases those in CA East. Consequently the angle differences between both CAs prompt the AGM to transmit power to the isolated CA East via the HVDC system. Particularly during primary load frequency control the directly adjacent converters within CA Germany (VSC 2 and 3) provide balancing power to the isolated CA East until the remaining power plant 9 in CA east fully makes up for the lack of power. If no HVDC overlay grid and no AGM would be applied, power plants of the interconnected area would not take part in load frequency control of the isolated area. After this primary load frequency control VSC 8 only imports a small amount of power from CA Germany which was transmitted via the AC system prior to the disturbance (see Fig. 4.13 and also Appendix I).

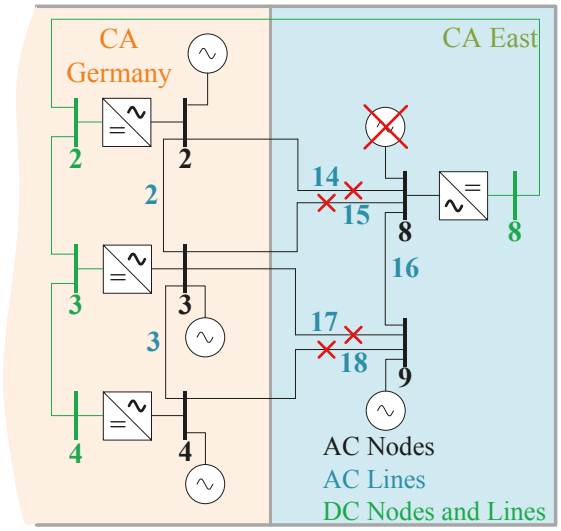

Fig. 4.12: Detail of the reference grid showing the disturbances leading to an islanding and demand for balancing power.

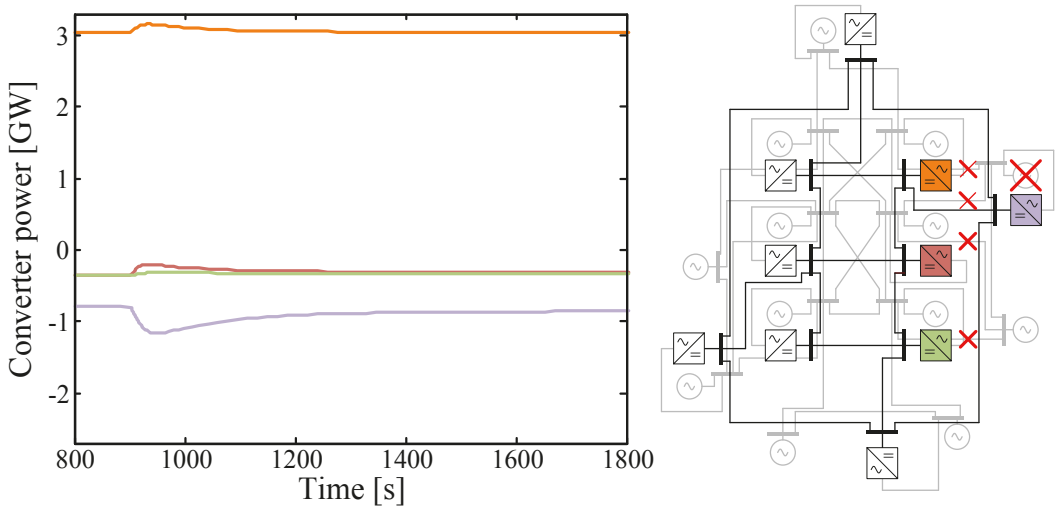

Fig. 4.13: Converter power values during islanding of AC nodes 8 and 9 with simultaneously partial trip of power plant 8.

4.5 Backup mechanisms for measurement value acquisition

The AGM fully relies on the measurement of an intact WAMS and thus on a communication system. Since AGM becomes active in case of disturbances of the grid, a certain degree of reliability should be ensured. Thus, this subchapter identifies alternative data sources if any WAMS equipment trips and provides a short discussion on the importance of a precise value of grid impedance between two converters' AC PCCs.

AGM, as proposed here, fully relies on a reliable provision of voltage angle difference information from a WAMS. This subchapter provides backup solutions for measurement value acquisition to keep the AGM and its basic functionality running. Different scenarios can occur (see Fig. 4.14):

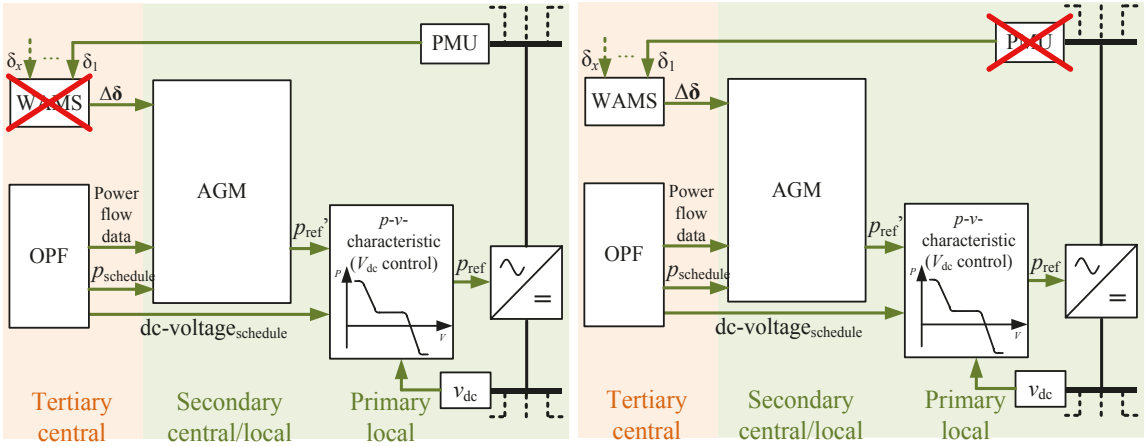

Fig. 4.14: Possible disturbances within WAMS' data acquisition and provision. On the left side disturbance scenario 1 and on the right side disturbance scenario 2.

- Scenario 1: Trip of entire WAMS or its communication towards convered control
- Scenario 2: Trip of a PMU or its communication towards WAMS

Scenario 2 assumes that all information, which has been provided by the WAMS is suddenly missing for a single or all converters. In the case of scenario 1, only one PMU measurement is missing but information from other PMUs are still available.

4.5.1 Scenario 1 - Trip of WAMS

It is possible that WAMS information is lost if the WAMS itself or the communication towards WAMS trips. When WAMS information is no longer provided and no measures are taken, the provided angle gradient vector $\mathbf{\Delta\delta}$ is no longer available for AGM and the global information on power flow gradients is lost.

A possible solution would be to maintain all converter power reference values until WAMS information is available again. This blocks AGM functionality and should be avoided.

Usually an HVDC converter is embedded in an appropriate AC substation. Thus all AC measurements as three phase voltage and current and the resulting apparent power for protection issues, for example, are also available for the converter [126]. In normal situations with an intact WAMS, information on the power flows between AC converter nodes are available (by WAMS) as well as the apparent power at each line outlet resulting from measurements within the AC substation. As such, a factor λ_{ij} between $p_{\mathrm{WAMS},ij}$ and the measured apparent power $s_{ij,x}$ (see Fig. 4.15) can always be defined according to (4.12).

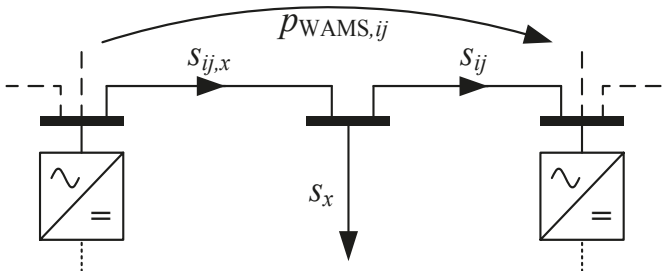

Fig. 4.15: Exemplary scenario for definition of power actor λ_{ij}.

$$\lambda_{ij} = \frac{p_{\mathrm{WAMS},ij}}{s_{ij,x}} \tag{4.12}$$

In case the WAMS trips the pre-trip factor λ_{ij} and the onsite measured apparent power $s_{ij,x}$ are still available. A multiplication of both delivers a replacement value for $p_{\mathrm{WAMS},ij}$ called $p_{\mathrm{WAMS},ij}$' according to (4.13).

$$p_{\mathrm{WAMS},ij}{}' = \lambda_{ij} \cdot s_{ij,x} \tag{4.13}$$

Apparent power also includes reactive power. Line earth faults are situations when apparent power increases significantly due to reactive power. Since line protection reacts immediately in the range of ms, it can be assumed that AGM which reacts in the range of 1-3 s, is not significantly affected. It is also possible to measure voltage. In case of a line earth fault

voltage would decrease significantly and a converter could provide short circuit power if it is needed. Simultaneously this can be an indicator to actively slow AGM time constants.

4.5.2 Scenario 2 - Trip of PMU

If PMU information is no longer provided and no measures have been taken, the provided angle gradient vector **Δδ** has non-determined values and AGM may interacts incorrectly at each involved converter or it no longer interacts. Since AGM is designed to relieve the AC system when it is put under additional stress in disturbed situations, whether or not the reliability of AGM can be maintained is analyzed, even if needed information is no longer available through WAMS.

The following measures are theoretically available:

- Measure 1: Disable AGM for all converters
- Measure 2: Using SCADA information
- Measure 3: Maintain last available PMU information
- Measure 4: Disable AGM for converter with tripped PMU information

Measure 1

Thus, the theoretically possible measure to maintain all involved converter power reference values is not reasonable, as long as a single PMU data is missing. If this measure would be applied AGM functionalities are blocked as long as single PMU information is missing. Thus, this measure is rejected.

Measure 2

Another posibility is to use SCADA information from the point in time when PMU information is lost. The SCADA estimates the missing voltage angle information based on global information and provides it instead of the measured PMU information. To be realized, it would need a very fast state estimation meeting time requirements related to second order swing equation (4.14).

$$\ddot{\delta} = \frac{\omega_0}{T_A} \cdot \left(p_m - p_e \right) - D \cdot \Delta\omega \tag{4.14}$$

$$\ddot{\delta} = 2\pi \dot{f} \tag{4.15}$$

According to [124] this is not possible today even if the use of PMUs can improve state estimation performance [124], [125]. At present, dynamic state estimation is under investigation and could make this option be possible in the future [110]-[113].

Measure 3

Thus, from the present point of view, a temporary solution is needed until SCADA information will be available after a time delay. This can be maintain the last known PMU information generated by the tripped PMU as long as online information is missing. That

includes the advantage that all other online PMU information are further used and that the AGM can provide its functionalities with the most available information. In case that no disturbance in the grid occurs, AGM would not change any converter power reference values, as it is required.

Measure 4

Alternatively the converter with missing PMU information maintains its reference value, which indicates a deactivated AGM for this converter but only for the converter where PMU information is missing.

Discussion

Assuming a disturbance the worst case is, if the PMU of the disturbance's closest converter trips. The change in voltage angle will be the highest there (close to the disturbance) and this change is unforeseeable for WAMS. The more distant an AC node is from a disturbed AC node, the less the voltage angle deviation will be. Therefore, the voltage angle differences $\Delta\delta_{ij}$ between the disturbed and all directly neighboring nodes is the most incorrect if the last available δ_i of the tripped PMU is maintained. That is disturbance surrounding PMUs (except the tripped one) will measure a decreasing voltage angle and the voltage angle information closest to the disturbance (at the tripped PMU) will remain unchanged according to measure 3. Thus, a power delivery from the power plant trip to the surrounding AC nodes is estimated (assuming measure 3) which is inverse to physical power flows (see Fig. 4.16 and Fig. 4.17 a). This can overload lines due to loop flows between DC and AC (refer to Fig. 4.17 b).

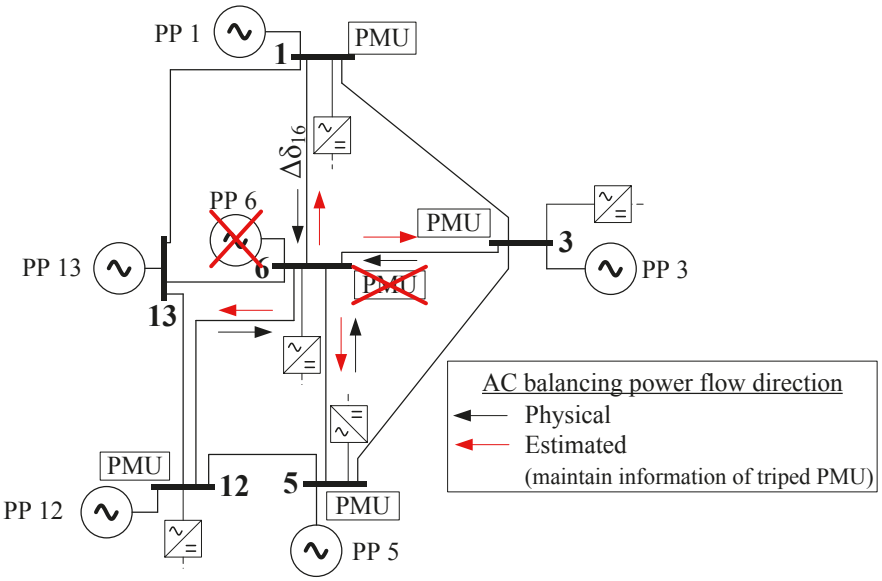

Fig. 4.16: Section of reference grid according to subchapter 2.4 around tripped power plant and simultaneously tripped PMU (nearby) – physical and estimated balancing power flow direction (assuming measure 3).

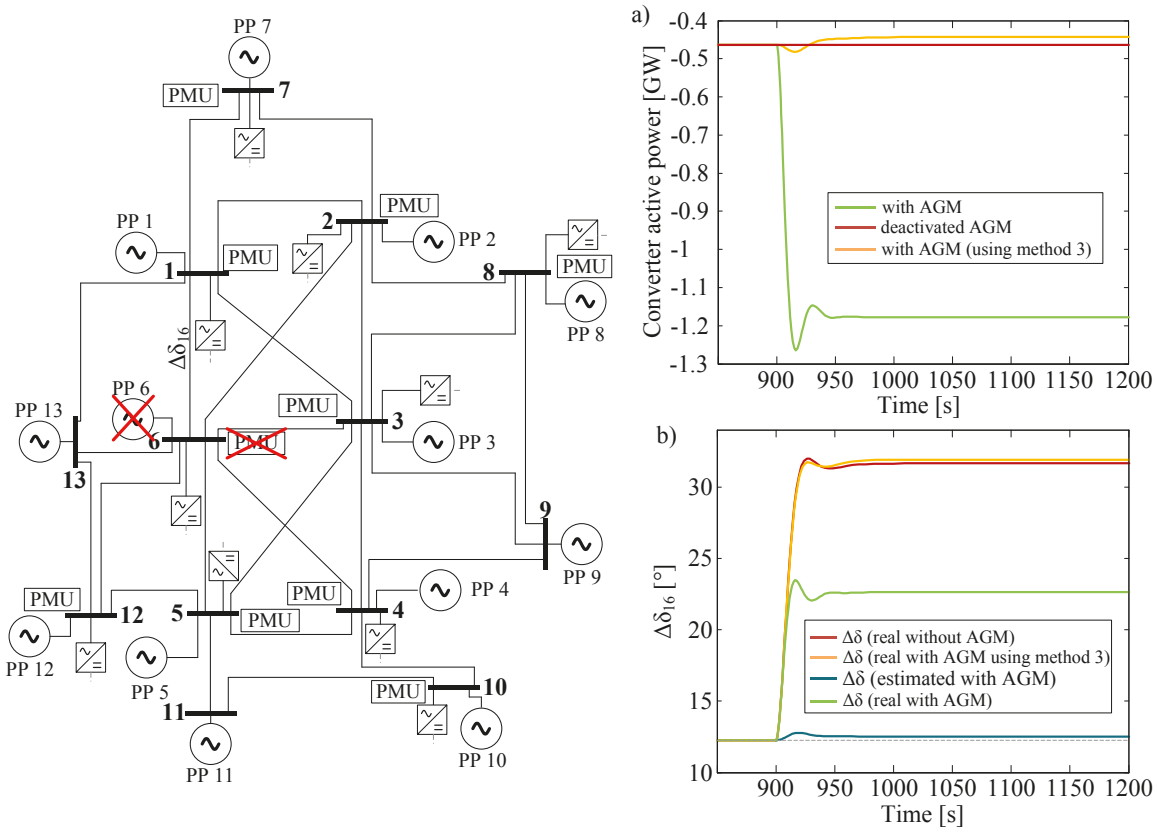

Fig. 4.17: Converter power (a) and voltage angle differences between node 1 and 6 $\Delta\delta_{16}$ (b) for a power plant trip at node 6 and simultaneous trip of PMU at node 6. Results are compared for AGM with all information available, AGM with unchanged information for tripped PMU and deactivated AGM.

The impact of method 3 using AGM is shown in Fig. 4.18 a) and b) for a line trip. Here a slightly positive effect occurs. Despite there are sometimes only a little difference in using a replacement value for missing PMU data or deactivating AGM, there is always a risk that further stress is placed on the grid by using a replacement value for tripped PMU's. Thus, maintaining the last voltage angle information seems to be inappropriate, particularly for PMU trips close to a disturbance.

Consequently, a converter related to a tripped PMU should not take part in AGM until SCADA information is available. Surrounding converters with intact PMUs will transmit balancing power, for example, as close as possible to the area it is needed, without placing additionally stress on the system. As soon as the SCADA estimates the missing voltage angle values, it is forwarded to all converters and AGM resumes full functionality.

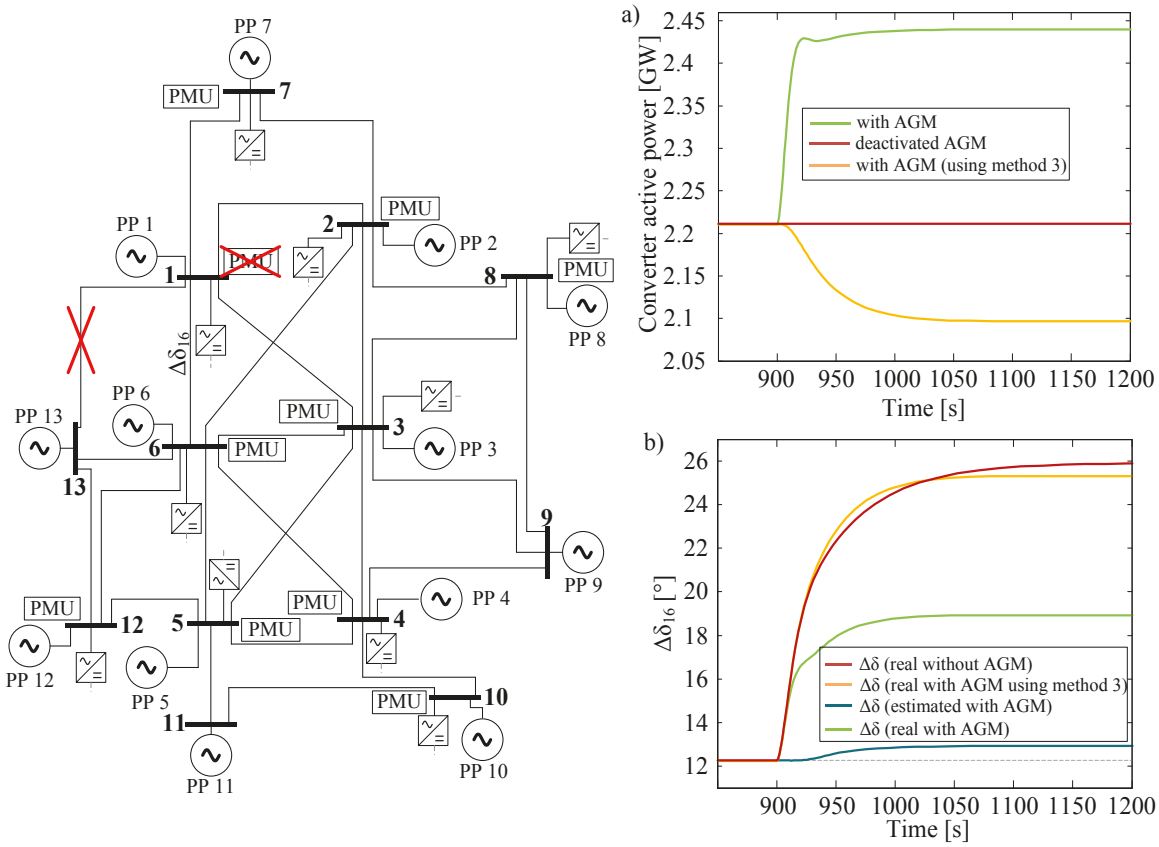

Fig. 4.18: Converter power (a) and voltage angle differences $\Delta\delta_{16}$ between node 1 and 6 (b) for a line trip between node 1 and 13 and simultaneous trip of PMU at node 1. Results are compared for AGM with all information available, AGM with unchanged information for tripped PMU and deactivated AGM.

4.6 Conclusion

In terms of long distance bulk power transmission, an HVDC grid should support the AC grid. For operational planning this can be fulfilled by implementing a mixed AC/DC OPF in order to calculate optimal converter reference values. Disturbances can lead to significant power flow changes in the AC gird. In this chapter a method is proposed which adapts the converter reference values using global voltage angle information (provided by PMUs and WAMS) and a local control accordingly. If significant AC power flow changes occur with regard to the schedule, the converter reference value is locally adapted in order to take part in the new power flow pattern. As it is based on detecting voltage angle gradients this method is introduced as Angle Gradient Method (AGM).

This is a fast measure which is supposed to be applied after disturbances in order to prevent instabilities or inadmissible equipment overload. As this is a local control, there is no optimized coordination among the converter realized. This can be made by a central controller afterwards with more time available as system security is ensured as much as possible by the AGM.

The proposed method has been validated using numerical case studies with several scenarios, as power plant trip, AC line trip or a partial converter trip. It has been demonstrated that AGM relieves the AC grid with an adjustable proportion of additional power flows and additionally improves dynamic behavior after disturbances regarding frequency stability.

A more efficient use of AC transmission capacities can be realized in normal operation as an adjustable amount of additional power flows in a disturbed system will be automatically transferred to the DC system. This makes the AGM very important as it ensures the backbone functionality of the HVDC system immediately after a disturbance and provides redundancy for the overall AC/DC system. It has therefore also been discussed how a backup can be realized if a single PMU measurement or the entire WAMS is not available, in order to provide a certain degree of robustness for the AGM.

5 DC energy balance – Primary control

This chapter addresses the general behavior of an HVDC grid with respect to the energy balance in the DC grid. The primary control is an instance which defines the final converter active power reference values in order to maintain DC energy balance based on the node voltage deviation from its reference value (see also subchapter 2.3). This final converter power reference value is the input signal for the inner converter control (current control loop) which realized the reference power if no higher priority events take place, for example related to protection issues. Based on its physical behavior, fundamental concepts for stable operation of an HVDC grid are derived. The measureable state variable which is strongly connected to DC energy balance is the DC node voltage. I.e. the DC node voltage control represents the final control instance (re-) defining reference values for internal converter control as indicated in Fig. 5.1.

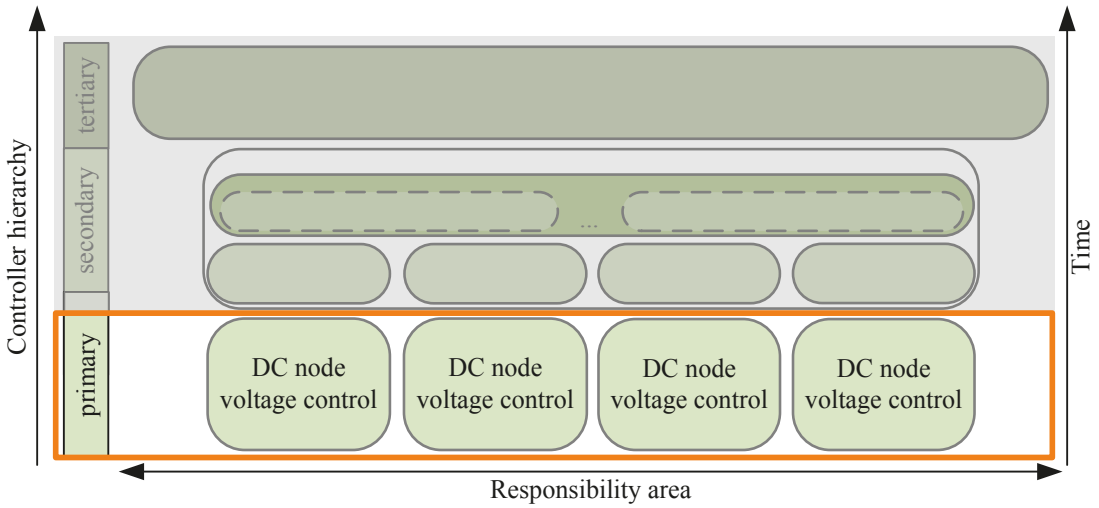

Fig. 5.1: Operation instance focused on in chapter 5.

In AC systems, the imbalance of energy causes a deviation from nominal frequency f_0. The frequency gradient in case of a lasting power imbalance is determined by the system inertia time constant T_A which is derived from the inertia of all synchronous generators directly connected to the grid (see (5.1)). System inertia time constant T_A is related to rotating masses of synchronous generators providing a kind of energy storage in the form of kinetic energy of rotation. Large T_A causes smaller frequency gradients. However an increasing amount of renewable energy (mainly connected to the AC grid using converters) and a decreasing amount of conventional power from synchronous generators decreases the system's T_A.

In DC grids, the imbalance of energy directly affects the DC node voltages. An energy imbalance (e_{in} - $e_{out} \neq 0$) results from a mismatch of input (p_{in}) and output active power (p_{out}) over a period of time dt while DC system losses are considered as an inherent output which is only indirectly controlable. As DC power flows are determined by differences in DC node voltage magnitudes, DC node voltage will differ from each other when the DC

system transmits power. However, the global indicator for an energy imbalance in a DC grid can be assumed to be the change of the mean value of DC node voltages.

The DC grid line capacitance C_L and converter capacitances C_C represent the DC grid capacitance C and therefore the short term storage capability of the DC grid (see Fig. 5.2). Therefore converter capacitances C_C of all converters n_C and line capacitances C_L of each DC line between nodes k and m sum up to DC grid capacitance C_{DC} according to (5.3). The DC grid capacitance increases its charge in case of an energy surplus causing an increase in system voltage and vice versa when a negative energy balance occurs (5.2). The converter capacitance is highly dependent on its technology. However, the total DC grid capacitance represents a very limited storage capacity compared to the power that will be transmitted via the HVDC grid. Thus, corresponding time constants in DC grids are much smaller than typical T_A in AC systems.

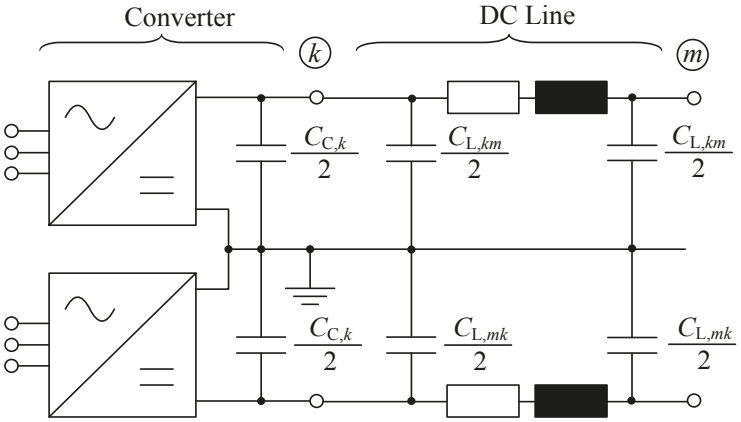

Fig. 5.2: Capacitances in the DC grid - simplified equivalent circuit diagram including a DC line and a bipolar converter.

$$f(t) = \frac{f_0}{T_A}\int_{t_0}^{t}\left(p_m(\tau) - p_e(\tau)\right)\mathrm{d}\tau + f_0 = f_0 + \frac{f_0}{T_A}\left(e_m(t_0,t) - e_e(t_0,t)\right) \tag{5.1}$$

$$v_{DC}(t) \cong \frac{1}{C_{DC}\cdot v_{0,DC}}\int_{t_0}^{t}\left(p_{in}(\tau) - p_{out}(\tau)\right)\mathrm{d}\tau + v_{0,DC} = v_{0,DC} + \frac{1}{C_{DC}\cdot v_{0,DC}}\left(e_{in}(t_0,t) - e_{out}(t_0,t)\right) \tag{5.2}$$

$$C_{DC} = \sum_k C_{C,k} + \sum_{km} C_{L,km} \tag{5.3}$$

If the mean DC voltage in general and particularly DC node voltages are bounded according to specified limits, the system is defined to be stable with regards to DC energy stability. In order to maintain DC energy stability, a DC balancing control is needed, namely DC node voltage control. This instance of control is comparable to AC systems' load frequency control [122]. This is mostly based on local voltage measurements. A state of the art analysis regarding this topic is given in subchapter 5.1.

5.1 State of the Art

5.1.1 Node voltage control without communication

Two terminal P2P schemes have been existing for many years. In such systems the energy balance is maintained by defining constant power control for one converter while the other converter controls the DC voltage. In the case of having multiple converters connected to a meshed HVDC system with changing power flow directions, this concept is difficult to realize and in large scale and bulk power HVDC grids it is nearly impossible. [127], [128]

Most voltage control concepts for multi terminal or meshed HVDC grids use local control variables based on a *p*-*v*- or *i*-*v*-characteristic defining the power or current reference value depending on the measured DC node voltage. Even if an *i*-*v*-characteristic, in contrast to a *p*-*v*-characteristic, represents a linear control behavior, hereinafter *p*-*v*-characteristic will be used since the use of power instead of current reference values is much more common in power systems. Regardless of the applied control characteristic certain limits have to be respected. These limits define the area permitted for safe operation (Fig. 5.3 and [130]):

- Power limit ($p_{conv,max}$): Assuming a constant AC voltage at PCC, the power limit is given by the maximum permitted current flowing through the converter's semiconductors.
- DC current limit ($i_{conv,max}$): Depending on the current-carrying capability of the DC equipment (e.g. DC lines) a maximum DC current limit can become active e.g. at low DC voltage.
- DC voltage limit ($v_{DC,max}$): Cost for high voltage insulation of HVDC equipment increases with increased permitted DC voltage. Thus, a maximum DC voltage of e.g. +5% [O-17], [48] is defined with additional safety margins. Additionally a minimum DC voltage can be necessary, very much depending on converter topology and its control, however this is not in the scope of this thesis.

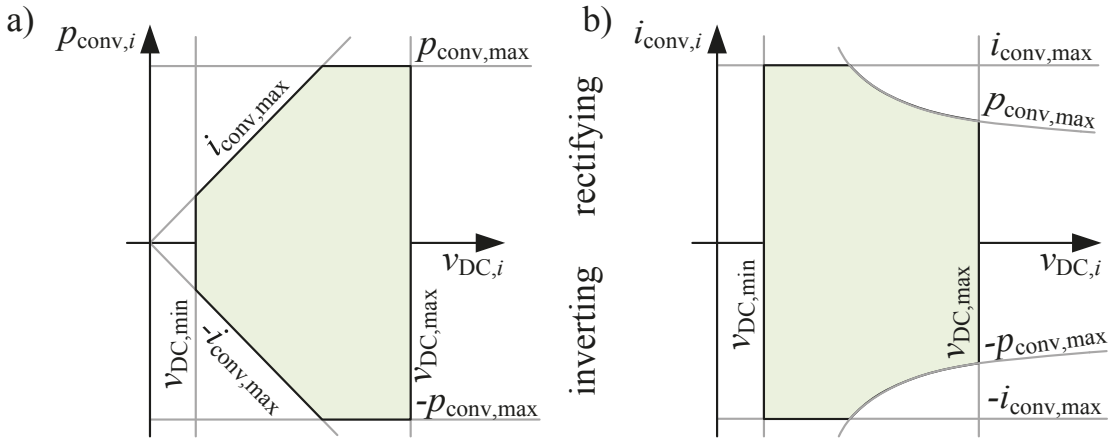

Fig. 5.3: Examples of permitted areas for safe operation for a) *p*-*v*-characteristic and b) *i*-*v*-characteristic assuming symmetrical operation range for converter power.

It is a requirement that the *p*-*v*-characteristic meets the reference point of the converter defined by a reference power $p_{\mathrm{conv,ref},i}$ and reference voltage $v_{\mathrm{DC,ref},i}$ [130]. Essentially, there are three different kinds of voltage control characteristics (see Fig. 5.4):

- Voltage droop
- Constant voltage
- Constant power control

Constant voltage and constant power control are special instances of voltage droop control, with a droop constant of converter i $k_{\Delta v,\mathrm{DC},i} \rightarrow 0$ and $k_{\Delta v,\mathrm{DC},i} \rightarrow \infty$ at the reference voltage $v_{\mathrm{DC,ref},i}$ respectively. The droop constant is the proportional factor between the two control variables voltage and power in the droop area:

$$k_{\Delta v,\mathrm{DC},i} = \frac{v_{\mathrm{DC},i}}{p_{\mathrm{conv},i}} \tag{5.4}$$

Constant voltage control was first proposed by [131], later re-established by [132], [133].

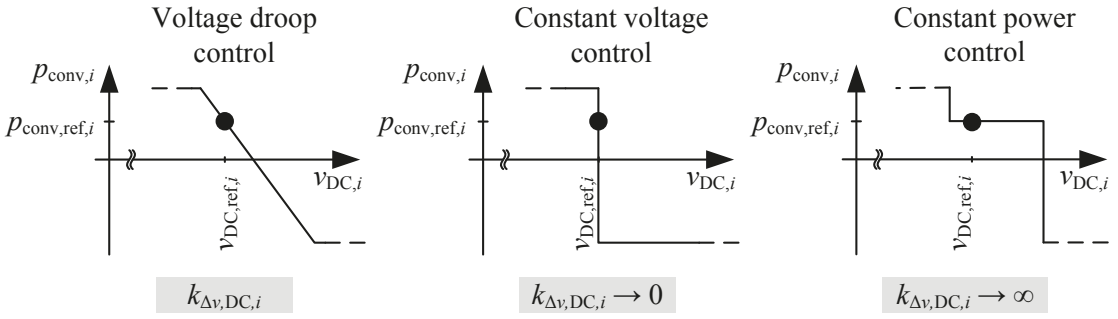

Fig. 5.4: Basic node voltage control characteristics.

This control concept can lead to voltage or power oscillations when applied to multiple converters within an HVDC system [128], [132], [134]. Thus, the voltage droop control was originally invented by [128] and re-established by [135]. It was shown that voltage droop control has several advantages over constant voltage control with regards to control's response time and transient performance [136]-[138]. For meshed HVDC grids a voltage droop control or a similar derivative is proposed in many publications, such as in [139]-[148]. A variety of voltage control characteristics can be derived from both. A compilation of general derivable control characteristic is given in [130] as shown in Fig. 5.5.

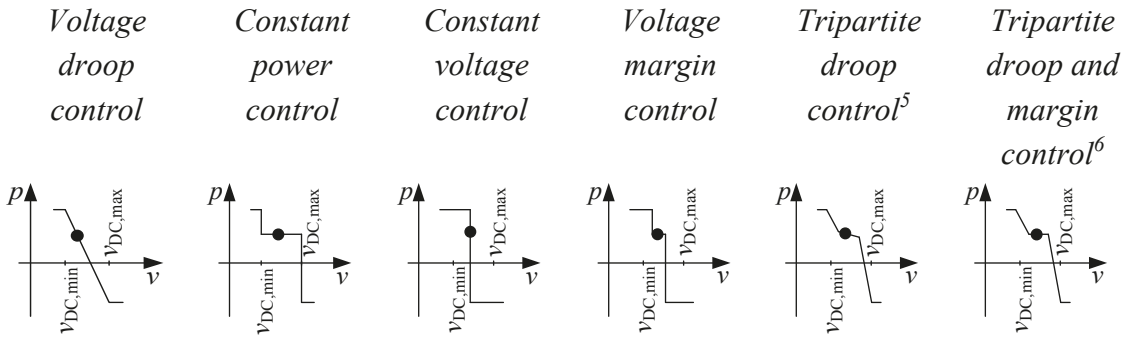

Fig. 5.5: Voltage control characteristics (continuous section by section).

Within an HVDC grid each converter can have a different voltage control characteristic, depending on the converters' principal duty [151], rated power, AC system characteristics at PCC or other criteria. Five different grid control strategies can be deduced here as also summarized in [130]:

- *Centralized voltage control*: A master controller is defined, acting as a slack-bus solely controlling voltage using a constant voltage control. Other converters are not participating in voltage control (constant power / current control).
- *Distributed Voltage control*: A voltage droop control or a tripartite droop control is implemented to some or even all converters of the HVDC grid.
- *Centralized voltage control with centralized back-up*: Similar to centralized voltage control with the addition of one converter acting as back up having a voltage margin control. If the primary constant voltage control fails, the back-up converter will reach the voltage margin limits and start controlling a constant voltage.
- *Centralized voltage control with distributed back-up*: Similar to centralized voltage control with the addition of a tripartite droop and margin control defined for all other converters. Thus, if central voltage control fails other converters are no longer in constant power control but in a voltage droop control mode whilst sharing balancing power.
- *Distributed voltage control with distributed back-up*: A Tripartite droop control is defined for all converters. It is also possible to define a tripartite droop and margin control for some converters instead of tripartite droop control.

All these concepts maintain DC energy balance on a basis of local measurements. Thus, neither communication or calculation delays (due to central optimization) nor loss of communication can endanger the DC system's stability. However, using DC voltage droop control or derived concepts can result in suboptimal operation due to higher losses caused by a lower mean DC voltage [139] as well as in deviation of converter power values from their set points [152], [154] or suboptimal balancing power charging among converters in terms of available converter capability [153].

[5] In literature also known as undead-band droop control [149], [150]
[6] In literature also known as dead-band droop control

5.1.2 Node voltage control with communication

[152], [154] propose a central control unit for DC voltage control using pilot voltage information. Pilot voltage can either be the voltage of a reference DC node or a mean value among all or selected DC nodes. The controller output is provided to all DC voltage controlling converters. Thus, all DC voltage controlling converters receive the same input and therefore provide the same amount of balancing power in case of a disturbance, assuming that there is no distribution factor that varies from converter to converter.

Another approach that is also based on coordination and communication is proposed in [155] and [156]. This agent based approach includes similar disadvantages as the central coordinated approach as mentioned before. In [156] delays are considered. The tolerable delay is highly dependent on line and converter capacitances and thus on their technology and line length. This crucial aspect is not mentioned in both publications.

The provision of a global reference, as is inherent in the AC system's frequency, can improve system behavior [153]. Even if a sufficient high speed communication can be achieved, loss of communication would still be a factor to endanger stability. Thus, a back-up methodology such as conventional voltage droop control or tripartite droop and margin control is needed (takes effect only if extended communication delays occur or a larger disturbance causes faster DC voltage changes).

Taking into account that communication causes a non-negligible delay, the basic idea of providing a global reference can take place as a kind of secondary control by resetting voltage reference values. This basic idea was proposed in [139].

5.1.3 Conclusion – State of the Art of Node Voltage Control

State of the art local DC node voltage characteristics are all piecewise defined functions with discontinuities. Under certain circumstances this fact can lead to oscillations when operating points are switching between those sections as it is described in subchapter 5.2. Additionally, when assuming state of the art DC node voltage control characteristics a decision must be made for exactly one of these control functions for each converter. A continuous characteristic has the inherent advantage of providing also "inter-characteristics" combining the advantages of two or more state of the art methods. Assuming that continuous characteristics parameters are determined according to surrounding grid conditions, no binary decision is necessary but the parameters can be defined automatically. A continuous characteristic is proposed in subchapter 5.3.

5.2 Sensitivity of DC energy stability

In HVDC systems oscillations can occur if more than one converter is in voltage control mode. This subchapter outlines factors which can cause oscillations at the equipment and

control side. To reduce complexity, all analyses are made using a P2P system topology. The results can be applied to HVDC grid topologies as well.

It is important to avoid significant oscillations in HVDC transmission grids for similar reason as in AC power systems where oscillations are damped by using power system stabilizers (PSS) [157]. Such oscillations block transmission capability and cause sub-optimal power flows or non-optimal use of physical transmission capacity. Additionally even transmission or generation equipment life cycles can be negatively influenced. Additionally DC oscillations can be transmitted to the AC system via converters. Thus, oscillations of that kind within the DC grid have to be avoided or well damped as they even might affect the AC system and deteriorate its stability. Therefore the influence of the following potentially causal factors for DC oscillations are analyzed separately while other parameters remain unchanged in each case:

- Dead time and delay of converter control
- Line and converter capacitances
- Line inductances
- Line length and type
- Uncoordinated converter reference values within the HVDC system
- Shape of *p*-*v*-characteristic for DC node voltage control

The analyses including software and hardware simulations and its results are published in [O-14]. For the following analyses a simulation is carried out using Matlab/Simulink including SimPowerSystems toolbox. Converters are modeled as ideal controlled current sources. This control includes a tripartite droop margin control as described in subchapter 5.1 and shown in Fig. 5.6, with a dead time (T_d = 4 ms) and a time delay (T_l = 10 ms) (see Fig. 5.7). The dead time represents the delay due to communication, computing time, measurement acquisition, processing, etc. while the converter's time constants - depending on internal converter control parameters and topology - are represented by the delay.

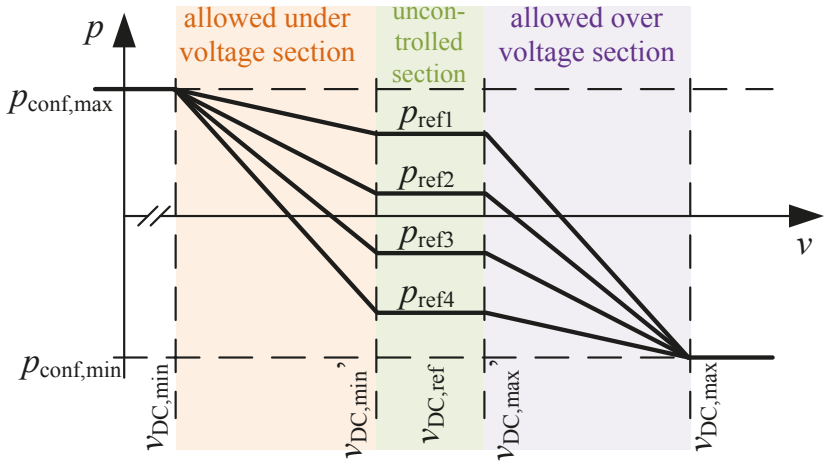

Fig. 5.6: General tripartite droop and margin control characteristic.

The DC line is modeled as a π equivalent according to Fig. 5.7 while the capacitances of the converters are included in the capacitance values of line's π equivalent named node capacitances C_k and C_m in Fig. 5.7 each with a value of 700 µF according to [O-14]. Line inductance L_{km} and line resistance R_{km} are defined as 3 Ω and 51 mH respectively as representing a 100 km long overhead transmission line for 500 kV voltage rating ([O-14]).

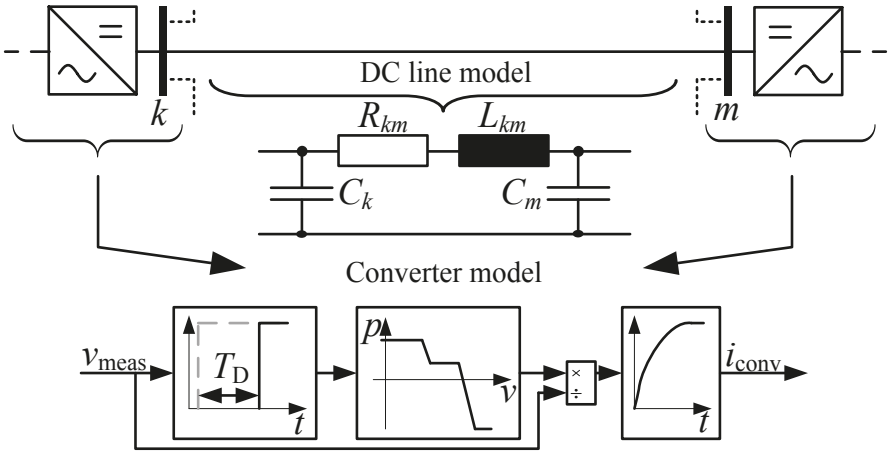

Fig. 5.7: Converter control representation and DC line model for oscillation analyses.

The stability of the overall system is analyzed using eigenvalues while the Simulik model is linearized for this purpose. Analyses show that the system is:

- *asymptotically stable* ($\mathrm{Re}\{\lambda_i\} < 0 \; \forall \, i$) when the operating points of both converters are within the uncontrolled section of the *p*-*v*-characteristic. In other words no operating point correction by the *p*-*v*-characteristic is necessary (Fig. 5.8 a)).
- *marginally stable* (eigenvalues with $\mathrm{Re}\{\lambda_i\} = 0$ have to be semisimple – algebraic multiplicity equal to geometric multiplicity – and all other eigenvalues with a negative real part) when both operating points oscillate between the uncontrolled section of the *p*-*v*-characteristic and either the maximum or minimum power limit and exactly one operating point is within the uncontrolled section at a time (Fig. 5.8 b)).
- *unstable* (if for any eigenvalues $\mathrm{Re}\{\lambda_i\} > 0$) when both operating points oscillate between maximum and minimum power limits of each converter with a phase shift against each other of 180°. The system is bounded by the converter limits but nevertheless unstable (Fig. 5.8 c)).

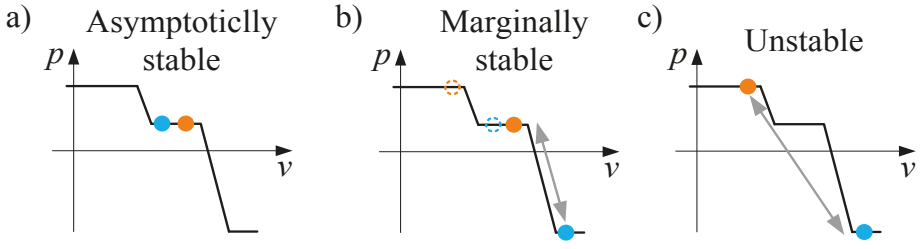

Fig. 5.8: Stability categorisation regarding operating points on the *p*-*v*-characteristic.

5.2.1 Dead time and delay of converter control

As is described on page 88 and shown in Fig. 5.8, the position of operating points is essential for system behavior. Thus, the influence of converter controller's delay and dead time is analyzed for operating points within the uncontrolled section (a in Fig. 5.9) and within one of the controlled sections (b in Fig. 5.9).

For system operating points only on the uncontrolled section and without a converter control time delay and dead time, the system is represented by eigenvalues with a negative real part and a conjugated complex pole pair. Since the real eigenvalues are dominant, the system does not tend to have oscillations. Even if a dead time and converter control's time delay add four more eigenvalues, the system behavior will not be fundamentally influenced since they are on the left side of the other eigenvalues and the other three eigenvalues are only marginally influenced (see Fig. 5.9 a).

Since control interaction is not required, dead time and converter control's time delay do not influence system behavior significantly when the operating points are on the uncontrolled region. The operating points will be within the uncontrolled section of the *p*-*v*-characteristic when converter's power reference values are well harmonized (see also subchapter 5.2.5) With an increasing line inductance the conjugated complex pole pair becomes dominant (see Fig. 5.13) and the system oscillates with the eigenfrequency of the system, determined by systems' inductances, capacitances and converter control dead times and time delays.

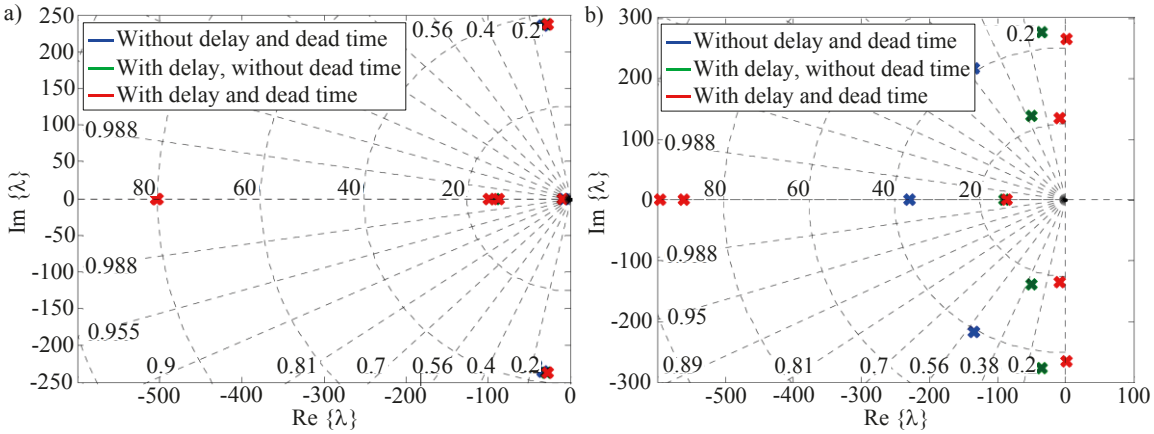

Fig. 5.9: Eigenvalues of a P2P connection and a converter representation as shown in Fig. 5.7 with operating points a) within the uncontrolled and b) within the controlled region of the *p*-*v*-characteristic (Fig. 5.6).

If one operating point is within one of the controlled regions of the *p*-*v*-characteristic, the eigenvalues of the system without dead time and converter control's time delay are more shifted to the left. In this case, there is no time delay influencing system response and the system is more stable when it is controlled (see Fig. 5.9 b). If the operating point is within the controlled region and dead time and time delay are considered eigenvalues move to the

right and their imaginary part is increased. Thus, the system will tend more to oscillations (lower damping). When adding a dead time and converter control's time delay, eigenvalues are shifted even more towards the imaginary axis, the system becomes less damped and an additional conjugated complex pole pair is added in comparison to the situation with an operating point only within the uncontrolled section. Depending on the specific time delay and dead time the system can become marginally stable or even unstable.

5.2.2 Line and converter capacitances

For stability analysis, the DC system's capacitances represented by line and converter capacitance are concentrated to node capacitances, which is permissible given that no traveling wave or related analyses are carried out. In the studies above a node capacitance of 700 μF each is used. To carry out the impact of DC system's capacitances this value is varied from 400 μF to 1500 μF in order to show the effect of different DC system capacitances.

As previously mentioned, the DC system's capacitances represent the "DC grid's inertia". Capacitances are essential for the DC system energy stability. Consequently, for very small capacitances the DC system will collapse if energy imbalances occur. The necessary dimension of the DC system's capacitances to prevent a voltage collapse is highly dependent on the speed of the converter control and therefore on its time delay and dead time. The smaller the time constants are the smaller the DC system's capacitances have to be.

When the DC system's capacitance is further increased, the three stability categories mentioned (instable, marginally stable and stable) are reached. Thus, the larger the DC system's capacitance becomes, the more stable the DC system will be. This is shown by the eigenvalue plot in Fig. 5.10. Primarily two conjugated complex pole pairs are affected by DC system capacitances. Their real part decreases with an increasing capacitance and simultaneously the imaginary part decreases as well. This leads to a higher damping and decreased oscillation frequencies. When the DC capacitance reaches a sufficiently high value, the system is stable even if the operating points of both converters are within the controlling sections of the p-v-characteristic.

A dead time within the converter control reduces the control speed, while capacitances within the DC system decelerating the inherent system response (due to its storage effect as explained on page 81). Thus, a higher system capacitance can compensate for the effect of dead or delay times since both, the system and its control, are decelerated. This aspect can be seen in Fig. 5.10.

Since all influencing factors are interdependent, there are system specific capacitance values for stable operation. Among others, it dependends on line resistances. The larger the line resistance becomes the lower the necessary DC system capacitance value will be to ensure stable operation due to the damping effect of the ohmic part.

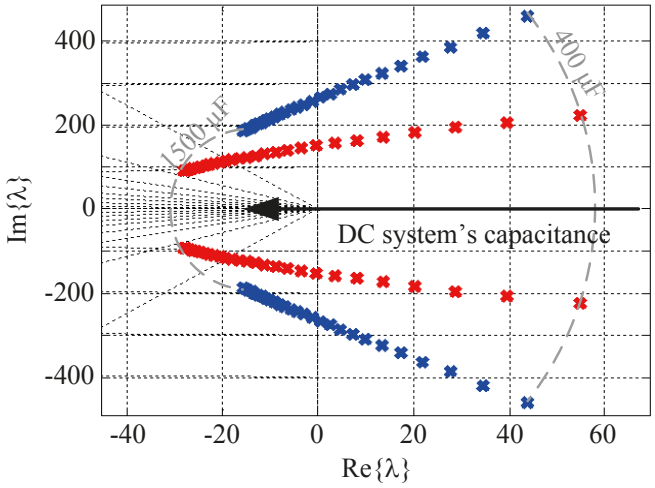

Fig. 5.10: Eigenvalue shift due to changed DC system capacitances.

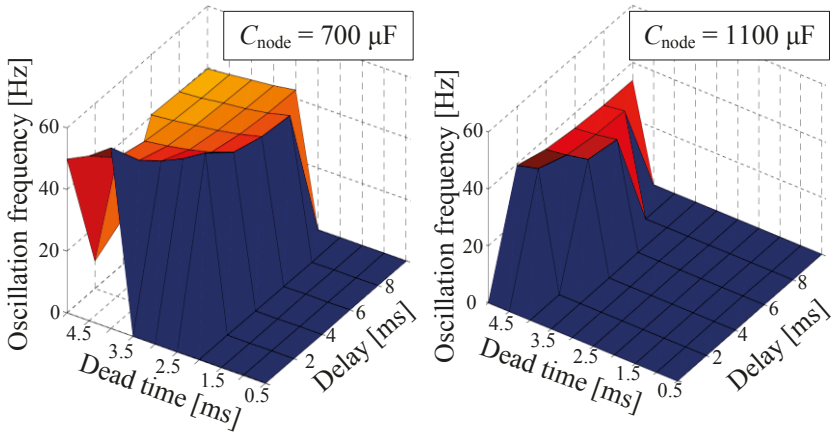

Fig. 5.11: Oscillation frequency as a function of converter control's dead time and time delay for two different node capacitances.

For the given setup, a DC node capacitance of 400 µF is necessary for stable operation if a line resistance of 5 Ω is assumed (see Fig. 5.12 a) while a DC node capacitance of 1300 µF is necessary assuming a line resistance of 2 Ω (see Fig. 5.12 a). The effect of low damping areas, as has been previously identified for line inductances, can also be identified for DC node capacitances. Those areas are further shifted to higher capacitance values the lower the line resistance becomes, again due to the damping effect of the ohmic part (see Fig. 5.12 b). Due to the described effect of voltage collapse for small capacitance values, there is no oscillation frequency or amplitude for very low DC node capacitances.

Comparing the effect of DC system capacitances and DC line inductances using Fig. 5.13 b and Fig. 5.10, a stabilizing effect can be identified, due to increasing DC system capacitances as well as a destabilizing effect caused by increasing DC line inductances. Consequently, the effect of high line inductances (e.g. caused by long overhead transmission

lines) can be compensated by additional capacitances (for example). Even an inherent compensation is possible having a DC system with overhead transmission lines and cables with an inherent higher capacitance.

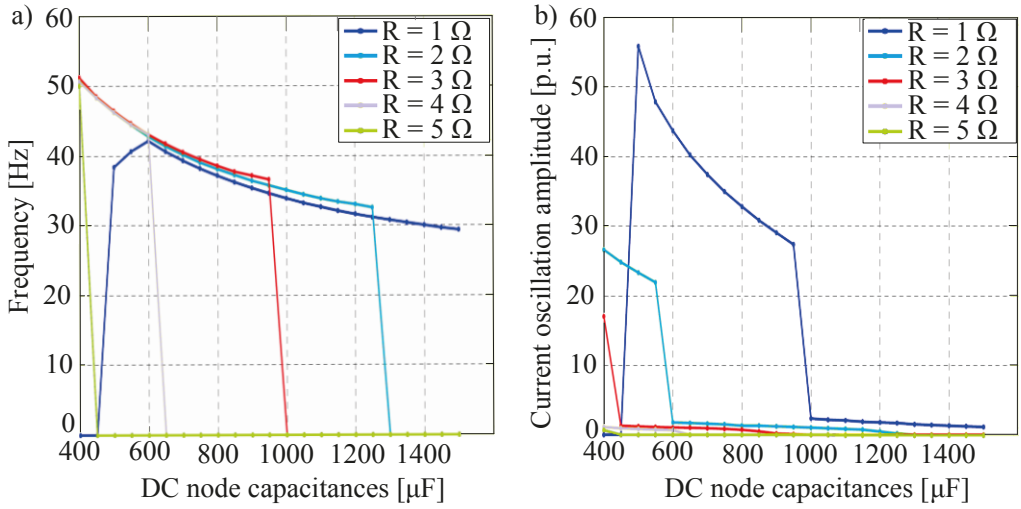

Fig. 5.12: Oscillation frequency (a) and current oscillation amplitude (b) influenced by DC node capacitance variation for a set of line resistances.

5.2.3 Line inductances

The eigenvalues are shifted more towards the imaginary axis with increasing line inductances (see Fig. 5.13). There are some eigenvalues that are shifted further with increased line inductances than others. Thus, when line inductances continuously increase, there is a change in the dominant conjugated complex pole pair and this results in an abrupt change of the system's dominant oscillation frequency (see Fig. 5.14 a).

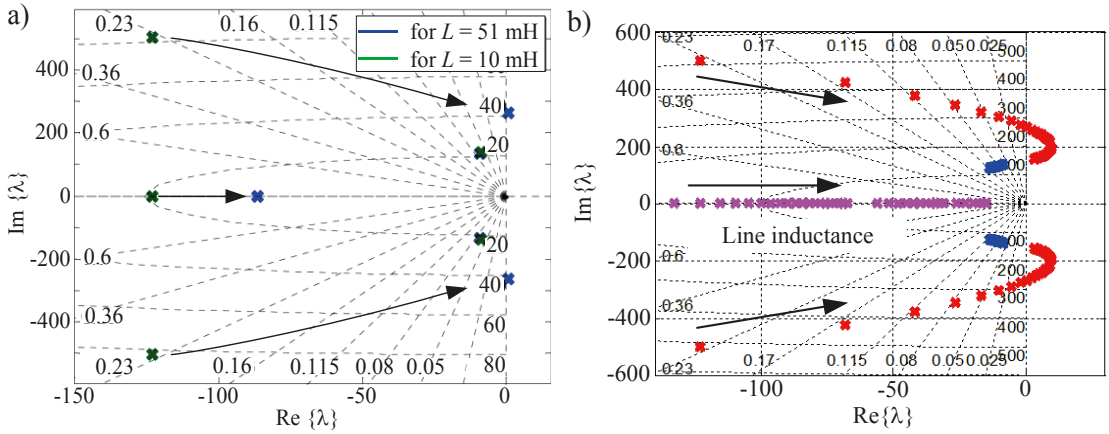

Fig. 5.13: Eigenvalue shift due to changed line inductances and consequently other dominant conjugated complex pole pair (a) and in b) for several line inductances.

Fig. 5.14 b) shows the existence of low damping areas for small line inductances and small line resistances. In these instances the system is unstable however returns to marginal stability with increasing line inductances or resistances. In Fig. 5.14 a) the effect as mentioned for Fig. 5.13 a) occurs again. For small line resistances and inductances a conjugated complex pole pair with an eigenfrequency of 22 Hz is dominant. With increasing line inductance another conjugated complex pole pair with an eigenfrequency of 40 Hz becomes abruptly dominant. For lines with higher line resistances and low line inductances, an eigenvalue with only a negative real part is dominant. Consequently, the eigenfrequency is 0 Hz. Increasing the line inductance makes the 40 Hz conjugated complex pole pair abruptly dominant as well as for higher resistances. Thus, for larger line inductances line resistances become less important.

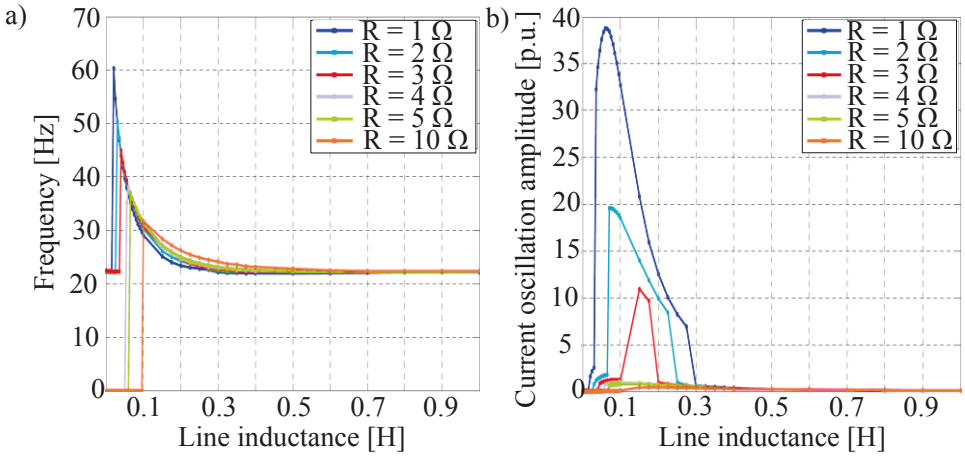

Fig. 5.14: Dominant oscillation frequency (a) and current oscillation amplitude (b) influenced by line inductance variation for a set of line resistances.

5.2.4 Line length and type

Beside converter topology, the DC system's capacitance as well as line inductance and resistance are primarily influenced by line length and technology. For comprehensive analysis parameters of overhead lines, cables and gas insulated lines are used as shown in Tab. 5-1.

Tab. 5-1: Line parameters of different technologies for a nominal voltage of 500 kV.

	***R'* [mΩ/km]**	***L'* [mH/km]**	***C'* [nF/km]**
Overhead line [159]	28	0.86	13.8
XLPE Cable [160]	19	0.73	183
GIL [160]	9.4	0.22	54

As previously mentioned line resistances have a damping effect. Even if the cables' resistance is much smaller than that of the overhead transmission lines, both have a similar oscillation characteristic (see Fig. 5.15) given that this is compensated by the cables' much

higher capacitances. Two technologies for low loss transmission are gas insulated transmission lines (GIL) and high temperature superconducting cables (HTC) as used for the Tres Amigas HVDC project [158].

GIL's small transmission losses are a consequence of its low resistance value. These low resistance and capacitance values have been identified as negatively impacting factors for DC system's stability. Conversely, a low line inductance has a positive effect on the system's stability. Since the distributed line inductance *L'* and resistance *R'* are the smallest they have the highest oscillation frequency in terms of GIL. The overall stability performance is better when using overhead transmission lines or cables, as can be seen in Fig. 5.15. For cables there is an area with low damping for short transmission lines which might become important if short sections are underground. However, this disadvantage can be compensated for by changing other influencing factors, as discussed later. Resistances of HTC are about 25•10³ times smaller than those of GIL [161]. These very low line resistances imply a very low inherent damping effect and together with smaller line capacitances a less stable system behavior.

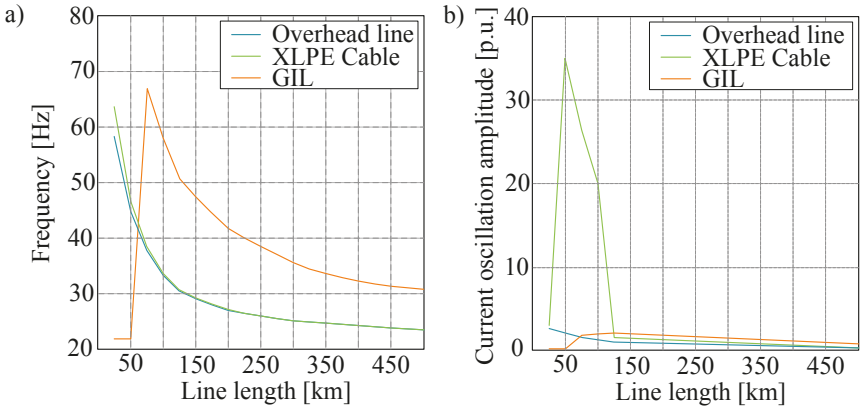

Fig. 5.15: Oscillation frequency (a) and current oscillation amplitude (b) influenced by different line technologies and variation in transmission line length.

Oscillation frequency as well as oscillation amplitude decrease with increasing line length for all considered transmission technologies. This is caused by the increasing damping effect due to the ohmic part (oscillation amplitude).

5.2.5 Uncoordinated converter reference values within the HVDC system

Even if oscillation frequency is not impacted by control issues, since oscillation frequency is only dependent on the equipment parameter (resistances, inductances and capacitances), oscillations can be provoked or avoided by control issues. One of these control issues is the coordination of converter power reference values.

If converter power reference values coordinate well with each other, all converter operating points will stay within the uncontrolled section of the *p*-*v*-characteristic and oscillations are avoided. The less the reference points are harmonized the higher the oscillation amplitude

will become (see Fig. 5.16). In existing HVDC point to point connection this effect does not occur as only one converter controls the voltage while the other converter controls the power. As mentioned above, the larger the HVDC system becomes and the more converters are included it becomes increasingly more reasonable to distribute balancing power to multiple converters (e.g. due to stress given to the AC system). I.e. more converters will be in voltage control mode and oscillations can occur. Thus, a large HVDC grid should have a coordination layer (distributed or central) as described in chapter 3.

5.2.6 Shape of p-v-characteristic for DC node voltage control

Besides the coordination aspect of converter's power references the shape of the *p*-*v*-characteristic also affects the oscillation potential of the system.

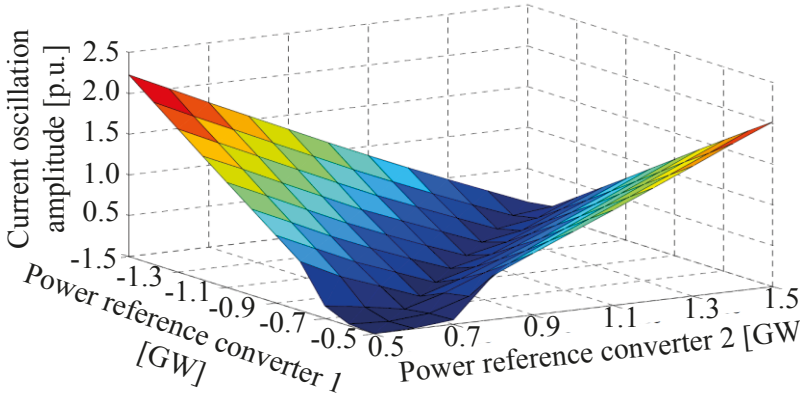

Fig. 5.16: Oscillation amplitude as a function of power references of a P2P connection.

If the shape of the *p*-*v*-characteristic is modified in a way that the uncontrolled section is extended, the droop will be larger for the controlled sections since the maximum and minimum voltage will be the same. Consequently, the eigenvalues will be shifted towards the imaginary axis. Thus, the system's damping will become smaller and oscillation amplitudes will increase. When modifying the tripartite droop and margin *p*-*v*-characteristic to a tripartite droop control (uncontrolled section modified to have a small droop) the system behavior can already be improved.

Operating points in the middle part of the characteristic will also be controlled (with a lower droop). Consequently, in some cases the operating points do not even reach the other two parts of the characteristic and unstable or marginally stale system conditions are avoided, as it is also described in [149] and [150]. Converter reference values do not need to be perfectly balanced to avoid oscillations. This is shown in Fig. 5.17 a), which is a result of numerous dynamically Simulink simulations using different set of converter power references for both converters of the P2P scheme and analyzing the oscillation frequency of the system.

Stability of a DC system depends on different impact factors while their interrelation determines the overall DC system stability. The negative effect of an influencing factor can be compensated by another one with positive impact.

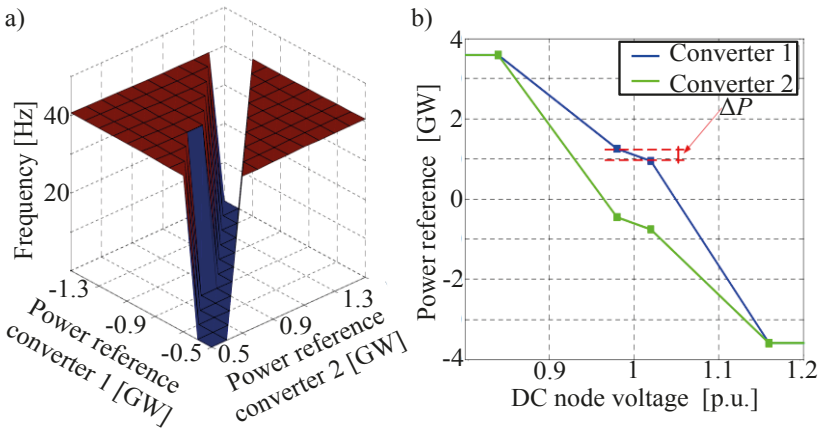

Fig. 5.17: Oscillation frequency as a function of converter power reference values (a) using a tripartite droop control (b).

5.2.7 Conclusion – Sensitivity of DC grid energy stability

Dead times and converter control delays in general have a destabilizing effect while dead times do have the most significant effect. This effect can be compensated by coordinating all converter power reference values in the DC system. Additionally a negative effect towards DC system stability is identified for voltage margin control sections within *p*-*v*-characteristic. When voltage margin control sections are replaced by voltage droop sections (e.g. with large droop constants) the risk for oscillations can be reduced even if discontinuities still bear a significant oscillation risk.

DC line parameters influence the DC system stability. Line inductances have a negative effect on DC system stability. However, with increasing line or converter capacitances on the DC side the stability can be significantly increased. As line resistances have a damping effect on oscillations, an increase in line resistance has a positive effect on DC system stability even if it increases transmission losses. Depending on its inductance, capacitance and resistances several line type have a more positive or negative effect on DC system stability. The most important factors are summarized in Tab. 5-2.

Tab. 5-2: Impact factors on DC system stability regarding equipment and control.

Impact factor	**stability**
Increasing dead times and converter control's delay	decreased
Increasing line resistances	increased
Increasing line inductances	decreased
Increasing line and converter capacitances	increased
Presence of voltage margin control sections in *p*-*v*-characteristic	decreased
Coordination of converter's reference values within the HVDC system	increased

In an HVDC grid with various line length and line technologies oscillation between two or multiple converters can occur, as it was shown for P2P schemes in this chapter. Oscillations between different converters can superimpose. However, the impacting factors will remain unchanged.

5.3 Continuous characteristic for DC node voltage control

Even with a tripartite droop control characteristic reference values should be coordinated as good as possible. This is trivial in the case if no disturbance occurs and a coordination layer (tertiary control see chapter 3) is in place. If a disturbance takes place (e.g. converter trip), converter reference values will be highly uncoordinated at least for the first moment until the power reference values are updated by an instance of coordination. A disturbance stresses the DC system, additional oscillations caused by a disturbance would further increase the system stress and should be avoided as much as possible. Equipment parameter influencing the oscillatory behavior (subchapter 5.2) may be not available for optimization issues due to footprint, economic or other reasons.

The tripartite droop control characteristic can avoid marginally or even unstable system states, but there is still an elevated risk of oscillations especially at discontinuities of the control function when an abrupt change in droop constant takes place as it is shown in Fig. 5.17. In order to overcome this problem a continuous DC node voltage control characteristic approach, as shown in Fig. 5.18 is proposed.

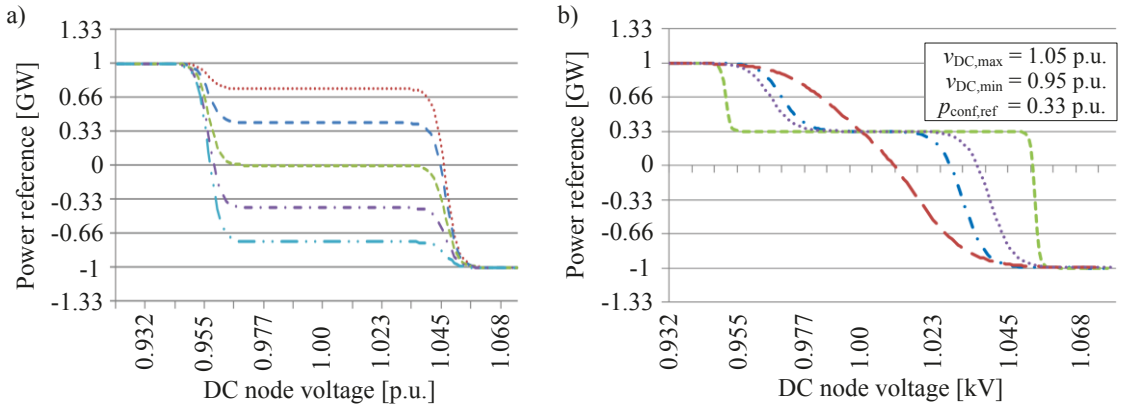

Fig. 5.18: Continuous DC node voltage control characteristic for different converter power reference values (a) and with different parameterization (b).

This continuous *p*-*v*- control characteristic is proposed as a set of two sigmoid functions according to (5.6). Using a sigmoid function makes it possible to approach the converter's power limits when voltage limits are reached without any risk of exceeding power limitations. A set of two sigmoid functions is therefore proposed in order to allow special treatment of the given reference value given by ($p_{conv,ref}$ and $u_{DC,ref}$). Around the reference operating point a much higher droop is possible resulting in a marginal participation in DC node voltage control actions. The sigmoid function on the right hand side has a (negative) offset

of the converter's maximum permissible active power in rectifier mode $p_{\mathrm{conv,min}}$. The mathematical description of the voltage control characteristic is known by each converter control. Its parameters are determined on a higher control hierarchy level (secondary or tertiary control – chapter 3 and 4) and submitted to each converter.

$$p_{\mathrm{conv,ref}}(v) = \frac{p_{\mathrm{conv,max}} - p_{\mathrm{conv,ref}}}{e^{h_{\mathrm{left}}(v_{\mathrm{DC}} - v'_{\mathrm{DC,min}})} + 1} + \frac{p_{\mathrm{conv,ref}} - p_{\mathrm{conv,min}}}{e^{h_{\mathrm{right}}(v_{\mathrm{DC}} - v'_{\mathrm{DC,max}})} + 1} + p_{\mathrm{conv,min}} \tag{5.5}$$

The proposed continuous *p*-*v*-characteristic avoids an abrupt change in voltage droop by smoothing the transition between higher droop and lower droop sections. Thus, depending on the characteristic's parameterization a wider area is created where no oscillations occur even with badly coordinated converter power reference values. Therefore the model used for the previous subchapter (Fig. 5.7) is used again to show the effect of continuous *p*-*v*-characteristics compared to tripartite characteristics as discussed in the previous section.

Fig. 5.19 shows two examples for different parameterization of continuous *p*-*v*-characteristic with a relatively small area surrounding the reference operating point with a larger droop constant (a and b) and with a larger area surrounding the reference operating point with a larger droop constant (c and d). For characteristics as shown in Fig. 5.19 d) with a wider area having a larger droop constant, the transition to areas with smaller droop constants is even smoother than in Fig. 5.19 d). The smoother transition allows for an even wider area for converter reference mismatches where no oscillations occur (see Fig. 5.19 c).

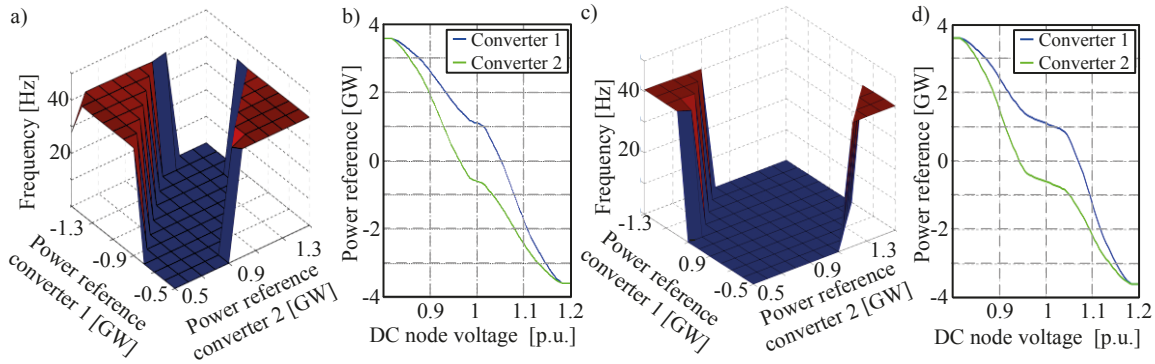

Fig. 5.19: Oscillation frequency as a function of converter power reference values using a tripartite droop control with a relatively small (a and b) respectively wide area (c and d) with a higher droop constant around the operating point.

A single sigmoid function is characterised by an upper bound ($p_{\mathrm{conv,max}}$ for the left and $p_{\mathrm{conf,ref}}$ for the right sigmoid) and lower bound ($p_{\mathrm{conf,ref}}$ for the left and $p_{\mathrm{conv,min}}$ for the right sigmoid) as it is illustrated in Fig. 5.20. For the set of both sigmoid functions, $p_{\mathrm{conv,max}}$ and $p_{\mathrm{conv,min}}$ represent the upper and lower bound of the continuous *p*-*v*-characteristic. Furthermore, each single sigmoid is characterised by its inflection point ($v'_{\mathrm{DC,min}}$ for the left and $v'_{\mathrm{DC,max}}$ for the right sigmoid) and slope (h_{left} for the left and h_{right} for the right sigmoid)

mainly determining the continuous *p*-*v*-characteristic's shape, as shown for different values (of inflection point and slope) in Fig. 5.18 b).

A single sigmoid is point-symmetrical to its inflection point. When superimposing two sigmoid functions, as is proposed for the continuous *p*-*v*-characteristic, point-symmetry for the left and right sigmoid are no longer exactly given. This is caused by superimposing both sigmoids with their asymptotic convergence to its bounds.

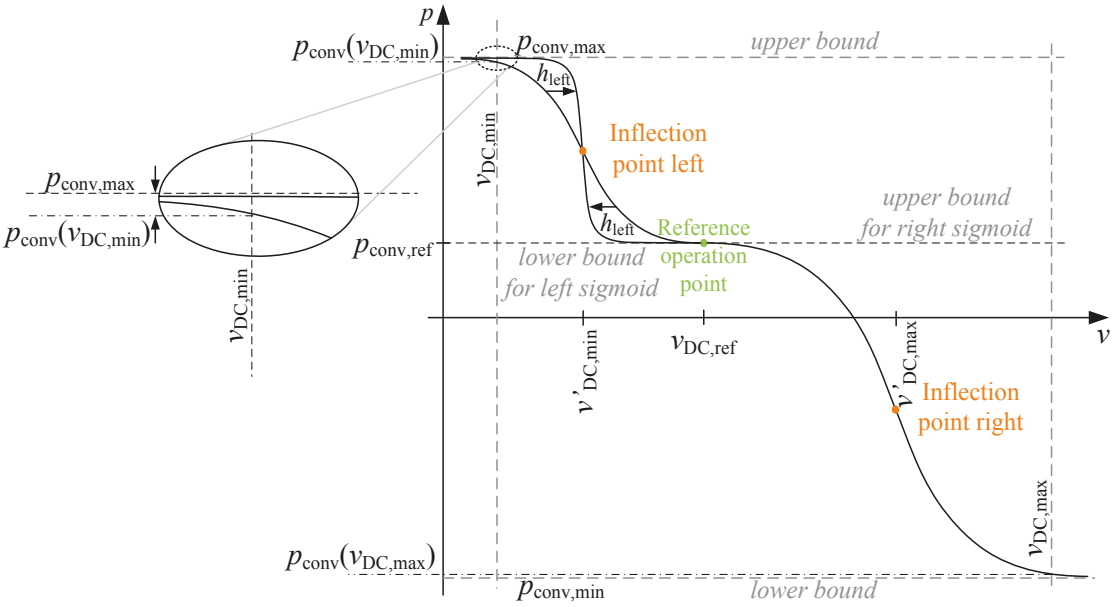

Fig. 5.20: Parameter of continuous *p*-*v*-characteristic.

Besides strict limits for the converter's active power, requirements for parameterization a set of sigmoid functions for a continuous *p*-*v*-characteristic also includes DC voltage limits. At the DC voltage limits $v_{DC,min}$ and $v_{DC,max}$ the converter's control characteristics in Fig. 5.5 defines the converter's power reference to be $p_{conv,max}$ and $p_{conv,min}$ respectively. This cannot be directly defined using a sigmoid function but must be inherently maintained when determining infection point and slope of the sigmoid. Since there will always be a small gap between the sigmoid function and the upper and lower power limit (except for $v_{DC,} \rightarrow \pm\infty$ as can be seen in Fig. 5.20) it is required that:

$$p_{conv,max} - p_{conv}(v_{DC,min}) \leq 10^{-4} \tag{5.6}$$

$$\left| p_{conv,min} - p_{conv}(v_{DC,max}) \right| \leq 10^{-4} \tag{5.7}$$

If a smaller accuracy is defined not all of the converters' capacity will be used when voltage limits $v_{DC,max}$ and $v_{DC,min}$ are reached.

The set of sigmoid functions should also meet the reference operation point with an even higher accuracy. Here, an accuracy of 10^{-5} is assumed. Therefore, the set of sigmoid functions underlies another requirement according to (5.8) that must be respected when determining the inflection point and slope for both sides.

$$\left| p_{\text{conf}} - p_{\text{conf}}(v_{\text{DC,ref}}) \right| \leq 10^{-5} \tag{5.8}$$

Both, left and right sigmoid, influence the other's shape. Thus, a separate consideration of both regarding the requirements (5.8) and (5.6) respectively (5.7) is not sufficiently correct for all parameter constellations. Thus, for general validity, the overall set of sigmoid functions must be considered.

Strategies for determining continuous *p*-*v*-characteristic's parameters (inflection points and slope) can be primarily subdivided into two tasks:

Parameterization with respect to:

- DC node's determined "role" within the DC grid in alignment to existing partial differentiable *p*-*v*-characteristics, as shown in Fig. 5.5.
- AC side grid characteristics and local conditions

Both strategies proposed here are described in the following two subchapters 5.4 and 5.5. As already mentioned in chapter 3, parameters for voltage control characteristics are determined by the tertiary control instance in the same time interval as for converters' power and DC node voltage references.

In case of a disturbance it may not only necessary to redefine converters' voltage and power reference values in a coordinated way but also the parameterization of the voltage control characteristics as it is possible that important constraints for node voltage control characteristic parameterization changed with the disturbance or power transfer between different areas significantly changed. For short term coordination this will be an issue for a coordinating secondary control instace as proposed in [145], for instance. For long term coordination this will be included in the next schedule which is provided by secondary control.

5.4 Parameterization of continuous p-v-characteristic based on DC nodes function

As described in subchapter 5.1, there are different partially differentiable *p*-*v*-characteristics to overcome a number of operational functions. Accordingly, these characteristics can be represented up to a certain extend with the proposed set of sigmoid functions but without points of discontinuity. It is shown in this subchapter that continuous characteristics can be used as an equivalent for piecewise linear state of the art characteristics without causing any further disadvantages. Therefore parameter limitations are defined for the state of the art characteristics to be represented by the continuous characteristic.

A central dispatch center as described in chapter 3 can, besides a schedule, also assign a role to each HVDC converter within the HVDC grid. Hence, one converter can define a fixed voltage within the HVDC grid, e.g. in order to maintain a high voltage level within the grid. An appropriate state of the art control characteristic would be a constant voltage control. Other converters can operate in tripartite margin droop control or other control characteristics according to Fig. 5.5. All of those can be represented with their main characteristics using an appropriate parameterization of continuous *p*-v-characteristic.

5.4.1 Constant voltage control

For constant voltage control both infection points of the set of sigmoid functions are set to the reference voltage value. For the following example it was set to $v_{DC,ref} = v'_{DC,max} = v'_{DC,min} = 1.04$ which is within the absolute voltage limits given by $v_{DC,min} = 0.95$ and $v_{DC,max} = 1.05$. Since a converter with such control characteristic is not controlling power in any manner, power reference is set to zero. In order to find a characteristic which is steep enough to emulate a constant voltage control, $v_{DC,max}$ and $v_{DC,min}$ should be redefined for requirements (5.6) and (5.7) to be very close to the reference voltage. For this example it was chosen according to (5.9) and (5.10).

$$v_{DC,ref} - v_{DC,min} = 10^{-4} \tag{5.9}$$

$$v_{DC,max} - v_{DC,ref} = 10^{-4} \tag{5.10}$$

The resulting continuous *p*-*v*-characteristic is shown in Fig. 5.21, while a) shows the characteristic within the complete permitted operation band, b) shows a detail around the reference voltage with redefined $v_{DC,min}$ and $v_{DC,max}$ and c) an even more detailed section to demonstrate the validity of requirement (5.6) exemplarily. Therefore, slopes of $h_{left} = 88{,}600$ and $h_{right} = 141{,}300$ are calculated as minimum values in order to meet all given requirements.

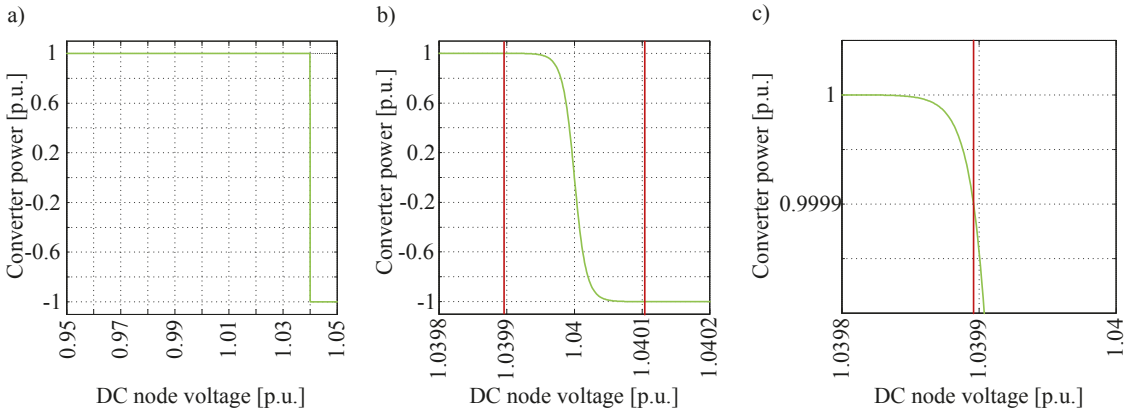

Fig. 5.21: Continuous *p*-*v*-characteristic for representation of constant voltage control a) for the complete permitted voltage operation band, b) detail around voltage reference and c) detail to show validity of (5.6).

5.4.2 Tripartite margin droop and tripartite droop control

Due to sigmoid function characteristics (droop constant always < ∞) a tripartite margin droop control cannot be represented with respect to a complete flat area by a continuous *p*-*v*-characteristic. But the area around the operating point can be considered being almost flat if the inflection points are set in the middle between reference operating point and voltage limits or even further towards voltage limits. Thus, for tripartite margin droop control (5.11) and (5.12) should be respected. For the example in Fig. 5.22 a) the middle between reference operating point and voltage limits was chosen. Minimum slopes in order to meet all given requirements in (5.6) - (5.8) are $h_{left} = 292$ and $h_{right} = 477$.

$$v_{DC,min} < v'_{DC,min} \leq v_{DC,min} + \frac{v_{DC,ref} - v_{DC,min}}{2} \tag{5.11}$$

$$v_{DC,max} > v'_{DC,max} \geq v_{DC,ref} + \frac{v_{DC,max} - v_{DC,ref}}{2} \tag{5.12}$$

Consequently if tripartite droop control behaviour is intended with a higher slope around the reference operating point (5.13) and (5.14) should be respected. An example is given in Fig. 5.22 b). Minimum slopes for that example in order to meet all given requirements in (5.6) - (5.8) are $h_{left} = 231$ and $h_{right} = 406$.

$$v_{DC,ref} > v'_{DC,min} \geq v_{DC,ref} - \frac{v_{DC,ref} - v_{DC,min}}{2} \tag{5.13}$$

$$v_{DC,ref} < v'_{DC,max} \leq v_{DC,ref} + \frac{v_{DC,max} - v_{DC,ref}}{2} \tag{5.14}$$

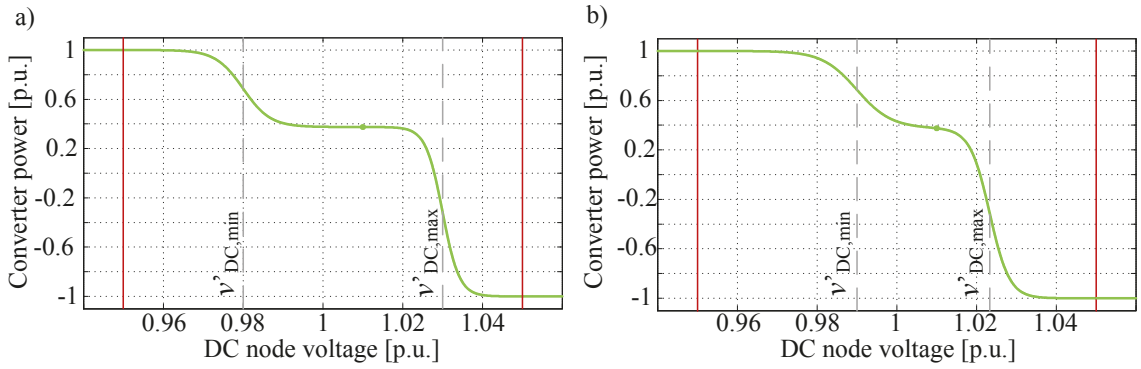

Fig. 5.22: Continuous *p*-*v*-characteristic for representation of a) tripartite margin droop control and b) tripartite droop control.

5.4.3 Voltage margin control

Voltage margin control defines a small area around the reference operating point (smaller than the permitted voltage band) where voltage is almost uncontrolled and then having

steep slopes towards $p_{conv,max}$ and $p_{conv,min}$. Thus, in order to fulfil (5.6) and (5.7) $v_{DC,max}$ and $v_{DC,min}$ must be redefined to be very close to $v'_{DC,max}$ and $v'_{DC,min}$ respectively. As an example $v_{DC,max}$ and $v_{DC,min}$ are chosen according to (5.15) and (5.16). Consequently, resulting in steep slopes of $h_{left} = 87{,}500$ and $h_{right} = 93{,}500$.

$$v_{DC,max} - v'_{DC,max} = 10^{-4} \tag{5.15}$$

$$v'_{DC,min} - v_{DC,min} = 10^{-4} \tag{5.16}$$

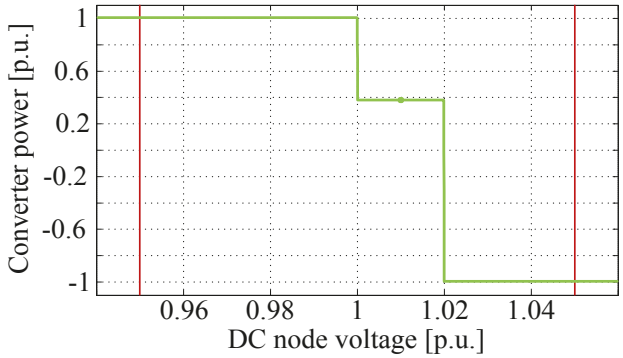

Fig. 5.23: Continuous *p*-*v*-characteristic for representation of voltage margin control.

5.4.4 Constant power control

Constant power control is similar to voltage margin control but here the complete permitted voltage band remains uncontrolled. Thus, $v_{DC,max}$ and $v_{DC,min}$ are still representing the limits for the permitted voltage band in (5.6) and (5.7). Here $v'_{DC,max}$ and $v'_{DC,min}$ must be set very close to these absolute voltage limits $v_{DC,max}$ and $v_{DC,min}$. As an example $v'_{DC,max}$ and $v'_{DC,min}$ are chosen according to (5.17) and (5.18). Thus, steep slopes of $h_{left} = 92{,}100$ and $h_{right} = 90{,}800$ result in order to meet the requirements according to (5.6) and (5.7). The continuous *p*-*v*-characteristic representing constant power control is shown in Fig. 5.24.

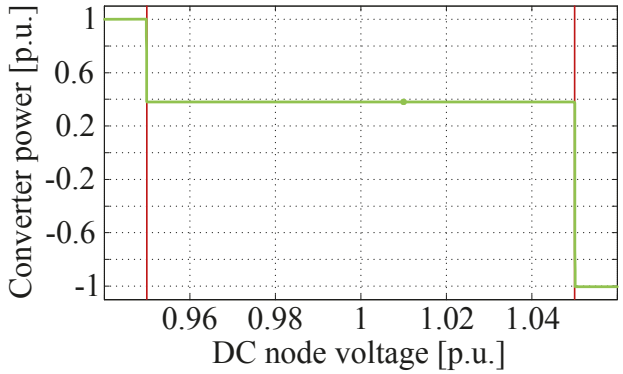

Fig. 5.24: Continuous *p*-*v*-characteristic for representation of constant power control.

$$v_{DC,max} - v'_{DC,max} = 10^{-4} \tag{5.17}$$

$$v'_{DC,min} - v_{DC,min} = 10^{-4} \tag{5.18}$$

5.4.5 Voltage droop control

In the literature, voltage droop control in literature is primarily defined over the entire operation range but not around a particular operation point. Using continuous *p*-*v*-characteristic, exemplary representatives are shown in Fig. 5.25 b) and c). Here only one sigmoid out of the set of two is needed, so the left one is exemplarily chosen. Since no specific operation point is intended for this kind of voltage droop control characteristic, $p_{conv,min}$ is replacing $p_{conv,ref}$ formerly used for the definition of the initial function (see (5.5)) if the left sigmoid is used ($p_{conv,max}$ if the right sigmoid is used), referring to the example. Examples are given in Fig. 5.25 where the (5.6) and (5.7) are fully respected (b) and where the accuracy for (5.6) and (5.7) is lowered from 10^{-4} to 10^{-2} (c). Decreasing the accuracy here means the converter's power capacity is not fully used for $v_{DC,min}$ and $v_{DC,max}$ respectively, but the *p*-*v*-characteristic's slope is less steep. For the Fig. 5.25 b) $h_{left} = 199$ and for Fig. 5.25 c) $h_{left} = 106$. As described, the left sigmoid is used here and therefore h_{right} is not affected and can have any value.

If voltage droop is intended around a specific reference operation point, the value for $p_{conv,ref}$ in (5.5) is replaced by $p'_{conv,ref}$ according to

- (5.19) if the reference operation point is defined by a positive converter reference power $p_{conv,ref}$
- (5.20) otherwise

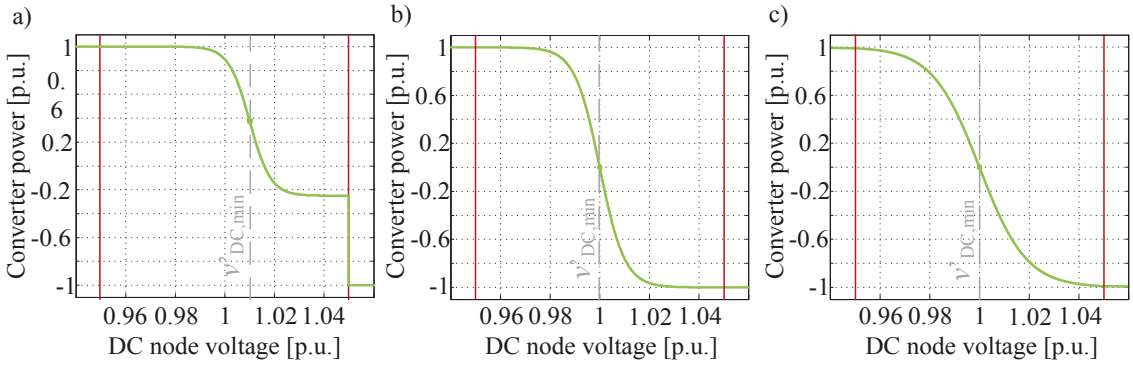

Fig. 5.25: Continuous *p*-*v*-characteristic for representation of voltage droop control a) droop around an operating point, b) droop around the midpoint of the permitted operation band respecting (5.6) and (5.7), c) droop around the midpoint of the permitted operation band respecting (5.6) and (5.7) with a limited accuracy of 0.99.

$$\left.\begin{aligned} p'_{\mathrm{conv,ref}} &= p_{\mathrm{conv,max}} - 2\cdot\left(p_{\mathrm{conv,max}} - p_{\mathrm{conv,ref}}\right) \\ v'_{\mathrm{DC,min}} &= v_{\mathrm{DC,ref}} \\ v'_{\mathrm{DC,max}} &= 0.9999\cdot v_{\mathrm{DC,max}} \end{aligned}\right\} p_{\mathrm{conv,ref}} > 0 \tag{5.19}$$

$$\left.\begin{aligned} p'_{\mathrm{conv,ref}} &= p_{\mathrm{conv,min}} - 2\cdot\left(p_{\mathrm{conv,min}} - p_{\mathrm{conv,ref}}\right) \\ v'_{\mathrm{DC,min}} &= 1.0001\cdot v_{\mathrm{DC,min}} \\ v'_{\mathrm{DC,max}} &= v_{\mathrm{DC,ref}} \end{aligned}\right\} p_{\mathrm{conv,ref}} \leq 0 \tag{5.20}$$

This inherently defines whether the right ($p_{\mathrm{conv,ref}} \leq 0$) or left ($p_{\mathrm{conv,ref}} > 0$) sigmoid will be used around the reference point. The other sigmoid (not used around the reference operating point) is needed in this case to meet the requirement, this is according to (5.7) for $p_{\mathrm{conv,ref}} > 0$ or (5.6) for $p_{\mathrm{conv,ref}} \leq 0$. Thus, the inflection point of this sigmoid function is defined to be very close to the according voltage limit (here 0.01% of voltage limit). Consequently, the inflection points of both sigmoid functions are defined according to (5.19) for $p_{\mathrm{conv,ref}} > 0$ and according to (5.20) for $p_{\mathrm{conv,ref}} \leq 0$. An example is given in Fig. 5.25 a) for a reference point given by $p_{\mathrm{conv,ref}} = 0.375$ and $v_{\mathrm{DC,ref}} = 1.01$. According to (5.6), (5.7) and (5.19) the slopes of the sigmoid function result to $h_{\mathrm{left}} = 114{,}402$ and $h_{\mathrm{right}} = 237$.

5.5 Parameterization of continuous p-v-characteristic based on AC side balancing power provision capability

As previously shown, continuous *p*-*v*-characteristic can emulate any state of the art voltage control characteristic. In addition to its continuous shape, another of its important advantage is that a smooth transition between each state of the art characteristic is possible and that it is not necessary to actively decide for one of these specific voltage control characteristics.

When parameterizing a continuous voltage control characteristic, it is important not only to consider its effect on the DC system but also its effect on the AC system since active power is affected by DC voltage control characteristics in case of a DC disturbance. If a converter activates DC balancing power this must be provided by the connected AC system. To different cases can be differentiated in this context:

1. An overlay HVDC grid without interconnection to another asynchronous AC grid
2. An HVDC grid which is also interconnecting asynchronous AC grids

In case 1 the DC balancing power that is obtained from the AC grid primarily leads to a power flow shift from the DC to the AC grid. If losses are not considered in this case the overall energy balance is no disturbed by a converter trip and the AGM, as described in chapter 4, will adapt converter power reference values in order to relieve the AC grid by some of the additional power flows.

In case 2, a scenario can occur that a converter trips which is supposed to import or export power from another asynchronous AC grid via the HVDC grid. Thus, balancing power is activated in at least one of both AC systems and transmitted to the corresponding converter.

If a converter activates DC balancing power that is surounded by a lot of available AC balancing capacities the AC transmission grid is less affected in in another scenario when available AC balancing capacities are remote. Thus, it is reasonable to activate that converter first that has available balancing capabilities nearby. Available balancing capability in this context means that the balancing power is physically as well as commercially available. Herinafter commercial availablitity is assumed and only physical availability is considered. However, the basic parameterization methodology will be the same if commercial availablility of balancing power is considered additionally.

Factors that affect the AC systems capability of providing DC balancing power are (see Fig. 5.26):

- Available balancing power from power plants nearby the considered converter $\sum p_{\text{AC\_balance},i}$
- Available balancing power from storage nearby the considered converter $\sum p_{\text{storage\_installed}}$
- Available balancing energy from storage nearby the considered converter $\sum e_{\text{storage}}$

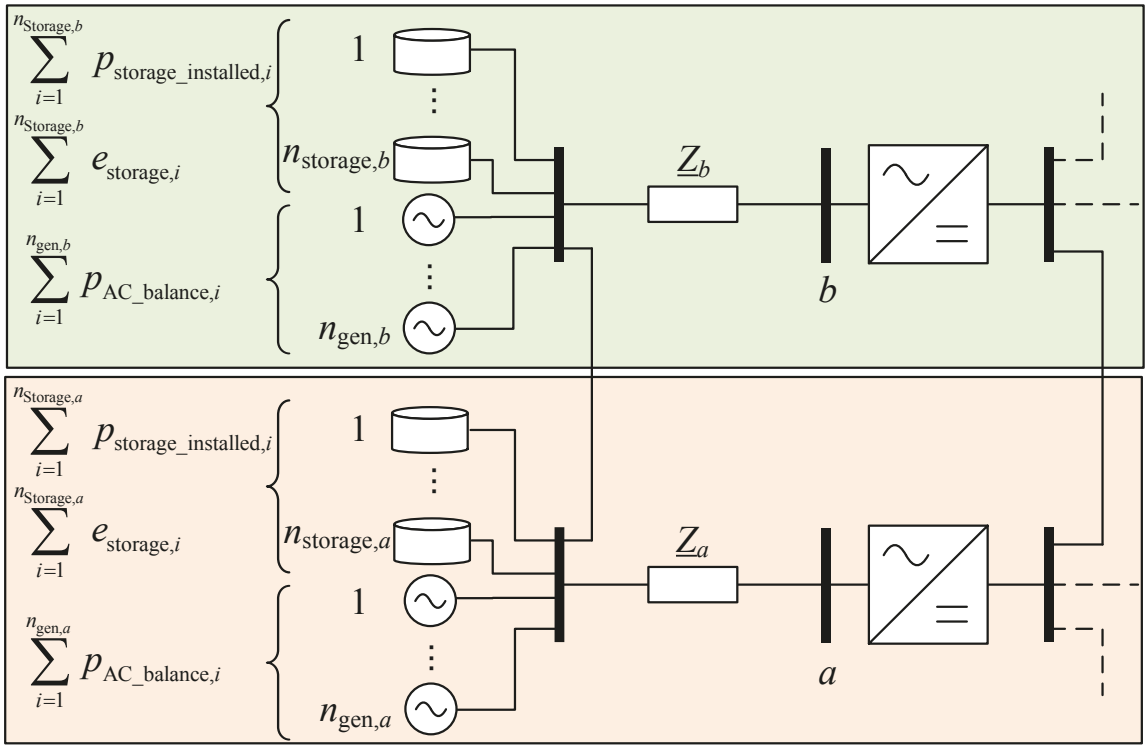

Fig. 5.26: Factors affecting AC system's capability for DC balancing of a nearby converter.

Normally the AC system is designed or reinforced according to where an HVDC converter is connected. Thus, the line(s) connecting the converter to the AC transmission system ($\underline{Z}$) will normally be large enough to transmit installed power. In rare cases, for example due to AC line trips where there is not enough transmission capability, $p_{\text{conv,max}}$ and $p_{\text{conv,min}}$ will be reduced for the voltage control characteristic by an overlayed control instance (tertiary

control) regardless of the voltage control characteristic. Therefore, available transmission capacity is inherently respected during parameterization of the continuous *p*-*v*-characteristic's by given values for minimum and maximum converter power $p_{conv,min}$ and $p_{conv,max}$.

As for parameterization, installed power of each converter is also not considered for DC balancing power purposes. This is inherent when assuming a control characteristic is limited not only by permitted voltage band but also by an permitted power band defined by $p_{conv,min}$ and $p_{conv,max}$ of a converter.

When considering a meshed HVDC overlay grid, some converters will collect bulk power (e.g. from offshore wind power plants) and others will feed power back into the AC grid where load centers or significant storage capacities are located. Consequently, regarding the provision of DC balancing power, the capability of each converter will differ. Converters can be surrounded by generation units which do not participate in balancing power transmission for the following reasons:

- The infeed comes from renewable resources (e.g. converters connected to offshore wind farms)
- Power plants which do not participate in energy balancing (e.g. due to commercial reasons)

On the contrary, if the converter location is in the vicinity of huge storage plants they can contribute to the balancing power. Here it is assumed that storages can be used for ancillary services as provision of DC balancing power. Furthermore, a distinction between capability of the surrounding AC system regarding positive and negative balancing power must be made. Some generators may have the capability to provide negative balancing power if it is strongly desired, however, no capacity to provide positive balancing power, as is the case for generation units of renewable energy.

It is described in chapter 3, that an overlayed tertiary control will provide converters with parameterisation of its *p*-*v*-characteristic. This also includes the reference converter power. The gap between power reference value as well as maximum and minimum converter power are defined as $p^{+}_{DC\_balance}$ and $p^{-}_{DC\_balance}$ (see Fig. 5.27 c). This is the maximum or minimum needed positive or negative DC balancing power. This implies the assumed that the whole allowed operation area between $p_{conv,min}$ and $p_{conv,max}$ can used in case of a DC energy imbalance. The more converter are involved in the HVDC grid, the more the needed balancing power can be devided among all converters. Therefor it could be defined that balancing power will be provided by a converter up to a maximum of ±10%-20% of its power reference value. $p^{+}_{DC\_balance}$ and $p^{-}_{DC\_balance}$ will be redefined in such a case.

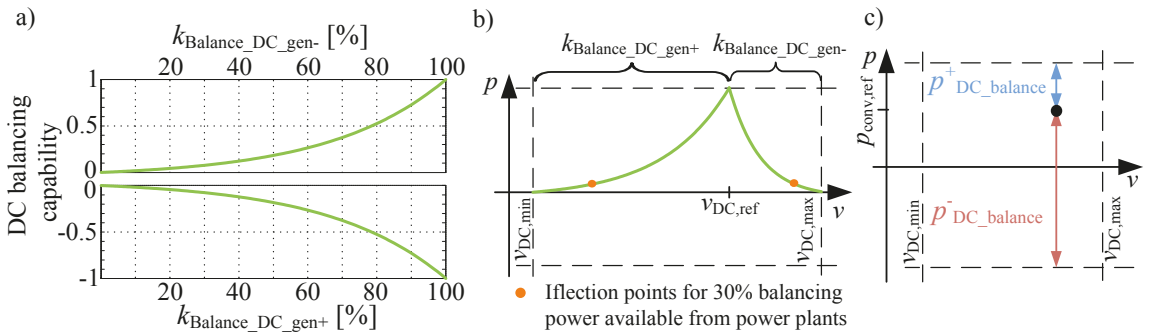

Fig. 5.27: Influence of available AC balancing power towards capability of participating in DC balancing (a), its meaning for inflection point placement for continuous *p*-*v*-characteristic (b) and maximum needed DC balancing power dependent on converters reference power of the considered converter (c).

If all generation units close to the converter (excluding storages) can provide the maximum required positive balancing power $p^{+}_{DC\_balance} = p_{conv,max} - p_{conv,ref}$ (see Fig. 5.27 a) the capability of the AC grid close to this converter is 100%. To measure and quantify this impact an indicator $k_{Balance\_DC\_gen+}$ is introduced in (5.21). The indicator is limited to 1 as this equals a balancing capability of 100%. The same is true for negative balancing power provision capability indicated by $k_{Balance\_DC\_gen-}$ which is limited to -1 (= 100% of negative balancing power provision capability).

$$k_{Balance\_DC\_gen+} = \frac{\sum_{i=1}^{n_{gen}} p^{+}_{AC\_balance,i}}{p_{conv,max} - p_{conv,ref}} \quad \text{for} \sum_{i=1}^{n_{gen}} p^{+}_{AC\_balance,i} \le \left(p_{conv,max} - p_{conv,ref}\right) \tag{5.21}$$

$$k_{Balance\_DC\_gen+} = 1 \qquad \text{else}$$

$$k_{Balance\_DC\_gen-} = \frac{\sum_{i=1}^{n_{gen}} p^{-}_{AC\_balance,i}}{p_{conv,min} - p_{conv,ref}} \quad \text{for} \sum_{i=1}^{n_{gen}} p^{-}_{AC\_balance,i} \le \left(p_{conv,min} - p_{conv,ref}\right) \tag{5.22}$$

$$k_{Balance\_DC\_gen-} = -1 \qquad \text{else}$$

As this is directly transferable to the location of the left inflection point of the continuous *p*-*v*-characteristic, this can be defined as being at nominal voltage Fig. 5.27 b) in this particular case. The same is true for negative balancing power and the right inflection point according to (5.25). Even if a generation unit is not capable of providing negative balancing power it can be recommended that generation is reduced when a certain DC voltage is exceeded, as is indicated in Fig. 5.27 a), b) and later on in Fig. 5.29. Interpolation for $k_{Balance\_DC\_gen+} = 0\ldots1$ and $k_{Balance\_DC\_gen-} = 0...-1$ is another subject to optimization. Here an exponential interpolation was used (see Fig. 5.27).

The more generation is installed without balancing capability in a grid the more storage becomes necessary to compensate their inherent volatility. In general, the presence of storage will have a positive impact on the capability of the AC system with regards to DC

balancing. However, this is not only dependent on the installed storage power but also on the storage level. An almost empty storage will allow the AC system enough capacitance for DC balancing in the event that the DC voltage reaches its maximum permitted value $v_{DC,max}$. However, this will not be able to provide an adequate balancing capability in the instance that DC voltage reaches it minimum permitted value, $v_{DC,min}$.

In order to combine storage level and installed storage power it is of interest to know how long and in which dimension storage near to a converter can provide DC balancing capability. As already described, it is assumed that the tertiary control will provide converters with parameterisation of its *p*-*v*-characteristic. Furthermore, it is assumed that this controller has knowledge of installed storage power, its storage level and its schedule.

It is proposed that parameterisation of *p*-*v*-characteristics is updated with the converter's voltage and power reference schedules which may be every 15 minutes, for example. For parameterisation of the *p*-*v*-characteristic and distribution of DC balancing capability among all converters of the HVDC grid it is important to know for how long storage near to the converter can absorb full positive ($p^+_{DC\_balance}$) or negative ($p^-_{DC\_balance}$) DC balancing power (see Fig. 5.28 c). This is possible with the aforementioned knowledge of the tertiary control.

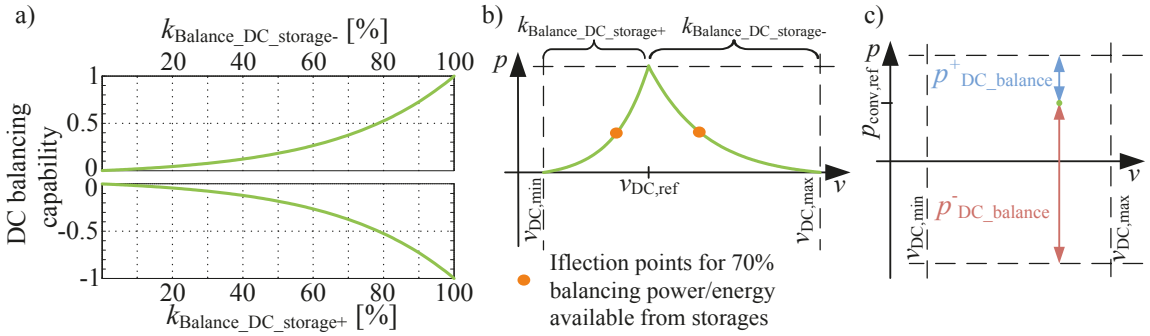

Fig. 5.28: Influence of storages towards capability of participating in DC balancing (a), its meaning for inflection point placement of continuous *p*-*v*-characteristic (b) and maximum needed DC balancing power dependent on converters reference power of the considered converter (c).

For 100% DC balancing capability of an AC PCC, enabled by storage, $p^+_{DC\_balance}$ or $p^-_{DC\_balance}$ (see Fig. 5.28 c) can be absorbed for 15 minutes, i.e. the maximum required energy $e^+_{DC\_balance}$ or $e^-_{DC\_balance}$ is available by storage. The less power which can be absorbed within 15 minutes, the smaller the DC balancing capability of the considered AC node will be (see Fig. 5.28 a). This is directly transferable to the location of inflection points of the continuous characteristic in the *p*-*v*-chart Fig. 5.28 b).

Capability of absorbing positive and negative DC balancing power by an AC node (enabled by storage) can be described as a percentage by (5.23) and (5.24) respectively. Thereby k_p represents the capability of installed storage power while k_{e+} and k_{e-} represent the capability of available energy enabled by storage for additional generation and additional load respectively.

$$k_{\text{Balance\_DC\_storage+}} = k_{\text{p+}} \cdot k_{\text{e+}} \cdot 100\% \tag{5.23}$$

$$k_{\text{Balance\_DC\_storage-}} = k_{\text{p-}} \cdot k_{\text{e-}} \cdot 100\% \tag{5.24}$$

$$k_{\text{p+}} = \frac{\left(\sum_{i=1}^{n_{\text{Storage}}} p_{\text{storage\_installed},i} \right)}{p_{\text{conv,max}} - p_{\text{conv,ref}}} \text{ for } \sum_{i=1}^{n_{\text{Storage}}} p_{\text{storage\_installed},i} \le (p_{\text{conv,max}} - p_{\text{conv,ref}}) \tag{5.25}$$
$$k_{\text{p+}} = 1 \qquad \text{else}$$

$$k_{\text{p-}} = \frac{\left(\sum_{i=1}^{n_{\text{Storage}}} p_{\text{storage\_installed},i} \right)}{\left| p_{\text{conv,min}} - p_{\text{conv,ref}} \right|} \text{ for } \sum_{i=1}^{n_{\text{Storage}}} p_{\text{storage\_installed},i} \le \left| p_{\text{conv,min}} - p_{\text{conv,ref}} \right| \tag{5.26}$$
$$k_{\text{p-}} = 1 \qquad \text{else}$$

$$\begin{aligned} e^{+}_{\text{DC\_balance}} &= (p_{\text{conv,max}} - p_{\text{conv,ref}}) \cdot 15\,\text{min} \\ e^{-}_{\text{DC\_balance}} &= (p_{\text{conv,min}} - p_{\text{conv,ref}}) \cdot 15\,\text{min} \end{aligned} \tag{5.27}$$

$$k_{\text{e+}} = \frac{\left(\sum_{i=1}^{n_{\text{Storage}}} e_{\text{storage\_installed},i} \cdot k_{\text{Stocklevel},i} \right)}{e^{+}_{\text{DC\_balance}}} \text{ for } \left(\sum_{i=1}^{n_{\text{Storage}}} e_{\text{storage\_installed},i} \cdot k_{\text{Stocklevel},i} \right) \le e^{+}_{\text{DC\_balance}} \tag{5.28}$$
$$k_{\text{e+}} = 1 \qquad \text{else}$$

$$k_{\text{e-}} = \frac{\left(\sum_{i=1}^{n_{\text{Storage}}} e_{\text{storage\_installed},i} \cdot \left(1 - k_{\text{Stocklevel},i}\right) \right)}{e^{-}_{\text{DC\_balance}}} \text{ for } \left(\sum_{i=1}^{n_{\text{Storage}}} e_{\text{storage\_installed},i} \cdot \left(1 - k_{\text{Stocklevel},i}\right) \right) \le \left| e^{-}_{\text{DC\_balance}} \right| \tag{5.29}$$
$$k_{\text{e-}} = -1 \qquad \text{else}$$

Indices resulting from both criteria, for the AC balancing capability by generation units $k_{\text{Balance\_DC\_gen}}$ as well as absorbable DC balancing power by storages within the AC grid $k_{\text{Balance\_DC\_sorage}}$ (including power and energy availability), are combined to the AC systems overall capability of DC balancing power at the converter's AC PCC $k_{\text{Balance\_DC}}$ according to (5.30) and (5.31). The overall capability of AC system's DC balancing at converter's AC PCC is limited to 1 (as illustrated in Fig. 5.29). According to Fig. 5.27 and Fig. 5.28, a capability of 1 in this case means, that the AC node is capable of handling maximum positive DC balancing power demand of the converter and therefore, the right inflection point is at the reference voltage.

Consequently, a capability of -1 in this case means that the AC node is capable of handling maximum negative DC balancing power demand of the converter and thus, the left inflection point is at the reference voltage. Hence, the upper and lower planes in Fig. 5.29 repre-

sent possible positions for the right and left inflection point of the continuous *p*-*v*-characteristic respectively, depending on the balancing power provision by AC generating units and available storage capabilities nearby the considered converter.

$$\begin{aligned} k_{\text{Balance\_DC+}} &= k_{\text{Balance\_DC\_gen+}} + k_{\text{Balance\_DC\_storage+}} && \text{if } k_{\text{Balance\_DC\_gen+}} + k_{\text{Balance\_DC\_storage+}} \le 1 \\ k_{\text{Balance\_DC+}} &= 1 && \text{else} \end{aligned} \tag{5.30}$$

$$\begin{aligned} k_{\text{Balance\_DC-}} &= k_{\text{Balance\_DC\_gen-}} + k_{\text{Balance\_DC\_storage-}} && \text{if } k_{\text{Balance\_DC\_gen-}} + k_{\text{Balance\_DC\_storage-}} \ge -1 \\ k_{\text{Balance\_DC-}} &= -1 && \text{else} \end{aligned} \tag{5.31}$$

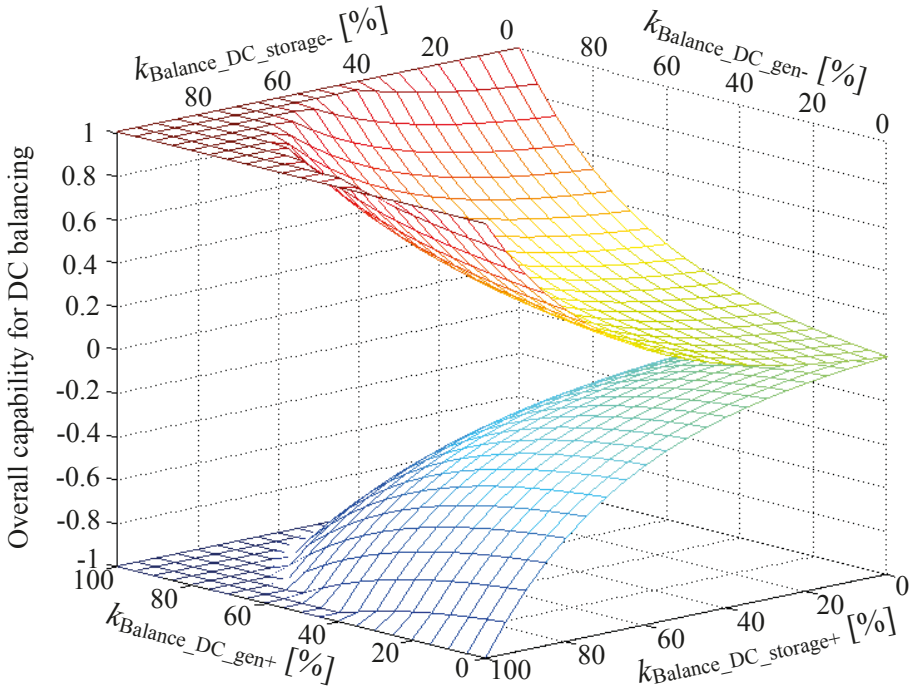

Fig. 5.29: AC system capability of DC balancing at converters AC PCC.

If only one of both inflection points is at or very nearby reference voltage a suitable solution that also meets (5.8) is not likely to be possible. Thus, in that case, the corresponding inflection point is displaced 1% beside $v_{\text{DC,ref}}$. It is also possible to have a scenario where both inflection points are defined to meet the reference voltage. In that scenario it is comparable to a voltage droop replication around an operating point as it is described on page 104.

5.6 Numerical Studies

Hereinafter examples are given for automatic parameterisation of continuous *p*-*v*-characteristics assuming three scenarios regarding available storage and AC balancing power capabilities nearby the considered converter station's AC PCC and another scenario assuming an overlay HVDC grid with five converters. Based on those four scenarios the impact of the proposed method we be demonstrated regarding shape of *p*-*v*-characteristic and impact on AC power flows in case of a disturbance on the DC side:

- Scenario 1: The assumed installed power of the storage is sufficient to cover all possible DC balancing power but storage levels allow only a limited provision in positive DC balancing (high DC balancing capability)
- Scenario 2: No storage or generating units are available for DC balancing power nearby the converter (no DC balancing capability)
- Scenario 3: Only 20% of maximum positive or negative DC balancing can be provided by generating units nearby the converter and support by storage is also limited (low DC balancing capability)
- Scenario 4: A whole overlay HVDC grid is considered and *p*-*v*-characteristics of all five converters are parameterized according to AC PCC's characteristics (overlay HVDC grid)

5.6.1 Scenario 1: High DC balancing capability

For scenario 1 it is assumed that installed power of the storage is sufficient to cover all DC balancing power. But the storage level determines that 90% of the maximum necessary DC balancing energy is available for negative balancing power (in case of $v_{DC} > v_{DC,ref}$) and only 10% for positive balancing power provision (in case of $v_{DC} < v_{DC,ref}$) as illustrated in Fig. 5.30. Additionally, 70% of the maximum required positive and negative DC balancing power can be covered from generation plants nearby the considered converter.

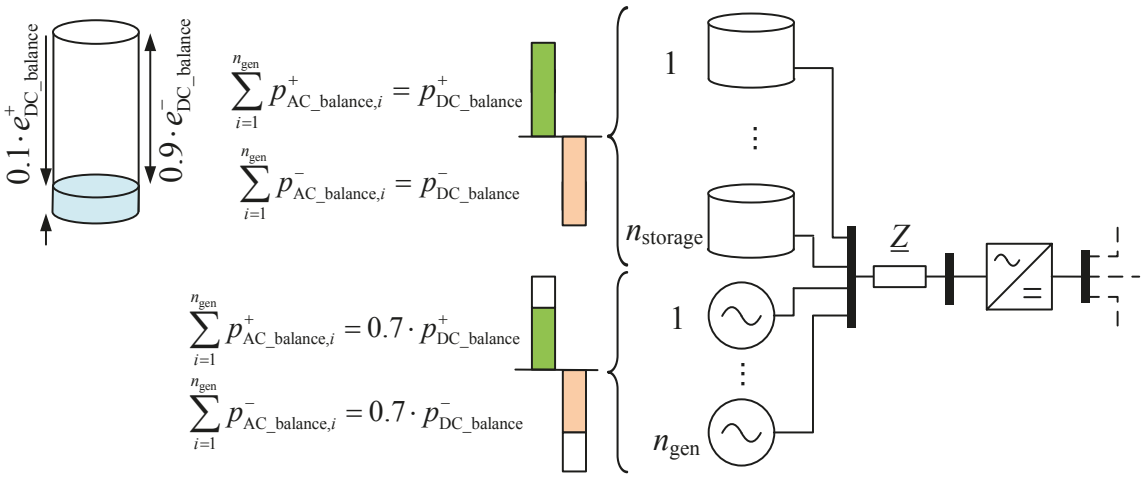

Fig. 5.30: Parameterization of continuous *p*-*v*-characteristic regarding AC side grid characteristics and local conditions – scenario 1.

Thus, storage can be almost used to its maximum in case of $v_{DC} > v_{DC,ref}$ and AC balancing power restrictions are limited. In case of $v_{DC} < v_{DC,ref}$ limitations are also very small but use of storages for positive DC balancing power is very limited. The operating reference point of the converter is defined at $v_{DC,ref} = 1.01$ p.u. and $p_{conv,ref} = 0.375$ p.u. Consequently, right inflection point is at $v'_{DC,min} = 1.0064$ and $v'_{DC,max} = 1.0105$. In order to meet (5.6) - (5.8), the smallest slope values are $h_r = 3{,}459$ and $h_l = 201$. The corresponding *p*-*v*-characteristic is shown in Fig. 5.31. The area nearby the operating point in overvoltage direction is very

steep due to the aforementioned high capability of storage for negative DC balancing power. Due to low storage capability for additional energy generation, slope in under voltage direction is much smaller than in over voltage direction.

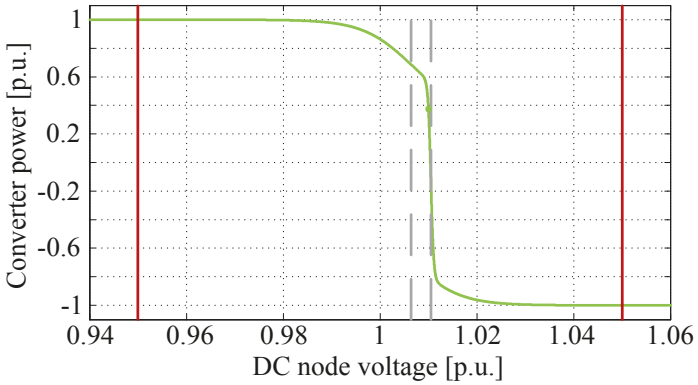

Fig. 5.31: Automatic parameterization of *p*-*v*-characteristic for 70% available AC balancing power for DC balancing, 10% generating and 90% consuming capability of storages nearby a converter.

5.6.2 Scenario 2: No DC balancing capability

This scenario outlines the case where there are no storage or generating units available for AC balancing power nearby the converter. This scenario is also illustrated in Fig. 5.32.

Consequently inflection points are defined in such a way that the converter does not take part in DC energy balance control until the DC voltage band is almost left (see Fig. 5.33 b). The right inflection point is defined by the automatic algorithm to be $v'_{DC,min} = 0.9501$ and $v'_{DC,max} = 1.04999$ and in order to meet (5.6) - (5.7) the minimum slope values are $h_r = 72{,}255$ and $h_l = 64{,}362$. Fig. 5.33 a) shows the resulting *p*-*v*-characterisitc.

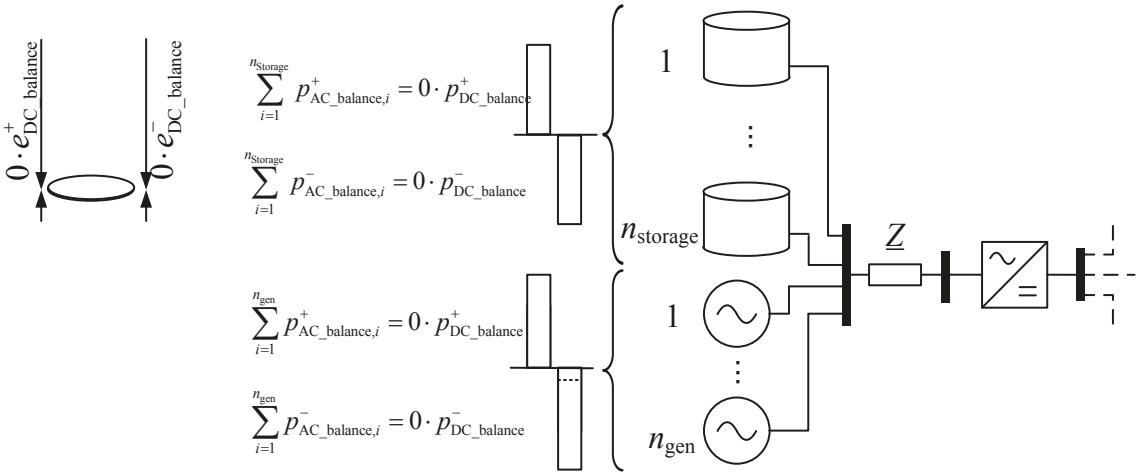

Fig. 5.32: Parameterization of continuous *p*-*v*-characteristic regarding AC side grid characteristics and local conditions – scenario 2.

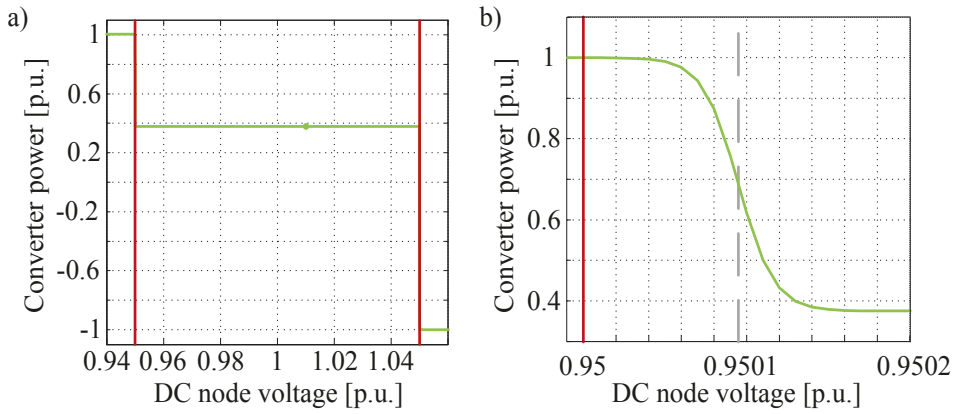

Fig. 5.33: Automatic parameterization of *p*-*v*-characteristic for 0% available AC balancing power for DC balancing and 0% balancing capability of storages nearby a converter a) complete characteristic and b) zoom around voltage limit.

5.6.3 Scenario 3: Low DC balancing capability

This scenario assumes that 20% of the maximum required positive and negative DC balancing power can be covered from AC generating units nearby the considered converter. Again it is assumed that installed storage power is capable of maximum required DC balancing power. Storable energy and storage level determine the capability of positive balancing capability by 20% and of negative balancing capability of 40% (see Fig. 5.34).

Automatic inflection point determination defines $v'_{\mathrm{DC,min}} = 0.9857$ and $v'_{\mathrm{DC,max}} = 1.0280$. Minimum slope for both sides is consequently $h_{\mathrm{l}} = 287$ and $h_{\mathrm{r}} = 434$. This scenario does not represent an extreme scenario since low AC balancing capability is compensated by storage. However, storage is not as capable as they could cope with all possible DC balancing scenarios. This therefore results in a very smooth *p*-*v*-characteristic as shown in Fig. 5.33.

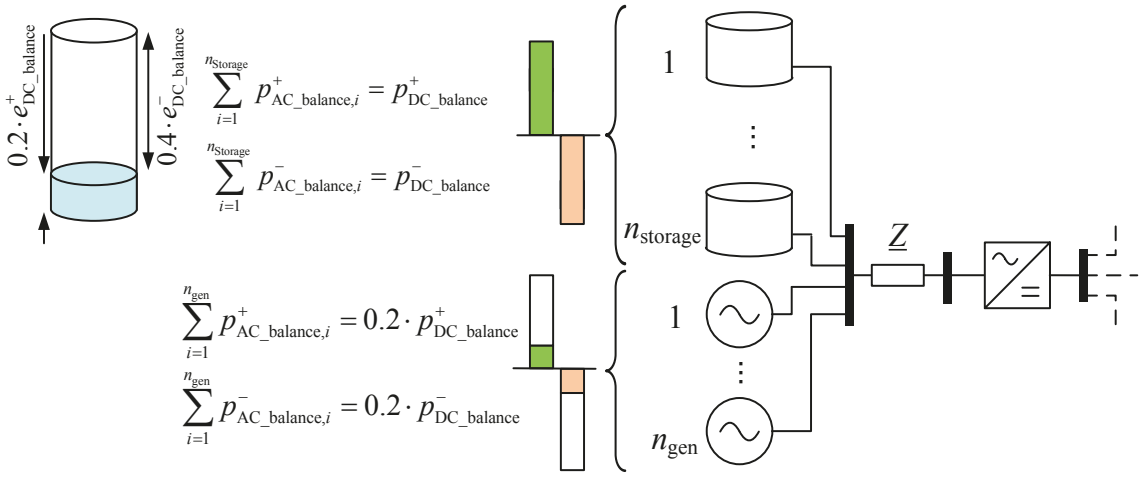

Fig. 5.34: Parameterization of continuous *p*-*v*-characteristic regarding AC side grid characteristics and local conditions – scenario 3.

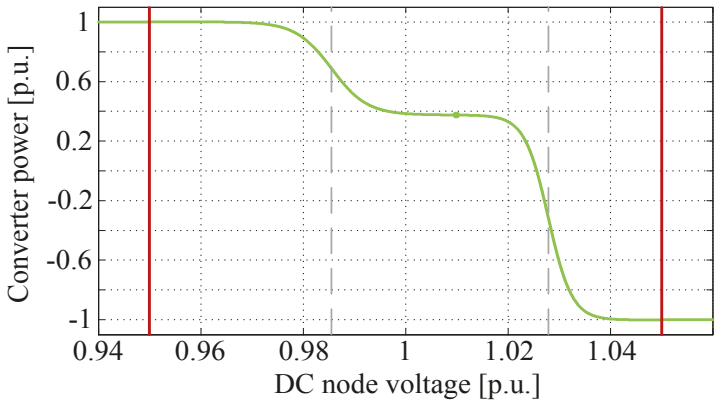

Fig. 5.35: Automatic parameterization of *p*-*v*-characteristic for 20% available AC balancing power for DC balancing, 40% generating and 20% consuming capability of storages nearby the converter.

The described methodology implies the advantage of adjusting the participation of each HVDC converter in DC balancing action according to its AC PCC. There is a methodology described in literature for voltage droop parameterisation [146]. This methodology defines the same droop constant for all converters that are participating in DC voltage control. Thus, no differences are made and special requirements of PCCs are not taken into consideration. This disadvantage is overcome with the proposed parameterization.

5.6.4 Scenario 4: Overlay HVDC grid

In order to show the effect of the proposed characterization on the AC grid, numerical simulations are carried out with an entire AC and DC grid. This is derived from the reference grid introduced in subchapter 2.4 (Fig. 2.5). In order to show the effect of the proposed parameterization of *p*-*v*-characteristics, the following requirements must be met by modifications:

- *Diverse characteristics of AC nodes connected to converters:* The proposed parameterization is based on balancing control capabilities of AC nodes connected to converters. Therefore, AC nodes with a high balancing capability, without balancing capability and with a limited capability should be considered.
- *AC nodes without converters:* The reference grid provides a converter for all AC nodes within Germany. Only some AC nodes outside Germany are not directly connected to a converter. It is intended to show the effect of the parameterization on power flows not only between converter connected AC nodes but also which effect the proposed parameterization has for other AC nodes.
- *Limited number of AC nodes:* The number of AC nodes that will be used for this scenario 4, should not exceed the number of AC nodes in the reference grid as is described in subchapter 2.4. Otherwise results can easily become confusing.

Therefore, only the central part (CA Germany) of the reference grid is considered here. In order to increase the number of AC nodes without a direct connection to a converter, three additional AC nodes are included and the number of converters is reduced by one. Additionally, not all AC nodes are connected to a power plant any more to achieve the desired diverse characteristic of AC nodes. This results in a 9 node AC and 5 node overlay HVDC grid.

All AC nodes nearby the converter including all relevant units for parameterization are aggregated to a single AC node in order to keep the number of AC nodes limited. This is a permissible simplification as global effects of parameterization are intended to show. The parameterization is made in such a way that converters connected to an AC node with a large potential for positive and / or negative balancing is controlling DC energy balance by a large amount if the reference voltage is marginally left. The less balancing potential is available at or nearby the converter's AC node, the more the DC node voltage differs from its reference until a significant participation of the converter in DC balancing is performed. This avoids DC balancing power flow in the AC grid as far as possible and AC transmission capacity can be used as originally intended.

For numerical case studies a nine node AC grid with four power plants with balancing capability and a five node DC grid is used according to Fig. 5.36. There is 1 GW of generation at node 2 with no balancing capability. The set points for generating units with balancing capacity and converters are given in Fig. 5.36 as well.

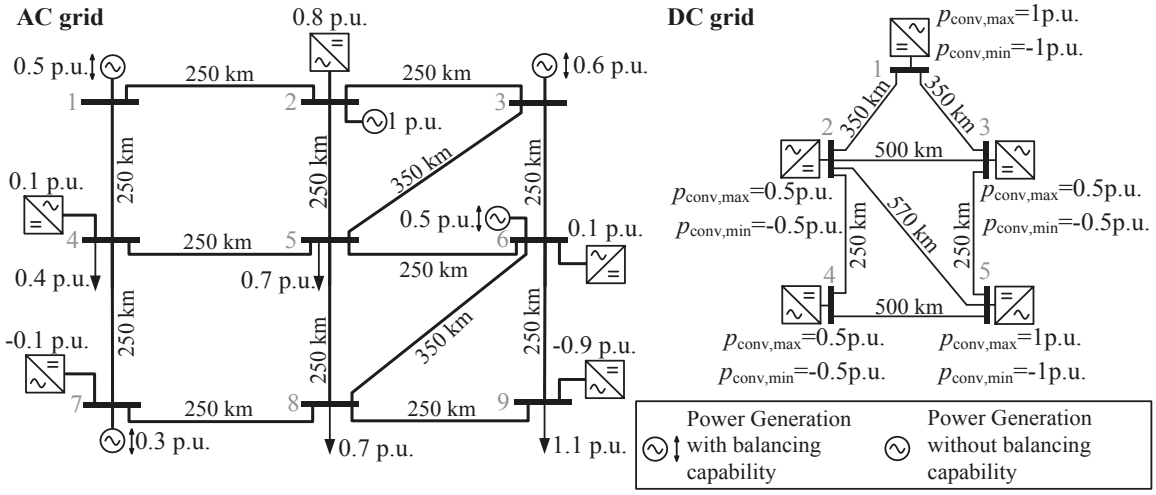

Fig. 5.36: AC and DC grid for numerical simulations regarding parameterization of continuous *p*-*v*-characteristic.

In a first scenario the proposed parameterization is not applied. Therefore, the inflection points are defined for each converter according to (5.32) for the left and according to (5.33) for the right inflection point. Thus, there is no consideration for balancing capability nearby or at the AC node the converter is connected to.

$$v'_{\mathrm{DC,min}} = v_{\mathrm{DC,ref}} - 0.55\left(v_{\mathrm{DC,ref}} - v_{\mathrm{DC,min}}\right) \tag{5.32}$$

$$v'_{\mathrm{DC,max}} = v_{\mathrm{DC,ref}} + 0.55\left(v_{\mathrm{DC,max}} - v_{\mathrm{DC,ref}}\right) \tag{5.33}$$

The reference values for all converters are assumed to be calculated by a tertiary control instance (operational planning) according to the following values:

Converter 1	$v_{\mathrm{DC1,ref}} = 1.04$	$p_{\mathrm{conv,DC1}} = 0.8$
Converter 2	$v_{\mathrm{DC2,ref}} = 0.9835$	$p_{\mathrm{conv,DC2}} = 0.1$
Converter 3	$v_{\mathrm{DC3,ref}} = 0.9796$	$p_{\mathrm{conv,DC3}} = 0.1$
Converter 4	$v_{\mathrm{DC4,ref}} = 0.9693$	$p_{\mathrm{conv,DC4}} = -0.1$
Converter 5	$v_{\mathrm{DC5,ref}} = 0.9611$	$p_{\mathrm{conv,DC5}} = -0.9$

The equilibrium of the DC grid is disturbed with -0.1 p.u. nearby DC node 1. In order not to superimpose different effects, the disturbance is not modeled as a partial converter trip but as a disturbance of the DC grid only. This could be the case if offshore wind generation is also connected to the DC grid. The AC grid is only affected by the DC balancing due to *p*-*v*-haracteristics.

In consequence of the disturbance, the overall DC voltage is decreasing. Before the disturbance takes place all converters are quite close at their reference values. The smallest voltage margin towards a significant impact of the control characteristic from this operation point exists for converter 5.

Additionally the control characteristic for converter 5 for voltages smaller than the reference voltage is very steep (see Fig. 5.37). Thus, converter 5 takes all necessary balancing power in order to balance the -0.1 p.u. disturbance by a reduced infeed into the AC grid. At the AC node of converter 5 no units are installed for provision of balancing power. Consequently, other generating units in the AC system with balancing power capability are providing the necessary balancing power.

The largest amount comes from AC node 6, which is the closest AC node with balancing capability to converter 5. This leads to a significant higher power flow from AC node 6 to AC node 9 where converter 5 is connected to (see Fig. 5.37). Before the disturbance took place AC node 9 provided AC node 8 with power as there is only a load and no generating unit or converter connected to.

This situation changes with the DC disturbance. AC node 9 significantly reduces power provision for AC node 8. Instead power is flowing from AC node 6 and AC node 5 to AC node 8. Fig. 5.37 summarizes the power flows, power generation and converter power values after reestablishing steady state of the overall system and provides information about change compared to the pre-disturbance situation for each value.

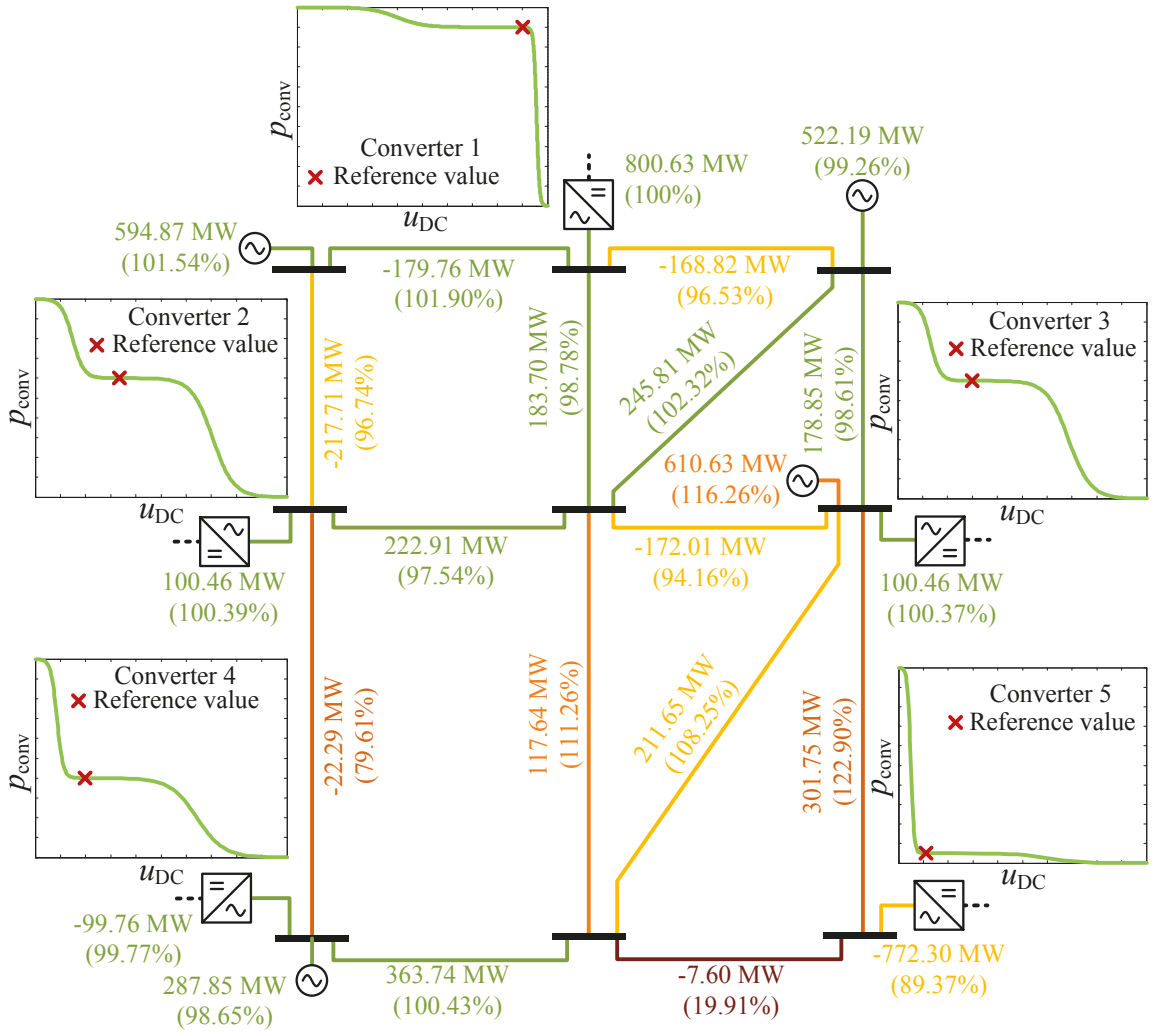

Fig. 5.37: Power flows and operating points in the AC grid after a -100 MW disturbance in the HVDC grid in absolute values (and its change compared to the pre-disturbance situation in brackets) with *p*-*v*-characteristics not respecting the available balancing power at AC nodes.

The proposed method for control characteristic parameterization intends to avoid those additional power flows within the AC grid caused by balancing power provision for the DC system. For simplification and as no significant storage capacities are available in Europe yet (compared to that amount that would be needed today and in the near future) only generating units' balancing capabilities are considered in this numerical simulation. It is assumed that generating units can provide a maximum of positive balancing power only limited by its power limitations. Additionally the nine node AC grid that is used here defines large distances between AC nodes (see Fig. 5.36). As the proposed parameterization methodology suggests taking into account balancing capabilities nearby the converter only, units connected to the same AC node as the converter are considered.

Thus, according to Fig. 5.36 and equations (5.21) and (5.22) the following positive and negative balancing capabilities indicators $k_{\text{Balance\_DC\_gen}}{}^{+}$ and $k_{\text{Balance\_DC\_gen}}{}^{-}$ at converters' AC nodes are identified:

AC node 2 – converter 1

$p_{\text{conv,ref,1}} = 0.8$ p.u.		$p_{\text{gen,1}} = 0$ p.u.	
$p_{\text{conv,max,1}} = 1$ p.u.	$p_{\text{conv,min,1}} = -1$ p.u.	$p_{\text{gen,max,1}} = 0$ p.u.	$p_{\text{gen,min,1}} = 0$ p.u.
$p_{\text{conv,max,1}} - p_{\text{conv,ref,1}} = 0.2$ p.u.		$p^{+}_{\text{AC\_balance,1}} = 0$ p.u.	
$p_{\text{conv,min,1}} - p_{\text{conv,ref,1}} = 1.8$ p.u.		$p^{-}_{\text{AC\_balance,1}} = 0$ p.u.	
$\boldsymbol{k_{\text{Balance\_DC\_gen+,1}} = 0}$		$\boldsymbol{k_{\text{Balance\_DC\_gen-,1}} = 0}$	

AC node 4 – converter 2

$p_{\text{conv,ref,2}} = 0.1$ p.u.		$p_{\text{gen,2}} = 0$ p.u.	
$p_{\text{conv,max,2}} = 0.5$ p.u.	$p_{\text{conv,min,2}} = -0.5$ p.u.	$p_{\text{gen,max,2}} = 0$ p.u.	$p_{\text{gen,min,2}} = 0$ p.u.
$p_{\text{conv,max,2}} - p_{\text{conv,ref,2}} = 0.4$ p.u.		$p^{+}_{\text{AC\_balance,2}} = 0$ p.u.	
$p_{\text{conv,min,2}} - p_{\text{conv,ref,2}} = -0.6$ p.u.		$p^{-}_{\text{AC\_balance,2}} = 0$ p.u.	
$\boldsymbol{k_{\text{Balance\_DC\_gen+,2}} = 0}$		$\boldsymbol{k_{\text{Balance\_DC\_gen-,2}} = 0}$	

AC node 6 – converter 3

$p_{\text{conv,ref,3}} = 0.1$ p.u.		$p_{\text{gen,3}} = 0.5$ p.u.	
$p_{\text{conv,max,3}} = 0.5$ p.u.	$p_{\text{conv,min,3}} = -0.5$ p.u.	$p_{\text{gen,max,3}} = 1$ p.u.	$p_{\text{gen,min,3}} = 0$ p.u.
$p_{\text{conv,max,3}} - p_{\text{conv,ref,3}} = 0.4$ p.u.		$p^{+}_{\text{AC\_balance,3}} = 0.5$ p.u.	
$p_{\text{conv,min,3}} - p_{\text{conv,ref,3}} = -0.6$ p.u.		$p^{-}_{\text{AC\_balance,3}} = 0.5$ p.u.	
$\boldsymbol{k_{\text{Balance\_DC\_gen+,3}} = 1}$		$\boldsymbol{k_{\text{Balance\_DC\_gen-,3}} = -0.833}$	

AC node 7 – converter 4

$p_{\text{conv,ref,4}} = -0.1$ p.u.		$p_{\text{gen,4}} = 0.3$ p.u.	
$p_{\text{conv,max,4}} = 0.5$ p.u.	$p_{\text{conv,min,4}} = -0.5$ p.u.	$p_{\text{gen,max,4}} = 0.8$ p.u.	$p_{\text{gen,min,4}} = 0$ p.u.
$p_{\text{conv,max,4}} - p_{\text{conv,ref,4}} = 0.6$ p.u.		$p^{+}_{\text{AC\_balance,4}} = 0.5$ p.u.	
$p_{\text{conv,min,4}} - p_{\text{conv,ref,4}} = -0.4$ p.u.		$p^{-}_{\text{AC\_balance,4}} = 0.3$ p.u.	
$\boldsymbol{k_{\text{Balance\_DC\_gen+,4}} = 0.833}$		$\boldsymbol{k_{\text{Balance\_DC\_gen-,4}} = -0.75}$	

AC node 9 – converter 5

$p_{conv,ref,5}$ = -0.9 p.u.		$p_{gen,5}$ = 0 p.u.	
$p_{conv,max,5}$ = 1 p.u.	$p_{conv,min,5}$ = -1 p.u.	$p_{gen,max,5}$ = 0 p.u.	$p_{gen,min,5}$ = 0 p.u.
$p_{conv,max,5}$-$p_{conv,ref,5}$ = 1.9 p.u.		$p^{+}_{AC\_balance,5}$ = 0 p.u.	
$p_{conv,min,5}$-$p_{conv,ref,5}$ = -0.1 p.u.		$p^{-}_{AC\_balance,5}$ = 0 p.u.	
$\boldsymbol{k_{Balance\_DC\_gen+,5}}$ **= 0**		$\boldsymbol{k_{Balance\_DC\_gen-,5}}$ **= 0**	

The resulting *p*-*v*-characteristics are shown in Fig. 5.38. The positive balancing capability at AC node 6 (converter 3) is 100%. Thus, if a negative voltage deviation at DC node of converter 3 occurs a significant amount of DC balancing power is provided immediately due to the steepness of the according continuous *p*-*v*-characteristic for negative DC node voltage deviations.

The same -100 MW disturbance is applied to the DC system as before. Converter 3 stops DC voltage decrease by providing the DC system with 100 MW from the AC grid. Due to the steepness of continuous *p*-*v*-characteristic of converter 3 for negative DC voltage deviations converter 4 is almost not participating in DC balancing. This is useful as AC node of converter 4 has a lower capability for positive balancing.

As a consequence of the proposed parameterization of the *p*-*v*-characteristics there are no significant power flow changes on the transmission lines of the considered AC grid. The DC balancing power that is provided by converter 3 for the DC grid is generated by a generating unit at the same AC node by means of AC balancing control (see Fig. 5.38). This proves the functionality of the proposed parameterization methodology for continuous *p*-*v*-characteristics.

It should be highlighted that converters with a *p*-*v*-characteristic with a steep shape for negative voltage deviations very close to their operating point ensure a high voltage level of the DC grid in case of a negative energy balance. Thus, such converters are very useful for the HVDC grid in means of providing a high voltage level for lower transmission losses.

The closer the reference operating point is to the upper voltage limit the steeper the *p*-*v*-characteristic will be for positive voltage deviations. However, this represents a vital function for the HVDC grid equipment in means of overvoltage protection within the allowed DC node voltage band.

5.7 Conclusion

All state of the art local DC node voltage control characteristics are piecewise linear characteristics. Except for voltage droop control characteristic there are points of discontinuity within the allowed operating band. It is shown that such characteristic can promote oscillations within the DC grid. A continuous DC node voltage control characteristic is proposed which reduces the probability of oscillations within the DC grid.

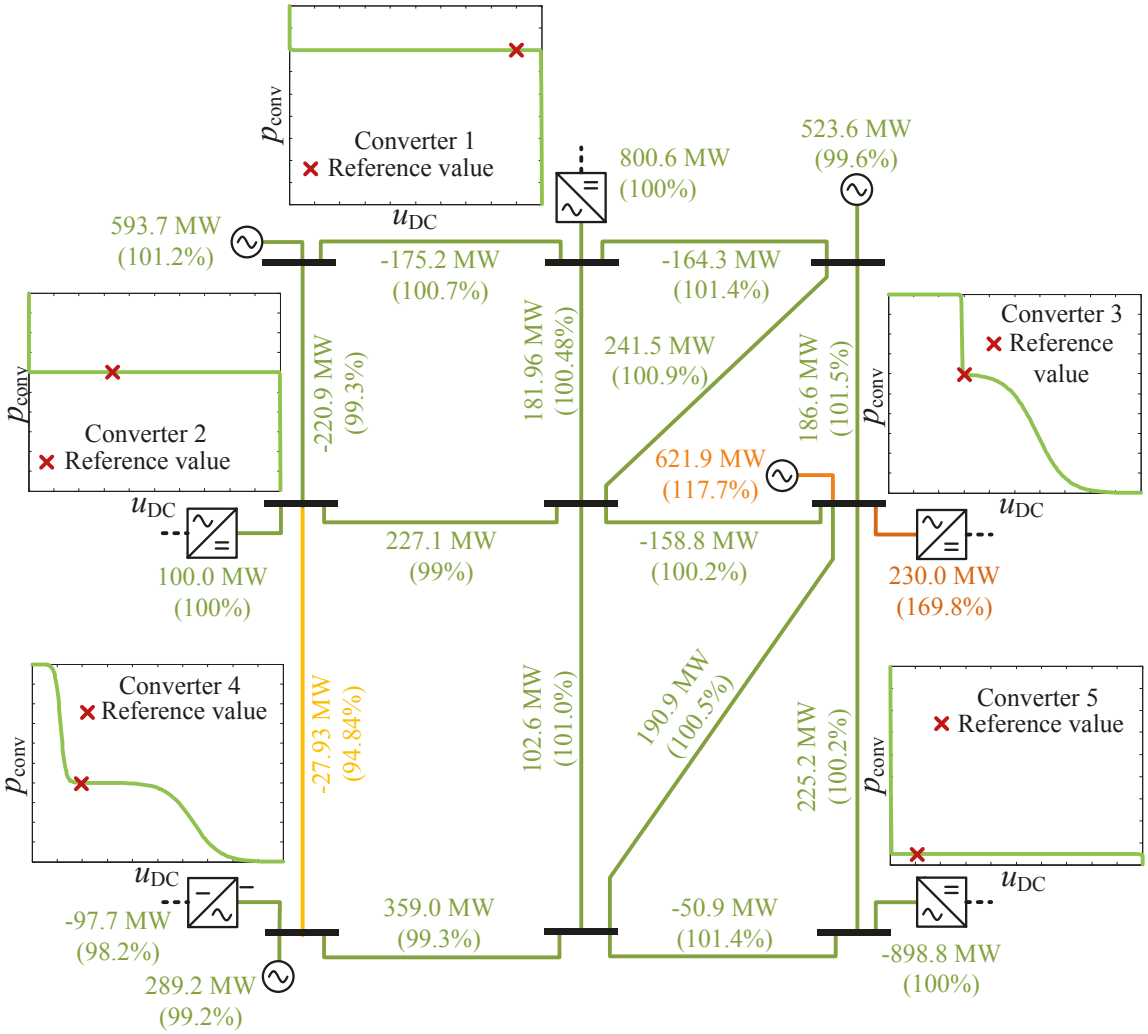

Fig. 5.38: Power flows and operating points in the AC grid after a 100 MW disturbance in the HVDC grid in absolute values (and its change compared to the pre-disturbance situation in brackets) with *p*-*v*-characteristics respecting the available balancing power at AC nodes.

It is shown that this continuous DC node voltage control characteristic can emulate the basic shape of all state of the art DC node voltage control characteristics but without points of discontinuity. The most important advantage of this proposed characteristic is a high level of variability due to its parameterization options. It enables the operator of an HVDC grid for automatic parameterization, e.g. according to AC grid characteristics at AC PCC.

A methodology for this automatic parameterization of the continuous DC node voltage control characteristic is proposed based on the availability of balancing power at or nearby the AC PCC. It is shown that this reduces additional AC power flows in case of DC energy equilibrium is disturbed. Thus, AC transmission capacities are available for their primarily duties and the AC system operator is not ask to save a lot of transmission reserves for DC ancillary services.

6 Conclusion and outlook

With Germany as its nucleus, the energy revolution defines a new European power transmission requirement: Long distance bulk power transmission. A possible solution to fulfill this requirement is the implementation of a transcontinental HVDC grid; that is a new network layer on top of the extra high voltage interconnected AC transmission grid (HVAC grid) will evolve in Europe. Both technological and operational issues of a (transcontinental) HVDC grid, operating on top of an interconnected HVAC grid, are completely new territory in engineering and science. This work is dedicated to answer the following research question:

How is it possible to operate a meshed HVDC grid overlaying an interconnected AC grid in order to maintain its own stability and interact with the AC system to ensure secure operation of both AC and DC and that an optimal operation point of the overall system can be reached?

The question is answered from an HVDC grid operator perspective. A three stage control and operation scheme for HVDC grids is proposed (see Fig. 6.1). They address the need for:

- A central control instance which operates centrally (e.g. HVDC grid control center) for operational planning, where set point schedules are determined and all relevant network data of the DC and affected AC system are available. This is introduced as **tertiary control** (chapter 3).
- A local control instance which operates on the converters' sites based on global data acquisition allowing converters to adjust their reference values accordingly to optimally cope with unscheduled network events in the AC and DC grid. To a certain extend this depends on telecommunication due to a global data acquisition approach (wide area monitoring). This is introduced as **secondary control** in chapter 4.
- A local control instance which operates at the converters' site and does not rely on a telecommunication system for safe operation. It ensures the DC energy balance of the HVDC grid. This is introduced as **primary control** in chapter 5.

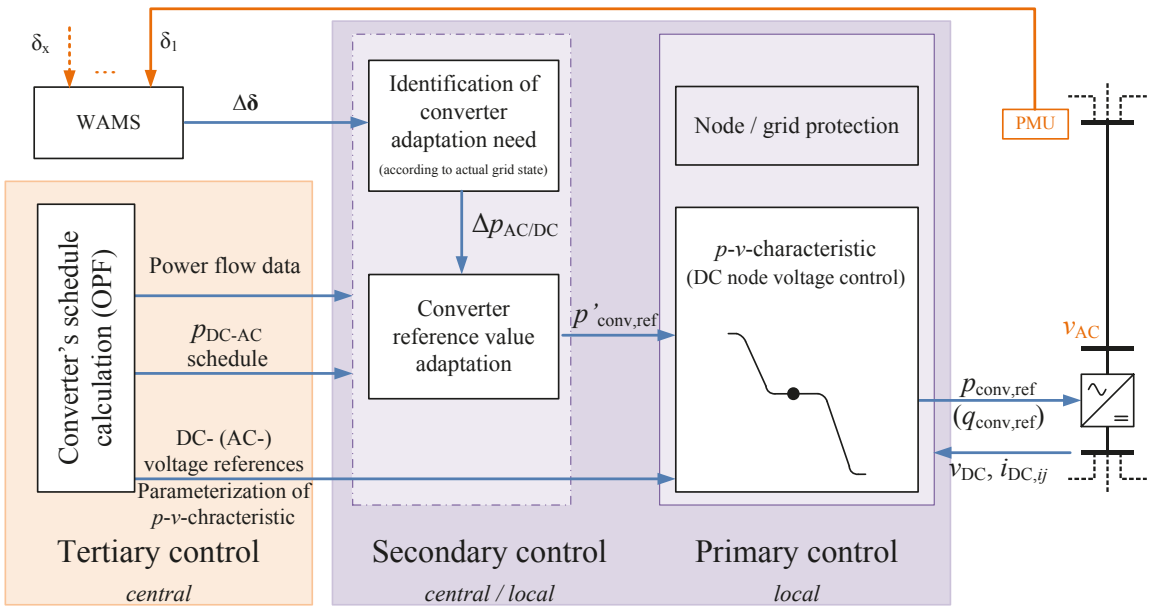

Fig. 6.1: Overall control concept for operation of overlay HVDC grids including tertiary, secondary and primary control instance.

6.1 Results

Tertiary control

Within the operational planning, schedules of converter reference values for certain time intervals (e.g. 15 min) are determined (chapter 3). This is based on the anticipated AC and DC grid topology, conventional power plant schedules, renewable generation and load forecasts. Thus, an instance that performs operational planning for an overlaying HVDC grid has ideally the system responsibility over the entire HVDC grid network layer and reasonable insights into the underlaying AC grid. In a scenario where there are separate organizations, an HVDC grid operator can derive recommendations for the AC transmission system operators (TSOs). If this is assumed, a mixed AC/DC optimal power flow (OPF) can be performed in order to find an overall optimal system state according to the defined objective function (OF) which can have single or multiple objectives included.

Such kind of mixed AC/DC optimization problems are characterized by high non-linearity, multiple local minima, a very wide permissible state space (e.g. each converter has a permissible operation range between maximum and minimum converter power). The use of conventional optimization algorithms implies a high risk for a non-convergence or convergence in a local minimum. Thus, an algorithm is used that is capable of robustly solving these types of optimization problems. Therefore, the Differential Evolution (DE) strategy is selected. The generic and heuristic character of DE reduces the risk for convergence in local minima or even non-convergence. Its properties and robust convergence behavior has been demonstrated with a numerical case study.

However, it is also shown that there is still a potential for further improvement of problem formulation in order to totally avoid convergence in local minima.

Operational planning not only provides optimized reference value schedules for all converters but also the most appropriate converter control parameters for local control actions such as for primary control. Thus, in the operational planning stage, the tertiary control determines a consecutive time series of sets of reference values for converters as well as optimized local converter control parameters in order to ensure a secure operation of the entire AC and DC grid.

Secondary Control

As soon as a disturbance occurs, schedules from the tertiary control may no longer be optimal and might no longer be able to guarantee stable operation. As such, a disturbance addresses an unplanned event causing equipment to become unavailable. This can be a consequence of a fault while the fault detection and clearing is not addressed in this work. Even if security constrained OPFs can limit the risk for reaching instabilities, an adaptation of converter reference values according to the new system state can help to relieve the AC system by additional power flows (due to the disturbance) until corrective actions are activated, for example. Such a method is proposed for the secondary control instance as a fast and local measure in chapter 4.

This proposed method uses global voltage angle differences provided by a phasor measurement unit (PMU) based wide area monitoring system (WAMS). From measured AC node voltage phase angle difference changes in the AC power flow directions and magnitudes can be observed. Significant deviations from the planned power flow schedule can also be detected. According to this, the converter active power reference values are locally adapted in order to support the AC transmission system by optimally adjusting the share of power flows between the AC and DC grid. The positive effect on the AC grid is shown in some numerical case studies.

The method is introduced as angle gradient method (AGM) as it is based on the measurement of AC node voltage angle gradients within the AC grid in order to identify significant unscheduled power flow changes. This means that the AGM relies on telecommunication based provisions of global measurements by a WAMS. Thus, it is also analyzed which effect the trip of a single PMU or the overall WAMS system has on AGM performance assuming different backup mechanisms for replacement data acquisition or favored actions of the AGM in case of a PMU trip, for example.

It is shown that in case of a PMU trip disabling AGM for the specific converter wich is in the vicinity of the tripped PMU is the most appropriate solution. The AGM for all other surrounding converters will operate as usual and ensures optimal share of the unplanned power flow changes between the HVDC and AC grid.

Primary Control

Due to the very small short term storage capacity of the DC grid (small "DC grid inertia" provided by its capacitances) a DC energy imbalance immediately causes a change in DC node voltages. A DC node voltage deviation is acceptable as long as it stays within small defined limits around the nominal voltage, primarily due to insulation requirements and secondarily due to optimal operation purposes.

Ensuring DC energy balance has been a topic on which has recently garnered a lot of research attention. As such, several control concepts have been proposed. These control concepts make use of locally applied and piecewise linear control characteritics. Oscilations within the DC grid can occur if more than one converter controls DC node voltage according to one of the many piecewise linear control characteristics (except voltage droop control). Oscillations mostly occur around the points of discontinuity. To overcome this, a continuous control characteristic is proposed in chapter 5.

This continuous control characteristic can be parameterized in such a way that state of the art DC node voltage control characteristics are emulated. Thus, the adjustment of control characteristics allows for the realization of different control objectives, voltage margin control, voltage droop control or constant voltage control, for example. But the biggest advantage of this characteristic is its high variability in shape. By adjusting its parameters a continuous modification is possible to dynamically change between various shapes of the control characteristics. Thus, it is no longer necessary to define a fixed particular control characteristic. Depending, for example, on the AC grid characteristic at the point of common coupling, an appropriate parameterization can automatically be realized A method is therefore proposed which adjusts the converter control characteristic with respect to the capability of AC balancing power provision at the converter's AC connection point.

As the DC node voltage control characteristic ensures the DC energy balance (DC balancing), the required DC balancing power is taken from the AC grid. The proposed parameterization algorithm forces those converters to provide DC balancing power immediately after there is a deviation from its DC node voltage reference which are connected to an AC node that has itself or can receive from nearby AC nodes all balancing power that might be in the worst case requested by the converter. Converters which are connected to AC nodes with little to no balancing power provision capability will remain in a power control mode until limits in the DC node voltage are almost reached.

This AC balancing power provision capability based parameterization method relieves the AC grid by additional DC balancing power flows as DC balancing power is requested where it can be provided by the AC grid. This positive effect of the proposed DC node voltage control characteristic parameterization method is demonstrated by a numerical case study.

The according parameterization corresponds to the AC balancing power provision capability based parameterization method is also provided by the tertiary control instance. It is

assumed that at the tertiary control level, there is grid information which allows for that. As the parameterization of the control characteristic may need to be adapted after a disturbance (e.g. power plant trip) there should be a short term optimization in place (e.g. within secondary control). Even if this optimization can only be based on a subset of the entire DC and AC grid due to time constraints a parameter adaptation can further increase system performance.

Main contributions

The main contribution of the thesis is a coherent approach for operating overlay HVDC grids. The approach is comprised of three levels corresponding to operational planning (tertiary control), reference value adaptation in case of significant unscheduled AC power flow changes (secondary control) and ensuring the DC energy balance (primary control). Particular contributions are:

- **Tertiary control:** An optimization algorithm is developed to determine converter reference schedules of an overlay HVDC grid. This algorithm takes the HVDC as well as all affected parts of the AC grid into account and performs a mixed AC/DC OF based on Differential Evolution (DE) strategy for optimization. This lowers the risk for non-convergence or convergence in local minima. Typical convergence of DE for such optimization problems is described and some significant potential for further improvement of problem formulation is identified.
  As this is a centralized approach assuming encompassing knowledge of the entire HVDC grid and all affected parts of the AC transmission level, a more decentralized approach is also proposed for the coordination of HVDC converters and optimizing their operation.
- **Secondary control**: A method that enables HVDC converters to share deviations from the AC power flow schedule between the HVDC and the underlaying AC grid is proposed. This is a fast acting control which is based on global measurement data acquisition using a wide area monitoring system and a local control at each converter station. The method automatically relieves the AC grid and avoids instability and transmission equipment overload. It is introduced as angle gradient method (AGM).
- **Primary control**: A continuous DC node voltage control characteristic is proposed that ensures DC energy balance based on a local control. Its continuous character reduces the risk for DC oscillations. Therefore, two parameterization methods for the local DC node voltage control characteristic are proposed:
  1. Approximation to piecewise linear DC node voltage control characteristics
  2. Parameter determination based on the capability of the AC system at point of common coupling for DC balancing power provision.

Exploitation of results

Most results that are presented in this thesis have been published continuously (see own publications in subchapter 7.1). Furthermore, some of these results and cognitions have contributed to the following task force and working groups:

- VDE task force “Aktive Energienetze im Kontext der Energiewende” [O-3],
- CIGRÉ working group B4.58 [O-6] and
- CENELEC working group CLC TC8x/WG 06 [O-7], [O-17].

Research question

Regarding the research question, this thesis proposes a methodology for structured operation of overlay HVDC grids.

An optimal operation point of the overall system (AC and DC) is assured for undisturbed operation using a mixed AC/DC OPF during operational planning. Thus, also an integrated operation of the HVDC within the AC system operation is realized by the mixed AC/DC OPF but also by the adaptation of converter active power reference value in case of a disturbance within the AC system.

This method shares the consequences of a disturbance in means of changed power flows between the AC and DC system by an adjustable division. The consequences for the AC grid due to a disturbance within the HVDC grid are limited due to the parameterization of converter DC node voltage control characteristics according to the AC nodes capability to provide balancing power. Significant additional power flows as a consequence of DC disturbances are avoided as much as possible. Thus an operation strategy for overlay HVDC grids is proposed including fast local control as well as slow operational planning instances.

There are still some open points for the operation of HVDC grids closely related to the research question which are addressed in the following subchapter 6.2.

6.2 Future Work

The contributions of this thesis for the operation of HVDC grids are a first step towards a standardized and practically implemented HVDC grid operation control. Topics for future work are identified in different categories. One corresponds to further development of the proposed methods and its application for HVDC grids and the other corresponds to the application of the proposed methods into other grid layers and their adaptations related to different special requirements. This primarily addresses the application in distribution grid layers as well as its extension to cover other equipment in the AC transmission layer such as flexible AC transmission systems or phase shifting transformers.

HVDC grids

Tertiary control

As suggested in subchapter 3.2, there is still significant potential for further improvement of problem formulation related to DE as optimization algorithm for mixed AC/DC OPF in terms of operational planning issues. This is primarily related to further increasing the probability for convergence in global minima.

Additionally, analyses are necessary to optimize DE regarding its convergence speed. Therefore one can take advantage of the fact that the operation point will probably not change drastically from one considered time step to another (e.g. 15 minutes later). This will significantly reduce the allowed state space that must be covered by DE. An inflexible definition of the allowed state space for the next time step can on the one hand decrease the computation time if no significant changes take place and on the other hand a stringent limitation of the allowed state space can exclude the global optimum if the generation and load pattern changed significantly. Hence, it is also possible to compare the change in generation and load pattern as well as change in topology from one considered time step to another and take this as a basis for dynamically defining the limited state space for the next time step.

A further development potential of DE AC/DC OPF problem formulation for operational planning is related to security constrained OPF in order to provide preventive actions. This can further improve the robustness of the overall AC/DC system regarding any disturbances as converter reference values are calculated with respect to possible disturbances. In this case the reference values are optimal or also optimal (if security constrains are only part of the objective function) with regards to a secure system state even if any disturbances take place.

It is also possible to develop a new optimization algorithm that perfectly matches the requirements for mixed AC/DC OPFs. At least further research can be made which focuses on the mixture of existing optimization methods in order to meet any special requirements.

Secondary control

Complementary to preventive actions, corrective actions can be taken into account for future work. If a disturbance takes place a coordinated adaptation of converter reference values is reasonable to optimize the system with respect to the changed boundary conditions. Stability margins can be maximized while losses are kept at a minimum. As central online optimization triggered by a certain disturbance is too time consuming, it is a feasible solution to calculate converter schedules for a defined contingency list in advance and deposit them locally for each converter. If a disturbance takes place the activation of the corresponding schedule is triggered.

The real time identification of a particular disturbance is another issue for future work (incident recognition). It would be ideal if local measurements within the converter's substation identify a particular disturbance. If such a method is not capable of identifying any particular disturbance within the whole grid a centralized identification can serve as a backup solution. This may cause further challenges on combining local and central fault identification, if some converters are quickly triggered whereas locally and others are slowly triggered centrally depending on fault identification capability of each converter control.

Preventive as well as corrective actions can be used to redefine the existing N-1 criterion of the AC transmission system towards the"diverse redundancy" of the overall AC and DC system. This is due to the fact that an AC equipment trip can not only be covered by an AC equipment but, if there is an overlay HVDC grid, it can also be covered by DC equipment by redefining the converters' power reference values. Having an HVDC overlay grid broadens the available redundancy capacities if it is defined and activated accordingly.

Primary control

Regarding the parameterization of local DC node voltage control characteristics a further improvement can be reached if the operational requirements corresponding to the AC and DC grid are combined. A fundamental requirement for the AC grid as proposed here is the reduction of DC balancing power flows in the AC transmission system. The proposed method considers available balancing power at or nearby the AC PCC of a converter. For the DC system it is important that there is a small DC voltage deviation in case of a disturbance. This implies that parameterization of DC node voltage control characteristics must be coordinated so as to ensure that there is always at least one activating significant DC balancing power immediately after its reference voltage is left.

As described in chapter 5 the parameterization of the DC node voltage control characteristic is performed by a tertiary control instance for operational planning purposes and can be adjusted by a secondary control instance after a disturbance has taken place. Thus, all significant instances described in this work are fully or partially subject to an HVDC control center. In this context, how to implement these control instances and control methods into an HVDC control center is also an operen issue. Which requirements exist, which data and which data preparation is needed and how to integrate an HVDC control center (e.g. located at TSC or CORESO) in existing AC operation and operation structure need to be adressed.

Besides the power transmission issues as addressed in this work there are also other services which can be provided to the AC systems if voltage source converters are used (e.g. AC voltage control or damping of AC power oscillations). A decoupled consideration of active and reactive power related issues is only possible as long as apparent power limits of the converter are not violated. Thus, a method for coordination of power transmission and other issues provided by converters with respect to the given hardware limits will be necessary.

Application in grid layers other than overlay HVDC grid

This work addresses operation issues for overlay HVDC grids. As there are tendencies towards meshed DC grids in lower grid layers, on the one hand to replace existing AC distribution topologies and on the other hand to build new large industrial complexes with DC electrification. Thus, it is also an important issue to transfer the methods developed for overlay HVDC grids here to lower voltage levels and islanded DC grids. Therefore, it is important to identify specific requirements of other voltage levels and applications.

The energy turnaround not only affects the transmission system as considered for this work but also the distribution system due to much renewable energy infeed in the lower grid levels. Some of the problems related to this fact may be overcome by fully controllable devices as converters between grid layers (as opposed to today's transformers) and also between separated parallel distribution grids of the same voltage layer (back to back converters on the distribution layer). Some coordination approaches as described in this work could also be applied to these vertical and horizontal couplings if they are modified according to its special requirements.

Moreover, the proposed approach can also be extended to the AC transmission layer in order to integrate the operation of flexible AC transmission systems and phase shifting transformers. This will be primarily a special issue for the described functionalities of secondary and tertiary control.

7 References

[1] H. Maier, „Erwin Marx (1893-1980) Ingenieurwissenschaftler in Braunschweig, und die Forschung und Entwicklung auf dem Gebiet der elektrischen Energieübertragung auf weite Entfernungen zwischen 1918 und 1950“, Ph.D. dissertation, Department for history of pharmacy and science, TU Braunschweig, GNT Verlag, ISBN 3-928186-11-6, Braunschweig, 1993.

[2] European Commission, Communication from the commission to the European parliament, the council, the European economic and social committee and the committee of the regions, “Energy Roadmap 2050”, Brussels, 15.12.2011.

[3] European Commission, Communication from the commission to the European council and the European Parliament, “An energy policy for Europe”, Brussels, 10.01.2007.

[4] European Commission, Communication from the commission to the council and the European parliament, “Renewable Energy road map – renewable energies in the 21st century: building a more sustainable future”, Brussels, 10.01.2007.

[5] European Council, EUCO 169/14, CO EUR 13, CONCL 5, Brussels, 24.10.2014.

[6] The European Wind Energy Association (EWEA), “Wind in power – 2013 European statistics”, 02/2014.

[7] The European Wind Energy Association (EWEA), “The European offshore wind industry – key trends and statistics 2013”, 01/2014.

[8] European Photovoltaic Industry Association (EPIA), “Global Market Outlook for Photovoltaics 2014-2018”, 2014.

[9] European Commission, Eurostat, Renewable energy statistics, [Online], Available: http://epp.eurostat.ec.europa.eu/statistics_explained/index.php/Renewable_energy_statistics (31.10.2014).

[10] ENTSO-E, Data Expert Group, “Electricity in Europe 2013 – Synthetic overview of ENTSO-E electric system consumption, generation and exchanges during 2013”, 03/2014.

[11] European Commission, M. Gimeno-Gutiérrez and R. Lacal-Arántegui, “Assessment of European potential for pumped hydropower energy storage – A GIS-based assessment of pumped hydropower storage potential”, JRC Scientific and Policy Reports, 2013.

[12] Eurelectric, O. Pirker et al., “Hydro in Europe: Powering Renewables – Synopsis Report”, Brussels, 09/2011.

[13] ENTSO-E, “Ten-Year Network Development Plan 2014 – Full Report”, 10/2014.

[14] 50Hertz Transmission, Amprion, TenneT and Transnet BW, „Netzentwicklungsplan Strom 2014 (NEP 2014)“, www.netzentwicklungsplan.de, 04/2014.

[15] Bundesministerium für Wirtschaft und Energie, „Erneuerbare Energien im Jahr 2013 – Erste vorläufige Daten zur Entwicklung der erneuerbaren Energien in

Deutschland auf der Grundlage der Angabe der Arbeitsgruppe Erneuerbare Energien-Statistik (AGEE-Stat)“, 02/2014.

[16] BDEW Bundesverband der Energie- und Wasserwirtschaft e.V., „Erneuerbare Energien und das EEG: Zahlen, Fakten, Grafiken (2014) – Anlagen, installierte Leistung, Stromerzeugung, EEG-Auszahlungen, Marktintegration der Erneuerbaren Energien und regionale Verteilung der EEG-induzierten Zahlungsströme“, 02/2014.

[17] A. Gustafsson, M. Saltzer, A. Farkas, H. Ghorbani, T. Quist and M. Jeroense, “The new 525 kV extruded HVDC cable system”, ABB Grid Systems, 08/2014.

[18] H. Koch, *GIL – Gas-insulated Transmission Lines*, vol. 1, Chichester, United Kingdom: J ISBN 9-780470665336, 2012.

[19] Inelfe, [Online], Available: http://www.inelfe.eu/ (01.11.2014).

[20] European Commission, “List of projects to be considered as potential Projects of Common Interest in energy Infrastructure – Electricity”, 2014.

[21] Western Link, [Online], Available: http://www.westernhvdclink.co.uk/ (01.11.2014).

[22] A. Aguado, Friends of the Supergrid, “An intelligent Pan-European Network: The Supergrid”, Presentation at FEPS, 12/2013, [Online], Available: http://slideplayer.us/slide/1191558/ last access (26.10.2014).

[23] J. Häfner and B. Jacobson, “Proactive hybrid HVDC breakers – a key innovation for reliable HVDC grids”, in *Proc. Cigré Symposion 2011*, Bologna, Italy, 09/2011.

[24] W. Grieshaber, J.-P. Dupraz, D.-L. Penache and L. Violleau, “Developement and test of a 120 kV direct current circuit breaker”, B4-301, in *Proc. Cigré Session 2014*, Paris, France, 08/2014.

[25] ENTSO-E, “Research & Development Roadmap 2013-2022”, Brussels, 12/2012.

[26] ENTSO-E, “ENTSO-E Draft Network Code on High Voltage Direct Current Connections and DC-connected Power Park Modules”, 04/2014.

[27] Twenties Projekt - transmitting wind, [Online], Available: www.twenties-project.eu (08.11.2014).

[28] Friends of the Supergrid, “Roadmap to the Supergrid Technologies - Update Report”, 06/2014.

[29] North Seas Countries’ Offshore Grid Initiative, “Final 2012 report”, 12/2012.

[30] J. Dorn, H. Huang and D. Retzmann, “Novel Voltage-Sourced Converters for HVDC and FACTS Applications”, in *Proc. Cigré Symposium 2007*, Osaka, Japan, 11/2007.

[31] J. Dorn, H. Huang and D. Retzmann, “A new Multilevel Voltage-Sourced Converter Topology for HVDC Applications”, in *Proc. Cigré Session 2008*, B4-304, Paris, France, 08/2008.

[32] V. Crastan and D Westermann, *Elektrische Energieversorgung 3 – Dynamik, Regelung und Stabilität, Versorgungsqualität, Netzplanung, Betriebsplanung und –*

führung, Leit- und Informationstechnik, FACTS, HGÜ, 3rd edition, Springer, ISBN 978-3-642-20099-1, 2012.

[33] C. Troitzsch, *Netzfehler in vermaschten HGÜ-Netzen – Ein Verfahren zur Berechnung, Detektion, Fehlerklärung, Ilmenauer Beiträge zur elektrischen Energiesystem-, Geräte- und Anlagentechnik*, Band 9, Universitätsverlag Ilmenau, ISBN 978-3-86360-076-1, 2014.

[34] J. Descloux, P. Rault, S. Nguefeu, J.-B. Curis, X. Guillard, F. Colas and B. Raison, "HVDC meshed grid: Control and protection of a multi-terminal HVDC system", in *Proc. Cigré Session 2012*, Paris, France, 08/2012.

[35] J. Descloux, "Protection contre les courts-circuits des réseaux à courant continu de forte puissance", Ph.D dissertation, Laboratoire de Génie Électrique de Grenoble (G2Elab), Iiversité de Grenoble, Grenoble, France, 09/2013.

[36] D. van Hertem, M. Ghandhari, J. B. Curis, O. Despouys and A. Marzin, "Protection requirements for a multi-terminal meshed DC grid", in *Proc. Cigré Symposion 2011*, Bologna, Italy, 09/2011.

[37] D. Jovcic, D. van Hertem, K. Linden, J.-P. Taisne and W. Grieshaber, "Feasibility of DC transmission networks", in *Proc. 2011 2nd IEEE PES International Conference and Exhibition on Innovative Smart Grid Technologies (ISGT Europe)*, Manchester, United Kingdom, 12/2011.

[38] L. Tang, "Control and Protection of Multi-Terminal DC Transmission Systems based on Voltage-Source Converters", Ph.D. dissertation, Department of Electrical and Computer Engineering, McGill University, Montreal, Canada, 01/2003.

[39] P. K. Murthy, J. Amarnath, S. Kamakshiah and B. P. Singh, "Wavelet Transform Approach for Detection and Location of Faults in HVDC System", in *Proc. IEEE Region 10 Colloquium and the Third Industrial and Information Systems (ICIIS)*, Kharagpur, India, 12/2008.

[40] K. de Kerft, K. Srivastava, M. Reza, D. Bekaert, S. Cole, D. van Hertem and R. Belmans, "Wavelet-based protection strategy for DC faults in multi-terminal VSC HVDC systems", *IET Generation, Transmission & Distribution*, vol. 5, pp. 496-503, 04/2011.

[41] P. Chen, B. Xu and J. Li, "A Traveling Wave Based Fault Locating System for HVDC Transmission Lines", in *Proc. IEEE International Conference on Power System Technology (PowerCon)*, Chongqing, China, 10/2006.

[42] D. Naidoo and N M. Ijumba, "HVDC Line Protection for the Proposed Future HVDC Systems", in *Proc. IEEE International Conference on Power System Technology (PowerCon)*, Singapore, Singapore, 11/2004.

[43] Cigré WG B4.46, Technical Brochure 492, "Voltage Source Converter (VSC) HVDC for Power Transmission – Economic Aspects and Comparison with other AC and DC Technologies", 04/2012.

[44] L. Tang and B.-T. Ooi, "Protection of VSC-Multi-Terminal HVDC against DC Faults", in *Proc. IEEE 33rd Annual Power Electronics Specialists Conference (PESC)*, Cairns, Australia, 06/2002.

[45] J. Arrillaga, *High Voltage Direct Current Transmission*, Stevenage (UK): The Institution of Engineering and Technology (IET), ISBN 978-0852969410, 1998.

[46] X. Li, Z. Yuan, J. Fu, Y. Wang, T. Liu and Z. Zhu, "Nanao multi-terminal VSC-HVDC project for integrating large-scale wind generation", in *Proc. 2014 IEEE PES General Meeting Conference & Exposition*, National Harbor, USA, 07/2014.

[47] ENTSO-E, "Supporting Document for the Network Code on Load-Frequency Control and Reserves", 28.06.2013.

[48] Cigré WG B4.58, "Devices for load flow control and methodologies for direct voltage control in a meshed HVDC grid", to be published in 2015.

[49] A. Egea-Alvarez, J. Beerten, D. van Hertem and O. Gomis-Bellmunt, "Primary and secondary power control of a multi-terminal HVDC grid", in *Proc. 10th IET International Conference on AC and DC Power Transmission*, Birmingham, United Kingdom, 12/2012.

[50] Cigré WG B4.52, Technical Brochure 533, "HVDC grid feasibility study", 04/2013.

[51] F. Akhter, D. E. Macpherson and G. P. Harrison, "Enhanced multi-terminal HVDC grid management for reliable AC network integration", in *Proc. 7th IET International Conference on Power Electronics, Machines and Drives*, Manchester, United Kingdom, 04/2014.

[52] K. Rouzbehi, A. Miranian, J. I. Candela, A. Luna and P. Rodriguez, "A hierarchical control structure for multi-terminal VSC-based HVDC grids with GVD characteristics", in *Proc. 2013 International Conference on Renewable Energy Research and Applications (ICRERA)*, Madrid, Spain, 10/2013.

[53] K. Rouzbehi, C. Gavriluta, J. I. Candela, A. Luna and P. Rodriguez, "Comprehensive analogy between conventional AC grids and DC grids characteristics", in Proc. 39th Annual Conference of the IEEE Industrial Electronics Society (IECON), Vienna, Austria, 11/2013.

[54] ENTSO-E, "Network Code on Operational Security", 24.09.2013.

[55] ENTSO-E, "Supporting Document for the Network Code on Operational Security", 2nd edition final, 24.09.2013.

[56] Transmission System Operator Security Cooperation (TSC), [Online], Available: http://www.tscnet.eu/ (11.10.2014).

[57] Coordination of Electricity System Operators (CORESO), [Online], Available: http://www.coreso.eu/ (11.10.2014).

[58] Electricity Coordinating Center (EKC), [Online], Available: http://www.ekc-ltd.com/ (11.10.2014).

[59] R. Foerst, G. Heyner, K. W. Kanngiesser and H. Waldmann, "Multiterminal Operation of HVDC Converter Stations", *IEEE Transactions on Power Apparatus and Systems*, vol. PAS-88, issue 7, pp. 1042-1052, 07/1969.

[60] E. E. George, H. W. Page and J. B. Ward, "Co-ordination of Fuel Cost and Transmission Loss by Use of the Network Analyzer to Determine Plant Loading Schedules", *AIEE Transactions*, vol. 68, issue 2, pp. 1152-1163, 07/1949.

[61] H. W. Dommel and W. F. Tinney, "Optimal Power Flow Solutions", *IEEE Transactions on Power Apparatus and Systems*, vol. PAS-87, no. 10, pp. 1866-1876, 10/1968.

[62] European Union, "Third Energy Package", 2009.

[63] R. K. Verma, H. Singh and L. Srivastava, "Optimal Power Flow Using Differential Evolution Algorithm with Conventional Weighted Sum Method", *International Journal of Computational Engineering Research (IJCER)*, vol. 2, issue 3, pp. 681-685, ISSN 2250-3005, 05-06/2012.

[64] Z. Qiu, G. Deconinck and R. Belmans, "A Literature Survey of Optimal Power Flow Problems in the Electricity Market Context", in *Proc. IEEE/PES Power Systems Conference and Exposition (PSCE)*, Seattle, USA, 03/2009.

[65] J. A. Momoh, M. E. El-Hawary and R. Adapa, "A Review of Selected Optimal Power Flow Literature to 1993 Part I: NonLinear and Quadratic Programming Approaches", *IEEE Transactions on Power Systems*, vol. 14, no. 1, 02/1999.

[66] J. A. Momoh, M. E. El-Hawary and R. Adapa, "A Review of Selected Optimal Power Flow Literature to 1993 Part II: Newton, Linear Programming and Interior Point Methods", *IEEE Transactions on Power Systems*, vol. 14, no. 1, 02/1999.

[67] D. W. Wells, "Method for Economic Secure Loading of a Power System", Proceedings of the Institution o Electrical Engineers, Vol. 115, no. 8, pp. 1190-1194, 08/1968.

[68] L. Castaing and O. Beck, "Optimal Operation of HVDC Links Embedded in an AC Network", in *Proc. IEEE PowerTech*, Grenoble, France, 06/2013.

[69] G. F. Reid and L. Hasdorff, "Economic Dispatch using Quadratic Programming", *IEEE Transactions on Power Apparatus and Systems*, vol. PAS-92 ,no. 6, pp. 2015-2023, 11/1973.

[70] K. R. Frisch, "Principles of Linear Programming – with Particular Reference to the Double Gradient Form of the Logarithmic Potential Method, Memorandum Institute of Economics", University of Oslo, 10/1954.

[71] P. E. Gill, W. Murray, M. A. Saunders, J. A. Tomlin and M. H. Wright, "On the Projected Newton Barrier Methods for Linear Programming and an Equivalence to Karkmarka's Projective Method", *Math Programming*, Vol. 36, pp. 183-209, 06/1986.

[72] T. S. Chung and Y. Z. Li, "A Hybrid GA Approach for OPF with Consideration of FACTS Devices", *IEEE Power Engineering Review*, vol. 21, no. 2, pp. 47-50, 02/2001.

[73] A. G. Bakirtzis, P. N. Biskas, C. E. Zoumas and V. Petridis, "Optimal Power Flow by Enhanced Genetic Algorithm", *IEEE Power Engineering Review*, vol. 17, no. 2, pp. 229-236, 05/2002.

[74] R. Storn and K. Price, "Differential Evolution – a simple and efficient adaptive scheme for global Optimization over Continuous Spaces", International Computing Science Institute, Berkley, 1995, [Online], Available: http://www.mat.univie.ac.at/~neum/glopt/mss/StoP95.pdf (01.12.2014).

[75] P. Attaviriyanupap, H. Kita, E. Tanaka and J. Hasegawa, "New Bidding Strategy Formulation for Day-Ahead Energy and reserve Markets Based on Differential Evolution", *Electrical Power Systems research*, Vol. 27, 2005.

[76] C. Muthamil Selvi and K. Gnanambal, "Power System Voltage Stability Analysis using Modified Differential Evolution", in *Proc. International Conference on Computer, Communication and Electrical Technology (ICCCET)*, Tamilnadu, India, 03/2011.

[77] B. Mahdad and K. Srairi, "Differential Evolution for Optimal Power Flow Considering FACTS Under Contingency Situation", in *Proc. 6th International Conference on Sciences of Electronics, Technologies of Information and Telecommunication (SETIT)*, Sousse, Tunisia, 03/2012.

[78] R. C. Eberhart and I. Kennedy, "A New Optimizer Using Particle Swarm Theory", in *Proc. 6th International Symposium on Micro Machine and Human Science (MHS)*, Nagoya, Japan, 10/1995.

[79] P. E. O. Yumbla, J. M. Ramirez and C. A. Coello, "Optimal Power Flow Subject to Security Constraints Solved with a Particle Swarm Optimizer", *IEEE Transaction on Power Systems*, vol. 23, no. 1, pp. 33-40, 02/2008.

[80] I. A. Hiskens and R. J. Davy, "Exploring the power flow solution space boundary", *IEEE Transactons on Power Systems*, vol. 16, no. 3, pp. 389-395, 08/2001.

[81] W. A. Buksh, A. Grothey, K. I. M. McKinnon and P. A. Trodden, "Local Solutions of the Optimal Power Flow Problem", *IEEE Transactions on Power Systems*, vol. 28, no. 4, pp. 4780-4788, 08/2013.

[82] J. Vesterstrom and R. Thomsen, "A Comparative Study of Differential Evolution, Practical Swarm Optimization and Evolutionary Algorithms on Numerical Benchmark Problems", in *Proc. Congress on Evolutionary Computation (CEC)*, Portland, USA, 06/2004.

[83] M. R. Nayak, K. R. Krishnanand and P. K. Rout, "Modified Differential Evolution Optimization Algorithm for Multi-constraint Optimal Power Flow", in *Proc. International Conference on Energy, Automation and Signals (ICEAS)*, Bhubaneswar Odisha, India, 12/2011.

[84] G. C. Onwubolu and D. Davendra, *Differential Evolution: A Handbook for Global Permutation-Based Combinatorial Optimization*, Berlin: Springer, ISBN 978-3-540-92150-9, 2009.

[85] S. Hernández, G. Leguizamón and E. Mezura-Montes, "A Hybrid Version of Differential Evolution with two Differential Mutation Operators Applied by Stages", in *Proc. 2013 IEEE Congress on Evolutionary Computation*, Cancun, Mexico, 06/2013.

[86] J. Cao, W. Du, H. Wang, and S. Bu, "Minimization of transmission loss in meshed AC/DC grids with VSC-MTDC networks," *IEEE Transactions on Power Systems*, vol. 28, no. 3, pp. 3047‑3055, 08/2013.

[87] W. Feng, L. A. Tuan, L. Bertling Tjernberg, A. Mannikoff and A. Bergman, „A New Approach for Benefit Evaluation of Multiterminal VSC–HVDC Using A Proposed Mixed AC/DC Optimal Power Flow", *IEEE Transactions on Power Delivery*, vol. 29, no. 1, pp. 432-443, 02/2014.

[88] R. Widget and G. Andersson, "Optimal Power Flow for Combined AC and Multi-Terminal HVDC Grids based on VSC Converters", in *Proc. IEEE PES General Meeting 2012*, San Diego, USA, 07/2012.

[89] M. Baradar, M. R. Hesamzadeh and M. Ghandhari, "Second-Order Cone Programming for Optimal Power Flow in VSC-Type AC-DC Grids", *IEEE Transactions on Power Systems*, vol. 28, no. 4, pp. 4282-4291, 11/2013.

[90] C. N. Ravi and C. C. Asir Rajan, "A Comparative Analysis of Differential Evolution and Genetic Algorithm for Solving Optimal Power Flow", in *Proc. IEEE 5th Power India Conference*, Murthal, India, 12/2012.

[91] M. .N. Suharto, M. Y. Hassan, M. S. Majid, M. P. Abdullah and F. Hussein, "Optimal Power Flow Solution Using Evolutionary Computation Techniques", in *Proc. IEEE Region 10 Conference (TENCON)*, Bali, Indonesia, 11/2011.

[92] H. A. Hejazi, H. R. Mohabati, S. H. Hosseinian and M. Abedi, "Differential Evolution Algorithm for Security-Constrained Energy and Reserve Optimization Considering Credible Contingencies", *IEEE Transactions on Power Systems*, vol. 26, no. 3, pp. 1145-1155, 08/2011.

[93] P. S. Jones and C. C. Davidson, "Calculation of Power Losses for MMC-based VSC HVDC Stations", in *Proc. 15th European Conference on Power Electronics and Applications (EPE)*, Lille, France, 09/2013.

[94] Airtricity, "European Offshore Supergrid® Proposal – Vision and Executive Summary", 2006.

[95] S. Mano, B. Ovgor, Z. Samadov, M. Pudlik, V. Jülich, D. Sokolov and J. Y. Yoon, "Gobitec and Asian Super Grid for renewable Energies in Northeast Asia", ISBN 978-905948-143-5, 01/2014.

[96] L. Fan, Z. Miao and D. Osborn, "Wind Farms With HVDC Delivery in Load Frequency Control", *IEEE Transactions on Power Systems*, vol. 24, issue: 4, 08/2009.

[97] L. Xu, L. Yao, M. Bazargan and Y. Wang, "The Role of Multiterminal HVDC for Wind Power Transmission and AC Network Support", in *Proc. IEEE Power and Energy Engineering Conference – Asia-Pacific (APPEEC)*, Chengdu, China, 03/2010.

[98] E. Rakhshani, A.Luna, K. Rouzbehi, P. Rodriguez and I. Etxeberria-Otadui, "Effect of VSC-HVDC on load frequency control in multi-area power systems", in *Proc. IEEE Energy Conversion Congress and Exposition (ECCE)*, Raleigh, USA, 09/2012.

[99] J. Dai, Y. Phulpin, A. Sarlette and D. Ernst, "Coordinated primary frequency control among non-synchronous systems connected by a multi-terminal high-voltage direct current grid", *IET Generation, Transmission & Distribution*, vol. 6, no. 2, pp. 99.108, 02/2012.

[100] C. Zhao, L. Li, G. Li and C. Guo, "A Novel Coordinated Control Strategy for Improving the Stability of Frequency and Voltage Based VSC-HVDC", in *Proc. IEEE 3rd International Conference on Electric Utility Deregulation and Restructuring and Power Technologies*, Nanjing, China, 04/2008.

[101] T. M. Haileselassie and K. Uhlen, "Primary Frequency Control of Remote Grids Connected by Multi-terminal HVDC", in *Proc. IEEE PES General Meeting* 2010, Minneapolis, USA, 07/2010.

[102] G. Adam, O. Anaya-Lara and K. Lo, "Grid Integration of Offshore Wind Farms using Multi-Terminal DC Transmission Systems (MTDC)", in *Proc. IEEE 5th IET International Conference on Power Electronics, Machines and Drives*, Glasgow, United Kingdom, 04/2010.

[103] T. M. Haileselassie, R. E. Torres-Olguin, T. K. Vrana, K. Uhlen and T. Undeland, "Main Grid Frequency Support Strategy for VSC-HVDC Connected Wind Farms with Variable Speed Wind Turbines", in *Proc. IEEE PowerTech*, Trondheim, Norway, 06/2011.

[104] C. Li, P. Zhan, J. Wen, M. Yao, N. Li and W.-J. Lee, "Offshore Wind Farm Integration and Frequency Support Control Utilizing Hybrid Multiterminal HVDC Transmission", *IEEE Transactions in Industry Applications*, vol. 50, no. 4, 07-08/2014.

[105] N. R. Chandhuri, R. Majunder and B. Chaudhuri, "System Frequency Support Through Multi-Terminal DC (MTDC) Grids, *IEEE Transactions on Power Systems*, vol. 28, no. 1, pp. 347-356, 02/2013.

[106] K. Wang, "Generalized Power Control Strategy with Droop Feedback for VSC-HVDC", in *Proc. IEEE PES General Meeting*, San Diego, USA, 07/2012.

[107] Y. Phulpin, "Communication-free inertia and frequency control for wind generators connected by an HVDC-link", *IEEE Transactions on Power Systems*, vol. 27, no. 2, 05/2012.

[108] P. Labra Francos, S. Sans Verdugo and S. Guyomarch, "New French-Spanish VSC link", B4-110, in *Proc. Cigré Session 2012*, Paris, France, 2012.

[109] G. Missout and P Girard, "Measurement of Bus Voltage Angle between Montreal and Sept-Iles", *IEEE Transactions on Power Apparatus and Systems*, vol. 99, no. 2, 03/1980.

[110] A. Jain and N. R. Shivakumar, "Power System Tracking and Dynamic State Estimation", in *Proc. IEEE/PES Power Systems Conference and Exposition (PSCE)*, Seattle, USA, 03/2009.

[111] A M. Glazunova and I. N. Kolosok, "Bad Data Detection by Dynamic State Estimation for the Case of Low Redundancy of Measurements", in *Proc. 2014 International Energy Conference*, Cavtat, Croatia, 05/2014.

[112] Y. Yang, W. Hu and Y. Min, "Projected Unscented Kalman Filter for Dynamic State Estimation and Bad Data Detection in Power Systems", in *Proc. 12th IET International Conference on Developments in Power System Protection*, Copenhagen, Denmark, 04/2014.

[113] L. Fan, Z. Miao and Y. Wehbe, "Application of Dynamic State and Parameter Estimation Techniques on Real-World Data", *IEEE Transactions on Smart Grid*, vol. 4, no. 2, pp. 1133-1141, 01/2013.

[114] G. Missout, J. Beland, and G. Bedard, "Dynamic Measurement of the Absolute Voltage Angle on Long Transmission Lines", *Transactions on Power Apparatus and Systems*, vol. 100, No. 11, 11/1981.

[115] P. Bonanomi, "Phase Angle Measurements with Synchronized Clocks – Principles and Applications", *IEEE Transactions on Power Apparatus and Systems*, vol. 100, No. 11, 11/1981.

[116] A. G. Phadke and J. S. Thorp, *Synchronized Phasor Measurement and Their Applications*, New York: Springer, ISBN 978-0-387-76535-8, 2008.

[117] A. G. Phadke, J. S. Thorp and M. G. Adamiak, "A New Measurement Technique for Tracking Voltage Phasors, Local System Frequency and Rate of Change of Frequency", *IEEE Transactions on Power Apparatus and Systems*, vol. 102, No. 5, 5/1983.

[118] *IEEE Standard for Synchrophasor Measurement for Power Systems*, IEEE Standard C37.118.1, 12/2011.

[119] Z. Lukszo, G. Deconinck and M. P. C. Weijnen, *Securing Electricity Supply in the Cyber Age: Exploring the Risk on Information and Communication Technology in Tomorrow's Electricity Infrastructure*, New York: Springer, ISBN 978-90-481-3593-6, 2010.

[120] C. Rehtanz and J. Bertsch, "A new wide area protection system", in Proc. 2001 Poto Power Techn Conference, Porto, Portugal, 09/2001.

[121] C. Rehtanz and J. Bertsch, "Wide Area Measurement and Protection System for Emergency Voltage Stability Control", in Proc. IEEE PES Winter Meeting, New York, USA, 01/2002

[122] ENTSO-E, *UCTE Operation Handbook*, Policy 1 and Appendix A1, 2009.

[123] ENTSO-E, Ad hoc Group "Geographical Distribution of Reserves", document 1-7, 07/2005.

[124] A. Z. Gamm, Y. A. Grishin, I. N. Kolosok A. M. Glazunova and E. S. Korkina, "New EPS State Estimation Algorithms Based on the Technique of Test Equations

and PMU Measurements", in *Proc. IEEE PowerTech 2007*, Lausanne, Switzerland, 06/2007.

[125] J. Amit and N. R. Shivakumar, "Impact of PMU in Dynamic State Estimation of Power Systems", 40th North American Power Symposium (NAPS) 2008, Calgary, Canada 11/2008.

[126] ABB Switchgear Manual, 12th edition, 2011.

[127] P. Thepparat, "Analysis of the Combined and Coordinated Control Method for HVDC Transmission", Ph.D. dissertation, Power System Department, TU Ilmenau, ISBN 978-3-8322-9045-0, 2010.

[128] B. K. Johnson, R. H. Lasseter, F. L. Alvarado and R. Adapa, "Expandable Multiterminal DC Sstems Based on Voltage Droop, *Transactions on Power Delivery*, vol. 8, no. 4, 10/1993.

[129] T. M. Haileselassie, "Control, Dynamics and Operation of Multi-terminal VSC-HVDC Transmission Systems", Ph.D. dissertation, Department of Electric Power Engineering, NTNU Trondheim, 12/2012.

[130] T. K. Vrana, J. Beerten, R. Belmans and O. B. Fosso, "A classification of DC Node Voltage Control Methods for HVDC Grids", *Electric Power System Research*, vol. 103, pp. 137-144, 2013.

[131] Y. Tokiwa, F. Ichikawa, K. Suzuki, H. Inokuchi, S. Hirose and K. Kimura, "Novel Control Strategies for HVDC Systems with Self-Contained Converter", *Electrical Engineering in Japan*, vol. 113, no. 5, p. 1-13, 1993.

[132] T. Nakajima and S. Irokawa, "A control system for HVDC Transmission by Voltage Sourced Converter", in *Proc. IEEE PES Summer Meeting*, Edmonton, Canada, 07/1999.

[133] T. M. Haileselassie, M. Molinas and T. Undeland, "Multi Terminal VSC-HVDC System for Integration of Offshore Wind Farms and Green Electrification of Platforms and the North Sea", in *Proc. Nordic Workshop on Power and Industrial Electronics (NORPIE)*, Espoo, Finland, 06/2008.

[134] J. Zhu and C. Booth, "Future Multi-Terminal HVDC Transmission Systems using Voltage Source Converter", in *Proc. 45th International Universities Power Engineering Conference (UPEC)*, Cardiff, United Kingdom, 09/2010.

[135] T. Haileselassie, K. Uhlen and T. Undeland, "Control of Multitermianl HVDC Transmission for Offshore Wind Energy", in *Proc. Nordic Wind Power Conference*, Bornholm, Denmark, 09/2009.

[136] W. Wang, M. Barnes and O. Marjanovic, "Droop Control Modeling and Analysis of Multi-Terminal VSC-HVDC for Offshore Wind Farms", in *Proc. 10th IET International Conference on AC and DC Power Transmission (ACDC 2012)*, Birmingham, United Kingdom, 12/2012.

[137] F: Gonzalez-Longatt and J. Roldan, "Effect of DC Voltage Control Strategy on Voltage Response on Multi-Terminal HVDC following Loss of a Converter Station", in *Proc. IEEE PES General Meeting*, Vancouver, Canada, 07/2013.

[138] M. Avendano-Mora, M. Barnes and J.Y. Chan, "Comparison of Control Strategies for Multiterminal VSC-HVDC Systems for Offshore Wind Farm Integration", in *Proc. 7th IET International Conference on Power Electronics, Machines and Drives (PEMD)*, Manchester, United Kingdom, 04/2014.

[139] C. D. Barker and R. S. Whitehouse, "Autonomous Converter Control in a Multi-Terminal HVDC System", in *Proc. 10th IET International Conference on AC and DC Power Transmission (ACDC 2010)*, London, United Kingdom, 12/2010.

[140] C. D. Barker and R. S. Whitehouse, "Further Development in Autonomous Converter Control in a Multi-Terminal HVDC System", in *Proc. 10th IET International Conference on AC and DC Power Transmission (ACDC 2012)*, Birmingham, United Kingdom, 12/2012.

[141] J. Beerten, D. Van Hertem and R. Belmans, "VSC MTDC Systems with a Distributed DC Voltage Control – A Power Flow Approach", in *Proc. IEEE PowerTech 2011*, Trondheim, Norway, 06/2011.

[142] C. Dierckxsens, K. Srivastava, M. Reza, S. Cole, J. Beerten and R. Belmans, "A Distributed DC Voltage Control Method for VSC MTDC Systems", *Electric Power Systems Research*, vol. 82, no. 1, 01/2012, pp. 54-58.

[143] T. M. Haileselassie and K. Uhlen, "Impact of DC line Voltage Drops and Power Flow of MTDC Using Droop Control", *IEEE Transactions on Power Systems*, vol. 27, no. 3, 08/2012.

[144] P. Karlsson, "DC Distributed Power Systems - Analysis, Design and Control for a Renewable Energy System", Ph.D. dissertation, Department of Industrial Electrical Engineering and Automation, Lund University, 2002.

[145] J. Beerten, O. Gomis-Bellmut, W. Guillaud, J. Rimez, A. van der Meer and D. van Hertem, "Modeling and control of HVDC grids: a key challenge for the future power system", in *Proc. 18th Power Systems Computation Conference (PSCC)*, Wroclaw, Poland, 08/2014.

[146] P. Rault, "Dynamic Modeling and Control of Multi-Terminal HVDC Grids", Ph.D. dissertation, University Lille, 2014.

[147] R. Pinto, S. Rodrigues, P. Bauer and J. Pierik, "Operation and control of a multi-terminal DC-Network", in *Proc. IEEE ECCE Asia-Downunder*, 06/2013.

[148] L. Xu, L. Yao and M. Bazargan, "DC Grid Management of a Multi-Terminal HVDC Transmission System for Large Offshore Wind Farms", in *Proc. International Conference on Sustainable Power Generation and Supply (SUPERGEN)*, Nanjing, China, 04/2009.

[149] T. K. Vrana, L. Zeni and O. B. Fosso, "Active Power Control with undead-bad voltage and frequency droop applied to a meshed DC grid Test system", in *Pro. IEEE International Energy Conference and Exhibition (ENERGYCON)*, Florence, Italy, 09/2012.

[150] T. K. Vrana, L. Zeni and O.B. Fosso, "Dynamic Active Power Control with Improved Undead-Band Droop for HVDC Grids", in *Proc. 10th IET International*

Conference on AC and DC Transmission (ACDC 2012), Birmingham, United Kingdom, 12/2012.

[151] H. Chen, C. Wang, F. Zhang and W. Pan, "Control strategy research of VSC based multiterminal HVDC system", in *Proc. IEEE PES Power System Conference and Exposition (PECE 2006)*, Atlanta, USA, 11/2006.

[152] B. Berggen, R. Majunder, C. Sao and K. Linden, "Method and Control Device for controlling power Flow within a DC Power Transmission Network", WIPO International Publication Number WO 2012/000549 A1, International Filing Date: 30. June 2019, International Publication Date: 05. January 2012.

[153] N. R. Chaudhuri and B. Chaudhuri, "Adaptive Droop Control for Effective Power Sharing in Multi-Terminal DC (MTDC) Grids", *IEEE Transactions on Power Systems*, 02/2013.

[154] B. Berggen, K. Linden and R. Majumder, "DC Grid Control Through the Pilot voltage Droop Concept – Methods for Establishing Set-Point Tracking", in *Proc. IEEE International Energy Conference (ENERGYCON 2014)*, Dubrovnik, Croatia, 05/2014.

[155] M. Nazari and M. Ghandhari, "Application of Multi-Agent Control to Multi-Terminal HVDC Systems", in *Proc. 2013 IEEE Electrical Power & Energy Conference (EPEC 2013)*, Halifax, USA, 08/2013.

[156] D. Babazadeh and L. Nordström, "Agent-based control of VSC-HVDC transmission grid – A Cyber Physical System perspective", in *Proc. 2014 Workshop on Modeling and Simulation of Cyber-Physical Energy Systems (MSCPES)*, Berlin, Germany, 04/2014.

[157] M. Eremia and M. Shahidehpour, *Handbook of electrical power system dynamics – Modelling, Stability and Control*, Wiley, 2013, p. 110.

[158] Electric Power Research Institute (EPRI), "Superconducting Power Equipment - Technology Watch 2011", 12/2011.

[159] P. Kundur, *Power System Stability and Control*, McGraw-Hill, ISBN 978-0-07-035958-1, 1994, p. 209-210.

[160] H. Koch, *Gas-Insulated Transmission Lines*, West Sussex (UK), Wiley, ISBN 978-0-47-066533-6, 2012, p. 326.

[161] R. Zuijderduin, O. Chevtchenko, J.J. Smit, G. Aanhaanen, I. Melnik and A. Geschiere, "AC HTS transmission cable for integration into the future EHV grid of the Netherlands Superconductivity Centennial Conference", *Physics Procedia 36*, Elsevier, pp. 1149-1152, 2012.

[162] G. Daelemans, K. Srivastava, M. Reza, S Cole and R. Belmans, "Minimization of steady-state losses in meshed networks using VSC HVDC", in *Proc. IEEE Power and Energy Society General Meeting*, Calgary, Canada, 07/2009.

[163] R. Marquardt, "Current rectification circuit for voltage source inverters with separate energy stores replaces phase blocks with energy storing capacitors", German patent DE10103031B4, January 2001.

[164] T. Modeer, H.-P. Nee and S. Norrga, "Loss comparison of different sub-module implementations for modular multilevel converters in HVDC applications", in *Proc. 14th European Conference on Power Electronics and Applications*, Birmingham, United Kingdom, 09/2011.

[165] P. S. Jones and C. C. Davidson, "Calculation of power losses for MMC-based VSC HVDC stations", in *Proc. 15th European Conference on Power Electronics and Applications*, Lille, France, 09/2013.

[166] Q. Tu and Z. Xu, "Power losses evaluation for modular multilevel converter with junction temperature feedback", in *Proc. IEEE Power and Energy Society General Meeting*, Detroit, USA, 07/2011.

[167] Z. Zhang, Z. Xu and Y. Xue, "Valve losses evaluation based on piecewise analytical method for MMC-HVDC links", in *Proc. IEEE Power and Energy Society General Meeting*, Detroit, USA, 07/2011.

[168] R. Mallipeddi and P. Suganthan, "Ensemble of Constraint Handling Techniques", *IEEE Transactions on Evolutionary Computation*, vol. 14, no. 4, pp. 561-579, 08/2010.

[169] K. Vasakh and L. R. Srinivas, "Differential Evolution based OPF with Conventional and Non-Conventional Cost Characteristics", in *Proc. Joint International Conference on Power System Technology and IEEE Power India Conference (POWERCON)*, New Delhi, India, 10/2008.

[170] P. S. Manoharan, P. S. Kannan, S. Baskar and M. W. Iruthayarajan, "Penalty Parameter-less Constraint Handling Scheme based Evolutionary Algorithm Solutions to Economic Dispatch", *IET Generation, Transmission & Distribution*, vol. 2, no. 4, pp. 478-490, 07/2008.

[171] B. Tessema and G. G. Yen, "A Self Adaptive Penalty Function Based Algorithm for Constrained Optimization", in *Proc. IEEE Congress on Evolutionary Computation (CEC 2006)*, Vancouver, Canada, 07/2006.

7.1 Own publications

Books and book contributions

[O-1] A.-K. Marten, „Integration der Betriebsführung eines HGÜ-Overlay-Netzes in die Leistungs-Frequenzregelung eines Drehstrom-Verbundnetzes", Ilmenauer Beiträge zur elektrischen Energiesystem-, Geräte- und Anlagentechnik, vol. 3, Universitätsverlag Ilmenau, date of defence: 24. Nov. 2011, ISBN 978-3-86360-038-9, 2012.

[O-2] A. Aguado Cornago, F, Schettler, A.-K. Marten, et al., "European Energy Studies Volume VII – The European Supergrid", Claeys & Casteels Publishing, ISBN 978 9077 644 263, 01/2015.

Reports

[O-3] B. M. Buchholz, M Luther, A.-K. Marten, et al., „Aktive Energienetze im Kontext der Energiewende – Anforderungen an künftige Übertragungs- und Verteilungsnetze unter Berücksichtigung von Marktmechanismen“, Studie der Energietechnischen Gesellschaft im VDE (ETG), 02/2013.

[O-4] W. Peters, E. Weingarten, H.-J. Koch, U. Prall, J. Vollprecht, D. Westermann and A.-K. Marten, „Umweltbelange und raumbezogene Erfordernisse bei der Planung des Ausbaus des Höchstspannungs-Übertragungsnetzes – Band I: Gesamtdokumentation, Umweltbundesamt“, Climate Change 11/2014, ISSN 1862-4359, 06/2014.

[O-5] W. Peters, E. Weingarten, H.-J. Koch, U. Prall, J. Vollprecht, D. Westermann and A.-K. Marten, „Umweltbelange und raumbezogene Erfordernisse bei der Planung des Ausbaus des Höchstspannungs-Übertragungsnetzes – Band II: Praxisnahe Empfehlungen, Umweltbundesamt“, Climate Change 12/2014, ISSN 1862-4359, 06/2014.

[O-6] K. Linden, J. Beerten, A.-K. Marten, et al., *“Cigré WG B4.58 - Devices for Load flow Control and Methodologies for Direct Voltage Control in a Meshed HVDC Grid”*, to be released in 2015.

[O-7] F. Schettler, B. Whitehouse, A.-K. Marten, et al., “CENELEC Working Group CLC TC8x/WG 06 – System Aspects of HVDC Grids”, ongoing.

Conference Paper

[O-8] A.-K. Marten and D. Westermann, “Participation in power flows of interconnected power system with an embedded HVDC Grid”, in *Proc. IEEE PES General Meeting*, San Diego, USA, 07/2012.

[O-9] A.-K. Marten and D. Westermann, “Power Flow Participation by an Embedded HVDC Grid in an Interconnected Power System”, in *Proc. IEEE PES Innovative Smart Grid Technologies Europe*, Berlin, Germany, 10/2012.

[O-10] A.-K. Marten and D. Westermann, “A novel operation method for meshed HVDC overlay grids and corresponding steady state and dynamic power flow calculation principle”, in *Proc. IET 10th International Conference on AC and DC Power Transmission (ACDC 2012)*, Birmingham, United Kingdom, 12/2012.

[O-11] A.-K. Marten, D. Westermann, M. Luginbühl and H. F. Sauvain, “Integration of a Multi Terminal DC Grid in an Interconnected AC Network”, in *Proc. IEEE PowerTech 2013*, Grenoble, France, 06/2013.

[O-12] A.-K. Marten, D. Westermann, M. Luginbühl and H. F. Sauvain, “Schedules for Converters of a Meshed HVDC Grid and a Contingency Schedule for Adaptation to Unscheduled Power Flow Changes”, in *Proc. IEEE PES General Meeting 2013*, Vancouver, Canada, 07/2013.

[O-13] A.-K. Marten and D. Westermann, "Local HVDC Grid Operation with Multiple TSO Coordination at a Global Optimum", in *Proc. IEEE International Energy Conference (Energycon 2014)*, Dubrovnik, Croatia, 05/2014.

[O-14] A.-K. Marten, D. Westermann, L. Vento and P. Favre-Perrod, "Factors influencing Oscillations within Meshed HVDC Grids and Implications for DC Voltage Control", in *Proc. 9th International Conference on Critical Information Infrastructures Security (CRITIS)*, Limassol, Cyprus, 10/2014.

[O-15] A.-K. Marten, C. Troitzsch and D. Westermann, "Non-telecommunication based DC line fault detection methodology for meshed HVDC grids", in *Proc. IET 11th International Conference on AC and DC Power Transmission (ACDC 2015)*, Birmingham, United Kingdom, 02/2015.

[O-16] A.-K. Marten, V. Vahrenholt, W. Fischer, K. Fuchs, F. Berger and D. Westermann, „Substation layout for multi-terminal HVDC systems and neutral conductor arrangements for reduced field emissions", in *Proc. IET 11th International Conference on AC and DC Power Transmission (ACDC 2015)*, Birmingham, United Kingdom, 02/2015.

[O-17] J. Dragon, F. Schettler, A.-K. Marten, et all, "Development of Functional Specifications for HVDC Grid Systems", in *Proc. 11th IET International Conference on AC and DC Transmission (ACDC 2015)*, Birmingham, United Kingdom, 02/2015.

[O-18] S. Bohn, M. Agsten, A.-K. Marten and D. Westermann, "A pan-European-MENA HVDC overlay grid for bulk energy exchange", in *Proc. IEEE PES Transmission and Distribution Conference and Exposition*, Chicago, USA, 04/2014.

[O-19] S. Bohn, M. Agsten, A.-K. Marten and D. Westermann, "Meshed HVDC Transmission in the content of Sustainable Power Transmission for the Future and its Environmental Impact", in *Proc IAFOR North American Conference on Sustainability, Energy and the Environment (NACSEE 2014)*, Providence, USA, 09/2014.

[O-20] S. Bohn, J. Kayser, M. Fetisova, M. Agsten, A.-K. Marten, and D. Westermann, "The Operation of a Meshed HVDC Grid – A Model-based Analysis of a Supergrid", in *Proc. Australian Utility Week*, Sydney, Australia, 11/2014.

[O-21] S. Bohn, M. Fetisova, M. Agsten, A.-K. Marten and D. Westermann, "A continuous DC voltage control function for meshed HVDC grids and the impact of the underlaying future AC grid due to renewable in-feed", in *Proc. 6th International Conference on Modeling, Identification and Control (IJMIC)*, Melbourne, Australia, 12/2014.

Journal Paper

[O-22] F. Schettler, J. Dragon, G. Imgrund, A.-K. Marten, D. Westermann, R. Whitehouse and W. Winter, „Standardization and common Grid Codes from the technical framework for European wide HVDC Grids", European Energy Journal, vol. 5, issue 2, May 2015.

[O-23] S. Bohn, I. Boie, C. Kost, M. Agsten, P. Bretschneider, A.-K. Marten, and D. Westermann, "Meshed HVDC Transmission in the content of Sustainable Power Transmission for the Future and its Environmental Impact", *invited for publication in* Journal of Strategic Innovation and Sustainability, ISSN 1718-2077, vol. 10(1), 2014.

Invited Presentations

[O-24] A.-K. Marten, "Load Frequency Control in an Interconnected Power System with Embedded HVDC Grid", *presentation*, 2012 IEEE PES General Meeting, San Diego, USA, 07/2012.

[O-25] A.-K. Marten, "Schedules for Converters of a Meshed HVDC Grid and a Contingency Schedule for Adaption to Unscheduled Power Flow Changes", 2013 IEEE PES General Meeting, Vancouver, Canada, 07/2013.

[O-26] A.-K. Marten, „Systemtechnische Aspekte von vermaschten HGÜ-Netzen", *presentation*, VDE Hochschulgruppe der Technischen Universität Ilmenau, 06/2014.

[O-27] A.-K. Marten, "Influencing factors for oscillations within meshed HVDC grids and consequences for DC voltage control", *presentation*, 2014 IEEE PES General Meeting, Washington D.C., USA, 07/2014.

[O-28] F. Schettler, S. Nguefeu, M. Zeller, A.-K. Marten, M. Hyttinen, P. Lundberg, R. Whitehouse and A. Morales, CENELEC TC 8X/WG 06, Workshop at Cigré Session 2014, Paris, 08/2014.

[O-29] A.-K. Marten, „Systemführung 2030", 50 Hertz Transmission Systemsicherheitskonferenz 2014, Magdeburg, 09/2014.

[O-30] A,-K. Marten, D. Westermann, V. Vahrenholt and W. Fischer, „Anforderungen an GIS-Schaltanlagen für Multi-Terminal HGÜ-Systeme", GIS Anwenderforum, Darmstadt, 10/2014.

[O-31] A.-K. Marten, "Operation of meshed HVDC Grids – Challenges and First Solutions", ISGT Europe, Istanbul, Turkey, 10/2014.

Appendix A Loss estimation of modular multilevel converters

All existing publications concerning mixed AC/DC OPF problems are using loss estimations for two or three level converters as in [162]. As modular multi-level converters (MMC) are more likely to be implemented in a future HVDC grid e.g. due to smaller losses and fewer harmonics, another more adequate loss model is needed.

The MMC technology is quite new (invented in 2001) [163] and the coordination and switching of converter vales is much more complex than with previous two or three level VSCs, MMC's loss computation is quite complex [164]-[167]. Applying such complex loss models would significantly increase the computational effort when applying for OPF analyses. Hence, it is proposed to use the same loss model (A.1) as for conventional VSCs but with adaptation of its parameters α, β and γ.

$$p_{\text{conv,loss}} = \left[\alpha + \beta \cdot \frac{i_{\text{conv}}}{i_{\text{conv,nominal}}} + \gamma \cdot \left(\frac{i_{\text{conv}}}{i_{\text{conv,nominal}}} \right)^2 \right] \cdot p_{\text{conv,nominal}} \tag{A.1}$$

$$i_{\text{conv}} = \frac{\sqrt{p_{\text{conv,AC}}^2 + q_{\text{conv,AC}}^2}}{\sqrt{3} v_{\text{conv,AC}}} \tag{A.2}$$

In [164] switching and conducting losses p_{loss} are given for half bridge, full bride and clamp double converter sub-module technology according to Tab. 7-1 for full converter load.

Tab. 7-1: Switching and conducting losses of MMC converters. [164]

	Topology of converter sub-modules		
	Half bride	Full bridge	Clamp double
$p_{\text{conv,loss}}$	0.4766%	0.8081%	0.6405%

The total MMC converter station losses are 1% at full load with half bridge sub-module topology [165]. Consequently, load independent station losses can be estimated according to (A.5).

$$\alpha = 0.01 - 0.004766 = 0.005234 \tag{A.3}$$

As [164]-[167] do not provide any detailed load dependent loss considerations it is assumed that distribution between linear and quadratic current dependent losses is equal to that of conventional VSCs according to [162]. Thus, 44% of load dependent losses are linear and 66% quadratic dependent on converter's current. Hence, loss model parameters are estimated as shown in Tab. 7-2.

Tab. 7-2: Parameter for simplified MMC loss model.

α	0.005234
β	0.002097
γ	0.003146

Appendix B Constraint handling for artificial intelligence optimization methods

As mentioned in subchapter 3.1.4 the major disadvantage of artificial intelligence methods for OPF optimization issues is constraint handling since those methods are originally indented to be used for unbounded problems. Different opportunities for constraint handlings exist and [168] gives a good overview of them.

In general constraint handling possibilities can be subdivided in two major groups. One of them is feasibility preserving and the other is based on penalty functions. Feasibility preserving according to [169] enforces optimization solutions compliance with given constraints. Population vectors are reset to boundary values during evolutionary optimization process according to (A.4). Alternatively, in case of any boundary violation population vectors can also be reset to any other value within the permitted state space.

$$x^{(G)} = \begin{cases} x_{min} & \text{if } x^{(G)} < x_{min} \\ x_{max} & \text{if } x^{(G)} > x_{max} \\ x^{(G)} & \text{otherwise} \end{cases} \tag{A.4}$$

Feasibility preserving is easy to implement but is an incisive intervention in the evolutionary optimization process. The intended learning effect fully disappears for populations that violate limits. Consequently, finding the global optimum cannot be maintained as it is illustrated in Fig. 7.1. Additionally solely limits regarding state variables can be sufficient respected. The effect of feasibility preserving can also be seen in Fig. 3.8 in subchapter 3.2.3.

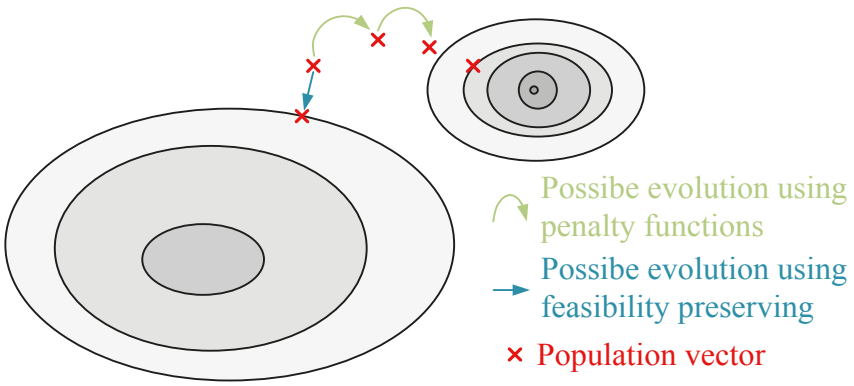

Fig. 7.1: Level curves of permissible state space and possible evolution of an exemplary population vector using penalty functions and feasibility preserving.

Using of penalty functions allows further constraints, is a less restrictive approach and allows population vectors to stay in restricted state space areas by adding a penalty function to the objective function which is weighting boundary violations as in (A.5) [168]. Conse-

quently, using penalty function $F_{\text{penalty}}(x,u)$ means no longer minimizing $F(x,u)$ but minimizing $F_{\text{fitness}}(x,u)$. $F_{\text{penalty}}(x,u)$ sums up all weighted boundary violations p as in (A.6) and the original OF is weighted using k_{fitness}.

$$F_{\text{fitness}}(x,u) = k_{\text{fitness}} F(x,u) + F_{\text{penalty}}(x,u) \tag{A.5}$$

$$F_{\text{penalty}}(x,u) = \sum_{p} k_{\text{penalty},p} \cdot \text{penalty}_{p}(u,x) \tag{A.6}$$

For defining the weighting of boundary violations again different approaches are described in literature. Mainly it can be static parameterization, parameter-less, adaptive parameterization. Static parameterization is using predefined weighting factors for penalty functions. The choice of weighting factor is directly influencing the evolution process during optimization. Thus a bad choice of weighting factors can lead to a deviation from the global optimum [170]. Since choosing static weighting factors is a more or less heuristic process an initialization or extension of an optimization problem causes a longer verification process.

This disadvantage is bypassed when there are no parameters to choose. The parameter-less method as in [170] evaluates the objective function under consideration of any boundary violation. Comparing two population vectors when both violating limits that one with the smaller violation is maintained. If two population vectors are compared where only one is violating the given limits the boundary violating one is rejected. Again this method bears the risk of not covering the complete permitted state space and consequently the global optimum may not be found as it was identified for feasibility preserving method [168].

Adaptive parameterization intends to improve static parameterization's disadvantages and does not need any user defined parameters. A possible method is described in [171]. The choice of penalty factors is dependent on the amount of population vectors within permitted state space areas. If a high number of population vectors are within permitted state space area the penalty factor is smaller while the penalty factor is larger when a high number of population vectors are violating limits. However, such an algorithm must be designed with care in order to ensure finding of global optimum.

Appendix C AC/DC grid model for OPF numerical case studies

For OPF numerical case studies a 6 AC and 4 DC node grid model is used while nominal voltage on the AC side is assumed to be 400 kV and on the DC side to be ±500 kV. For simplifications reasons transmission line length between two AC or DC nodes is defined to 500 km with the same type of line for both grids. Depending on the connection a different number of parallel systems are implemented. Tab. 7-3 includes load and generation at AC nodes as well as its reactive power limits and Tab. 7-4 converter's power limits. AC and DC grid topologies are given in Tab 7-6 and Tab 7-5 respectively while also AC and DC line parameters and their maximum transmission capability are included.

Tab. 7-3: Fixed load and generation on AC nodes including reactive power limits.

AC node	P_{load} [MW]	Q_{load} [MVar]	P_{gen} [MW]	Q_{min} [MVar]	Q_{max} [MVar]
1	1,150	775	13,000	-20,000	20,000
2	4,740	2,370	2,270	-4,800	4,800
3	2,490	1,245	2,100	-3,500	3,500
4	1,740	870	200	-2,000	2,000
5	6,660	3,330	800	-5,500	5,500
6	1,590	795	400	-2,500	2,500

Tab. 7-4: Converter's active power limits and connected AC nodes.

DC node	$P_{conv,AC,max}$ [MW]	$P_{conv,AC,min}$ [MW]	Connected AC node
1	15,000	-15,000	1
2	5,000	-5,000	3
3	5,000	-5,000	5
4	5,000	-5,000	6

Tab. 7-5: DC grid topology, DC line parameters and maximum transmission capacity.

DC line	From DC node	To DC node	R' [Ω]	Maximum transmission capacity [MW]
1	1	2	0.01	4,000
2	1	3	0.01	4,000
3	2	3	0.03	4,000
4	2	4	0.03	4,000
5	2	5	0.01	4,000

Tab. 7-6: AC grid topology, AC line parameters and maximum transmission capacity.

AC line	From AC node	To AC node	R' [Ω]	X' [Ω]	Maximum transmission capacity [MW]
1	1	2	0.01	0.083	2,250
2	1	3	0.01	0.083	2,250
3	2	3	0.03	0.25	750
4	2	4	0.03	0.25	750
5	2	5	0.01	0.083	2,250
6	3	4	0.01	0.083	2,250
7	3	5	0.03	0.25	750
8	4	5	0.03	0.25	750
9	4	6	0.03	0.25	750
10	5	6	0.03	0.25	750

Appendix D Mixed AC/DC OPF results

Tab. 7-7: Result of differential evolution mixed AC/DC OPF – $|v_{AC,min}| = 0.95$ p.u., $|v_{AC,max}| = 1.05$ p.u., $v_{DC,min} = 0.95$ p.u., $v_{DC,max} = 1.05$ p.u..

	1	2	3	4	5	6	7	8	9	10	11	12	13	14	15	16	17	18	19	20
$P_{conv,loss}$ [MW]	835.59	822.55	861.05	889.85	832.05	829.40	822.51	897.49	822.43	829.33	894.52	889.25	882.94	872.35	856.95	822.44	863.08	837.04	822.49	833.06
No. of iterations	6000	5993	6000	3002	3414	6000	6000	3002	5285	5458	3008	6000	3002	6000	5397	5813	4229	3490	5310	6000
$\|v_1\|$ [pu]	1.012	1.019	1.016	0.950	1.016	1.012	1.017	0.950	1.017	1.009	0.950	0.950	0.966	0.950	0.950	1.019	0.950	1.014	1.0176	1.007
$\|v_2\|$ [pu]	1.00	1.000	1.000	1.000	1.000	1.000	1.000	1.000	1.000	1.000	1.000	1.000	1.000	1.000	1.000	1.000	1	1.000	1.000	1.000
$\|v_3\|$ [pu]	1.050	1.050	1.050	1.050	1.050	1.049	1.050	1.050	1.050	1.050	1.050	1.050	1.050	1.050	1.050	1.050	1.050	1.050	1.050	1.050
$\|v_4\|$ [pu]	0.950	1.049	0.950	1.036	1.041	1.049	1.049	1.035	1.050	1.025	1.050	1.029	1.050	1.040	1.048	1.050	1.017	1.004	1.050	1.032
$\|v_5\|$ [pu]	1.0316	1.044	1.031	1.050	0.951	1.024	1.050	1.028	1.050	1.031	1.049	1.031	1.050	1.046	1.042	1.050	0.989	0.959	1.048	0.950
$\|v_6\|$ [pu]	1.0485	1.050	1.049	0.950	1.049	0.958	1.049	0.950	1.050	0.974	1.050	0.951	1.044	1.050	1.050	1.050	0.950	1.013	1.050	1.047
δ_{v1} [°]	40.65	40.21	40.38	44.05	40.29	40.67	40.32	44.57	40.32	40.82	44.56	44.09	43.67	44.14	44.11	40.24	44.10	40.54	40.30	40.98
δ_{v2} [°]	0.00	0.00	0.00	0.00	0.00	0.00	0.00	0.00	0.00	0.00	0.00	0.00	0.00	0.00	0.00	0.00	0.00	0.00	0.00	0.00
δ_{v3} [°]	8.92	9.34	8.63	9.73	8.81	9.07	9.63	8.13	9.43	8.84	7.99	9.85	7.86	11.18	9.86	9.42	9.28	7.90	9.75	8.80
δ_{v4} [°]	-8.46	-7.83	-8.72	-9.34	-8.19	-8.31	-7.84	-11.34	-7.90	-8.47	-11.18	-9.43	-11.20	-8.10	-9.06	-7.84	-9.23	-8.57	-7.79	-8.66
δ_{v5} [°]	-9.90	-9.95	-10.10	-10.14	-10.13	-9.87	-10.03	-9.36	-9.94	-9.73	-9.24	-10.24	-9.17	-10.86	-9.83	-9.96	-9.86	-9.69	-10.10	-10.00
δ_{v6} [°]	5.39	4.66	4.95	-3.05	4.96	4.54	3.93	-11.07	4.00	4.37	-11.22	-3.50	-11.01	-0.46	-3.66	4.40	-0.40	6.69	3.960	2.49
$Q_{gen,1}$ [MVar]	1623.4	1639.2	1648.3	1345.3	1642.5	1619.9	1624.6	1428.0	1629.9	1615.3	1431.3	1344.7	1498.2	1312.2	1347.0	1625.2	1362.2	1660.7	1622.7	1607.5
$Q_{gen,2}$ [MVar]	3348.9	3143.4	3327.6	3481.2	3497.6	3252.5	3133.9	3572.1	3132.6	3270.3	3480.1	3559.6	3397.6	3507.8	3497.0	3131.1	3717.6	3521.7	3140.3	3559.3
$Q_{gen,3}$ [MVar]	2675.2	2241.9	2663.6	2650.8	2427.9	2313.4	2236.5	2762.3	2241.1	2419.7	2681.8	2700.8	2600.2	2598.5	2607.2	2235.2	2806.9	2582.9	2234.7	2516.8
$Q_{gen,4}$ [MVar]	640.6	1336.4	639.5	1371.8	1396.9	1493.4	1335.8	1403.0	1333.8	1262.4	1354.5	1346.7	1360.3	1285.0	1344.9	1336.1	1296.7	1151.6	1339.4	1328.5
$Q_{gen,5}$ [MVar]	3849.3	3822.9	3844.1	3965.5	3143.0	3764.5	3869.2	3714.4	3862.6	1820.0	3718.4	3821.1	3730.8	3866.1	3740.6	3855.2	3514.2	3269.6	3857.0	3125.8
$Q_{gen,6}$ [MVar]	953.2	803.1	954.6	554.4	937.1	604.5	789.5	603.7	791.2	662.3	804.0	587.5	786.4	795.6	788.8	795.1	652.6	889.0	793.4	933.3
$v_{DC,1}$ [pu]	1.050	1,050	0.986	0.984	1.050	1.050	1.050	0.983	1.050	1.050	0.983	0.984	0.983	1.031	1.050	1.050	1.050	1.050	1.050	1.050
$v_{DC,2}$ [pu]	1.028	1,027	0.962	0.961	1.027	1.028	1.027	0.960	1.027	1.027	0.960	0.961	0.960	1.007	1.028	1.027	1.028	1.028	1.027	1.028
$v_{DC,3}$ [pu]	1.020	1,020	0.954	0.952	1.019	1.020	1.020	0.950	1.020	1.019	0.950	0.952	0.950	1.000	1.020	1.020	1.020	1.019	1.020	1.020
$v_{DC,4}$ [pu]	1.016	1.016	0.950	0.950	1.015	1.017	1.016	0.950	1.016	1.016	0.950	0.950	0.950	0.997	1.018	1.016	1.017	1.016	1.016	1.017
$P_{conv,AC,1}$ [MW]	-7024.6	-7063.2	-7015.2	-7029.0	-7025.5	-7033.6	-7077.0	-6900.0	-7064.6	-7015.3	-6894.1	-7041.1	-6885.9	-7110.2	-7039.5	-7066.5	-7008.7	-69682	-7084.7	-7007.5
$P_{conv,AC,2}$ [MW]	278.9	388.7	255.9	518.6	293.1	359.1	438.8	345.9	406.9	311.6	328.8	531.5	306.9	712.2	517.0	402.6	397.0	136.6	456.7	303.8
$P_{conv,AC,3}$ [MW]	4446.3	4405.2	4442.2	4619.2	4453.7	4489.8	4402.1	4978.7	4418.5	4514.1	4985.2	4622.8	4992.4	4421.6	4633.3	4406.7	4631.5	4515.3	4390.1	4534.5
$P_{conv,AC,4}$ [MW]	1879.1	1850.3	1869.9	1456.6	1857.0	1765.9	1817.4	1135.3	1820.6	1770.8	1141.3	1441.9	1148.6	1660.6	1472.4	1838.5	1560.3	1894.6	1819.1	1748.9

Tab. 7-8: Result of differential evolution mixed AC/DC OPF – $|v_{AC,min}|$ = 0.95 p.u., $|v_{AC,max}|$ = 1.05 p.u., $v_{DC,min}$ = 0.95 p.u., $v_{DC,max}$ = 1.05 p.u..

	21	22	23	24	25	26	27	28	29	30	31	32	33	34	35	36	37	38	39	40
$P_{conv,loss}$ [MW]	860,6	848,1	822,5	831.4	835,7	882,9	839,6	828,0	857.1	848.1	824.4	839	847.6	822.67	824.7	822.7	882.9	883.0	835.8	860.6
No. of iterations	6815	6502	7268	4099	5287	3720	5388	4059	8000	5977	6626	8000	5950	8000	5609	6320	4224	4238	5741	4241
$\|v_1\|$ [pu]	0.950	1.023	1.020	1.015	1.014	0.966	1.009	1.017	0.950	1.022	1.013	1.008	1.023	1.021	1.021	1.019	0.966	0.966	1.009	0.951
$\|v_2\|$ [pu]	1.000	1.000	1.000	1.000	1.000	1.000	1.000	1.000	1.000	1.000	1.000	1.000	1.000	1.000	1.000	1.00	1.000	1.000	1.000	1.000
$\|v_3\|$ [pu]	1.050	1.050	1.050	1.050	1.050	1.050	1.050	1.049	1.050	1.050	1.050	1.050	1.050	1.050	1.050	1.050	1.050	1.050	1.050	1.049
$\|v_4\|$ [pu]	1.034	1.050	1.050	1.050	0.950	1.050	0.950	1.025	1.046	1.050	1.045	0.950	1.050	1.050	1.040	1.050	1.050	1.050	0.950	1.031
$\|v_5\|$ [pu]	1.018	1.043	1.048	0.950	1.050	1.042	1.025	1.050	1.032	1.045	1.050	1.016	1.043	1.046	1.046	1.036	1.044	1.039	1.040	1.026
$\|v_6\|$ [pu]	0.964	1.050	1.050	1.050	1.050	1.047	0.950	1.050	1.049	1.050	1.045	0.977	1.050	1.049	1.050	1.050	1.048	1.044	1.047	0.955
δ_{v1} [°]	44.16	39.93	40.17	40.49	40.52	43.67	40.85	40.31	44.06	40.01	40.61	40.94	39.93	40.09	40.08	40.23	43.67	43.67	40.82	43.97
δ_{v2} [°]	0.00	0.00	0.00	0.00	0.00	0.00	0.00	0.00	0.00	0.00	0.00	0.00	0.00	0.00	0.00	0.00	0.00	0.00	0.00	0.00
δ_{v3} [°]	10.468	9.17	9.41	9.05	9.19	7.89	9.34	9.19	9.97	9.24	8.08	9.72	8.92	9.45	7.92	9.19	7.79	7.898	8.80	10.56
δ_{v4} [°]	-9,129	-8.03	-7.79	-8.20	-8.29	-11.22	-8.52	-7.82	-8.88	-8.07	-8.50	-8.41	-8.09	-7.71	-8.15	-7.90	-11.23	-11.23	-8.63	-8.72
δ_{v5} [°]	-10.203	-10.21	-9,97	-10.22	-9.98	-9.20	-10.12	-9.93	-9,94	-10.21	-9,30	-10.32	-10.09	-10.02	-9.36	-9.91	-9.15	-9.21	-9.78	-10.30
δ_{v6} [°]	-3.727	4.28	4.75	4.06	5.64	-11.12	6.37	5.77	-2,70	3.86	3.78	5.52	4.46	5.11	6.30	4.70	-10.99	-11.13	4.61	-1.17
$Q_{gen,1}$ [MVar]	1332	1662	1640	1630	1624	1497	1600	1637	1339	1655	1650	1584	1669	1644	1687	1642	1500	1497	1616	1332
$Q_{gen,2}$ [MVar]	3606	3123	3125	3498	3275	3426	2294	3163	3532	3123	3153	3436	3121	3127	3126	3174	3416	3435	3334	3572
$Q_{gen,3}$ [MVar]	2686	2224	2230	2399	2632	2610	2694	2325	2626	2228	2320	2705	2230	2223	2296	2258	2609	2613	2684	2652
$Q_{gen,4}$ [MVar]	1392	1343	1334	1470	618	1368	779	1147	1335	1340	1286	759	1341	1341	1250	1351	1362	1377	631	1370
$Q_{gen,5}$ [MVar]	3699	3817	3859	3125	4006	3665	3933	3909	3683	3831	3833	3835	3810	3847	3827	3749	3681	3648	3902	3801
$Q_{gen,6}$ [MVar]	626	803	798	925	935	805	717	834	801	798	783	788	804	801	822	814	804	800	934	601
$v_{DC,1}$ [pu]	1,050	0.986	1.050	1.050	1.050	0.983	1.050	1.050	1.050	0.986	1.050	1.049	0.987	1.050	1.050	1.050	0.983	0.983	1.050	1.050
$v_{DC,2}$ [pu]	1,027	0.962	1.027	1.028	1.028	0.960	1.028	1.027	1.028	0.962	1.028	1.026	0.963	1.027	1.028	1.028	0.960	0.960	1.028	1.027
$v_{DC,3}$ [pu]	1,020	0.953	1.020	1.020	1.020	0.950	1.020	1.019	1.020	0.954	1.020	1.018	0.955	1.019	1.019	1.020	0.950	0.950	1.020	1.020
$v_{DC,4}$ [pu]	1.018	0.950	1.016	1.016	1.016	0.950	1.016	1.016	1.017	0.950	1.017	1.015	0.951	1.016	1.016	1.016	0.950	0.950	1.016	1.017
$P_{conv,AC,1}$ [MW]	-7067	-7062	-7069	-7037	-7044	-6888	-7043	-7054	-7051	-7063	6976	-7063	-7047	-7074	-6983	-7053	-6882	-6888	-7012	-7086
$P_{conv,AC,2}$ [MW]	606	384	399	340	319	312	347	345	523	397	200	402	344	404	157	363	296	313	266	600
$P_{conv,AC,3}$ [MW]	4612	4389	4396	4456	4411	4991	4444	4389	4594	4397	4556	4417	4408	4380	4485	4420	4996	4990	4482	4535
$P_{conv,AC,4}$ [MW]	1432	1842	1855	1820	1894	1147	1831	1901	1516	1824	1803	1822	1850	1871	1922	1851	1152	1147	1844	1531

Tab. 7-9: Result of differential evolution mixed AC/DC OPF – $|v_{AC,min}|$ = 1.00 p.u., $|v_{AC,max}|$ = 1.05 p.u., $v_{DC,min}$ = 0.95 p.u., $v_{DC,max}$ = 1.05 p.u..

	1	2	3	4	5	6	7	8	9	10	11	12	13	14	15	16	17	18	19	20
$P_{conv,loss}$ [MW]	825,7	1021.6	826.2	827.1	1048.1	824.8	822.5	827.1	1020.6	825.0	1020.6	826.4	825.7	1020.6	826.2	827.1	824.8	822.5	827.1	1020.6
No. of iterations	8000	3002	4624	8000	3002	5830	7355	3973	3002	3529	3002	7549	8000	3002	4624	8000	5830	7355	3973	3002
$\|v_1\|$ [pu]	1.017	1.000	1.000	1.017	1.000	1.016	1.018	1.015	1.000	1.014	1.000	1.000	1.017	1.000	1.000	1.017	1.016	1.018	1.015	1.000
$\|v_2\|$ [pu]	1.000	1.000	1.000	1.000	1.000	1.000	1.000	1.000	1.000	1.000	1.000	1.000	1.000	1.000	1.000	1.000	1.000	1.000	1.000	1.000
$\|v_3\|$ [pu]	1.050	1.050	1.050	1.050	1.050	1.050	1.050	1.050	1.050	1.050	1.050	1.050	1.050	1.050	1.050	1.050	1.050	1.050	1.050	1.050
$\|v_4\|$ [pu]	1.042	1.050	1.050	1.000	1.000	1.050	1.050	1.000	1.050	1.050	1.050	1.049	1.042	1.050	1.050	1.000	1.050	1.050	1.000	1.050
$\|v_5\|$ [pu]	1.007	1.050	1.049	1.041	1.000	1.000	1.050	1.044	1.000	1.044	1.000	1.041	1.007	1.000	1.049	1.041	1.000	1.050	1.044	1.000
$\|v_6\|$ [pu]	1.028	1.000	1.050	1.050	1.000	1.050	1.050	1.049	1.000	1.037	1.000	1.050	1.028	1.000	1.050	1.050	1.050	1.050	1.049	1.000
δ_{v1} [°]	40.31	41.43	41.42	40.36	41.43	40.42	40.31	40.48	41.43	40.55	41.43	41.43	40.31	41.43	41.42	40.36	40.42	40.31	40.48	41.43
δ_{v2} [°]	0.00	0.00	0.00	0.00	0.00	0.00	0.00	0.00	0.00	0.00	0.00	0.00	0.00	0.00	0.00	0.00	0.00	0.00	0.00	0.00
δ_{v3} [°]	10.17	7.48	9.40	9.34	7.56	9.17	9.49	9.44	7.44	9.37	7.44	9.35	10.17	7.44	9.40	9.34	9.17	9.49	9.44	7.44
δ_{v4} [°]	-7.66	-11.38	-8.73	-7.97	-11.83	-8.05	-7.87	-8.03	-11.55	-8.06	-11.55	-8.76	-7.66	-11.55	-8.73	-7.97	-8.05	-7.87	-8.03	-11.55
δ_{v5} [°]	-10.50	-9.20	-9.72	-10.01	-9.41	-10.01	-9.97	-10.01	-9.27	-9.91	-9.27	-9.73	-10.50	-9.27	-9.72	-10.01	-10.01	-9.97	-10.01	-9.27
δ_{v6} [°]	4.78	-10.70	-0.82	5.37	-11.35	4.15	4.06	4.74	-10.99	3.49	-10.99	-0.82	4.78	-10.99	-0.82	5.37	4.15	4.06	4.74	-10.99
$Q_{gen,1}$ [MVar]	1611	1620	1565	1630	1618	1631	1629	1620	1621	1616	1621	1565	1611	1621	1565	1630	1631	1629	1620	1621
$Q_{gen,2}$ [MVar]	3299	3214	3226	3231	3456	3314	3132	3232	3391	3172	3391	3258	3299	3391	3226	3231	3314	3132	3232	3391
$Q_{gen,3}$ [MVar]	2309	2423	2347	2441	2676	2322	2238	2447	2493	2271	2493	2363	2309	2493	2347	2441	2322	2238	2447	2493
$Q_{gen,4}$ [MVar]	1370	1416	1335	970	1106	1400	1334	967	1487	1359	1487	1343	1370	1487	1335	970	1400	1334	967	1487
$Q_{gen,5}$ [MVar]	3601	3791	3808	3868	3472	3476	3865	3887	3405	3827	3405	3738	3601	3405	3808	3868	3476	3865	3887	3405
$Q_{gen,6}$ [MVar]	805	672	777	877	800	858	792	869	736	762	736	790	805	736	777	877	858	792	869	736
$v_{DC,1}$ [pu]	1.050	0.983	1.050	1.050	0.983	1.050	1.050	1.050	0.983	1.049	0.983	1.050	1.050	0.983	1.050	1.050	1.050	1.050	1.050	0.983
$v_{DC,2}$ [pu]	1.027	0.960	1.028	1.027	0.960	1.028	1.027	1.027	0.960	1.026	0.960	1.028	1.027	0.960	1.028	1.027	1.028	1.027	1.027	0.960
$v_{DC,3}$ [pu]	1.019	0.950	1.020	1.020	0.950	1.020	1.020	1.020	0.950	1.018	0.950	1.020	1.019	0.950	1.020	1.020	1.020	1.020	1.020	0.950
$v_{DC,4}$ [pu]	1.016	0.950	1.017	1.016	0.950	1.016	1.016	1.016	0.950	1.015	0.950	1.017	1.016	0.950	1.017	1.016	1.016	1.016	1.016	0.950
$P_{conv,AC,1}$ [MW]	-7110	-6918	-7030	-7058	-6923	-7046	-7069	-7060	-6916	-7055	-6916	-7027	-7110	-6916	-7030	-7058	-7046	-7069	-7060	-6916
$P_{conv,AC,2}$ [MW]	508	284	435	361	278	361	417	379	279	402	279	426	508	279	435	361	361	417	379	279
$P_{conv,AC,3}$ [MW]	4344	5000	4580	4397	5000	4442	4411	4409	5000	4448	5000	4585	4344	5000	4580	4397	4442	4411	4409	5000
$P_{conv,AC,4}$ [MW]	1836	1156	1600	1881	1158	1824	1823	1853	1158	1786	1158	1600	1836	1158	1600	1881	1824	1823	1853	1158

Tab. 7-10: Result of differential evolution mixed AC/DC OPF – $|v_{AC,min}|$ = 1.00 p.u., $|v_{AC,max}|$ = 1.05 p.u., $v_{DC,min}$ = 1.00 p.u., $v_{DC,max}$ = 1.05 p.u..

	1	2	3	4	5	6	7	8	9	10	11	12	13	14	15	16	17	18	19	20
$P_{conv,loss}$ [MW]	824.9	822.5	826.4	823.1	832.8	826.2	1020.4	831.6	837.7	1019.7	828.5	822.5	1019.7	822.6	822.6	827.1	822.7	825.2	328.3	825.3
No. of iterations	3931	7177	7437	3955	3791	6578	3002	3883	3646	3002	3859	5245	3002	7074	6518	4767	7178	5178	3670	7880
$\|v_1\|$ [pu]	1.015	1.018	1.000	1.021	1.016	1.004	1.000	1.016	1.050	1.000	1.004	1.018	1.000	1.020	1.018	1.014	1.017	1.016	1.022	1.017
$\|v_2\|$ [pu]	1.000	1.000	1.000	1.000	1.000	1.000	1.000	1.000	1.000	1.000	1.000	1.000	1.000	1.000	1.000	1.000	1.000	1.000	1.000	1.000
$\|v_3\|$ [pu]	1.050	1.050	1.050	1.050	1.050	1.050	1.050	1.050	1.050	1.050	1.050	1.050	1.050	1.050	1.050	1.050	1.050	1.050	1.050	1.050
$\|v_4\|$ [pu]	1.050	1.050	1.047	1.047	1.000	1.049	1.050	1.006	1.050	1.050	1.000	1.050	1.050	1..049	1.050	1.000	1.050	1.050	1.049	1.050
$\|v_5\|$ [pu]	1.000	1.048	1.038	1.049	1.039	1.050	1.000	1.050	1.000	1.000	1.047	1.050	1.000	1.049	1.047	1.040	1.050	1.039	1.050	1.036
$\|v_6\|$ [pu]	1.046	1.050	1.046	1.048	1.050	1.028	1.050	1.050	1.050	1.000	1.050	1.050	1.000	1.050	1.046	1.050	1.044	1.000	1.050	1.000
δ_{v1} [°]	40.44	40.29	41.43	40.06	40.40	41.19	41.43	40.39	38.28	41.43	41.14	40.25	41.43	40.14	40.29	40.50	40.32	40.39	40.04	40.36
δ_{v2} [°]	0.00	0.00	0.00	0.00	0.00	0.00	0.00	0.00	0.00	0.00	0.00	0.00	0.00	0.00	0.00	0.00	0.00	0.00	0.00	0.00
δ_{v3} [°]	9.43	9.46	9.53	10.01	9.14	9.18	7.82	9.06	8.18	7.82	9.56	9.45	7.82	9.68	9.51	9.47	9.66	9.33	9.24	9.83
δ_{v4} [°]	-7.99	-7.86	-8.71	-7.53	-8.14	-8.61	-11.37	-8.15	-6.77	-11.38	-8.48	-7.84	-11.38	-7.69	-7.85	-8.04	-7.83	-8.00	-7.82	-7.84
δ_{v5} [°]	-10.13	-9.97	-9.82	-10.28	-9.98	-9.68	-9.21	-9.89	-10.20	-9.21	-9.94	-9.97	-9.21	-10.10	-10.00	-10.04	-10.05	-9.95	-9.98	-10.20
δ_{v6} [°]	3.98	4.19	-0.78	5.01	4.89	0.71	-11.43	4.74	14.66	-11.14	1.75	4.34	-11.14	4.72	4.21	4.67	3.97	4.70	5.04	4.57
$Q_{gen,1}$ [MVar]	1622	1631	1560	1631	1632	1584	1610	1636	1805	1610	1576	1634	1610	1635	1630	1617	1623	1628	1653	1616
$Q_{gen,2}$ [MVar]	3320	3137	3272	3122	3241	3204	3392	3192	3128	3392	3277	3127	3392	3123	3143	3246	3135	3176	3109	3190
$Q_{gen,3}$ [MVar]	2319	2241	2369	2216	2454	2333	2481	2416	2144	2481	2502	2234	2481	2222	2241	2453	2236	2264	2223	2256
$Q_{gen,4}$ [MVar]	1409	1335	1340	1320	971	1352	1423	1002	1422	1491	963	1333	1491	1331	1345	971	1343	1418	1326	1428
$Q_{gen,5}$ [MVar]	3484	3851	3728	3896	3843	3850	3343	3918	3585	3407	1882	3867	3407	3874	3845	3859	3877	3842	3873	3829
$Q_{gen,6}$ [MVar]	847	795	785	797	877	725	869	854	952	737	853	793	737	797	786	875	777	683	798	687
$v_{DC,1}$ [pu]	1.050	1.050	1.050	1.050	1.035	1.050	1.031	1.036	1.050	1.031	1.050	1.050	1.031	1.050	1.050	1.050	1.050	1.050	1.035	1.050
$v_{DC,2}$ [pu]	1.027	1.027	1.028	1.027	1.012	1.028	1.009	1.013	1.027	1.009	1.027	1.027	1.009	1.027	1.027	1.027	1.027	1.027	1.012	1.027
$v_{DC,3}$ [pu]	1.020	1.019	1.020	1.019	1.004	1.019	1.000	1.005	1.020	1.000	1.019	1.019	1.000	1.019	1.020	1.020	1.020	1.020	1.004	1.020
$v_{DC,4}$ [pu]	1.016	1.016	1.017	1.016	1.000	1.017	1.000	1.001	1.014	1.000	1.016	1.016	1.000	1.016	1.016	1.016	1.016	1.016	1.000	1.016
$P_{conv,AC,1}$ [MW]	-7061	-7068	-7037	-7108	-7045	-7024	-6938	-7041	-7057	-6938	-7048	-7069	-6938	-7085	-7071	-7062	-7079	-7057	-7.062	-7087
$P_{conv,AC,2}$ [MW]	401	410	452	490	337	393	328	330	151	328	416	409	328	441	419	384	444	394	375	470
$P_{conv,AC,3}$ [MW]	4426	4410	4569	4332	4421	4560	5000	4431	4190	5000	4493	4405	5000	4371	4406	4408	4401	4435	4392	4394
$P_{conv,AC,4}$ [MW]	1814	1829	1600	1866	1861	1654	1146	1855	2290	1146	1721	1836	1146	1854	1827	1850	1815	1809	1870	1804

Tab. 7-11: Result of differential evolution mixed AC/DC OPF – $|v_{AC,min}| = 1.00$ p.u., $|v_{AC,max}| = 1.05$ p.u., $v_{DC,min} = 1.00$ p.u., $v_{DC,max} = 1.05$ p.u., 20,000 iterations.

$P_{conv,loss}$ [MW]	**822.58**
No. of iterations	20,000
$\|v_1\|$ [pu]	1.020
$\|v_2\|$ [pu]	1.000
$\|v_3\|$ [pu]	1.050
$\|v_4\|$ [pu]	1.047
$\|v_5\|$ [pu]	1.048
$\|v_6\|$ [pu]	1.050
δ_{v1} [°]	40.17
δ_{v2} [°]	0.00
δ_{v3} [°]	9.52
δ_{v4} [°]	-7.75
δ_{v5} [°]	-10.03
δ_{v6} [°]	4.75
$Q_{gen,1}$ [MVar]	1637
$Q_{gen,2}$ [MVar]	3129
$Q_{gen,3}$ [MVar]	2236
$Q_{gen,4}$ [MVar]	1317
$Q_{gen,5}$ [MVar]	3865
$Q_{gen,6}$ [MVar]	801
$v_{DC,1}$ [pu]	1.050
$v_{DC,2}$ [pu]	1.027
$v_{DC,3}$ [pu]	1.020
$v_{DC,4}$ [pu]	1.016
$P_{conv,AC,1}$ [MW]	-7075
$P_{conv,AC,2}$ [MW]	415
$P_{conv,AC,3}$ [MW]	4386
$P_{conv,AC,4}$ [MW]	1855

Appendix E Power flow equations

Derivation of power flow equations for the transmission level.

$$s_{ij} = v_i \cdot i_{ij}^* \qquad \text{and} \qquad i_{ij}^* = \frac{v_i - v_j}{r_{ij} + j \cdot x_{ij}} \tag{A.7}$$

$$s_{ij} = v_i \frac{v_i^* - v_j^*}{r_{ij} - j \cdot x_{ij}} \tag{A.8}$$

Formulation in Polarcoordinates

$$s_{ij} = v_i(\cos(\delta_i) + j \cdot \sin(\delta_i)) \frac{v_i\,(\cos(\delta_i) - j \cdot \sin(\delta_i)) - v_j(\cos(\delta_j) - j \cdot \sin(\delta_j))}{r_{ij} - j \cdot x_{ij}} \tag{A.9}$$

$$s_{ij} = \frac{v_i^2 r_{ij} + j \cdot x_{ij} v_i^2 - v_i v_j r_{ij} \cos(\Delta\delta) - j \cdot v_i v_j x_{ij} \cos(\Delta\delta) - j \cdot v_i v_j r_{ij} \sin(\Delta\delta) + v_i v_j x_{ij} \sin(\Delta\delta)}{r_{ij}^2 + x_{ij}^2} \tag{A.10}$$

Using the following assumptions for transmission grids:

- $r/x << 1$
- $v_i \approx v_j$
- $\Delta\delta \rightarrow 0$

$$p_{ij} = \frac{v_i v_j}{x_{ij}} \sin(\Delta\delta) \tag{A.11}$$

Appendix F WAMS and PMU

Voltage angles can be quickly obtained using PMUs connected to a WAMS. A phasor represents a sinusoidal signal of a fixed frequency. While (A.12) describes the instantaneous value of a sinusoidal variable depending on its angular frequency ω, its peak value *M* and phase angle φ, (A.13) defines the transition to a phasor formulation. The phasor is represented by the RMS value of the original signal as its magnitude and by the phase angle φ. A phasor is no longer dependent on a frequency since it is only valid for a single frequency. Thus, when extracting a phasor from a real measurement a Fourier analysis is necessary at first and a phasor can be calculated for each measured frequency. PMUs use microprocessor applicable derivatives of the Fourier transformation (FT) namely discrete FT or fast FT.

$$x(t) = M \cdot \cos(\omega t + \varphi) \tag{A.12}$$

$$x(t) \longleftrightarrow x = \frac{M}{\sqrt{2}} \cdot e^{j\varphi} \tag{A.13}$$

First measurements of phase angle differences took place in the early 1980s using different sources for time synchronization [109]-[115]. Those early phasor measurements provided an accuracy of approximately 40μs, which is too much for a wide area measurement system [116]. Consequently, these early approaches were not further developed.

Shortly after, in 1983, the starting point for modern PMUs was given. The impetus for developing the PMU concept was based on a new fault detection algorithm for transmission lines using a symmetrical components analysis of voltages and currents. At this time, information from the global positioning system (GPS) have been fully available making a measurement synchronization possible. The first PMU prototype was built at Virginia Tech in the early 1980s and the first commercially available PMU was available in 1991 from Macrodyne. [117] Today, a PMU is defined as a device providing at least a synchronized phasor (angle and magnitude), frequency and change of frequency of its input signal which can be voltage and/or current while using a time synchronizing signal [118].

Each measurement by a PMU is stamped with a time signal at the measurement unit itself. Thus, transmission time of measurements to an analyzing unit is not critical. The time tag is provided by GPS. The most important signal provided by the GPS for that purpose is the one puls-per-second signal, which is received almost coincidently [116]. A synchronization accuracy of 1μs is achieved [116], [117] while a GPS provided time has an accuracy of 0.2 μs [118]. For 50 Hz systems 1μs accuracy results in a phasor angle error of 0.018° (≙ 0.005%) which is quite small. The requirements given by the according IEEE standard [118] permits a maximum of ±31 μs but only if there is no measurement error for *V* respectively *I*. This is derived from a maximum permissible total vector error *TVE* of 1% which is defined for a phasor of time stamp *n* by (A.14) [118]:

$$TVE(n) = \sqrt{\frac{\left(\hat{x}_R(n) - x_R(n)\right)^2 + \left(\hat{x}_I(n) - x_I(n)\right)^2}{\left(x_R(n) - x_I(n)\right)^2}} \tag{A.14}$$

This is also illustrated in Fig. 7.2 while the TVE is normalized to the length of the real vector in order to specify the TVE in percentage.

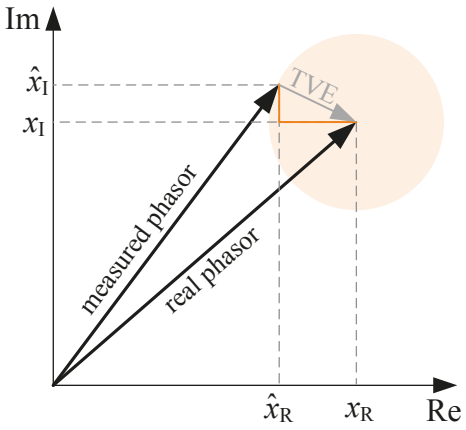

Fig. 7.2: Total vector error of a synchrophasor.

A WAMS collects all PMU data (see Fig. 7.3) and calculates angle differences between the measured synchrophasors (phasors with the same time stamp) (see Fig. 4.5). The latency between PMU measurement, data transmission to WAMS and back to an application device takes approximately 50-200 ms while a WAMS updates every 0.05 - 0.1 s [120]. With phasor data availability within this time frame several applications are possible and can be divided in three categories [116], [119]:

- *Wide area monitoring* – monitoring complex voltage $\underline{v}$ and frequency f within a grid and also improving state estimation
- *Wide area protection* – special power system protections e.g. backup protection (due to latency of remote measurements)
- *Wide area control* – e.g. electromechanical oscillations, certain overload phenomena

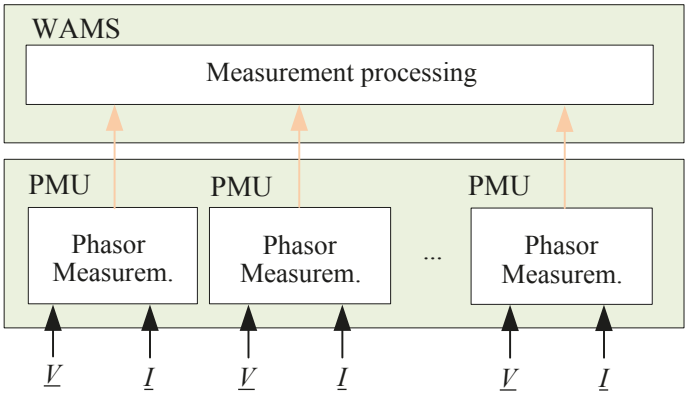

Fig. 7.3: Architecture of a wide area measurement system and its integration into data acquisition and application context. According to [120] and [121].

Appendix G AGM – Scenario power plant trip

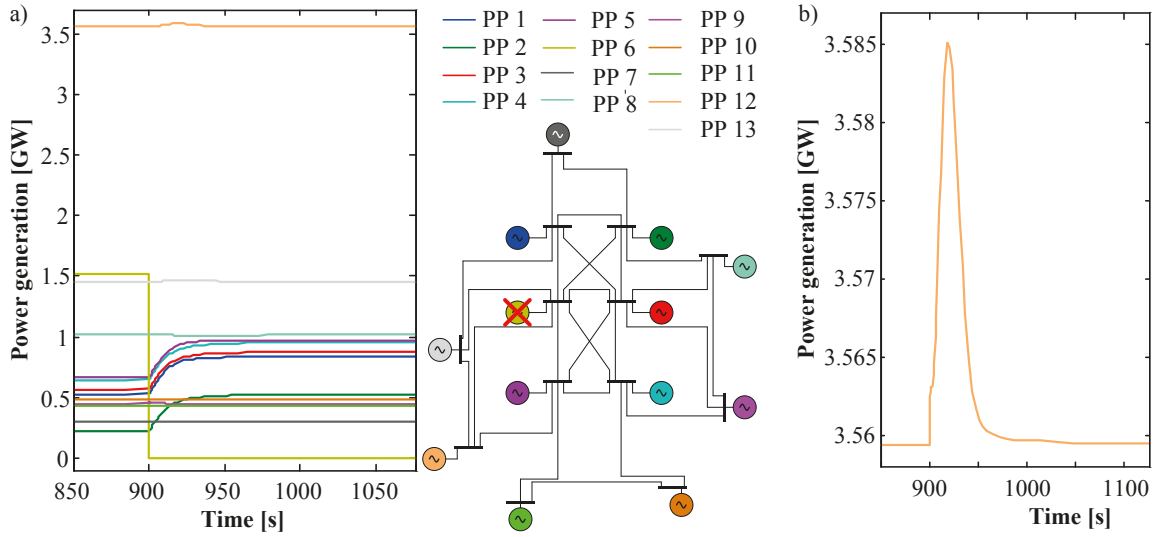

Fig. 7.4: Power generation of all power plants after trip of power plant 6 including primary and secondary load frequency control (a) and power plant 12 (as an example of an undisturbed control area) (b).

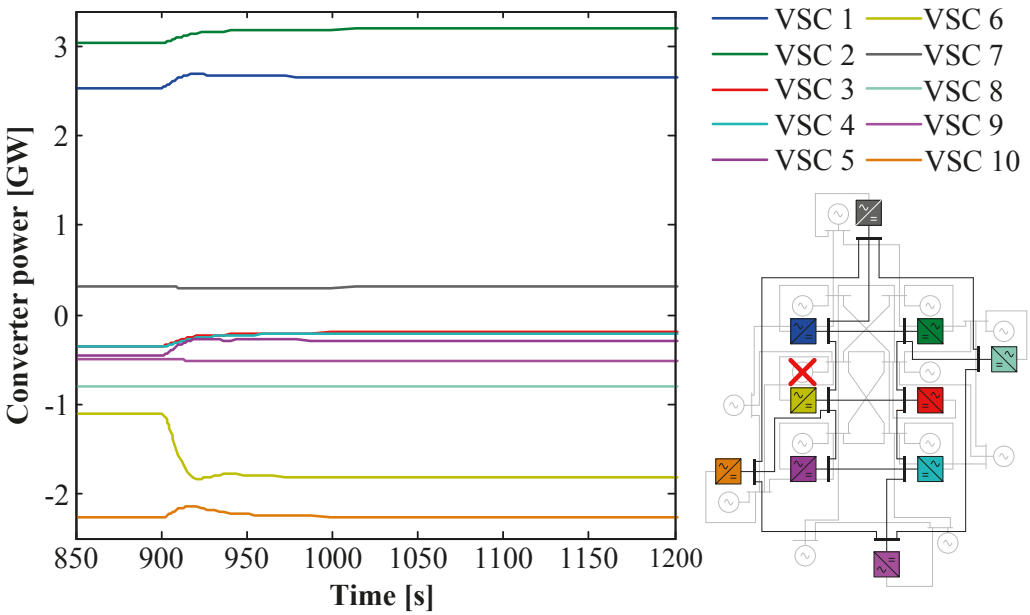

Fig. 7.5: HVDC converter power after trip of power plant 6.

Appendix H AGM – AC line trip

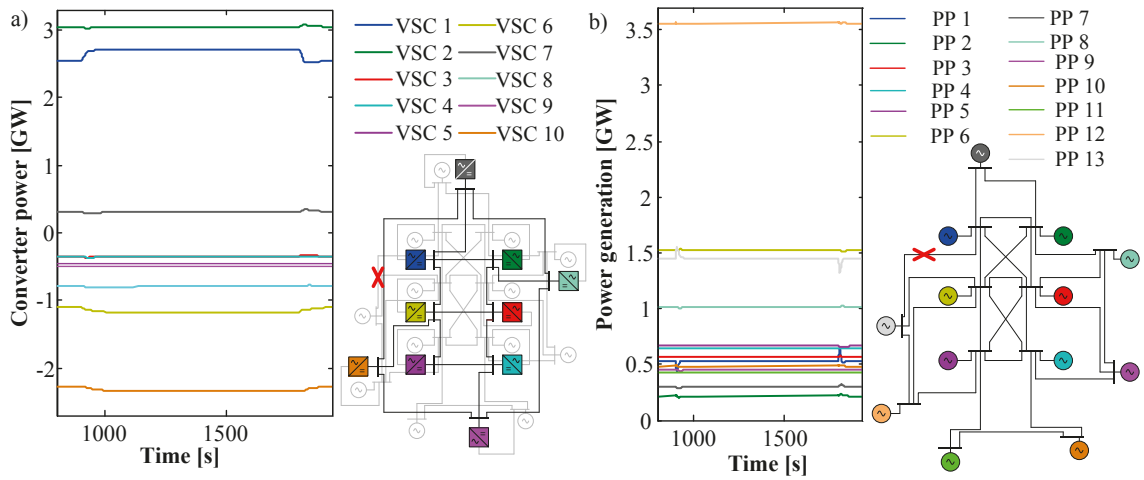

Fig. 7.6: a) HVDC converter power during and after an AC line 26 trip and b) corresponding power plant power generation.

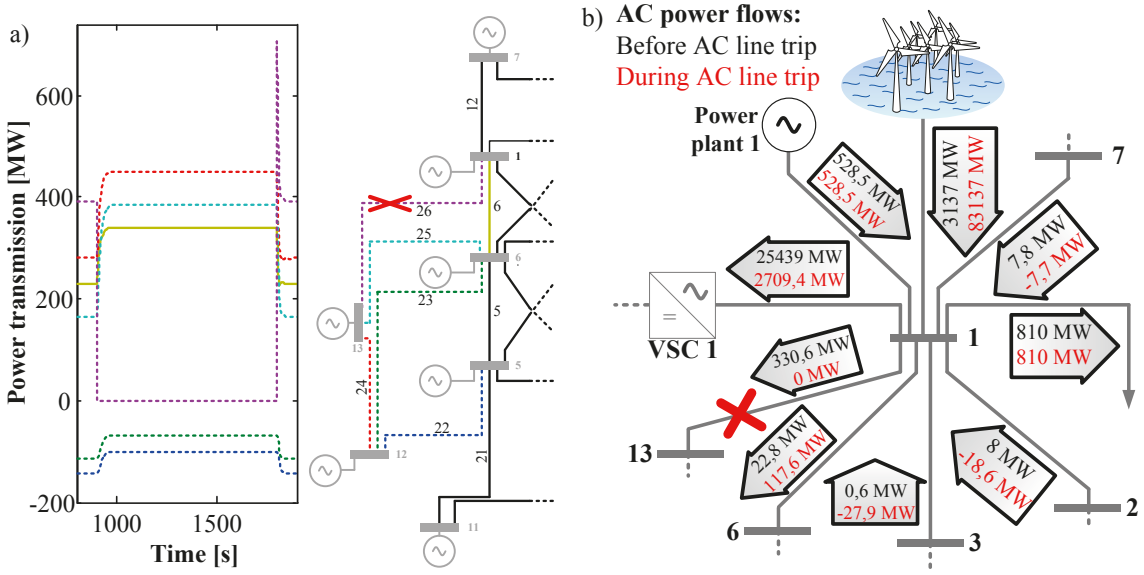

Fig. 7.7: a) AC power flows around tripped AC line 26 and b) reallocation of AC power flows around AC node 1 before and during AC line 26 trip.

Appendix I Overlay grid as remaining connection to an islanded area

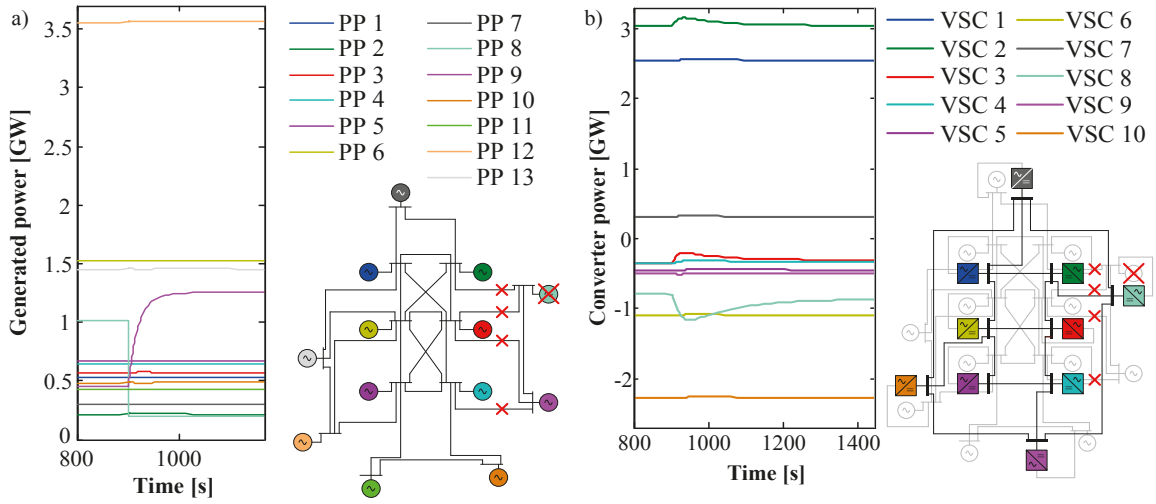

Fig. 7.8: a) Power generation of power plants during islanding of AC nodes 8 and 9 with simultaneously partial trip of power plant 8 and b) Converter power values during islanding of AC nodes 8 and 9 with simultaneously partial trip of power plant 8.

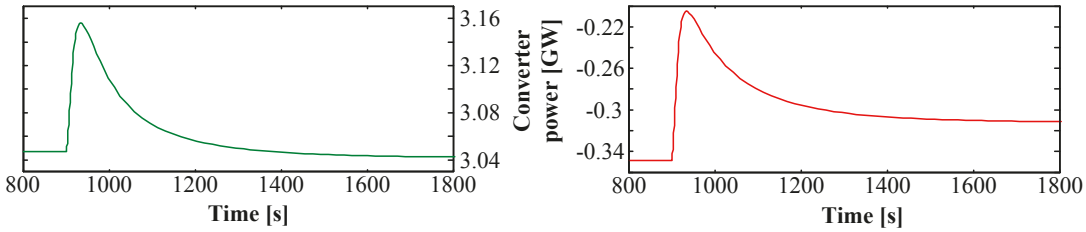

Fig. 7.9: Converter power of VSC 2 and 3during islanding of AC nodes 8 and 9 with simultaneously partial trip of power plant 8.

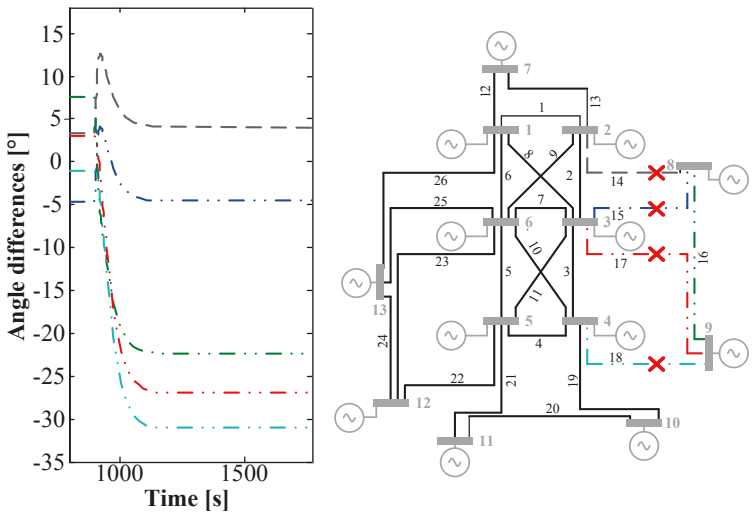

Fig. 7.10: Angle differences over AC lines during and after islanding of AC nodes 8 and 9 with simultaneously partial trip of power plant 8.

Appendix J Impedance influence on AGM simplification – line length distribution using random numbers

Tab. 7-12: Line length distribution using random numbers between -250 and +250.

AC line	Random number	Resulting AC line length [km]
Line 1	-9	491
Line 2	163	663
Line 3	-72	418
Line 4	60	560
Line 5	120	620
Line 6	75	575
Line 7	172	672
Line 8	-66	434
Line 9	53	553
Line 10	46	546
Line 11	-87	413
Line 12	125	625
Line 13	-8	492
Line 14	-238	262
Line 15	-102	398
Line 16	124	624
Line 17	97	597
Line 18	-52	448
Line 19	64	564
Line 20	-138	362
Line 21	-184	316
Line 22	11	511
Line 23	100	600
Line 24	-128	372
Line 25	51	551
Line 26	-172	328

List of Abbreviations

AGM	Angle Gradient Method
AI	Artificial Intelligence
CA	Control Area
CORESO	Coordination of Electricity System Operators
DE	Differential Evolution
EKC	Electricity Coordination Center
ENTSO-E	European Network of Transmission System Operators for Electricity
FACTS	Flexible AC Transmission System
FT	Fourier Transformation
GA	Generic Algorithm
GIL	Gas Insulated Line
GPS	Global Positioning System
HVDC	High Voltage Direct Current
HTC	High Temperature super conducting Cable
IP	Interior Point
ISO	Independent System Operator
LCC	Line Commutated Converter
LP	Linear Programming
MMC	Modular Multilevel Converter
NLP	Non Linear Programming
OF	Objective Function
OPF	Optimal Power Flow
P2P	Point-to-point (HVDC scheme – primarily considered as VSC technology)
PCC	Point of Common Coupling
PMU	Phasor Measurement Unit
PSO	Particle Swarm Optimization
PSS	Power System Stabilizer
PWM	Pulse Width Modulation

QP	Quadratic Programming
RMS	Root Mean Square
RSCI	Regional Security Cooperation Initiatives
SCADA	Supervisory Control And Data Acquisition
TSC	Transmission System Operator Security Cooperation
TSO	Transmission System Operator
TVE	Total vector error
TYNDP	Ten Year Network Development Plan
VSC	Voltage Source Converter
WAMS	Wide Area Monitoring System

List of Symbols

$k_{\Delta v_{DC}}$	Converter's DC voltage control droop constant
$\hat{x}_I$, $\hat{x}_R$	Measured value by PMU (imaginary and real part)
$\|v_{AC}\|$	AC voltage magnitude
$\|v_{Slack,AC}\|$	AC voltage magnitude of Slack bus
a	Weighting factor for a part of a multi objective function
b	Constant factor of objective function
c	Linear factor of objective function
C	Matrix of HVDC converter observability area center nodes of directly adjacent responsibility areas to the considered one
C_C	Converter capacitance at the DC grid side
C_{DC}	Overall DC grid capacitance
C_L	DC Line capacitance
C_m, C_k	DC node capacitance at node m and k
CR	Crossover constant (Differential Evolution optimization algorithm)
D	Generators damping constant
d	Quadratic factor of objective function
e_{DC}	Energy of the DC grid
$e^+_{DC\_balance}$ / $e^-_{DC\_balance}$	Maximum available energy for positive / negative balancing power provision for the DC grid by storages at or nearby considered AC node
e_{in} / p_{in}	Energy / power input in a system
e_{out} / p_{out}	Energy / power output out of a system
$e_{storage}$	Energy available for balancing power from storage at or nearby a considered AC node
f	frequency
$F(u,x)$	Objective function
f_{eig}	Eigenfrequency
$F_{fitness}(x,u)$	Fitness function containing weighted objective function and penalty function (Differential Evolution optimization algorithm)

f_M	Mutation constant (Differential Evolution optimization algorithm)
G	Generation (Differential Evolution optimization algorithm)
$g(u,x)$	Inequality constraints
$h(u,x)$	Equality constraints
h_{left} / h_{l}	Parameter for slope definition of left part of continuous p-v-characteristic (left sigmoid function)
h_{right} / h_{r}	Parameter for slope definition of right part of continuous p-v-characteristic (left sigmoid function)
I, i	Current
i_{conv}	Converter current
$i_{\text{conv,max}}$	Maximal converter current
$i_{\text{conv,nominal}}$	Nominal converter current
k	Number of equality constraints
$k_{\text{AC-DC}}$	Division factor between AC and DC power flows at a specific node
$k_{\text{Balance\_DC\_gen+}}$ / $k_{\text{Balance\_DC\_gen-}}$	Capability of generating units (except storages) connected to or nearby a considered AC node for positive / negative balancing power provision for the DC grid
$k_{\text{Balance\_DC\_storage+}}$ / $k_{\text{Balance\_DC\_storage-}}$	Capability of storages connected to or nearby a considered AC node for positive / negative balancing power provision for the DC grid
$k_{\text{Balance\_DC+}}$ / $k_{\text{Balance\_DC-}}$	Overall positive / negative DC balancing capability of a considered AC node
$k_{\text{e+}}$ / $k_{\text{e-}}$	Capability of storages connected to or nearby a considered AC node for positive / negative balancing power provision by means of available energy
$k_{\text{p+}}$ / $k_{\text{p-}}$	Capability of storages connected to or nearby a considered AC node for positive / negative balancing power provision by means of installed storage power
k_{penalty}	Penalty weighting factor (Differential Evolution optimization algorithm)
$k_{\Delta f}$	Converter's frequency control droop constant
l	Number of Inequality constraints
L_{km}	DC line inductance
M	Amplitude of a sinusoidal function / signal

n_{conv}	Number of converters in the grid
n_{DC_line}	Number of lines in the HVDC grid
n_{gen}	Number of generating units (except storages) at or nearby a considered AC node
n_{OF}	Number of objective functions
NP	Number of populations (Differential Evolution optimization algorithm)
$n_{storage}$	Number of storages at or nearby a considered AC node
$P^{(G)}$	Population vector of generation G (Differential Evolution optimization algorithm)
$p^{+}_{AC\_balance}$	Available positive AC balancing power from generating units (except storages)
$p^{+}_{DC\_balance}$	Maximum positive DC balancing power requested by a considered converter
$p_{AC,loss}$	AC transmission losses
$p^{-}_{AC\_balance}$	Available negative AC balancing power from generating units (except storages)
$p_{conv,AC}$	Converter active power on the AC grid side
$p_{conv,AC,exchange}$	Part of converter reference value for a special exchange with another converter
$p_{conv,AC,max}$	Maximum converter active power on the AC grid side
$p_{conv,AC,min}$	Minimum converter active power on the AC grid side
$p_{conv,nominal}$	Nominal converter active power
$p_{conv,schedule}$	Scheduled converter reference value from tertiary control
$p_{DC,loss}$	DC transmission losses
$p^{-}_{DC\_balance}$	Maximum negative DC balancing power requested by a considered converter
p_{el}	Generated electrical power
$p_{exchange}$	Market based power exchange between transmission system operators
p_{gen}	Generated active power
p_{ij}	Power flow on a DC line

p_{load}	Vertical system load (active power)
p_{loss}	Losses
$p_{\text{loss\_conv}}$	Converter losses
$p_{\text{loss\_DC\_line}}$	DC Line losses
p_{m}	Mechanical power from generators turbine
$p_{\text{schedule},ij}$	Scheduled power flow between node i and j
$p_{\text{storage:installed}}$	Installed storage power at or nearby a considered AC node
$p_{\text{WAMS},ij}$	WAMS measured power flow between node i and j
$q_{\text{conv,AC}}$	Converter reactive power (AC grid side)
q_{load}	Vertical system load (reactive power)
r_{ij}	Line resistance between node i and j
R_{km}	DC line resistance
s_{ij}	Apparent power flow on an AC transmission line
$s_{\text{VSC,max}}$	Converter's maximum allowed apparent power
$s_{\text{VSC,min}}$	Converter's minimum allowed apparent power
t	Time
T_{l}	Delay time
T_{A}	Generator time constant
T_{d}	Dead time
TVE	Total vector error (accuracy of PMU measurement)
u	Optimization vector
u'	Optimization vector (containing redundant information)
$u_{rs}^{(G)}$	Trial vector elements of generation G (Differential Evolution optimization algorithm)
$u_{s}^{(G)}$	Trial vector of generation G (Differential Evolution optimization algorithm)
V, v	Voltage
$v'_{\text{DC,max}}$	Right inflection point of continuous p-v-characteristic (right sigmoid function)
$v'_{\text{DC,min}}$	Left inflection point of continuous p-v-characteristic (left sigmoid function)

v_{AC}	AC voltage
$v_{AC,max}$	Maximum allowed AC voltage magnitude
$v_{AC,min}$	Minimum allowed AC voltage magnitude
$v_{conv,AC}$	AC voltage on converter's AC side
v_{DC}	DC voltage
$v_{DC,max}$	Maximum allowed DC voltage magnitude
$v_{DC,min}$	Minimum allowed DC voltage magnitude
$v_{DC,ref}$	Reference DC node voltage
$v_{rs}^{(G)}$	Elements of mutation vector of generation G (Differential Evolution optimization algorithm)
$v_s^{(G)}$	Mutations vector of generation *G* (Differential Evolution optimization algorithm)
x	State vector
x_{best}	Best known population (Differential Evolution optimization algorithm)
x_I, x_R	Physical / real value (imaginary and real part)
x_{ij}	Line inductance between node *i* and *j*
$x_{r,best}^{(G)}$	Vector elements of best known population until generation G (Differential Evolution optimization algorithm)
$x_{rs}^{(G)}$	Vector elements of population $x_s^{(G)}$ (Differential Evolution optimization algorithm)
$x_{rs,max}$	Vector of maximum limits for optimization variables (Differential Evolution optimization algorithm)
$x_{rs,min}$	Vector of minimum limits for optimization variables (Differential Evolution optimization algorithm)
$x_s^{(G)}$	Population of generation *G* (Differential Evolution optimization algorithm)
$\underline{Z}$	AC grid impedance
α	Converter losses (voltage dependent)
β	Converter losses (linear dependent on converter current)
γ	Converter losses (quadratic dependent on converter current)
δ_{AC}	AC voltage angle

Δf	Frequency deviation
Δp_{bound}	Converter reference value boundary violation
$\Delta p_{\text{neg,margin}}$	Margin between converter reference value and most restrictive boundary for minimum converter reference value
$\Delta p_{\text{pos,margin}}$	Margin between converter reference value and most restrictive boundary for maximum converter reference value
$\Delta p_{\text{ref},n,f}$	Change in converter power reference due to frequency droop control of converter n
$\Delta p_{\text{ref},n,v}$	Change in converter power reference due to DC node voltage droop control of converter n
$\Delta p_{\text{schedule},ij}$	Difference between measured and scheduled power flow between node i and j
$\delta_{\text{Slack,AC}}$	AC voltage angle of slack bus
$\Delta\delta$	Voltage angle difference between AC nodes
ε	Radius of convergence (Differential Evolution optimization algorithm)
λ_i	Eigenvalue i
λ_{ij}	Share between active power measured by WAMS and apparent power measured at AC line outlet parallel to DC line between converter connected AC node i and j
φ	Phase angle of sinusoidal function / signal
ω	Angular velocity
ω_0, f_0	Reference angular velocity / reference frequency
$p_{\text{loss\_TSO}}$	Total losses (AC and DC) within a TSO HVDC converter observability area caused by an power exchange with another TSO p_{export}
$p_{\text{loss\_global}}$	Total losses (AC and DC) caused by an power exchange between TSOs p_{export}
$p_{\text{loss\_transit\_TSO}}$	AC losses within a TSO HVDC converter observability area caused by an power exchange between two other TSOs p_{export}
$n_{\text{transit\_TSO}}$	Number of considered transit TSO for a decentralized coordination of converter power references